The role of cysteine rich with epidermal growth factor-like domains 2 in skeletal development and homeostasis.

Ella Patricia Dennis

Thesis submitted for Doctor of Philosophy

Institute of Genetic Medicine

June 2018

Abstract

Cysteine-rich with epidermal growth factor (EGF)-like domains 2 (CRELD2) has previously been identified as a genotype-specific endoplasmic reticulum (ER) stress-inducible gene implicated in the pathogenesis of skeletal dysplasias. The function of *Creld2* is largely unknown despite putative roles described in protein folding and trafficking. *Creld2* is expressed in mouse embryonic skeletal tissues and interestingly a novel role has been identified for *Creld2* in mesenchymal stem cell osteogenic differentiation. To further study the role of *Creld2* in skeletal development and homeostasis, conditional *Creld2* knockout mice were generated and phenotyped.

The data presented in this thesis revealed that cartilage-specific *Creld2* knockout mice display a distinctive chondrodysplasia phenotype characterised by disproportionate short statue and a disrupted cartilage growth plate. The ablation of *Creld2* in the growth plate significantly reduces chondrocyte differentiation, proliferation and survival resulting in regions of hypocellularity. Interestingly, analysis of the growth plate shows a striking misalignment of chondrocytes within individual chondrons would result from the impaired organisation of primary non-motile cilia. CRELD2 binds to low density lipoprotein receptor-related protein 1 (LRP1) in chondrocytes and it can therefore be hypothesised that CRELD2 plays a role in chondrocyte differentiation by modulating LRP1 trafficking.

This study also focused on generating and phenotyping bone-specific *Creld2* knockout mice. These mice display an osteopenic phenotype characterised by a reduction in bone mass, with impaired bone microarchitecture. The deletion of *Creld2* in osteoblasts significantly impairs osteoblast differentiation and activity and interestingly induces the upregulation of osteoblast-derived osteoclastogenic cytokine production, disrupting the balance between bone formation and resorption indicating that CRELD2 plays an anabolic role in osteoblasts.

Therefore *Creld2* plays distinct roles in bone and cartilage and points to an important role for *Creld2* in chondrocyte differentiation, osteoblast function and skeletal development.

Table of contents

List of figures

List of tables

Acknowledgments

Firstly, I would like to thank my supervisor, Professor Michael Briggs, for all his support and knowledge; which without, this thesis would not have been possible. I would also like to thank my second supervisor, Dr Katarzyna Piróg for her encouragement and guidance during my PhD. Thanks are also due to all the lab members, past and present, for their friendship and experimental assistance during my project. A special thanks to Robert Jackson for going through all the ups and downs of this PhD with me, coffee is the key to success!

I would like to express my gratitude to Professor Anna Teti, Dr Nadia Rucci and Dr Mattia Capulli for teaching me a wide range of experimental techniques and welcoming me into their group during my visit to the University of L'Aquila.

Thanks are also due to Dr Sarah Edwards (University of Manchester) for generating the *Creld2* conditional mouse model.

Special thanks to the Functional Genomics Unit at Newcastle University for assisting with the animal care.

GATC Biotech are greatly acknowledged for their help with RNA sequencing.

Thanks to Dr David Knight and the Biological Mass Spectrometry Unit at The University of Manchester for the help with Mass Spec.

Thanks are also due to the Electron Microscopy Research Services at Newcastle University.

The SYBIL consortium is gratefully acknowledged for financial support.

I would like to express my gratitude to my family - my Granny, Granda, Mum, Nigel, Eoin and David, for teaching me, encouraging me, supporting me and loving me. (And for their patience!).

Finally, my heartfelt thanks to Richard, for all his love and for believing in me.

Abbreviations

ACVR1	Type I activin receptor
ADAM	A disintegrin and metalloproteinase
ADP	Adenosine diphosphate
AKT	Protein kinase B
ALK2	Activin receptor-like kinase-2
ALP	Alkaline phosphatase
AME	2-methoxyethyl-acetate
AP1	Activator protein 1
APC	Adenomatosis polyposis coli
ARMET	Arginine-rich, mutated in early-stage tumors
ASPA	Animals (Scientific Procedures) Act
ATF	Activating transcription factor
ATP	Adenosine triphosphate
ATPase	Adenylpyrophosphatase
AVSD	Atrioventricular septal defects
BAX	BCL2-like protein 4
BBF2H7	BBF2 human homolog on chromosome 7
BCA	Bicinchoninic acid assay
BCL2	B-cell lymphoma 2
BFR	Bone formation rate
bHLH	Basic helix-loop-helix
BIP	Binding immunoglobulin protein
BMP	Bone morphogenic protein
BMP1RA	Type IA BMP receptor
BMP1RB	Type IB BMP receptor
BMP2R	Type II BMP receptor
BPO	Luperox ® A75 Bonzoyl peroxidase
BrdU	Bromodeoxyuridine
BS	Bone surface
bZIP	Basic leucine zipper
C-CBL	E3 Ubiquitin Protein Ligase
Calcr	*Calcitonin Receptor*

cAMP	Cyclic adenosine monophosphate
CBFA1	Core-binding factor subunit alpha-1
CCL	C-C Motif Chemokine Ligand
CD	Cluster of differentiation
CDK4	Cyclin dependant kinase 4
CDKN1A	Cyclin dependent kinase inhibitor 1A
CHOP	C/EBP homologous protein
CK1α	Casein kinase 1α
Col2	*Collagen Type II Alpha 1 Chain*
Co-IP	Co-Immunoprecipitation
COMP	Cartilage oligomeric matrix protein
COPA	Coatomer protein subunit alpha
COPG	Coatomer subunit gamma-1
CPNY4	Canopy 4
CREB	cAMP responsive element-binding protein
CREB3L2	cAMP Responsive element binding protein 3 like 2
CRELD	Cysteine-rich with EGF-like domains
***Creld2*$^{Bone\Delta Ex3\text{-}5}$**	*Creld2* bone-specific knockout
***Creld2*$^{Cart\Delta Ex3\text{-}5}$**	*Creld2* cartilage-specific knockout
CSF1	Colony stimulating factor
CTGF	Connective tissue growth factor
Ctsk	*Cathepsin K*
CXCL	C-X-C Motif chemokine ligand 10
CYR61	Cysteine-rich angiogenic-inducer 61
DAG	Diacylglycerol
DKK1	Dickkopf WNT signalling pathway inhibitor 1
DLL	Delta–like
DMEM	Dulbecco's Modified Eagle Medium
DMP1	Dentin matrix acidic phosphoprotein 1
DMPT	N,N-Dimethyl-p-toluidine
DMSO	Dimethyl sulfoxide
DNA	Deoxyribonucleic acid
DNMT3	DNA methyltransferase 3
DPBS	Dulbecco's phosphate-buffered saline

DSH	Dishevelled
DSL	Delta/Serrate/lag
DSP	Dithiobis(succinimidyl propionate
DTT	Dithiothreitol
dUTP	Deoxyuridine triphosphate
EBPB4	Ephrin receptor B4
ECM	Extracellular matrix
EDTA	Ethylenediaminetetraacetic acid
EGF	Epidermal growth factor
EHD4	EH domain-containing protein 4
eIF2α	Eukaryotic translation initiation factor 2α
ER	Endoplasmic reticulum
ERAD	ER-associated degredation
ERK	Extracellular signal–regulated kinase
ERO1A	ER oxidoreductase 1-like protein alpha
ERp	Endoplasmic reticulum resident protein
ERSE	ER stress-responsive cis-acting element
EtOH	Ethanol
FAT4	FAT Atypical Cadherin 4
FBN2	Fibrilin-2
FBS	Fetal bovine serum
FGF	Fibroblast growth factor
FGFR	Fibroblast growth factor receptor
FGU	Functional genomics unit
FLK1	Fetal liver kinase 1
FLT1	Fms related tyrosine kinase 1
FOP	Fibrodysplasia ossificans progressiva
FOX	Forkhead box
FZD	Frizzled
GADD	Growth arrest and DNA damage inducible
GANAB	Alpha glucosidase 2 alpha neutral subunit
GDF	Growth and differentiation factor
GLG1	Golgin 1
GPCR	G-protein-coupled receptors

GREM1	Gremlin 1
H&E	Hematoxylin and Eosin
HBSS	Hank's buffered saline solution
HCl	Hydrochloric acid
HES	Hairy and enhancer of split-1
HEY	Hairy/enhancer-of-split related with YRPW motif protein 1
HIF1α	Hypoxia-inducible factor 1α
HSP	Heat shock protein
HYOU1	Hypoxia upregulated protein 1
IBSP	Integrin binding sialoprotein/Bone sialoprotein
ICAM1	Intercellular adhesion molecule 1
ICD	Inner canthal distance
ID4	Inhibitor of DNA binding 4
IGF1	Insulin growth factor 1
IHC	Immunohistochemistry
IHH	Indian hedgehog
IL	Interleukin
IP3	Inositol triphosphate
IRE1	Inositol-requiring enzyme 1
IRF1	Interferon regulatory factor 1
KDEL	Lysine-aspartic acid-glutamic acid-leucine
KDR	Kinase Insert Domain Receptor
KIF3A	Kinesin family member 3A
LC-MS/MS	Liquid chromatography tandem-mass spectrometry
LEF	Lymphoid enhancer factor
LMAN1	ER-Golgi intermediate compartment protein 53
LRP	Low density lipoprotein receptor-related protein
MAML	Mastermind-like
MANF	Mesencephalic astrocyte-derived neurotrophic factor
MAPK	Mitogen-activated protein kinase
MAR	Mineral apposition rate
MCP1	Monocyte chemotactic protein 1
MCSF1	Macrophage colony stimulating factor 1
µCT	Micro-computed tomography

MED	Multiple epiphyseal dysplasia
MEF	Myocyte Enhancer Factor
MEFs	Mouse embryonic fibroblasts
MEMα	Minimum Essential Medium Eagle Alpha Modification
MEPE	Matrix extracellular phosphoglycoprotein
MESDC2	Mesoderm development candidate 2
MMA	Methyl methacrylate
MMP	Matrix metalloproteinase
MOGS	Mannosyl-oligosaccharide glucosidase
mRNA	Messenger RNA
MS	Mineralising surface
MSC	Mesenchymal stem cell
MSDS	Metaphyseal dysplasia type Schmid
nAChR	Nicotinic acetylcholine receptor
NaCl	Sodium chloride
NCAD	Neural cadherin
NCAM	Neural cell adhesion molecule
NCID	Notch intracellular domain
NFATc1	Nuclear factor of activated T-cells 1
NFκB	Nuclear factor kappa-light-chain-enhancer of activated B cells
NPG	Nonylphenyl-polyethyleneglycol acetate
OASIS	cAMP-responsive element-binding protein 3-like protein 1
OC	*Osteocalcin*
OCIF	Osteoclast inhibitory factor
OPG	Osteoprotegerin
OST	Oligosaccharyltransferase
OSX	Osterix
P3H1	Prolyl 3-hydroxylase 1
P4HA2	Prolyl 4-hydroxylase subunit alpha 2
PBS	Phosphate buffered saline
PCR	Polymerase chain reaction
PDI	Protein disulphide isomerase
PERK	Protein kinase ribonucleic acid (RNA)-like ER kinase
PHEX	Phosphate regulating endopeptidase homolog, X-linked

Pi	Inorganic phosphate
PI3K	Phosphatidylinositol-4,5-bisphosphate 3-kinase
PIP2	Phosphatidylinositol 4,5-bisphosphate
PKC	Protein kinase C
PLC	Phospholipase C
PLOD	Procollagen-lysine,2-oxoglutarate 5-dioxygenase
POFUT2	Guanine diphosphate-fucose protein O-fucosyltransferase 2
PP2A	Protein phosphatase 2A
PPI	Peptidyl–prolyl cis/trans isomerases
PPi	Inorganic pyrophosphate
PS	Presenilin
PSACH	Pseudoachondroplasia
PTCH1	Patched 1
PTHRP	Parathyroid hormone related protein
qPCR	Quantitative real-time PCR
R26R	ROSA 26
RANK	Receptor activator of NFκB
RANKL	Receptor activator of NFκB ligand
RBPjK	Recombining binding protein suppressor of hairless protein
rER	Rough Endoplasmic reticulum
RHOA	RAS homolog gene family, member A
RIN	RNA integrity number
RNA	Ribonucleic acid
RNA-seq	RNA sequencing
ROI	Region of intrest
RPL15	Ribosomal protein L15
RPN1	Dolichyl-diphosphooligosaccharide—protein glycosyltransferase subunit 1
RTN3	Reticulon-3
RUNX2	Runt Related Transcription Factor 2
S15A	40S ribosomal protein S15a
SDS	Sodium dodecyl sulphate
SEM	Standard error of the mean
SEMA3E	Semaphorin 3E

SEP15	Selenoprotein F
SERPINH1	Serpin family H member 1
SMAD	Mothers against decapentaplegic homolog
SMO	Smoothened
SOST	Sclerostin
SOX	SRY-box
SP7	Osterix
SPP1	Osteopontin
SSC	Saline sodium citrate
STAT1	Signal transducer and activator of transcription 1
T2R	Taste 2 receptor
TACE	Tumour necrosis factor-alpha converting enzyme
TAE	Tris-Base, acetic acid and EDTA
TCF	T-cell factor
TEM	Transmission electron microscopy
TGF	Transforming growth factor
TMED9	Transmembrane P24 trafficking protein 9
TNF	Tumour necrosis factor
TRAF	TNF Receptor Associated Factor
TRAcP	Tartrate-resistant acid phosphatase
TSG6	TNF-stimulated gene 6 protein
TSP	Thrombospondin
TUNEL	Terminal deoxynucleotidyl transferase dUTP nick end labelling
TWIST2	Twist Family BHLH Transcription Factor 2
UDP	Uridine diphosphate
UGGT1	UDP-glucose:glycoprotein glucosyltransferase 1
UPR	Unfolded protein response
UPRE	Unfolded protein response element
V-H$^+$-	Vacuolar-type H$^+$-adenylpyrophosphatase
VCAM1	Vascular cell adhesion molecule 1
VEGF	Vascular endothelial growth factor
vWFA	Von Willebrand factor A domain
WE	Tryptophan-aspartic acid
WNT	Wingless-type MMTV integration site

XBP1s	X-box binding protein 1 spliced
XBP1u	X-box binding protein 1 unspliced
X-gal	5-bromo-4-chloro-3-indolyl-β-D-galactopyranoside

Chapter 1. Introduction

Chapter 1. Introduction

Skeletal dysplasias result from a defect in the formation of the osseous skeleton. Individually these diseases are rare and phenotypes are grouped by clinical, radiographic and molecular presentation, ranging from mild to severe bone conditions and lethal diseases. Skeletal dysplasias are characterised by disproportionate short stature with malformations and deformations of the skeleton and a disrupted epiphyseal growth plate. In a previous study the novel endoplasmic reticulum (ER) stress-inducible gene, *Creld2,* encoding Cysteine rich with epidermal growth factor (EGF)-like domains (CRELD) 2, was found to be upregulated in several skeletal dysplasias; however, the precise role of this protein is not understood (Hartley et al., 2013).

The purpose of this thesis was to analyse the role of *Creld2* in the molecular mechanisms involved in longitudinal bone development and homeostasis. The reader will be introduced to skeletal development and homeostasis, focusing on endochondral ossification and the biology of bone turnover and maintenance. The role of *Creld2* to date will be reviewed and unanswered questions will be highlighted. The main focus of this thesis is to identify the role of *Creld2* in cartilage and in bone, which will be dissected using conditional knockout mouse models.

1.1 Committed differentiation of mesenchymal stem cells

Mesenchymal stem cells (MSCs) were first described by Alexander Friedenstein as a population of bone marrow derived stem cells, distinct from hematopoietic stem cells, that are capable of osteogenic differentiation *in vivo* (Friedenstein, 1976). MSCs were later found to carry out two essential functions. They not only have a high capacity for self-renewal in order to restore the MSC population, but are also precursors to cells of the mesodermal lineage. MSCs exhibit a unique combination of cell surface antigens and can differentiate into a variety of cell types including the chondrocytic, osteogenic, adiopogenic and myogenic lineages *in vitro* (Prockop, 1997, Pittenger et al., 1999) (Figure 2).

The key step in initiating endochondral ossification is the condensation and differentiation of osteochondroprogenitor MSCs into chondrocytes. The decision to differentiate into cells of the skeletal system is controlled by transcription factors. Under the control of the transcription factor SRY-box (SOX) 9, osteochondroprogenitor MSCs give rise to small round chondrocytes (Figure 3) (Akiyama et al., 2002). These chondrocytes then undergo maturation in the growth plate controlled by the combined transcriptional action of SOX9 as well as SOX5 and SOX6 and a wide range of other signalling molecules including bone morphogenic proteins (BMPs), members of the fibroblast growth factor (FGF) family, Wingless-Type MMTV Integration Site (WNT) family members, Indian hedgehog (IHH) and parathyroid hormone related protein (PTHrP) that will be discussed later in this thesis (Kozhemyakina et al., 2015).

Osteoblast differentiation of osteochondroprogenitor stem cells is controlled by transcription factors such as Runt Related Transcription Factor 2 (RUNX2), Osterix and β-catenin (Komori, 2006) (Figure 2). Studies have shown that WNT signalling and β-catenin are crucial for determining the commitment of MSCs to the osteoblast lineage and the formation of bone, as demonstrated by the gain and loss of function mouse models (Day et al., 2005, Hill et al., 2005, Hu et al., 2005, Bennett et al., 2007, Cawthorn et al., 2012b). It was shown that WNT signalling inhibits *Sox9* expression and the subsequent chondrogenic differentiation of MSCs, directing the cells to undergo osteoblastogenesis (Hill et al., 2005). Consistent with this, the inactivation of β-catenin suppressed osteoblastogenesis and MSCs were found to differentiate into chondrocytes (Day et al., 2005).

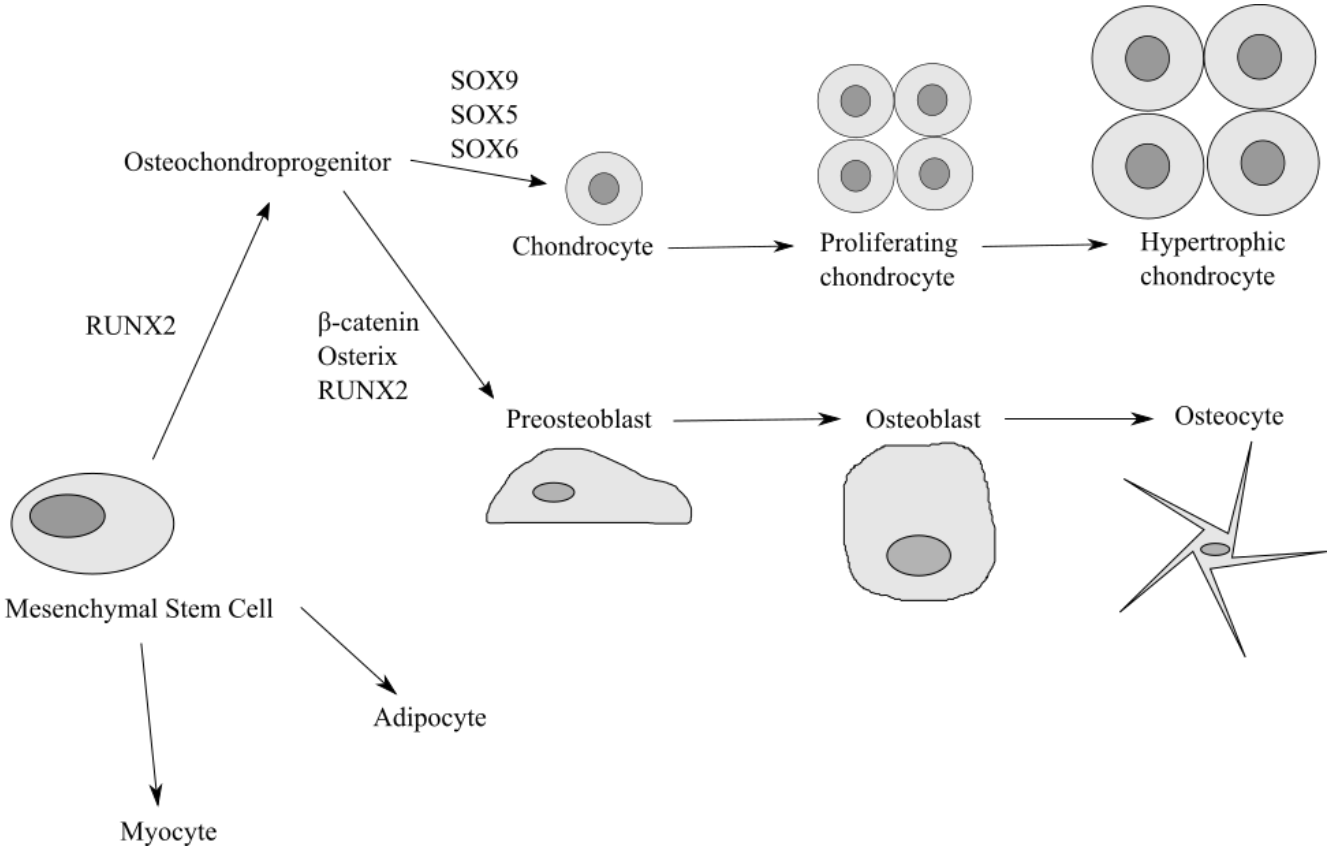

Figure 1. **Mesenchymal stem cells give rise to cells of the chondrogenic, osteogenic, adipogenic and myogenic lineages.**

Under the control of specific transcription factors they give rise to cells of the chondrogenic, osteogenic, adipogenic and myogenic lineages. RUNX2 is important for the differentiation of MSCs to osteochondroprogenitor cells. SOX9 is an important transcription factor driving chondrogenesis. Chondrocyte differentiation and osteoblastogenesis is further controlled by canonical WNT signalling involving the transcription factor β-catenin, that acts to inhibit chondrocyte differentiation and promote osteoblastogenesis.

1.2 Skeletal development

Bone is a dynamic connective tissue, which is formed within the third month of foetal development and is constantly adapted during postnatal life to maintain skeletal structure, function and integrity. The mature adult skeleton consists of 206 bones that form the appendicular and axial skeleton and function to offer support and protection whilst also acting as a mineral store for the body.

Bone formation, or osteogenesis, occurs by two distinct processes; intramembranous or endochondral ossification (Gilbert, 2000). The formation of membranous bones such as the facial and cranial bones occurs by intramembranous ossification in which the migrating neural crest mesenchymal cells and in some cases mesodermal differentiate into cells of the osteoblast lineage and form bone directly (Jiang et al., 2002). The formation of long bones on the other hand occurs by a process called endochondral ossification. Endochondral ossification describes the process in which the mesenchyme forms a cartilaginous template that is gradually calcified to form bone.

1.2.1 Intramembranous ossification

Intramembranous ossification describes the formation of flat bones such as the craniofacial bones and parts of the clavicle from the mesenchyme (Gilbert, 2000). This process begins with the migration and proliferation of mainly neural crest-derived MSCs; however, some of the bones are also formed by mesodermal mesenchymal cells (Jiang et al., 2002). Stem cells condense, differentiate into osteoblasts and secrete unmineralised bone known as osteoid in between the embryonic blood vessels that will later become calcified forming a network of trabeculae known as spongy bone.

The vascularised mesenchyme on the external face of the forming bone then condenses, forming the bone collar known as the periosteum. The trabeculae adjacent to the periosteum thicken and form a woven bone collar that is later replaced by mechanically strong compact lamellar bone.

1.2.2 Endochondral ossification

Endochondral ossification is the process responsible for the development of the vertical appendicular and axial skeleton, postnatal longitudinal bone growth and the natural healing of fractures. This distinct process of bone formation requires an initial cartilaginous model that is gradually replaced by bone (Figure 2) (Mackie et al., 2008). Endochondral ossification describes a highly regulated process and the mechanisms that control it have been extensively studied.

Endochondral ossification begins with the migration and condensation of MSCs that is mediated by the adhesion molecules neural cadherin (NCAD) and neural cell adhesion molecule (NCAM) (Jiang et al., 1993, Oberlender and Tuan, 1994). These cells then differentiate into chondrocytes, professional secretory cells that secrete an extracellular matrix rich in type II collagen and aggrecan that forms the primordial avascular cartilage model (Gentili and Cancedda, 2009).

On the surface of this model, the MSCs differentiate into a tissue called the perichondrium. Following a subsequent vascularisation of the perichondrium, they differentiate into osteoblasts and form the periosteum, a bone collar surrounding the cartilage anlage (Dwek, 2010).

Endochondral ossification is driven by differentiation-induced changes in chondrocyte morphology and secretory activity. Upon entering hypertrophy, chondrocytes upregulate the expression of matrix metalloproteinases (MMPs), predominantly MMP13, which degrade the cartilage matrix, and vascular endothelial growth factor (VEGF), a signal protein that stimulates vasculogenesis and angiogenesis (Gerber et al., 1999, Tuckermann et al., 2000). This results in the formation of the primary centre of ossification. These hypertrophic chondrocytes then facilitate calcification of the cartilaginous matrix before undergoing apoptosis.

Osteoblast precursors that invade the tissue via the newly formed blood vessels then use the calcified cartilage matrix as a scaffold for bone formation, beginning at the primary centre of ossification in the centre of the bone shaft (Maes et al., 2010). Bone formation then persists through the shaft allowing for bone elongation.

Later in development, secondary centres of ossification also form at the ends of the bone (epiphyses) and are separated from the bone shaft (diaphysis) by the growth plate or physis, a specialised cartilage tissue responsible for embryonic and postnatal

longitudinal bone growth. The epiphyseal growth plates at either end of the long bones continue depositing cartilage matrix and only fuse once maturity has been reached and bone growth stops (Shim, 2015). The resulting mature bone is completely calcified except for a fibrous matrix of hyaline cartilage at articulating surfaces, which allows for flexibility and support at the strain.

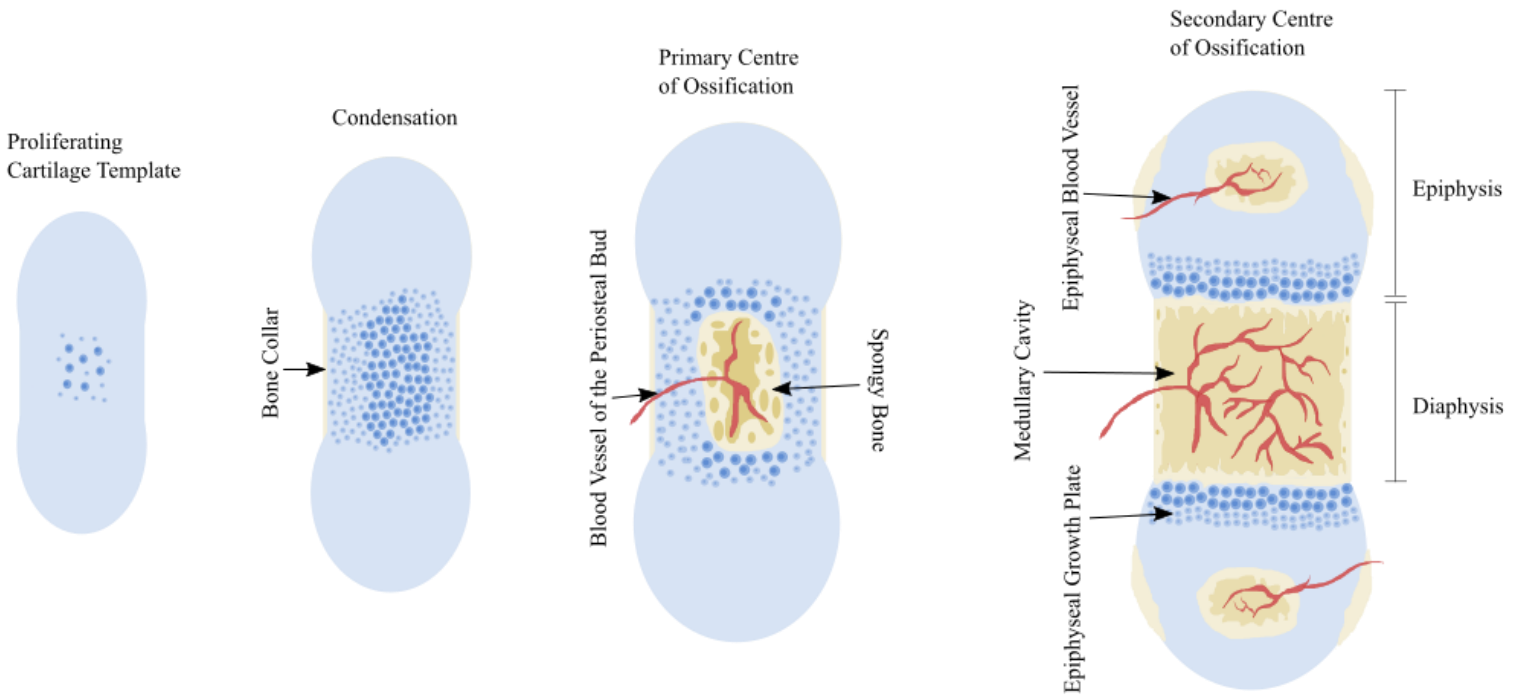

Figure 2. **The process of endochondral ossification**

The process of endochondral ossification begins with the condensation of MSCs that differentiate into chondrocytes, forming a cartilaginous model that is gradually replaced by bone. Bone formation begins at the primary centre of ossification or the diaphysis and persists throughout the shaft. Secondary centres of ossification form at the epiphyses and are separated from the diaphysis by a cartilaginous growth plate responsible for longitudinal bone growth.

1.3 Postnatal growth plate and longitudinal bone growth

1.3.1 Cartilage growth plate structure and function

The epiphyseal growth plate (physis) is a specialised form of hyaline cartilage found at the proximal and distal ends of long bones that is responsible for postnatal longitudinal bone growth. The single cell type found in the physis is called the chondrocyte. Chondrocytes are professional secretory cells that are present in small cavities called lacunae within a vast extracellular matrix. They are able to interact with and subsequently modify the environment of the matrix in which they reside. Chondrocytes are arranged in a highly ordered fashion and maintain their spatial location throughout their life cycle despite changes in morphology and secretory activity. In the physis, chondrocytes undergo highly regulated maturation processes involving differentiation, proliferation and hypertrophy. The growth plate is organised into four distinct zones depending on the state of differentiation of the chondrocytes. These are the resting or germinal zone, the zone of proliferation, the zone of hypertrophy or maturation and finally the zone of calcification (Figure 3) (Burdan et al., 2009).

The resting zone consists of a random arrangement of small rounded chondrocytes with a low proliferative capacity. Due to the presence of a high number of lipid bodies and vacuoles inside resting chondrocytes it is postulated that they are forming nutrient stores for later in life in the hypoxic growth plate (Brighton et al., 1973).

As cells progress in maturation from the resting zone, they adopt a highly proliferative phenotype. The proliferative zone comprises half the height of the physis due to the rapid rate of mitosis. Proliferative chondrocytes secrete a cartilaginous extracellular matrix rich in type II collagen and aggrecan that will be later used as a scaffold for bone formation (Gentili and Cancedda, 2009). In the proliferative zone the cells adopt a flattened shape and become polarised. Here they divide perpendicularly to the axis of bone formation, then migrate and align into longitudinal columns known as chondrons that are aligned along the axis of bone growth. This re-orientation of dividing proliferative chondrocytes may be controlled by primary non-motile cilia that project into the extracellular matrix and interact with matrix molecules such as collagens, via a number of receptors including integrins transducing signals from the extracellular

matrix (Ruhlen and Marberry, 2014). Interestingly primary cilia are also the centre for modulating WNT and IHH signalling and therefore regulate chondrocyte differentiation and maturation within the growth plate (Song et al., 2007, Haycraft and Serra, 2008).

Chondrocytes existing in the proliferative stage then undergo hypertrophy, the final step in the maturation process. Hypertrophic chondrocytes become more rounded and swell in size due to an increase in metabolic activity (Hunziker et al., 1987). The increasing glycogen content and dry mass of the hypertrophic chondrocytes is regulated by insulin growth factor 1 (IGF1) signalling (Wang et al., 1999). As well as changing the morphology, hypertrophic chondrocytes also alter their secretory activity. Chondrocytes in this zone cease the secretion of type II collagen and aggrecan and instead secrete hypertrophic markers such as type X collagen, alkaline phosphatase and proteins such as osteopontin and osteocalcin, facilitating mineralisation of the cartilaginous matrix (Kielty et al., 1985, Lian et al., 1993, Miao and Scutt, 2002). MMP13 is also upregulated in the hypertrophic chondrocytes in order to prepare the matrix for calcification (Stickens et al., 2004).

The final zone of the epiphyseal growth plate is the zone of calcification. Here the chondrocytes are dying or are dead. This is due to the mineralisation of the matrix creating a hypoxic environment depleted of nutrients. The chondrocytes initially undergo anaerobic respiration until the glycogen stores built up early in life are depleted and then are proposed to die. The subsequently empty lacunae are invaded by blood vessels sprouting into the cartilage analge due to hypertrophic chondrocytes expressing VEGF (Gerber et al., 1999). The invading blood vessels allow access for osteoblasts and osteoclasts to degrade the matrix and lay down a bone matrix on the mineralised cartilage scaffold (Maes et al., 2010).

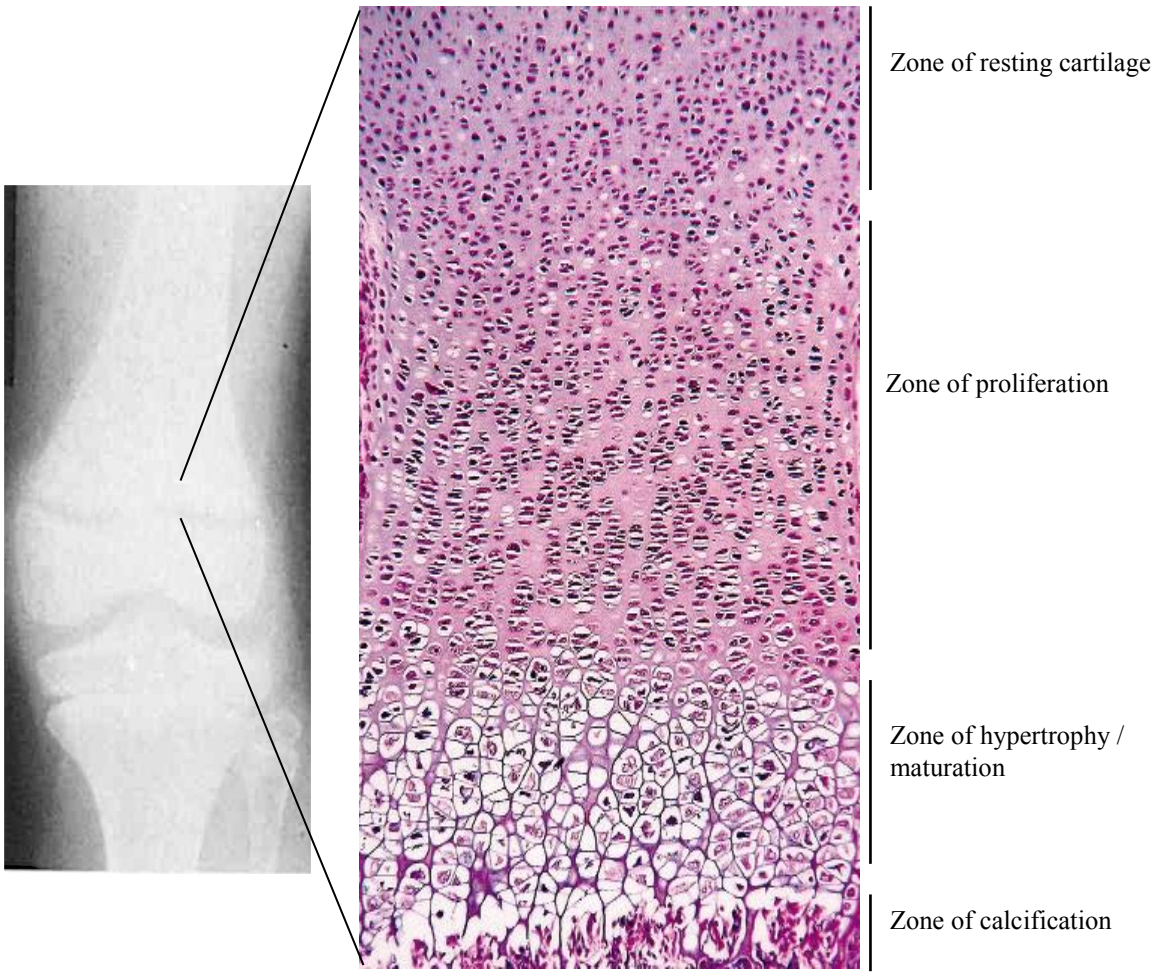

Figure 3. **Morphology of the epiphyseal growth plate.**

The growth plate is a highly ordered tissue divided into four distinct zones depending on the differentiation state of chondrocytes; the zone of resting cartilage where cells are in a random orientation, the zone of proliferation where cells arrange into longitudinal columns, the zone of hypertrophy/maturation where chondrocytes increase in size and the zone of calcification where the matrix becomes calcified prior to bone deposition. *Adapted from:* (Burdan et al., 2009)

1.3.2 Fate of hypertrophic chondrocytes

1.3.2.1 Apoptosis or chondrocyte programmed cell death

The condensed chondrocytes identified at the chondro-osseous junction were first described by Farnum and Wilsum as "dark chondrocytes" because of artifacts of transmission electron microscopy (Figure 8A & 8B) (Wilsman et al., 1981). "Dark chondrocytes" have also been identified in rabbits, chick embryos as well as articular cartilage (Erenpreisa and Roach, 1998, Roach and Clarke, 2000, Kouri-Flores et al., 2002). These chondrocytes have been postulated to undergo a distinct non-classical form of apoptosis that has been described as "chondroptosis" (Roach et al., 2004).

Hypertrophic chondrocytes at the vascular invasion front do not display the distinct morphological features of apoptosis. For example, despite the shrinking of cells and the condensation of chromatin in the nucleus, the chromatin in hypertrophic chondrocytes is not restricted into a solid mass (Figure 8C & 8D) (Ahmed et al., 2007, Roach and Clarke, 1999). Instead, it is spread through the unusually convoluted nucleus. Despite this, DNA cleavage must occur in terminal hypertrophic chondrocytes as apoptotic chondrocytes in the growth plate have been identified using the terminal deoxynucleotidyl transferase deoxyuridine triphosphate (dUTP) nick end labelling (TUNEL) method (Hatori et al., 1995, Zenmyo et al., 1996, Aizawa et al., 1997).

As hypertrophic chondrocytes have a different structure to apoptotic cells, evidence points to a second method of programmed cell death. Not only do the hypertrophic chondrocytes undergo nuclear changes, but they also undergo cytoplasmic changes (Roach et al., 2004). Terminal chondrocytes exhibit an expansion in rough endoplasmic reticulum (rER) that is seen at all stages of death together with an expansion of the Golgi apparatus (Figure 8C & 8E) (Ahmed et al., 2007). Interestingly, these chondrocytes are abundant in autophagic vacuoles; however, unlike classical apoptosis no apoptotic bodies are present (Ahmed et al., 2007).

The final stage of chondroptosis is characterised by empty lacunae following the final disintegration of cellular material (Farnum and Wilsman, 1989). This is distinct from classical apoptosis in which cells undergo a second necrosis phase leading to permeabilisation of lysosomal membranes and the release of lysosomal enzymes which result in cell elimination (Hatori et al., 1995, Don et al., 1977, Silva, 2010).

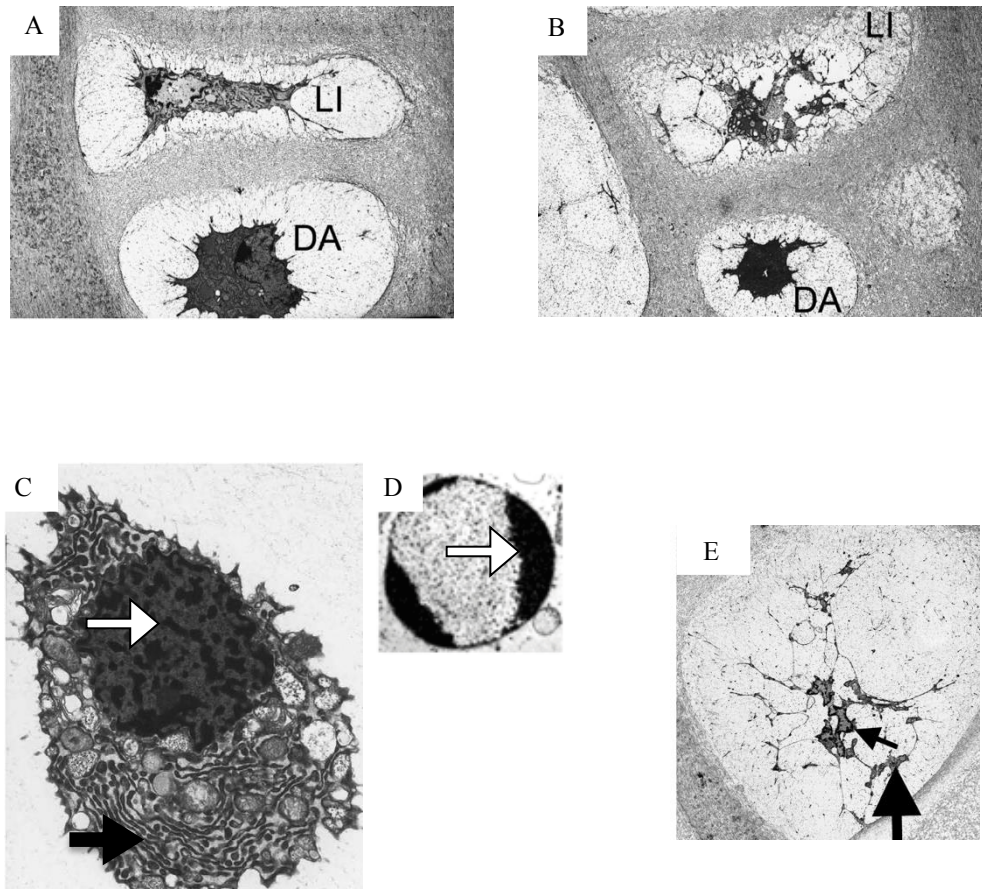

Figure 4. **Morphology of cells undergoing chondroptosis in the growth plate.**

"Dark chondrocytes" at the chondro-osseous junction undergo a distinct non-classical form of apoptosis described as "chondroptosis" (**A & B**) (LI= light chondrocytes, DA= dark chondrocytes). This type of cell death is distinct from apoptosis. For example, despite the shrinking of cells and the condensation of chromatin in the nucleus; the chromatin in hypertrophic chondrocytes is not restricted into a solid mass (**C**) as seen in the nuclei from cells undergoing classical apoptosis (**D**) (outlined by white arrow). Cytoplasmic changes are also evident as cells undergo an expansion of the Golgi apparatus and increase in rER (**C**) (outlined by black arrow). Interestingly in late stages of cell death, the nucleus of the chondrocytes appears to remain intact (**E**) (outlined by small arrow) and the rER remains visible at all stages (**C & E**) (outlined by large arrow). (Picture **A, B, E**, *taken from* (Ahmed et al., 2007), Picture **C** *taken from* (Roach et al., 2004), Picture **D** *taken from* (Volbracht et al., 2001).)

1.3.2.2_Transdifferentiation

A crucial step in the process of endochondral ossification is the conversion of cartilage to bone by the action of osteoblasts. The source of these osteoblasts is not well defined and the fate of the hypertrophic chondrocytes at the chondro-osseous border has been the subject of controversy for some time.

An alternative fate has been suggested for hypertrophic chondrocytes, postulating their conversion into osteoblasts in a process called transdifferentiation. Transdifferentiation describes the lineage reprogramming of cells without going through a pluripotent cell stage (Kelaini et al., 2014). Recent advances have shown remarkable differentiation plasticity of differentiated mammalian cells (Jopling et al., 2011). It is therefore possible that hypertrophic chondrocytes undergo a dedifferentiation process before they redifferentiate into osteoblasts as seen in other cases of cellular transdifferentiation.

This lineage reprogramming of hypertrophic chondrocytes into osteoblast-like cells has been identified in both *in vitro* and *in vivo* studies (Silbermann et al., 1983, Moskalewski and Malejczyk, 1989, Thesingh et al., 1991, Descalzi Cancedda et al., 1992, Gentili et al., 1993, Yang et al., 2014a, Yang et al., 2014b, Zhou et al., 2014, Park et al., 2015b). A number of *in vitro* studies have shown that given the right cues the hypertrophic chondrocytes differentiate in culture and become osteoblast-like cells with the ability of producing a mineralised matrix (Descalzi Cancedda et al., 1992, Gentili et al., 1993). Interestingly, it has also been shown that the hypertrophic chondrocytes express a number of genes associated with osteoblasts such as alkaline phosphatase, osteopontin and osteocalcin (Lian et al., 1993, Miao and Scutt, 2002).

Recently several *in vivo* lineage tracing studies using transgenetic mouse models have provided strong evidence for the transdifferentiation of hypertrophic chondrocytes to osteoblasts (Yang et al., 2014a, Yang et al., 2014b, Zhou et al., 2014). Interestingly, it was shown that up to 60 % of osteoblasts were derived from terminal growth plate chondrocytes (Zhou et al., 2014). However, this study contradicts a previous report using tamoxifen-induced genetic recombination using the *Col2a1-Cre*^{ERT} transgenic mouse line, which showed that osteoblasts did not derive from growth plate chondrocytes (Maes et al., 2010).

1.3.3 Local regulation of the growth plate chondrocytes

Skeletal development and postnatal longitudinal bone growth are highly organised processes. Chondrogenesis and the growth of the skeleton requires precise regulation of the commitment of cells to the chondrogenic lineage and the control of growth plate differentiation from proliferation to hypertrophy. Major signalling pathways including IHH/PTHrP, WNT proteins, BMPs, FGFs and hormones act together to control skeletogenesis (Kozhemyakina et al., 2015). Work is ongoing to outline their roles in both chondrogenesis and osteogenesis.

1.3.3.1 Indian hedgehog (IHH)/Parathyroid hormone related protein (PTHRP)

IHH is a member of the hedgehog family of proteins and has been found to play an important role in the development and growth of the vertebral skeleton (St-Jacques et al., 1999). It is considered a master regulator of endochondral ossification, controlling chondrocyte and osteoblast differentiation. In the absence of IHH ligand binding, its receptor protein patched homolog 1 (PTCH1) is localised to the primary cilium where it represses the accumulation of and activity of smoothened (SMO), a seven-pass transmembrane protein that shares structural similarities to G-protein-coupled receptors (GPCRs) (Taipale et al., 2002, Corbit et al., 2005, Wilson et al., 2009). The interaction between IHH and PTCH1 results in the intracellular signal transduction following the removal of its repressive effect on SMO by an undetermined mechanism (Marigo et al., 1996, van den Heuvel and Ingham, 1996, Taipale et al., 2002, Corbit et al., 2005, Wilson et al., 2009).

IHH is expressed by prehypertrophic and hypertrophic chondrocytes in the cartilage growth plate (Figure 4). Conversely its receptor, PTCH1, is found on the primary cilium of proliferating and perichondrial chondrocytes (Rohatgi et al., 2007). Several studies have indicated an important role for IHH in chondrogenesis and osteogenesis, controlling chondrocyte proliferation and bone formation by exerting its effects both directly and indirectly via PTHrP.

The function of IHH in skeletal development was first proposed in relation to PTHrP, a secreted protein that is expressed in proliferating and perichondral chondrocytes (Figure 4) (Lanske et al., 1996, Vortkamp et al., 1996). In contrast, the gene encoding its receptor, *PTH1R*, is expressed in prehypertrophic chondrocytes.

Several gain-of-function and loss-of-function studies have elucidated that PTHrP modulates chondrocyte differentiation and keeps chondrocytes proliferating by supressing their maturation into hypertrophy (Amizuka et al., 1994, Karaplis et al., 1994, Lanske et al., 1996, Weir et al., 1996, Schipani et al., 1997). Interestingly the overexpression of *Ihh*, or the constitutive activation of IHH signalling following the ablation of *Ptch1* expression, leads to delayed chondrocyte hypertrophy and the upregulation of *Pthrp* expression. Furthermore, postnatal *Ihh*-null mice displayed a striking skeletal phenotype with a disrupted growth plate, a reduction in the size of the cartilage growth plate proliferative zone and an increase in chondrocyte hypertrophy (Maeda et al., 2007). Together these studies indicate that the interactions of the two paracrine factors, PTHrP and IHH, control the transition of proliferating chondrocytes to hypertrophic chondrocytes in a positive feedback loop (Vortkamp et al., 1996).

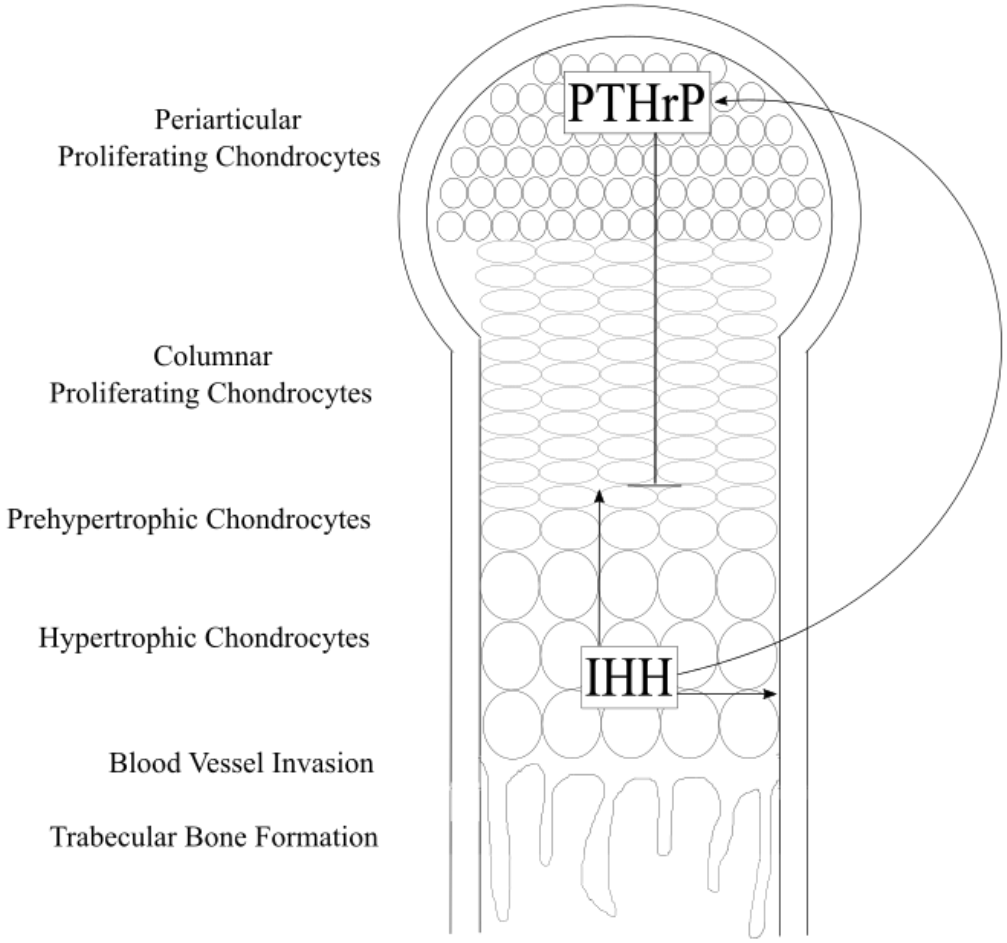

Figure 5. **Indian hedgehog (IHH)/Parathyroid hormone related protein (PTHRP) signalling in endochondral ossification.**

Ihh is expressed by prehypertrophic and hypertrophic chondrocytes in the cartilage growth plate and acts on proliferating and perichondrial chondrocytes. IHH controls chondrocyte proliferation and bone formation by exerting its effects both directly and indirectly via PTHrP. PTHrP modulates chondrocyte differentiation by keeping the chondrocytes proliferating and supressing their maturation into hypertrophy. *Adapted from:* (Kronenberg, 2003)

1.3.3.2 Bone morphogenic proteins (BMPs)

BMPs, also known as growth and differentiation factors (GDFs) are members of the transforming growth factor (TGF)-β cytokine superfamily that act via precisely controlled signalling pathways; regulating cellular differentiation, maturation and ultimately skeletal patterning and growth. A large number of ligands and receptors in this protein family play vital roles in endochondral ossification (Pogue and Lyons, 2006, Wu et al., 2016).

BMPs were first shown to play complex roles in chondrogenesis and osteogenesis due to their ability to form ectopic cartilage (Wozney et al., 1988). Studies in mice have also shown that BMP genes, *Bmp2, Bmp4, Bmp5* and *Bmp7,* are expressed in early condensing mesenchyme, demonstrating an important role for BMPs in the committed condensation and chondrogenic differentiation of MSCs (Lyons et al., 1995, Winnier et al., 1995, Dudley and Robertson, 1997, Solloway and Robertson, 1999, Buxton et al., 2001).

Not only are BMPs required for condensation and differentiation of MSCs, but they also play complex roles in the cartilage growth plate at later stages of development. BMPs were found to induce proliferation in the growth plate as mice with a *Noggin* knockout, that encodes a BMP antagonist, had over grown skeletal bones (Brunet et al., 1998). Furthermore, overexpression of *Noggin* resulted in a smaller growth plate with reduced proliferation and advanced differentiation of hypertrophic chondrocytes (De Luca et al., 2001, Minina et al., 2001, Tsumaki et al., 2002).

Further studies have outlined the presence of a BMP signalling gradient within the growth plate; with *Bmp2, Bmp4* and *Bmp6* highly expressed in hypertrophic chondrocytes, *Bmp7* highly expressed in proliferating chondrocytes and BMP antagonists, such as *Bmp3,* highly expressed in the resting zone (Nilsson et al., 2007). Not only do the regions of the growth plate express a well-defined pattern of BMP ligands but they also express a pattern of BMP receptors, with type IB BMP receptor (*Bmp1rb*) expressed throughout the growth plate, type IA BMP receptor (*Bmp1ra*) expressed in proliferative and hypertrophic chondrocytes and Activin receptor-like kinase-2 (*Alk2*) expressed in proliferating and resting chondrocytes (Zou et al., 1997, Rigueur et al., 2015). This well-defined pattern of BMP expression and signalling suggests that the development and maturation of chondrocytes is controlled by a series of signals in which BMP signalling is important at every stage.

The mechanisms controlling the maturation of chondrocytes within the growth plate is unclear; however, recent studies have provided evidence that this gradient of BMP expression pattern directs chondrocyte proliferation and hypertrophy (De Luca et al., 2001, Nilsson et al., 2007, Garrison et al., 2017). Furthermore, moderate levels of exogenous BMP2 were required to increase chondrocyte proliferation, whilst it took high levels to induce chondrocyte hypertrophy (De Luca et al., 2001). Additionally, overexpression of *Bmp1ra* lead to a reduction in proliferation and accelerated hypertrophy with an upregulation of maturation markers, suggesting distinct roles at each stage (Kobayashi et al., 2005).

BMP2 has been identified as playing a key role in chondrocyte proliferation and maturation in the growth plate as chondrocyte-specific *Bmp2* knockout mice display a severe chondrodysplasia phenotype with profound effects on chondrocyte proliferation and maturation (Shu et al., 2011). In cartilage, BMPs mediate their effects mainly through the canonical mothers against decapentaplegic homolog (SMAD) 1/5/8 pathway (Retting et al., 2009). Briefly, BMP signals through a taste 2 receptor (T2R) phosphorylated Serine/Threonine receptor inducing SMAD proteins such as SMAD1/5/8 to form a complex with SMAD4 that translocates to the nucleus and induces transcription. *In vitro* studies show that BMP2 inhibits the ubiquitylation of RUNX2 by downregulating cyclin dependant kinase 4 (CDK4) and so promoting proliferation (Shu et al., 2011). Furthermore, BMP2 was found to induce the expression of type X collagen and alkaline phosphatase and induced the expression of growth arrest and DNA damage inducible β (GADD45β) via SMAD1/RUNX2 in late hypertrophic chondrocytes which in turn activates MMP13, a hypertrophic marker (Valcourt et al., 2002, Ijiri et al., 2005). Together these findings indicate that BMP2 is important for chondrocyte proliferation and maturation.

Studies have shown that there is also considerable crosstalk between the signalling pathways that regulate the growth plate. For example, it has been shown that *Ihh* is a target of BMP signalling and that the *Ihh* promoter contains multiple SMAD binding sites (Seki and Hata, 2004). BMPs therefore induce proliferation and stimulate prehypertrophic chondrocytes to express *Ihh*. This in turn can indirectly increase proliferation and delay hypertrophy via PTHrP. Interestingly, exposing cartilage to noggin, a BMP specific antagonist, resulted in reduced *Ihh* expression *in vitro* (Minina et al., 2001). Not only does BMP signalling induce the expression levels of *Ihh*, but IHH also maintains the levels of BMPs, such as BMP2 and BMP4, in a positive feedback

loop (Pathi et al., 1999). This presents a much more complex view to the control of the growth plate as there is significant overlap between the regulatory signalling pathways.

1.3.3.3 Fibroblast growth factors

Canonical and hormone-like FGFs have also been shown to play a crucial role in endochondral ossification (Ornitz and Marie, 2015). There are 22 distinct members of the FGF family that interact with heparin sulphate proteoglycans and activate four cell-surface FGF receptors (Ornitz, 2000, Schlessinger et al., 2000, Ornitz and Itoh, 2001). Binding of ligands induces receptor dimerisation and subsequent autophosphorylation (Furdui et al., 2006). This leads to activation of downstream signalling pathways such as Ras/Mitogen-activated protein kinase (MAPK), Phosphatidylinositol-4,5-bisphosphate 3-kinase (PI3K)/ protein kinase B (Known as AKT), Phospholipase C (PLC) and Protein Kinase C (PKC) as well as stimulating members of the signal transducer and activator of transcription 1 (STAT1)/ cyclin-dependent kinase inhibitor 1 (Also known as $p21^{wad/cip1}$) pathway (Figure 5) (Su et al., 2014).

FGFs are expressed during all stages of development and play an essential role in limb morphogenesis (Martin, 1998). In the earliest stages of limb bud formation fibroblast growth factor receptor (FGFR) 1 and FGFR2 are expressed in the undifferentiated limb bud mesenchyme (Orr-Urtreger et al., 1991, Sheeba et al., 2010). In the condensing limb bud mesenchyme, there is a uniform expression pattern of *FGFR1* whereas *FGFR2* expression overlaps with areas of *SOX9* expression (Orr-Urtreger et al., 1991, Sheeba et al., 2010). As MSCs differentiate into chondrocytes, the expression of *FGFR3* is upregulated along with the expression of *SOX9* and *Col2a1* whereas the expression of *FGFR2* is downregulated (Peters et al., 1992, Peters et al., 1993, Purcell et al., 2009)

In vitro studies indicate an important role for FGFR signalling in the chondrogenic differentiation of MSCs. *In vitro* studies have shown that FGF signalling induces *SOX9* expression in MSCs and primary chondrocytes (Murakami et al., 2000, Shung et al., 2012). Furthermore, FGF signalling via the extracellular signal–regulated kinase (ERK) 1/2 pathway inhibits silencing of the *SOX9* gene by WNT-induced methylation in limb bud mesenchymal chondrogenesis (Kumar and Lassar, 2014).

FGFR signalling is also important in growth plate development. *FGFR2* expression in the resting zone is low, proliferative chondrocytes express *FGFR3* and hypertrophic chondrocytes express high levels of *FGFR1* (Peters et al., 1992, Peters et al., 1993, Delezoide et al., 1998, Hamada et al., 1999, Jacob et al., 2006, Karolak et al., 2015). *In vivo* studies have identified that immature chondrocytes express *Fgfr3*, which promotes proliferation and differentiation (Iwata et al., 2000). However, after the formation of the secondary centre of ossification, *Fgfr3* expression in proliferative chondrocytes inhibits chondrocyte proliferation and maturation via activation of STAT1, ERK1/2 and p38 pathways and the upregulation of the cell cycle inhibitor $p21^{wad/cip1}$ (Figure 5) (Aikawa et al., 2001, Legeai-Mallet et al., 2004). Furthermore, gain-of-function mutations in the *FGFR3* gene have been associated with several forms of skeletal dysplasia including achondroplasia, thanatophoric dysplasia, and hypochondroplasia (Rousseau et al., 1994, Shiang et al., 1994, Foldynova-Trantirkova et al., 2012). It has been postulated that activating mutations exert their effect indirectly by stabilising *Sox9* expression in prehypertrophic chondrocytes via the upregulation of Retinoblastoma-like protein 1 (Murakami et al., 2000, Shung et al., 2012, Kolupaeva et al., 2013, Kurimchak et al., 2013, Zhou et al., 2015). *Fgfr1* is expressed by hypertrophic chondrocytes however the precise reason why is not entirely understood (Jacob et al., 2006). The expression pattern however suggests a potential role for FGFR1 in cell death.

FGFR3 also indirectly regulates chondrocyte maturation via the regulation of PTH1R signaling and IHH, WNT and BMP proteins although the molecular mechanisms by which it acts are not understood. Mouse models with constituitively active FGFR3 signalling displayed a reduction in *Bmp4*, *Ihh* and *Pth1r* expression (Naski et al., 1998, Chen et al., 2001). The role of FGF signalling in the growth plate therefore opposes the role of BMP that signals to upregulate *Ihh* (Seki and Hata, 2004). FGF signalling also activates WNT signalling *in vitro* to inhibit chondrocyte differentiation to hypertrophic chondrocytes (Krejci et al., 2012, Buchtova et al., 2015). These studies and different expression patterns of the FGF receptors in the growth plate suggest that FGF signalling plays an important role in controlling chondrocyte proliferation and maturation.

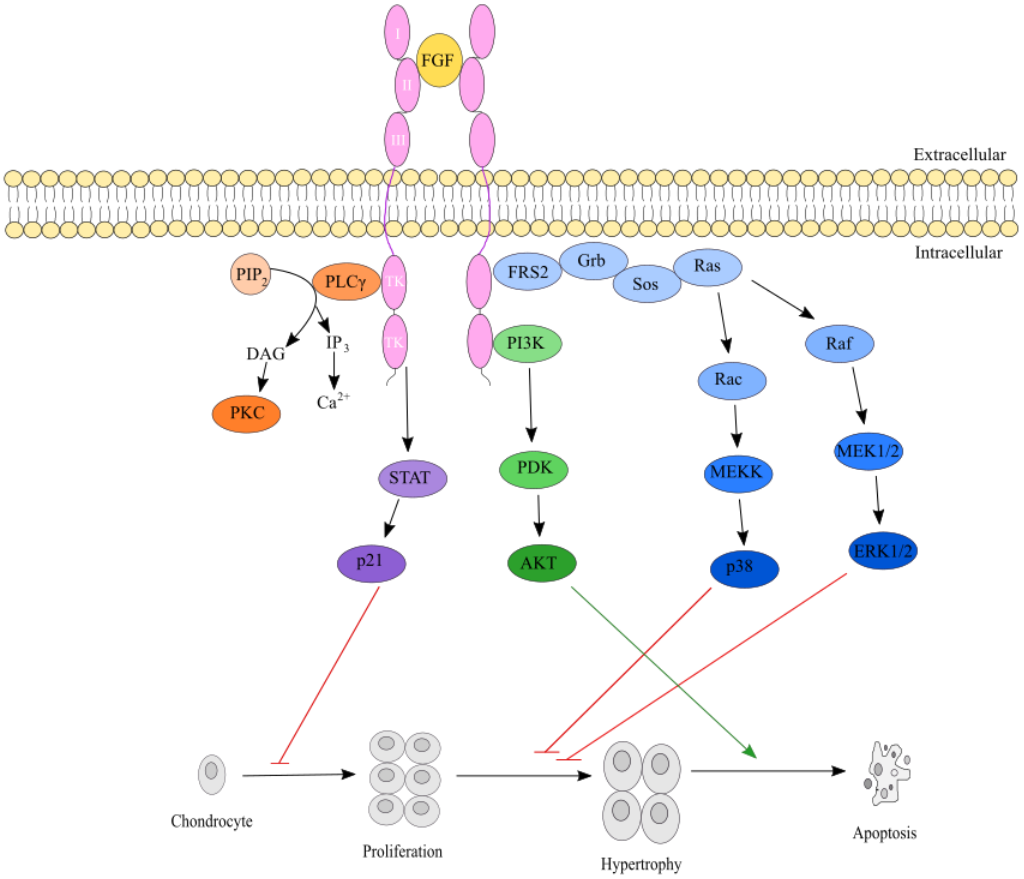

Figure 6. **Fibroblast growth factor (FGF) signalling in endochondral ossification.**

Binding of FGF ligands to their receptors induces receptor dimerisation and subsequent autophosphorylation. This leads to activation of downstream signalling pathways such as MAPK, PI3K/AKT, PLC and PKC as well as the STAT1/p21$^{wad/cip1}$ pathway. FGF signalling plays a crucial role in endochondral ossification regulating every step of chondrocyte differentiation. For FGFs inhibit chondrocyte proliferation and maturation via activation of STAT1, ERK1/2 and p38 pathways and upregulation of the cell cycle inhibitor p21$^{wad/cip1}$, while stimulating apoptosis via the AKT pathway. *Adapted from:* (Su et al., 2014)

1.3.3.4 WNT Proteins

The WNT signalling pathway is important in development and has been implicated in the patterning, development and growth of the skeleton (Geetha-Loganathan et al., 2008, Macsai et al., 2008). In vertebrates the WNT family of proteins consists of 19 secreted lipid-modified glycoproteins that exert their effect via canonical or non-canonical signaling, based on β-catenin dependency, to regulate gene expression (Komiya and Habas, 2008). The canonical β-catenin pathway involves the accumulation of the transcription factor β-catenin and the non-canonical signalling pathway involving the increase of intracellular calcium concentration and activation of PKC due to the activation of PLC (Figure 6) (Sheldahl et al., 2003, Kohn and Moon, 2005, Komiya and Habas, 2008).

The β-catenin dependant pathway is initiated by WNT binding to the receptor complex of frizzled (FRZ)/low density lipoprotein receptor-related protein (LRP) 5/6. This leads to binding of the dishevelled (DSH) and inactivation of the destruction complex comprising axin, adenomatosis polyposis coli (APC), casein kinase 1α (CK1α), protein phosphatase 2A (PP2A) and glycogen synthase kinase 3 (GSK3) that normally functions in targeting β-catenin for ubiquitination and destruction. Downstream interaction and phosphorylation of these destruction complex proteins results in the phosphorylation and subsequent stabilisation of β-catenin. β-catenin then accumulates in the cytoplasm and following translocation to the nucleus, it functions as a co-activator of T-cell factor/lymphoid enhancer factor (TCF/LEF) transcription factors (Cadigan and Waterman, 2012).

The non-canonical pathway involves altering intracellular calcium concentrations to mediate signalling (Kohn and Moon, 2005). Following the binding of FDZ to G-proteins, PLC is activated (Sheldahl et al., 2003). This hydrolyses membrane bound phosphatidylinositol 4,5-bisphosphate (PIP2) generating two messengers diacylglycerol (DAG) and inositol triphosphate (IP3) that activate PKC and stimulate calcium immobilisation from the ER respectively (Takai et al., 1979, Streb et al., 1983). This induces the expression of genes controlling cellular adhesion and migration and represses signalling via canonical β-catenin dependent signalling.

Through the use of animal models it has become clear that during mouse embryonic development the canonical and non canonical WNT signalling pathways

play opposing roles in cartilage development and growth (Usami et al., 2016). During embryogenesis, the overexpression of *WNT5A* and *WNT5B* that signal via the non-canonical calcium pathway induces chondrogenic differentiation (Church et al., 2002). In contrast, the over expression of *WNT1, WNT4* and *WNT8A* that signal via canonical WNT signalling inhibits chondrogenesis (Rudnicki and Brown, 1997, Hartmann and Tabin, 2000, Church et al., 2002). Additionally the constitutive expression of *Ctnnb1* (encoding β-catenin) in developing cartilage results in skeletal deformations and a disrupted growth plate with reduced chondrocyte differentiation marked by a reduction in the levels of SOX9 (Akiyama et al., 2004) Interestingly, the overexpression of *WNT5A* and *WNT5B* had opposing effects on proliferation but delayed the differentiation of chondrocytes (Yang et al., 2003). Taken together these results show that non-canonical WNT signalling via changes in intracellular calcium levels is important during development whereas non- canonical β-catenin dependant pathway is inhibitory.

During postnatal growth, both the canonical and non-canonical WNT signalling pathways are required for regulation of chondrocytes in the growth plate. Of the 19 WNT family members, 6 were found to be expressed in the growth plate (Andrade et al., 2007). Canonical WNT signalling is induced by WNT2, WNT4 and WNT10B whereas non-canonical WNT signalling was induced by WNT5A, WNT5B and WNT11 (Andrade et al., 2007). With the exception of *Wnt2b*, the expression of WNT signalling proteins was highest in the proliferative zone, decreasing in expression in the hypertrophic zone suggesting that WNT signalling regulates chondrocyte proliferation and maturation into hypertrophic chondrocytes (Andrade et al., 2007).

Studies have shown that β-catenin dependent signalling is important for maintenance of cartilage development in the growth plate as inactivation of *Ctnnb1* (encoding β-catenin) in chondrocytes reduces proliferation and delays hypertrophic maturation (Akiyama et al., 2004). Additionally, cartilage-specific *Ctnnb1* knockout mice have a disrupted growth plate and display delayed chondrocyte maturation with reduced proliferation (Chen et al., 2008). Interestingly, these mice showed a delay in angiogenesis marked by a decrease in the expression of *Mmp13* and *Vegf* (Chen et al., 2008). Furthermore, studies have shown that canonical WNT signalling in the growth plate requires the co-receptors LRP5/LRP6 as mice null for both *Lrp5* and *Lrp6* display the same phenotype as *Ctnnb1*-null mice (Joeng et al., 2011).

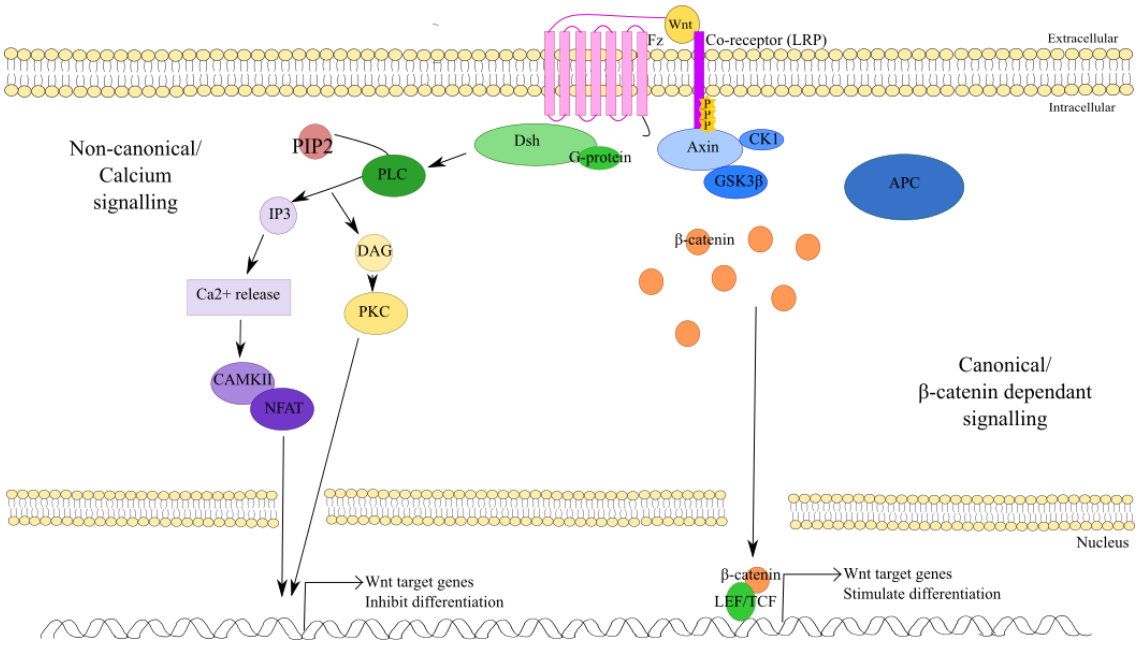

Figure 7. **(Wingless-Type MMTV Integration Site) WNT signalling in endochondral ossification.**

WNT signalling can initiate two distinct signalling pathways, canonical (β-catenin dependant) and non-canonical (β-catenin independant) WNT signalling. Canonical WNT signalling is initiated by WNT binding to the receptor complex of FRZ/LRP5/6. This leads to binding of the DSH, inactivation of the destruction complex comprising axin, APC, CK1α, PP2A and GSK3 and stabilisation of β-catenin. β-catenin then translocates to the nucleus and functions as a co-activator of TCF/LEF transcription factors. In the non-canonical pathway the FRZ receptor stimulates the activation of PLC that hydrolyses PIP2, generating DAG and IP3. DAG then activates PKC and IP3 stimulates calcium mobilisation from the ER resulting in the induction of genes controlling cellular adhesion and migration but repressing signalling via canonical β-catenin dependent signalling.

1.3.3.5 Vascular endothelial growth factor

Endochondral ossification and angiogenesis are tightly connected and critical to skeletal development (Yang et al., 2012). VEGF is a mitogenic factor for vascular endothelial cells and mediates cartilage remodelling and angiogenesis during long bone formation (Dvorak et al., 1995). VEGF exerts its effects on endothelial cells by binding the respective tyrosine kinase receptors Fms related tyrosine kinase 1 (FLT1) (Known as VEGF Receptor 1) and fetal liver kinase 1 (FLK1)/kinase insert domain receptor (KDR) (Known as VEGF Receptor 2) (Koch and Claesson-Welsh, 2012).

The expression of *Vegf* during mouse embryonic development is essential as loosing just one allele embryonic lethal between days 11 and 12 of development due to lack of vasculature (Carmeliet et al., 1996, Ferrara et al., 1996). Moreover, mice null for either of the receptors die between days E8.5 and 9.5. The segmentation for limb bud positioning was also lost in *Vegf*-null mice (Ferrara et al., 1996).

VEGF is also required during postnatal growth. Chondrocytes secrete four VEGF family members, VEGFA, VEGFB, VEGFC and VEGFD as well as the angiogenic stimulators and inhibitors, depending on their differentiation state (Bluteau et al., 2007). For example resting and proliferating chondrocytes express strong anti-angiogenic effects (Moses et al., 1990, Pepper et al., 1991, Moses et al., 1992); whereas terminal hypertrophic chondrocytes stimulated neovascularisation *in vitro* (Brown and McFarland, 1992). Interestingly, it was shown that VEGF signalling plays an important role in chondrocyte survival as hypertrophic chondrocytes do not undergo cell death in the absence of angiogenesis resulting in a thicker growth plate (Gerber et al., 1999).

It has been postulated that the primary trigger for *VEGF* expression and angiogenesis is hypoxia (Lin et al., 2004). *VEGF* expression in the growth plate is high in the avascular, hypoxic hypertrophic zone but low in the resting and proliferative zones (Horner et al., 1999). VEGF expression in the hypertrophic zone triggers vascular invasion into the mineralised cartilage matrix. The invading blood bring osteoblasts that form bone on the mineralised cartilage scaffold (Maes et al., 2010). VEGF has also been found to stimulate vascular endothelial cells to produce cytokines and growth factors to aid in the osteogenic differentiation of MSCs (Shum et al., 2004). VEGF is therefore essential for neovascularisation, coordinating chondrocyte death, cartilage remodeling and bone formation.

1.3.3.6 Transcription factors

Several transcription factors have been found to drive chondrogenesis and maturation in the growth plate (Figure 7) (Kozhemyakina et al., 2015). Early stages of chondrogenesis are controlled by members of the SRY-box family of transcription SOX9, SOX5 and SOX6 (Lefebvre et al., 2001, Akiyama et al., 2002). Chondrocyte maturation and progression through the growth plate is then controlled by RUNX2, myocyte enhancer factor (MEF) 2C/D and forkhead box (FOX) A2/3 (Kim et al., 1999, Arnold et al., 2007, Ionescu et al., 2012).

Research into SOX9 began following the discovery that heterozygous mutations in the *SOX9* gene result in campomelic dysplasia, a severe dwarfing condition affecting endochondral ossification (Foster et al., 1994, Wagner et al., 1994). *In vivo* studies have shown that *Sox9* is expressed in the developing limb bud by MSCs and is involved in the survival and formation of precartilagenous condensations (Akiyama et al., 2002). Within the developing embryo SOX9 is a master regulator of chondrogenesis, stimulating mesenchymal chondrogenic differentiation. Studies have shown that SOX9 physically interacts with RUNX2 driving differentiation to chondrocytic fates and inhibiting osteoblast differentiation (Akiyama et al., 2002, Zhou et al., 2006).

Sox9 is expressed by hypertrophic chondrocytes in the growth plate; however, its exact role remains unclear. Initial studies involving the inactivation of *Sox9* in chondrocytes suggested that SOX9 reduced proliferation (Akiyama et al., 2002). In contrast, recent studies using conditional *Sox9* knockout induced by a doxycycline-inducible *Cre* transgene have shown that SOX9 is necessary for chondrogenesis through to proliferation, delaying prehypertrophy and preventing premature hypertrophy; however, the evidence for its role in hypertrophy is contradicting (Dy et al., 2012). For example, early studies suggested that SOX9 inhibited chondrocyte hypertrophy as *Sox9* expression was reduced in hypertrophic chondrocytes however the protein was found to outlive the gene expression and acts as a transcriptional co-activator along with MEF2C, for cartilage markers such as *Col10a1* (Akiyama et al., 2002, Dy et al., 2012). Interestingly, the embryonic deletion of *Sox9* resulted in premature apoptosis and increased osteoblast differentiation of prehypertrophic chondrocytes suggesting a role for SOX9 in maintaining the chondrocyte lineage (Dy et al., 2012). It was found that SOX9 was able to block osteoblastogenesis by downregulating *Runx2* and suppressing WNT/β-catenin signalling by inducing proteosomal degradation of β-catenin (Akiyama

et al., 2004, Dy et al., 2012). This provides an interesting insight into the terminal fate of hypertrophic chondrocytes suggesting that they do not undergo apoptosis at the vascular front but instead may be able to transdifferentiate into osteoblasts.

SOX9 induces the expression of *SOX5* and *SOX6* (Akiyama et al., 2002). These transcription factors work together as a chondrogenic SOX trio to activate chondrocyte differentiation and maintain survival via the PI3K-AKT pathway (Ikegami et al., 2011). SOX5 and SOX6 do not physically interact with SOX9 but enhance its binging to deoxyribonucleic acid (DNA) therefore increasing its action as a transcriptional activator by an unknown mechanism (Han and Lefebvre, 2008). The SOX trio was also found to target chondrocyte markers such as type II collagen and aggrecan (Bell et al., 1997, Lefebvre et al., 1997, Lefebvre et al., 1998, Han and Lefebvre, 2008).

Sox9 expression is maintained by key signalling pathways in the growth plate such as IHH, BMP and FGF signalling (Hatakeyama et al., 2004). On the other hand, *SOX9* expression is reduced by WNT signalling that results in repressive methylation of CpG sites in the promoter of *SOX9* by DNA methyltransferase 3 (DNMT3) (Kumar and Lassar, 2014). This effect however is counteracted by FGF signalling which phosphorylates DNMT3A via ERK1/2 inhibiting its recruitment to the *SOX9* promoter (Kumar and Lassar, 2014).

The runt-domain gene family of family transcription factors comprises of RUNX1, RUNX2, and RUNX3 are important transcription factors for chondrocyte and osteoblast differentiation (Komori, 2015). RUNX1 is involved in early chondrogenesis following parathyroid hormone stimulation and the activation of protein kinase A in mesenchymal progenitor cells; however, it is redundant in chondrocyte maturation (Wang et al., 2013).

RUNX2, also known as core-binding factor Subunit alpha-1 (CBFA1), is widely known for its ability to stimulate the differentiation of MSCs to mineralising skeletal cells (Komori, 2010). Despite the most well known function of RUNX2 implicated in osteoblastogenesis, it is also a major transcription factor in the cartilage growth plate and is essential for promoting proliferation and terminal hypertrophic chondrocyte differentiation (Chen et al., 2014b). Interestingly, *RUNX2* expression is upregulated by canonical WNT signalling in chicken chondrocyte and therefore could explain how WNT controls hypertrophy (Dong et al., 2006). Studies have also shown that the

transcription factor MEF2C lies upstream of RUNX2 as chondrocyte loss of function downregulates hypertrophy and RUNX2 (Arnold et al., 2007).

RUNX2 is also found to interact with SMAD proteins regulated by BMP stimulation therefore transducing BMP signals to possibly stimulate chondrocyte hypertrophy (Leboy et al., 2001).

Runx2 expression was first identified in murine hypertrophic chondrocytes at E13.5 and correlated with chondrocyte maturation (Inada et al., 1999). During late chondrogenesis, *Runx2* levels were highly upregulated in terminal hypertrophic chondrocytes between E14.5 and E16.5 (Inada et al., 1999). In the growth plate *Runx2* is lowly expressed by resting and hypertrophic cells and upregulated in the hypertrophic zone (Inada et al., 1999).

In vivo transgenic animal studies of *Runx2* highlight the essential role for RUNX2 in in ossification. Both ablation and dominant negative forms of *Runx2* reduced chondrocyte hypertrophy (Inada et al., 1999, Kim et al., 1999, Ueta et al., 2001). *Runx2*-null mice die at birth due to the lack of ossification of endochondral bones including the rib cage that lead to breathing difficulties (Komori et al., 1997). Matrix mineralisation was absent from the majority of the skeleton and bones remained cartilaginous however calcification was observed in the distal limbs (tibia, fibula, radius and ulna). In the distal limbs, the chondrocyte differentiation was mildly impaired. The bones of *Runx2*-null mice had disrupted terminal differentiation at E18.5 marked by a narrow proliferative and enlarged hypertrophic zone. Additionally type X collagen, IHH and BMP6 were present in the distal limbs. However, there was a defect in vascular invasion in the distal limbs of these mice as the matrix was mineralised without vascularisation. This is potentially due to the absence of calmodulin-1, MMP13, bone sialoprotein (IBSP) and osteopontin expression in hypertrophic chondrocytes, suggesting that these genes are directly regulated by RUNX2. In other parts of the skeleton such as the thoracic cage and proximal limbs (femur and humerus), PTH1R, type X collagen, IHH and BMP6 expression was completely absent. Chondrocyte proliferation is controlled in part by IHH and was reduced in the *Runx2*-null mice (Yoshida et al., 2004). Several RUNX2 binding sites were found in the promoter of *Ihh* outlining that RUNX2 is important in regulating its expression (Yoshida et al., 2004). RUNX2 has also been found to bind the promoters of *Vegf*, *Col10a1* and *Mmp13* (Selvamurugan et al., 2000, Zelzer et al., 2001, Drissi et al., 2003). Together these findings outline a maturational blocking of

chondrocytes following *Runx2* ablation.

In contrast, the phenotype of the *Runx2*-null mouse was reversed following the transgenic expression of RUNX2 (Takeda et al., 2001). This ectopic expression of RUNX2 increased premature maturation *in vivo* and *in vitro* inducing hypertrophic markers such as type X collagen expression (Enomoto et al., 2000, Takeda et al., 2001, Ueta et al., 2001). Interestingly, overexpression of dominant negative forms of RUNX2 lead to lethality at birth due to impaired ossification whereas overexpression of RUNX2 also lead to lethality at birth due to the accelerated maturation of chondrocytes and subsequently abnormal ossification (Ueta et al., 2001).

Besides MEF2C and RUNX2, a novel family of transcription factors known as the forkhead box A family was found to stimulate chondrocyte hypertrophy as loss of function mutations in *FoxA2* and *Foxa2*-null chondrocytes lead to a reduction in hypertrophic markers including type X collagen and MMP13 (Ionescu et al., 2012).

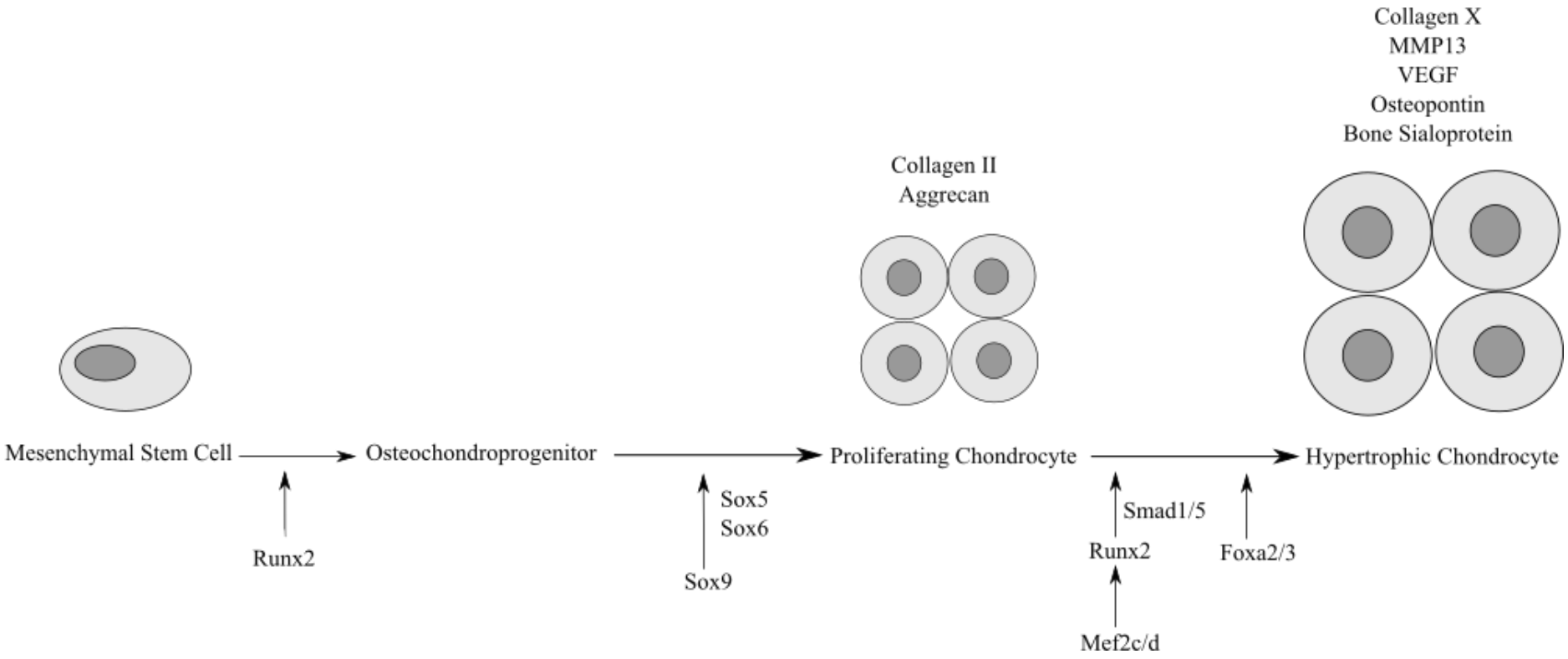

Figure 8. **Differentiation and maturation of chondrocytes.**

The differentiation of MSCs to osteochondroprogenitors is controlled by RUNX2. Early stages of chondrogenesis are then controlled by members of the SRY-box family of transcription SOX9, SOX5 and SOX6. Chondrocyte maturation and progression through the growth plate to hypertrophic chondrocytes is then controlled by RUNX2, MEF2C/D and FOXA2/3. The morphology and the secretory activity change during differentiation, with proliferating chondrocytes expressing type II collagen and aggrecan and hypertrophic chondrocytes expressing type X collagen and genes involved in aiding matrix mineralisation.

1.4 Bone Structure and function

Bone is a dynamic organic matrix comprising of type I collagen that is mineralised by calcium hydroxylapatite crystals providing great tensile strength (Florencio-Silva et al., 2015). Bone functions to provide support and protection for the body whilst supporting haematopoiesis and playing a role in mineral metabolism. There are two major forms of bone; cortical and trabecular bone, that differ morphologically (Clarke, 2008).

Cortical or compact bone, forming the outer shell of bones, is arranged into concentric layers known as lamellae. Each lamellae is formed by densely packed collagen fibrils that lay perpendicular in adjacent lamellae (Eriksen, 1994). The concentric lamellae surround a central canal, known as the haversian canal that is packed with blood vessels that together form the fundamental functional unit of cortical bone called "the osteon" (Eriksen, 1994). Trabecular bone, also known as cancellous bone, forms the inner bone and has a spongy appearance comprising of a porous network of trabeculae formed by mineralised collagen fibrils (Eriksen, 1994).

1.4.1 Cell types of bone

Four cell types are required for the formation, growth and homeostasis of the dynamic bone tissue; osteoprogenitors, osteoblasts, osteocytes and osteoclasts (Florencio-Silva et al., 2015).

1.4.1.1 Osteoblast

Osteoprogenitor or osteogenic cells derive from the mesenchymal lineage and are precursors for osteoblasts. Commitment to differentiation of these cells requires the WNT signalling pathway along with the transcription factors RUNX2 and osterix (OSX) (Ducy et al., 1997, Nakashima et al., 2002, Huang et al., 2007).

Osteoblasts are mononucleated cells that vary in morphology based on their activity. In the active form, the osteoblasts are found lining the bone and are cuboidal in shape. The principle function of osteoblasts is to form and mineralise the extracellular

bone matrix (Caetano-Lopes et al., 2007). First, they secrete an unmineralised organic matrix comprising mainly of type I collagen known as “osteoid”. Following this, the matrix becomes calcified by the deposition of calcium and hydroxyapatite crystals. Calcium and phosphate are sequestered into vesicles budding from osteoblasts forming form hydroxyapatite crystals within the vesicles (Anderson, 2003, Orimo, 2010). These are then transported to the matrix where they are deposited between collagen fibrils. Osteoblasts also secrete alkaline phosphatase (ALP) a basic phosphatase enzyme that hydrolyses inorganic pyrophosphate (PPi), an inhibitor to hydroxyapatite formation, to inorganic phosphate (Pi), a step crucial for mineralisation (Orimo, 2010).

1.4.1.2 Osteocyte

Despite being post-mitotic, osteoblasts are not terminally differentiated cells. When osteoblasts become entrapped in the osteoid matrix they become osteocytes, quiescent fully differentiated osteoblasts (Franz-Odendaal et al., 2006, Bonewald, 2011). Osteocytes lie within the osteoid in lacunae and directly regulate osteoid signaling and mineralisation. They also form a living network of cytoplasmic extensions known as canaliculi that run through the bone (Palumbo et al., 1990). Within their lacunae osteocytes function as integral mechanosensors of bone and regulating bone mass by controlling the actions of osteoblasts and osteoclasts (Bonewald, 2006).

As an osteoblast differentiates into an osteocyte its gene expression pattern changes. For example, the expression of ALP is reduced where as the expression of osteocyte markers such as phosphate regulating endopeptidase homolog, X-linked (PHEX), dentin matrix acidic phosphoprotein 1 (DMP1), matrix extracellular phosphoglycoprotein (MEPE), FGF23 and sclerostin (SOST) are upregulated (Mikuni-Takagaki et al., 1995, Nampei et al., 2004, Poole et al., 2005, Feng et al., 2006, Liu et al., 2006, Bonewald, 2011, Martin et al., 2011). Interestingly, under certain conditions osteocytes are found to also express markers of osteoclasts such as tartrate-resistant acid phosphatase (TRAcP) and cathepsin K in order to aid in perilacunar matrix remodeling (Qing et al., 2012).

1.4.1.3 Osteoclast

Osteoclasts are multinucleated cells that belong to the monocyte family and are derived from hematopoietic cells (Boyle et al., 2003). These multinucleated osteoclasts are found lining bone surfaces and function to degrade the bone matrix and immobilise calcium.

The multistep process of bone resorption begins with the proliferation of mononuclear osteoclast precursors. Osteoclast precursors then fuse and form large multinuclear mature osteoclasts capable of resorbing bone. Studies using competitive ligands to integrins have outlined that α2β3 integrin is necessary for the recognition of bone by the osteoclasts (Engleman et al., 1997). Here, multinucleated osteoclasts which are highly polarised, can rearrange their cytoskeleton to form a sealing zone and a ruffled border on the basal side of the cell resorbing bone on the basal area of the cell (Figure 9) (Vaananen and Horton, 1995).

Groups of podosomes rich in F-actin along with additional proteins such as vinculin, talin and α-actinin form the sealing zone, the site of attachment between the osteoclast and the matrix (Marchisio et al., 1984, Lakkakorpi et al., 1989). This creates a segregated resorption lacuna or howship lacuna that lies under a ruffled border.

Acidification of the resorption lacuna and demineralisation of the bone matrix precedes matrix degradation by lysosomal enzymes (Teitelbaum, 2000). Acidification of the howship lacuna to a pH of ~4.5 results from proton release from the vacuolar-type H^+-adenylpyrophosphatase (V-H^+-ATPase) and the $2Cl^-/H^+$ antiporter (Silver et al., 1988, Blair et al., 1989, Mattsson et al., 1994, Schlesinger et al., 1997). Following this acidification, the osteoclast secretes several hydrolases, including cathepsin K and TRAcP to degrade the demineralised matrix (Burstone, 1959, Gowen et al., 1999).

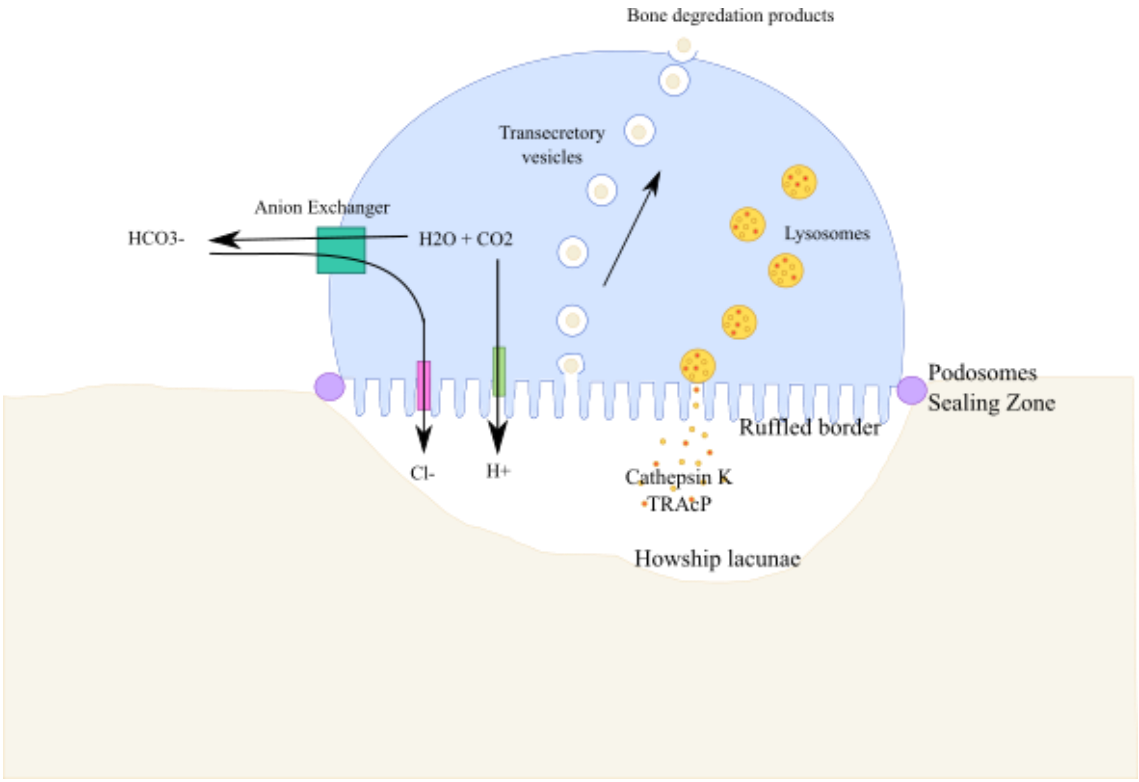

Figure 9. **Bone resorption by osteoclasts.**

Mature multinucleated osteoclasts are highly polarised and can rearrange their cytoskeleton to form a sealing zone and a ruffled border on the basal side of the cell, creating an acidic lacuna in order to resorb bone. Bone resorption occurs in two phases; acidification of the resorption lacuna, achieved from proton release, and demineralisation of the bone matrix followed by matrix degradation by lysosomal enzymes including cathepsin K and TRAcP. The products from bone degradation, such as calcium and collagens, are endocytosed by the resorbing osteoclast and released for reuse on the opposite side to bone resorption.

1.5 Differentiation and maturation of the osteoblast lineage

In osteoblastogenesis, mature osteoblasts are preceeded by an intermediate cell type of proliferative pre-osteoblasts and followed by terminally differentiated osteoblasts known as osteocytes. Osteoblastogenesis occurs in three distinct stages including proliferation, matrix maturation and mineralisation (Rutkovskiy et al., 2016). Each stage of osteoblast differentiation is characterised by distinctive gene expression of sequentially expressed genes (Figure 10) (Huang et al., 2007). For example, following MSC commitment to the osteoblast lineage, the differentiation of osteochondroprogenitors to preosteoblasts and preosteoblasts to mature osteoblasts is controlled by the action of three transcription factors, RUNX2, OSX and β-catenin. Proliferative preosteoblasts express RUNX2 and type I collagen as well as markers of osteoblast differentiation such as bone sialoprotein (IBSP), osteonectin, osteopontin, ALP and OSX. Mature osteoblasts are then found to express type I collagen, IBSP, osteonectin, osteopontin, ALP and osteocalcin.

Studies have shown that marker genes are differentially expressed at different stages in mature osteoblasts. In general; ALP, IBSP and type I collagen are highly expressed in early maturation whereas osteocalcin appears late in maturation with the onset of mineralisation and this differentiation is inhibited by the action of RUNX2, OSX and β-catenin (Roach, 1994, Huang et al., 2007). Additionally, osteocalcin is the second most abundant protein in bone after type I collagen and studies have shown that with the expression of osteocalcin, the levels of ALP expression fall (Gaur et al., 2005).

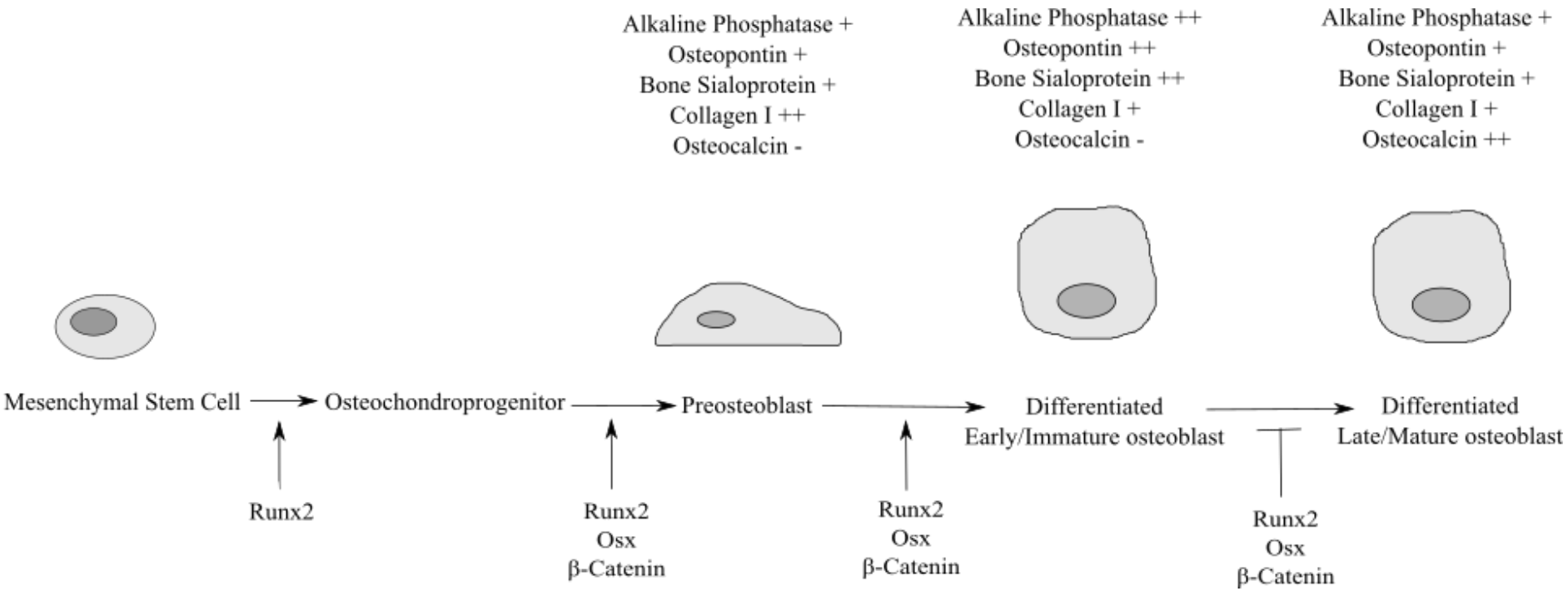

Figure 10. **Differentiation and maturation of the osteoblast lineage.**

Each stage of osteoblast differentiation is characterised by distinctive gene expression of sequentially expressed genes. Proliferative preosteoblasts express RUNX2 and type I collagen I as well as markers of osteoblast differentiation such as IBSP, osteonectin, osteopontin, ALP and osterix. The differentiation of preosteoblasts to early-differentiated osteoblasts is controlled by the combined action of Runx2, OSX and β-catenin. In general ALP, IBSP and type I collagen I are high in early maturation whereas osteocalcin appears late in maturation with mineralisation.

1.5.1 Regulation of osteoblast differentiation and maturation

The commitment and differentiation of osteoblasts is tightly controlled by a series of transcription factors that act together to ensure correct differentiation (Marie, 2003, Komori, 2006, Yavropoulou and Yovos, 2007, Canalis, 2008, Chen et al., 2012). Several recent publications have explored the integration of signalling pathways such as BMP, WNT, notch, hedgehog, and fibroblast growth factors in MSC osteoblast differentiation.

1.5.1.1 Transcription factors

In osteoblastogenesis, transcription factors RUNX2 and OSX are required for the commitment and differentiation of MSCs to osteoblasts and terminally differentiated osteocytes (Ducy et al., 1997, Nakashima et al., 2002, Huang et al., 2007). RUNX2 plays a central role in the commitment of MSCs to cells of the osteoblast lineage as *Runx2*-null mice display a complete absence of osteoblasts and subsequently a lack of bone formation (Komori et al., 1997, Otto et al., 1997). Interestingly, *Runx2*-null calvarial cells were found to spontaneously differentiate into adipocytes and chondrocytes *in vitro* (Kobayashi et al., 2000).

Preosteoblasts and immature osteoblasts express *Runx2*. RUNX2 binding sites have been identified in the promoters of *Col10a1*, *Spp1* (Encoding osteopontin), *Ibsp* and *Bglap* (Encoding osteocalcin) and *in vitro* studies have shown that RUNX2 induced the expression of these genes encoding bone matrix proteins (Harada et al., 1999, Javed et al., 2001, Kern et al., 2001, Komori, 2002). Conversely, during osteoblast maturation RUNX2 is downregulated. This identifies RUNX2 as the initial transcription factor directing cells to the osteoblast lineage and maintaining immature osteoblasts however RUNX2 must be downregulated for mature osteoblast differentiation. Confirming this, overexpression of RUNX2 in immature osteoblasts of transgenic mice in which *Runx2* expression was under the control of the 2.3kb *Col1a1* promoter resulted in inhibited osteoblast maturation (Liu et al., 2001). Furthermore, *Spp1* expression was increased whereas osteocalcin, a marker of mature osteoblasts was decreased. Moreover, there was a significant decrease in the number osteocytes. On the other hand, overexpression of the dominant negative form of *Runx2* under the same promoter resulted in increased mineralisation and resulted in trabecular bone with the appearance of mature compact

cortical bone (Maruyama et al., 2007). Therefore, RUNX2 drives the differentiation of MSC to osteoblast and regulates bone maturity via controlling the maturational stage of osteoblasts.

Osterix, also known as transcription factor SP7, belongs to the SP family transcription factors and plays a crucial role for the differentiation of preosteoblasts (Zhang, 2010). Like with *Runx2*-null mice, *Sp7*-null mice display a complete lack of endochondral and intramembranous ossification due to the diminished differentiation of osteoblasts (Nakashima et al., 2002).

Osterix is down stream of RUNX2 as RUNX2 is expressed in MSCs of *Sp7*-null mice, however Osterix is absent from MSCs of *Runx2*-null mice (Nakashima et al., 2002). Despite the expression of RUNX2, *Sp7*-null embryos do not express osteoblast markers such as type I collagen, osteonectin, osteopontin, IBSP and osteocalcin (Nakashima et al., 2002). As *Sp7*-null cells are arrested in differentiation, this suggests that Osterix induces *Runx2* expressing preosteoblasts to differentiate into mature functional osteoblasts and so is an anabolic regulator of bone. Despite these findings, overexpression of *Sp7* under the 2.3kb *Col1a1* promoter was found to result in osteopenia due to inhibition of osteoblast differentiation and an increase in the number of immature osteoblasts (Yoshida et al., 2012). This suggests that Osterix expression must be tightly controlled to promote correct differentiation of osteoblasts and bone formation.

1.5.1.2 WNT Proteins

WNT signalling has been shown to play a major role in controlling skeletal development and homeostasis regulating the differentiation and function of MSCs, chondrocytes, osteoblasts and osteoclasts. Therefore affecting bone formation and bone resorption.

WNT signals through β-catenin dependant and independent pathways (Figure 6). During skeletal development WNT/β-catenin signalling has been linked to osteoblastogenesis (Yavropoulou and Yovos, 2007). WNT6, WNT10A and WNT10B signal via β-catenin to stimulate osteoblastogenesis and promote bone formation (Cawthorn et al., 2012a). The conditional deletion of *β-catenin* results in reduced osteoblast differentiation and interestingly increased chondrocyte differentiation

therefore suggesting that WNT/β-catenin signalling inhibits chondrogenesis and stimulates osteoblastogenesis. (Day et al., 2005, Hill et al., 2005). Additionally, the overexpression of WNT signalling in osteoprogenitors mesenchymal cells was found to block chondrogenesis *in vivo* and *in vitro* (Rudnicki and Brown, 1997). WNT signalling through non canonical pathways also plays a role in determining the fate of MSCs as WNT3A and WNT7B signalling was found to stimulate osteoblastogenesis via PKC, independent of β-catenin (Tu et al., 2007).

WNT signalling in osteoblast differentiation is complex; as despite stimulating the osteoblastogenic differentiation of MSCs, it blocks the terminal differentiation of cells of the osteoblast lineage to mature osteoblasts (Kahler and Westendorf, 2003, Kahler et al., 2006, Kahler et al., 2008). Additionally, β-catenin signalling was found to inhibit the transcriptional activation of the *Osteocalcin* promoter by RUNX2 (Kahler and Westendorf, 2003). Further to this, WNT signalling plays an important role in controlling the function of mature osteoblasts. Studies show that deletion of *Ctnnb1* in mature osteoblasts results in increased osteoclastogenesis and low bone mass whereas constitutive activation of *Ctnnb1* results in high bone mass due to a reduction in osteoclasts (Glass et al., 2005, Holmen et al., 2005). Osteoprotegerin (OPG), an inhibitor of osteoclastogenesis, has been shown to be a direct target of β-catenin. Deletion of *Ctnnb1* therefore results in a reduction in *OPG* expression and interestingly results in higher levels of Receptor activator of nuclear factor kappa-light-chain-enhancer of activated B cells (NFκB) ligand (RANKL), an osteoclastogenic stimulator (Glass et al., 2005, Holmen et al., 2005).

WNT signalling via the canonical β-catenin dependant pathway is essential for osteoblast differentiation and promoting osteoblast function and bone formation as shown by several *in vivo* studies. WNT signalling is transduced by the LRP5/6 co-receptor both of which are expressed by osteoblasts. Transgenic mice lacking the LRP5 receptor had reduced bone mass resulting from reduced osteoblast proliferation. (Kato et al., 2002). Furthermore, missense mutations in *Lrp6* result in delayed ossification and osteoporosis (Kokubu et al., 2004). Conversely, gain of function mutations in *Lrp5* results in a high bone density due to increased bone formation (Little et al., 2002, Babij et al., 2003). Furthermore, transgenic mice heterozygous for dickkopf WNT signalling pathway inhibitor 1 (DKK1), a modulator of LRP5 activity, resulted in mice with a higher bone mass phenotype whereas overexpression of *Dkk1* in osteoblasts resulted in

osteopenia due to diminished osteoblast numbers and decreased bone formation (Li et al., 2006, Morvan et al., 2006).

There is significant crosstalk between WNT signalling and other anabolic pathways of bone. For example, WNT signalling induces the expression of *Bmp2* mediated through the TCF/LEF response elements in the promoter of *Bmp2* (Zhang et al., 2013c). Additionally the ability of BMP9 to induce the expression of *Alpl* and *Osteocalcin* was increased in the presence of WNT3A (Tang et al., 2009a). Furthermore the responsiveness of osteoblasts to BMP2 was reduced following *Ctnnb1* deletion resulting in impaired osteoblast differentiation and proliferation (Zhang et al., 2009).

Interestingly, several factors including PTH and FGF stimulate osteoblast differentiation and function via canonical WNT/β-catenin signaling (Fei et al., 2011, Tian et al., 2011). Studies show that in *Fgf2*-null mice, the expression of WNT genes such as *Wnt10b, Lrp6* and *β-catenin* are reduced suggesting that the anabolic effect of FGF2 signalling in osteoblast differentiation and function is modulated by the WNT pathway (Fei et al., 2011). Taken together, these results show that WNT signalling is tightly coupled to other signalling pathways and is essential in controlling osteoblast differentiation and function.

1.5.1.3 Fibroblast growth factors

Fibroblast growth factors play a central role in controlling chondrogenesis during endochondral ossification and play a central role in differentiation and maturation of cells of the osteoblast lineage (Marie, 2003). FGF signalling activates the MAPK, PI3K/AKT, PLC/PKC and STAT1/p21$^{wad/cip1}$ pathways and regulates proliferation, differentiation and apoptosis of cells of the osteoblast lineage (Ornitz and Marie, 2015).

The effects of FGF signalling in osteoblastogenesis are complex and depend on the type of ligand/receptor expressed and the stage of cell maturation. *Fgfr* expression and function differs at different stages of differentiation. FGFR signalling is downregulated by receptor internalisation, ubiquitination by CBL proto-oncogene, E3 ubiquitin protein ligase (c-CBL) and proteosomal degradation (Lemmon and Schlessinger, 2010). To further support the role for FGFR signalling in stimulating osteoblastogenesis, ubiqutination of FGFR2 by c-CBL reduces osteoblast differentiation

whereas inhibition of c-CBL stimulates osteoblastogenesis (Dufour et al., 2008, Severe et al., 2013).

FGFR1 is an example of a receptor that controls different stages of development (Jacob et al., 2006). In osteoprogenitors cells, conditional inactivation of FGFR1 stimulated proliferation while differentiation and mineralisation was delayed. However, in mature osteoblasts the lack of *Fgfr1* resulted in an increased bone mass and accelerated mineralisation. These data suggest that FGFR1 inhibits MSC proliferation, promotes osteoblast differentiation while also inhibiting mineralisation.

In MSCs FGFR2 signalling was found to maintain a high population of self-renewing cells (Di Maggio et al., 2012). Studies show that FGF signalling via the FGFR2 initiates stimulated proliferation therefore expanding the osteoblast precursor pool and also promoted osteogenic differentiation of MSCs via ERK1/2 (Choi et al., 2008, Miraoui et al., 2009). Two important FGF ligands implicated in the positive regulation of osteogenesis are FGF2 and FGF18. *In vivo* studies show that *Fgf2*-null mice and mice lacking *Fgf18* are characterised by reduced bone formation and a reduction in osteoblast differentiation (Montero et al., 2000, Liu et al., 2002, Ohbayashi et al., 2002, Xiao et al., 2010). Not only does FGF signalling promote differentiation in osteoblast precursors, but it also promotes survival. FGF2 was found to promote survival signalling via the PI3K/AKT signalling pathway (Debiais et al., 1998). Furthermore, binding of FGF2 to the FGFR1 receptor causes a signalling cascade resulting in alteration of the B-cell lymphoma 2 (BCL2)/ BCL2-like protein 4 (BAX) ratio promoting osteoblast survival (Debiais et al., 1998).

In osteoblasts, FGF signalling via ERK1/2 and PKC results in the upregulation of osterix and promotes the stabilisation of RUNX2 (Kim et al., 2003, Park et al., 2010, Niger et al., 2013, Felber et al., 2015). This leads to upregulation of osteoblast specific genes, such as osteocalcin (Xiao et al., 2002). Unlike promoting survival in osteoblast progenitors, FGF signalling via the FGFR2 in differentiated osteoblasts induces apoptosis (Mansukhani et al., 2000).

There is also crosstalk between the pathways controlling osteoblastogenesis. For example FGF interacts with other pathways including BMP and WNT signalling to control osteoblast differentiation. FGF2 was found to stimulate *Bmp2* expression *in vitro* via promoting the nuclear localisation of phosphorylated SMAD1/5/6 and RUNX2 (Choi et al., 2005, Agas et al., 2013). FGFs including FGF2 and FGF18, were also

found to inhibit the expression of the BMP antagonist *Noggin* (Fakhry et al., 2005, Reinhold et al., 2004). Consistently, *Fgf*-null mice show reduced expression of *Bmp2* (Naganawa et al., 2008). *Fgf*-null mice also display a reduction in the expression of WNT genes (Fei et al., 2011). Interestingly, in *Fgf*-null mice, exogenous FGF2 rescues osteoblast differentiation partly by modulating the canonical WNT/β-catenin signalling pathway as addition of FGF signalling resulted in nuclear accumulation of β-catenin.

Overall, the studies to date have outlined a central role of FGF signalling in osteoblastogenesis in which multiple pathways are activated to modulate all steps of osteoblast differentiation.

1.5.1.4 Transforming growth factor β (TGFβ) and bone morphogenic proteins

The TGFβ cytokine superfamily consists of over 40 members including TGFβ and BMPs. Following binding of a TGFβ cytokine family member, type I and type II serine/threonine receptor are found to heterodimerise and initiate a signalling cascade through the phosphorylation of SMAD proteins (canonical) or activation of the ERK-MARK pathway (non-canonical) to initiate transcription of genes controlling differentiation, maturation and growth.

Canonical and non-canonical TGFβ signalling has been shown to play an important role in endochondral and intramembranous ossification as conditional knockout mouse models of genes involved in *Tgfβ* signalling have disrupted bones and impaired osteogenic cell proliferation and differentiation (Baffi et al., 2004, Oka et al., 2007, Matsunobu et al., 2009, Greenblatt et al., 2010, Gunnell et al., 2010, Iwata et al., 2010, Hiramatsu et al., 2011). TGFβ is one of the most abundant cytokines in the bone matrix and has been shown to regulate the differentiation and activity of osteoblasts. TGFβ was found to promote the recruitment of MSCs to sites of bone formation and stimulates the proliferation of osteoprogenitors (Tang et al., 2009b, Jian et al., 2006). It also plays a role in early osteoblastogenesis due to its cooperation with WNT signalling (Zhou, 2011). Despite inducing early osteoblast differentiation, TGFβ has been shown to inhibiting terminal osteoblast differentiation by repressing RUNX2 via the activation of SMAD3 and results in a decrease in *Osteocalcin* expression (Alliston et al., 2001).

BMP signalling has long been implicated in embryogenesis and the development of the skeletal system, controlling both chondrogenesis and osteogenesis

(Bandyopadhyay et al., 2006). Interestingly, there is a strong connection between TGFβ and BMP signalling in osteogenesis as studies show that TGFβ1 enhances BMP2-stimulated osteoblast differentiation and bone formation (Tachi et al., 2011).

In vivo studies show that BMP ligands exert their osteogenic effects by signalling through 4 BMP receptors, BMPR1A, BMPR1B, type II BMP receptor (BMP2R) and type I activin receptor (ACVR1). Activating mutations in *Acvr1* have been linked to Fibrodysplasia ossificans progressiva (FOP) a disease characterised by extra-skeletal bone formation (Shore et al., 2006). Mechanistic studies show that constitutive activation of the ACVR1 receptor resulted in increased sensitivity of MSCs to BMP (van Dinther et al., 2010). This subsequently resulted in ectopic osteoblastogenesis and bone formation. Not only does BMP signalling play a role in osteoblastogenesis but it also regulates osteoblast function. In mice expressing the dominant negative form of BMP2R, skeletal development was delayed and resulted in decreased bone formation due to a reduction in SMAD1/5/8 phosphorylation (Yang et al., 2010). Additionally, the osteoblast-specific deletion of *Bmpr1a* lead to reduced mineralisation due to impaired osteoblast function (Mishina et al., 2004). Furthermore, overexpression of the BMP inhibitor *Noggin* resulted in reduced osteoblast differentiation and osteopenia *in vivo* (Devlin et al., 2003).

There are 14 BMP ligands that induce signalling via SMAD and non-SMAD pathways inducing the expression of genes involved in osteoblastogenesis and bone formation. BMP signalling leads to the activation of SMAD1/5/8 that form a complex with SMAD4 resulting in RUNX2 transcription (Lee et al., 2002). BMP/SMAD signalling has been found to play an essential role in osteoblast differentiation and postnatal bone formation. SMAD1 plays a central role in coordinating the osteogenic effects of BMPs as shown by osteoblast-specific *Smad1* knockout mice. The osteoblast specific ablation of *Smad1* resulted in an osteopenic phenotype with reduced osteoblast differentiation and proliferation (Wang et al., 2011). Additionally deletion of *Smad4* in pre-osteoblasts results in impaired differentiation and mineralisation by osteoblasts (Salazar et al., 2013). BMP ligands also induce signalling via non-SMAD pathways, signalling also via p38 MAPK (Rigueur et al., 2015). It has been shown that signalling via the non-SMAD dependant pathway leads to the phosphorylation of RUNX2 and Osterix, enhancing their binding potential to bind promoters of osteoblast-specific genes thus inducing osteoblast differentiation (Ortuno et al., 2010, Ge et al., 2012).

Of the 14 BMP ligands, studies have shown that 6 ligands, BMP2, BMP4, BMP5, BMP6, BMP7 and BMP9 induce bone formation (Sheldahl et al., 2003). Short-term stimulation of MSCs with BMP2 resulted in osteogenesis and bone formation (Noel et al., 2004). MSC-specific ablation of both *Bmp2* and *Bmp4* severely affected bone (Bandyopadhyay et al., 2006). Interestingly, this effect was not seen in *Bmp2/Bmp7* double null mice suggesting that BMP2 exerts its effects in coordination with BMP4 to stimulate osteoblast differentiation and osteogenesis (Bandyopadhyay et al., 2006). BMP2 was found to induce osteoblastogenesis *in vitro* by upregulating Osterix via RUNX2 dependant and independent mechanisms (Matsubara et al., 2008). In addition, BMP2 treatment lead to an upregulation of alkaline phosphatase and osteocalcin via RUNX2-dependant activating transcription factor (ATF) 6 activation (Huang et al., 2010, Jang et al., 2012). Taken together, these studies imply that BMP signalling is important for osteoblastogenesis and bone formation. Conversely, the non-canonical BMP, BMP3, opposes the anabolic functions of the other BMP family members (Kokabu et al., 2012). Through the use of transgenic mouse models it was identified that BMP3 is expressed by osteoblasts and osteocytes and functions to negatively regulate bone formation. For example, the ablation of *Bmp3* results in increased bone mass whereas overexpression resulted in impaired skeletal mineralisation (Daluiski et al., 2001, Gamer et al., 2009, Kokabu et al., 2012). BMP3 mediates its effects via SMAD2/3 antagonising the osteogenic activity of SMAD1/5/8 (Matsubara et al., 2008).

Osteoblast differentiation is enhanced with synergistic BMP and WNT signalling (Rawadi et al., 2003, Rodriguez-Carballo et al., 2011). *In vitro* studies showed that Smad proteins form a complex with TCF/LEF/β-catenin and induce high levels of *Runx2* expression (Rodriguez-Carballo et al., 2011). Interestingly BMP signalling plays a dual role in modulating WNT signalling. BMPs promote bone formation, but also negatively regulate bone mass, signalling via BMP1RA to upregulate the WNT inhibitors DKK1 and SOST (Kamiya et al., 2010). Furthermore, SMAD proteins were found to bind competitively to β-catenin and inhibit its interaction with the TCF/LEF transcription complex (Salazar et al., 2013). BMP signalling also stimulates WNT signalling by inducing the expression of *Lrp5* (Zhang et al., 2009).

BMP can also regulate FGF signalling during osteoblastogenesis. The cooperation between these two factors is essential for osteoblast differentiation; as in the absence of FGF2, the osteogenic effects of BMP2 is inhibited (Naganawa et al., 2008).

Furthermore FGFs induce *Bmp2* expression and enhances the nuclear localisation of RUNX2 and phosphorylated SMAD1/5/8 in BMP2 signalling (Naganawa et al., 2008, Agas et al., 2013). Interestingly BMPs and FGFs also play opposing roles in different stages of osteoblast differentiation. For example, BMP2 stimulates mineralisation whereas FGF2 inhibits mineralisation by osteoblasts (Hughes-Fulford and Li, 2011).

BMP ligands therefore act in all stages of endochondral ossification, controlling both chondrocyte and osteoblast differentiation and maturation, acting via both SMAD dependant and non-SMAD dependant signalling pathways to stimulate the expression of key osteoblast transcription factors inducing osteoblastogenesis and promoting bone formation.

1.5.1.5 Notch

Notch signalling between neighbouring cells has long been implicated in skeletal development controlling cell fate during embryogenesis and later in postnatal life (Artavanis-Tsakonas et al., 1999, Chiba, 2006).

Notch receptors are evolutionarily conserved single pass T1 receptors. In mammals there are four notch receptors that are activated by ligands and perform unique functions. The canonical mammalian notch ligands are characterised by a Delta/Serrate/lag-2 (DSL) domain and fall under two categories, either Delta–like (DLL1, DLL3, DLL4) or Serrate (Jagged)-like (Jagged 1 and 2) (Kopan and Ilagan, 2009). The canonical ligands that bind Notch receptors are single pass transmembrane proteins that stimulate Notch signalling via cell-cell interactions. Ligands can also interact autonomously inhibiting Notch signalling.

Following trans-interactions with ligands on neighbouring cells, the Notch receptor is activated and following a series of proteolytic cleavage events the intracellular domain is released to function as a Notch signal transducer (Figure 11) (Schroeter et al., 1998). The proteolysis of Notch is initiated by cleavage of the extracellular ligand-binding domain by a disintegrin and metalloproteinase (ADAM) followed by an intramembrane cleavage by γ-secretase complex containing either presenilin (Ps)-1 or presenilin-2 as the catalytic subunit releasing the Notch intracellular domain (NCID). The NCID then translocated to the nucleus where in complex with the CSL DNA binding protein (CBF1 in humans, suppressor of hairless in

drosophila, LAG in *Caenorhabditis elegans*; also called recombining binding protein suppressor of hairless protein (RBPjK) in mice) and co-activators such as mastermind-like (MAML) proteins it induces the expression of Notch target genes, including hairy and enhancer of split-1 (HES) and Hairy/enhancer-of-split related with YRPW motif protein 1 (HEY) (Lin et al., 2002, Wu et al., 2002, Iso et al., 2003, Kopan and Ilagan, 2009).

In vivo studies have outlined a role for Notch signalling in skeletal development as skeletal defects were observed in *Dll3* and *Ps1* global null mice (Wong et al., 1997b, Dunwoodie et al., 2002). Mesenchymal-specific *Notch1* and *Notch2* gene knockout results in a skeletal phenotype in adolescent mice characterised by an accumulation of cancellous bone with in the diaphysis cavity at 8 weeks old and a reduction in mesenchymal progenitors (Hilton et al., 2008). With age, these mice developed osteopenia as the mesenchymal progenitor pool is depleted. Studies showed that Notch signalling mediated by RBPjK suppresses osteoblast differentiation through inhibition of RUNX2 activity and suppression of *Nuclear factor of activated T-cells (NFatc1)* transcription (Tu et al., 2012). HEY1, induced by Notch signalling, was found to antagonise RUNX2 transcriptional activity upon direct physical interaction as identified by co-Immunoprecipitation studies (Zamurovic et al., 2004, Hilton et al., 2008). This outlines an inhibitory role of Notch signalling in early osteoblastogenesis, suppressing osteoblast maturation and function.

As with RUNX2, BMP and WNT signalling is also mediated by Notch signalling in osteogenesis. Overexpression of the intracellular domain of the Notch receptor abolished the positive effects of BMP2 and WNT3A signalling in osteoblast function as outlined by a reduction in ALP activity (Deregowski et al., 2006). As *Alp* is not a target gene of BMP2 signalling, it is therefore postulated that it exerts its downstream effects via WNT signalling. Furthermore, the overexpression of the Notch NCID resulted in a decrease in β-catenin levels however did not alter the phosphorylation of SMAD proteins downstream of BMP signalling (Deregowski et al., 2006).

Interestingly, Notch signalling in cells of the osteoblast lineage also regulates bone homeostasis. Notch induces the expression of *Opg* and suppresses osteoclast formation (Yamada et al., 2003, Engin et al., 2008). In line with this, the overexpression of *Notch* in committed osteoblasts resulted in a significant increase in trabecular bone

due to a reduction in osteoclast number and subsequently less bone resorption (Canalis et al., 2013).

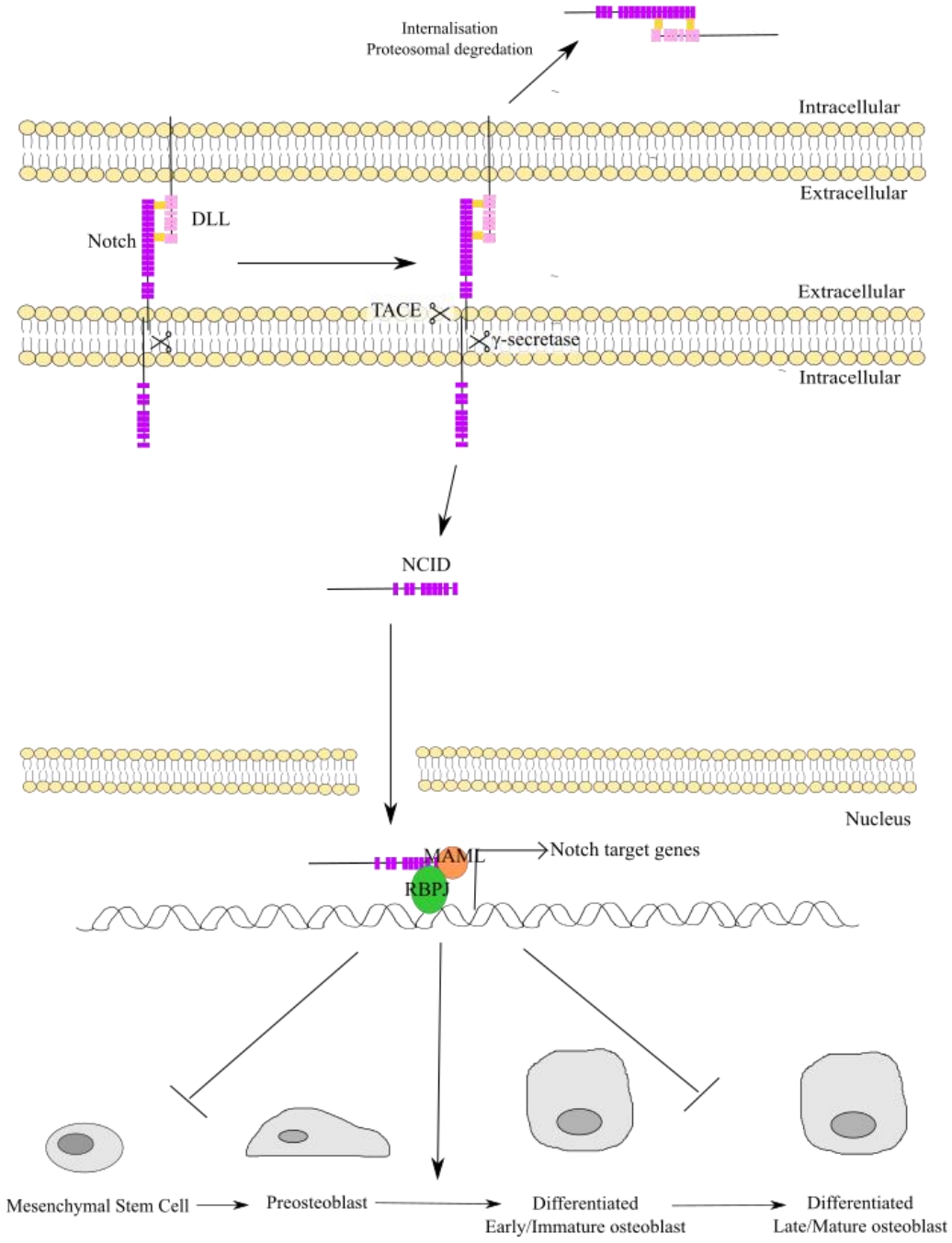

Figure 11. **Notch signalling in osteoblast differentiation and maturation.**

The Notch receptor binds ligands such as DLL on neighbouring cells and is activated by a series of cleavage by the metalloproteinase tumour necrosis factor-alpha converting enzyme (TACE). The NICD is then released to function as a Notch signal transducer, forming a complex with DNA binding proteins to induce the expression of Notch target genes. Notch1 plays a central role in osteoblast differentiation and maturation as Notch1 signalling in early osteoblastogenesis suppresses osteoblast maturation and function.

1.6 Bone homeostasis

Bone is a dynamic connective tissue that is remodelled throughout life to maintain skeletal structure and function. Bone remodelling is a highly controlled process carried out by a temporary functional anatomic structure known as the basic multicellular unit (Sims and Martin, 2015). Bone turnover requires the synchronised action of osteoclasts and osteoblasts that remodel bone in response to mechanical stress and hormones, serving to repair micro-damage and skeletal integrity as well as maintaining calcium homeostasis.

The bone remodelling process consists of three distinct phases (Hadjidakis and Androulakis, 2006). First, it has been postulated that osteocytes sense mechanical loading and micro-damage and initiate bone remodelling upon recruitment of osteoclast precursors to the site of bone turnover by osteoblast expression of chemokines such as monocyte chemotactic protein 1 (MCP1) where they differentiate into mature resorbing osteoclasts (Li et al., 2007). Stage 1 begins with the resorption of bone by the mature osteoclasts (Stage 1: Resorption). Concurrent with resorption, MSCs and osteoprogenitors are recruited to the site of bone remodelling where they differentiate into osteoblasts (Stage 2: Reversal). Here they secrete an osteoid matrix that becomes mineralised (Stage 3: Formation).

Bone remodelling must be tightly controlled as disruption to this fundamental process results in bone disorders such as osteoporosis (Feng and McDonald, 2011). It is controlled by a series of local and systemic factors that control osteoblast and osteoclast function including growth factors released from the bone matrix such as TGFβ, insulin growth factor 1 (IGF1) and BMP during the resorption phase (Hadjidakis and Androulakis, 2006). Most importantly, bone homeostasis is controlled by the crosstalk between bone cells with the RANKL/OPG pathway being the most researched to date (Boyce and Xing, 2007). The RANKL/OPG axis is critical for bone homeostasis and most hormones and cytokines that influence bone homeostasis act through regulating *Tnfsf11* (encoding RANKL) and *Tnfsf11b* (encoding OPG) expression (Figure 12) (Boyce and Xing, 2007).

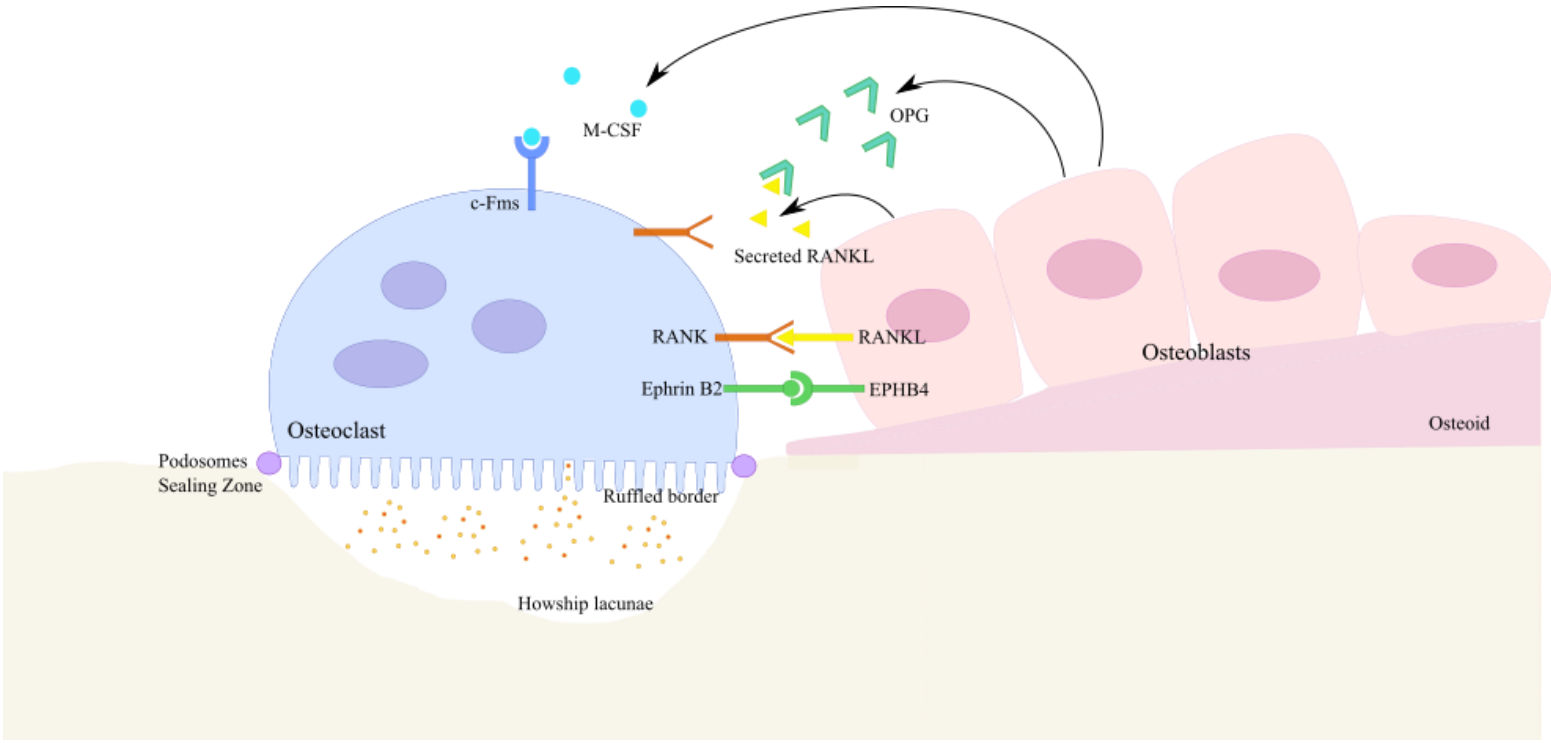

Figure 12. **Osteoclastic bone resorption is modulated by the action of osteoblasts through the RANKL/OPG axis.**

The interaction between osteoblasts and osteoclasts is central to maintaining bone homeostasis, coupling bone resorption and formation. There are several modes of osteoblast-osteoclast cross talk including direct membrane coupling via ephrin B2 and RANKL, growth factors released from the matrix during the resorption phase and via cytokines including RANKL and M-CSF. Osteoblasts also modulates RANKL signalling by expressing OPG, a decoy receptor for RANKL, negatively regulating its activity.

1.6.1 Osteoblast-osteoclast communication in bone homeostasis

There are several modes of osteoblast-osteoclast cross talk including membrane coupling, direct membrane coupling, the liberation of growth factors from the matrix during the resorption phase, and via small molecules such as cytokines (Matsuo, 2008).

The initiation phase of bone remodelling begins with the recruitment of hematopoietic precursors and their differentiation into osteoclasts, stimulated by cells of the osteoblast lineage. Osteoblasts secrete MCP1 and macrophage colony stimulating factor 1 (MCSF1) that promote recruitment and survival of cells of the macrophage-osteoclast lineage (Lagasse and Weissman, 1997, Graves et al., 1999). The interaction between receptor activator of NFκB (RANK) expressed on pre-osteoclasts and RANKL expressed by osteoblasts is essential for osteoclastogenesis and the initiation of bone remodelling.

RANKL, a type II membrane protein and member of the tumour necrosis factor (TNF) superfamily is expressed in the surface of osteoblasts and stromal cells (Boyce and Xing, 2007). It has also been shown that RANKL is proteolytically cleaved from the plasma membrane by matrix metalloproteases or ADAMs (Lum et al., 1999, Lynch et al., 2005, Hikita et al., 2006). Membrane bound and secreted RANKL is a potent stimulator of osteoclastogenesis as *in vivo* studies show that *Tnfsf11*-null mice develop osteopetrosis due to a lack of osteoclasts, a phenotype that is rescued upon lymphocyte *Rankl* expression (Li et al., 2000, Kim et al., 2000).

The receptor for RANKL, RANK is a type I membrane protein and a member of the TNF receptor superfamily (Boyce and Xing, 2007). RANK is expressed as a homotrimeric transmembrane protein on the surface of osteoclast precursors and mature osteoclasts. As with *Tnfsf11*-null mice, mice lacking *Tnfsf11a* (encoding RANKL) display the same osteopetrotic phenotype as they do not develop osteoclasts (Galli et al., 2008). Conversely, activating mutations in exon 1 of *Rank* resulted in an upregulation of NFκB signalling and lead to increased osteoclastogenesis and osteolysis (Hughes et al., 2000).

Upon RANKL binding, the intracellular domain of RANK binds to TNF receptor associated factor (TRAF) 6, resulting in its trimerisation and the stimulation of the NFκB, AKT and MAPK downstream signalling cascades (Wong et al., 1999, Mizukami et al., 2002, Feng, 2005, Lamothe et al., 2007). RANKL also induces the

expression of c-FOS that activates the activator protein 1 (AP1) complex which plays a role in controlling cellular differentiation, proliferation and apoptosis (Huang et al., 2006). NFκB and AP1 also induce the expression of the master regulator of osteoclastogenesis, NFATc1, that upregulates the expression of osteoclast specific genes resulting in osteoclast differentiation and bone resorption (Asagiri et al., 2005, Gohda et al., 2005).

Following the resorption phase of bone remodelling, bone resorption stops and RANKL-stimulated osteoclastogenesis is inhibited by OPG. OPG, also known as osteoclast inhibitory factor (OCIF) is a secreted member of the TNF receptor superfamily that is expressed by a number of cell types including osteoblasts and stromal cells (Boyce and Xing, 2007). OPG functions as a decoy receptor for RANKL, negatively regulating its activity and performing an osteoprotective role. OPG is upregulated in osteoblasts in response to canonical WNT signalling (Holmen et al., 2005, Glass et al., 2005). Furthermore the promoter of *Tnfsf11b* (encoding OPG) contains early B-cell factor 2 (EBF2) binding sites that regulate its expression and subsequently osteoblast-induced osteoclastogenesis (Kieslinger et al., 2005). *In vivo* studies show that *Tnfsf11b*-null mice develop osteoporosis whereas overexpression of *Opg* results in osteopetrosis (Bucay et al., 1998, Simonet et al., 1997).

Osteoblastic bone formation is promoted by the secretion of anabolic growth factors including BMP5 and WNT10B from osteoclasts, liberation of growth factors such as TGFβ from the matrix during the resorption phase and the direct interaction between osteoblasts and osteoclasts (Pfeilschifter and Mundy, 1987, Matsuo, 2008, Pederson et al., 2008). It has been proposed that osteoblasts and osteoclasts are also coupled by membrane interactions and bidirectional signalling. *In vivo* studies show that ephrin B2 is expressed on the surface of osteoclasts and binds its receptor ephrin receptor B4 (EBPB4) on osteoblasts, coupling the osteoblasts and osteoclasts (Zhao et al., 2006). Ephrin B2 signals into osteoclasts to inhibit differentiation by blocking the action of NFATc1 and c-FOS (Zhao et al., 2006). Conversely, EPHB4 signalling in MSCs was found to stimulate osteoblastogenesis potentially via the inhibition of RAS homolog gene family, member A (RHOA) (Zhao et al., 2006). Additionally EPHB4 signals to upregulate OPG to further inhibit osteoclastogenesis. A novel form of membrane coupling between osteoblasts and osteoclasts involves the cell membrane bound RANKL on osteoblasts (Furuya et al., 2013). Studies show that a peptide agonist for RANKL binding inhibits osteoclastogenesis and promotes bone formation (Aoki et

al., 2006). It has also been proposed that a direct interaction between Notch receptors on osteoblasts and notch ligands on osteoclasts also controls osteoclastogenesis, by resulting in the upregulation of *Opg* (Bai et al., 2008).

Osteocytes also play a role in regulating bone mass. For example, following bone formation osteocytes produce SOST that inhibits the canonical WNT/B-catenin pathway in osteoblasts by binding LRP5/6 and promoting apoptosis (Sutherland et al., 2004, Li et al., 2005). Interestingly *SOST* mutations in human results in high bone mass, a phenotype seen in mice bearing a deletion of *Sost* (Li et al., 2008, Piters et al., 2010).

1.7 The role of the endoplasmic reticulum (ER) in development and disease

1.7.1 Function of the ER

The endoplasmic reticulum is the largest organelle within the cell and primarily functions as a site for protein synthesis, folding and trafficking as well as a major site for carbohydrate metabolism, calcium storage and lipid synthesis (Caro and Palade, 1964, Eisen and Reynolds, 1985, Clapham, 2007, Fagone and Jackowski, 2009, Braakman and Hebert, 2013, Schwarz and Blower, 2016).

The synthesis of secreted, membrane and cytosolic proteins requires ribosomes on the cytosolic face of the ER (Caro and Palade, 1964, Reid and Nicchitta, 2015). The ribosome associates with a multiprotein complex, the Sec61 translocon, allowing for co-translational translocation of the nascent synthesised protein into the ER lumen (Rapoport, 2007). The nascent protein must then undergo proper folding to its native functional state of lowest gibbs free energy. It also undergoes post-translational modifications, including disulphide bond formation and N-liked glycosylation, mediated by protein folding chaperones and enzymes (Braakman and Hebert, 2013). Following proper folding, if the protein is targeted for secretion it is released by the chaperones and travel through the secretory pathway to its final destination. As skeletal cells are highly secretory cells the ER therefore plays an important role in development and homeostasis.

1.7.2 ER folding chaperones

As mentioned, the correct folding of proteins to their native functional form is monitored by ER resident folding enzymes and chaperones. A folding chaperone is defined as a protein that aids in folding of the maturing protein but is not part of the final structure (Ellis and van der Vies, 1991). Within the ER there are two types of chaperone, classical chaperones that recognise exposed hydrophobic regions that are normally buried within the native protein fold and non-classical lectin chaperones that recognise a monoglucosylated N-linked hydrophilic glycan. These two chaperone systems are regulated by a series of cofactors within the ER that work together to aid in the folding of immature proteins, prevent aggregation and refold misfolded proteins thus maintaining trafficking through the secretory pathway.

1.7.2.1 Classical chaperones

Classical ER chaperones include heat shock proteins, such as the heatshock protein (HSP) 70 proteins. The HSP70 family member Binding immunoglobulin protein (BIP) is regarded as the master regulator of protein folding and trafficking, binding most of the proteins that travel through the ER (Flynn et al., 1991).

BIP is locked onto the substrate upon hydrolysis of the adenosine triphosphate (ATP) to adenosine diphosphate (ADP) by HSP40 family members (Flynn et al., 1989). These proteins not only induce ATPase activity but also aid in positioning of BIP at the SEC61 translocon and potentially play a role in folding themselves following substrate binding (Alder et al., 2005). Nucleotide exchange factors then exchange ATP back into the nucleotide-binding cleft that reopens the chaperone and allows for release of the protein chain (Chung et al., 2002).

Later in the maturation process other chaperones act on the folding protein, these include members of the HSP90 family of chaperones, including GRP94 however its exact mechanism of action is unknown (Melnick et al., 1994).

1.7.2.2 Lectin chaperones

The second system of chaperones within the ER are the non-classical lectin chaperones (Braakman and Hebert, 2013). These include the molecular chaperones calnexin and calreticulin that bind to unfolded glycoproteins. Once translocated through the translocon pore into the ER lumen, the nascent protein undergoes N-linked glycosylation on asparagine residues (Aebi, 2013). This involves the addition of three glucose, nine mannose and two N-aceltylglucosamine residues ($Glc_3Man_9GlcNAc_2$) to an asparagine residue in an asparagine-X-serine/threonine glucosylation consensus sequence. This glycan then undergoes co-translational trimming by glucosidase I and II leaving a single glucose residue that is identified and bound by lectin chaperones, including calnexin and calreticulin (Hammond et al., 1994, Hebert et al., 1995, Peterson et al., 1995). Calnexin and calreticulin perform a range of functions within the ER. Primarily they aid in proper protein folding by slowing down the rate of folding and stabilising the process (Hebert et al., 1996, Hebert et al., 1997). They also prevent aggregation of the folding protein and retain the protein until it has reached its functional form (Hebert et al., 1996, Vassilakos et al., 1996). Interestingly, they also

promote disulphide bond formation by associating with the co-chaperone endoplasmic reticulum resident protein (ERp) 57, a thiol oxidoreductase (Zapun et al., 1998).

Upon cleavage of the last glucose by glucosidase II, the binding site for lectin chaperones is lost and the protein is free to fold. If the substrate has not folded correctly, the quality control sensor uridine diphosphate (UDP)-glucose:glycoprotein glucosyltransferase 1 (UGGT1) transfers a glucose residue back onto the unfolded protein resulting in its re-association with lectin chaperones in an attempt to fold it to the functional form (Hammond et al., 1994, Hebert et al., 1995, Sousa and Parodi, 1995, Van Leeuwen and Kearse, 1997, Pearse et al., 2008).

1.7.2.3 Protein folding enzymes

The rate of protein folding within the ER is increased by the ER resident enzymes. There are two classes of folding enzymes including peptidyl–prolyl cis/trans isomerases (PPIs) and oxidoreductases or protein disulphide isomerases (PDIs) . The rate limiting steps of protein folding is the *cis/trans* isomerisation of prolyl-peptide bonds and the formation of disulphide bonds and each of these steps are catalysed by PPIs and PDIs respectively.

During synthesis of the nascent protein strand, proline resides are inserted by the ribosome in the *cis* conformation. However, for the protein to fold to its native state the proline residues must be in the *trans* conformation. This isomerisation process is catalysed by PPIs and is crucial to proper protein folding (Figure 13A).

The folding and tertiary structure of proteins are often stabilised by the formation of disulphide bonds between two cysteine residues. The ER provides a calcium rich redox environment for correct folding of proteins, suitable for disulphide bond formation. PDIs are ER resident enzymes due to a perfect C-terminal lysine-aspartic acid-glutamic acid-leucine (KDEL) sequence. These enzymes function within the ER to mediate oxidative protein folding by catalysing the formation of disulphide bonds (oxidase activity) while rearranging incorrect disulphide bonds (isomerase activity) to allow the protein to fold it its native conformation (Figure 13B).

The folding activity of PDIs was first described in PDI. PDI is an abundant 55 kDa protein that contains four thioredoxin-like domains, two of which are catalytically

active and contain the canonical CxxC motif (Chivers et al., 1996). In the oxidised state, the catalytically active disulphide is transferred to the protein substrate to catalyse its oxidation leaving the active site reduced and vice versa. The two cysteine residues play distinct roles in the formation of disulphide bonds and allow the PDIs to act as a donor and acceptor for the substrate, catalysing substrate cysteine oxidation and reduction.

PDI is an important enzyme in procollagen assembly within the ER as it catalyses both inter- and intra-molecular disulphide bonds between the C-propeptides as these fold individually. Studies have shown that PDI also acts as a chaperone protein in the ER contributing to the ER quality control system (Cai et al., 1994, Song and Wang, 1995). PDI binds to monomeric C-propeptides leading to their retention within the ER until they assemble to form full length procollagen. PDI also forms the β-subunit of the prolyl-4-hydrocylase complex which catalyses the hydroxylation of proline within the collagen alpha helical structure (Wilson et al., 1998).

PDI is one of a family of 20 mammalian related proteins that vary in protein domain structure and length, but all share one common feature of at least one thioredoxin-like domain. Most of the PDI family members comprise both catalytic and non-catalytic thioredoxin-like domains however some family members such as ERp29 and 27 contain no reactive sites and so are non-catalytically active (Alanen et al., 2006, Mkrtchian and Sandalova, 2006). These non-catalytic thioredoxin like domains do not share a conserved sequence and structure like the catalytic thioredoxin-like domains and are postulated to be involved in substrate recruitment. This family of PDIs is therefore not grouped on function but on similarities in sequence, structure and localisation.

Due to the high number of PDI family members, it can be hypothesised that they have diverse functions with distinct specificities; however, there is little in vivo information on PDI enzyme substrates. Most information is currently available on the substrates of ERp57. The functions of ERp57 are not clear, however, a knockout mouse model is embryonically lethal at E13.5 and this is postulated to be due to ERp57 modulating STAT3 signalling upon interaction of ERp57 with STAT3 (Coe et al., 2010). *In vitro* studies of an *ERp57* knockout show that ER stress levels are not changed and so suggesting a compensatory mechanism by the PDI family members (Torres et al., 2015). ERp57 catalyses both the formation and isomerisation of disulphide bonds *in vitro*. The thiol-disulphide exchange forming mixed-disulphides between PDIs and their substrate can be utilised to identify specific PDI substrates. This has been shown by

Jessop *et al.* 2007, by introducing trapping mutants which prolong the covalent complex between the substrate and the PDI, the mixed-disulphide, upon mutation of a C-terminal active site cysteine residue (Jessop et al., 2007). Using this approach, ERp57 substrates were identified by immunoprecipitation using a V5-tagged ERp57 trapping mutant. It was shown that ERp57 binds monoglycosylated proteins both *in vivo* and *in vitro* and so acts as a glycoprotein specific PDI due to binding calnexin and calreticulin. This was further backed up by the reduced folding of Hemagglutinin *in vitro* upon the treatment of mouse fibroblasts with castanopermine, an indolisine alkaloid that inhibits glucosidase enzymes (Jessop et al., 2009). It is important to note that not all glycoproteins are substrates for ERp57, therefore the family of PDIs is very complex, and the substrate specificities of PDI enzymes are very distinct require further research.

A.

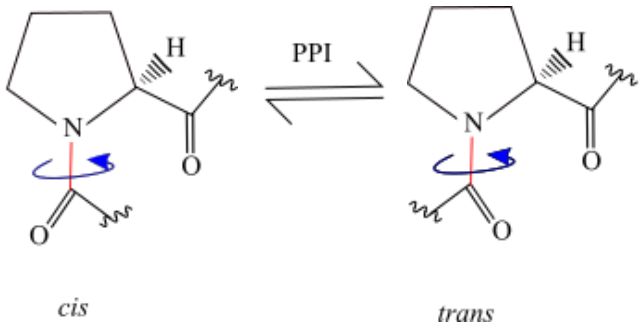

B.

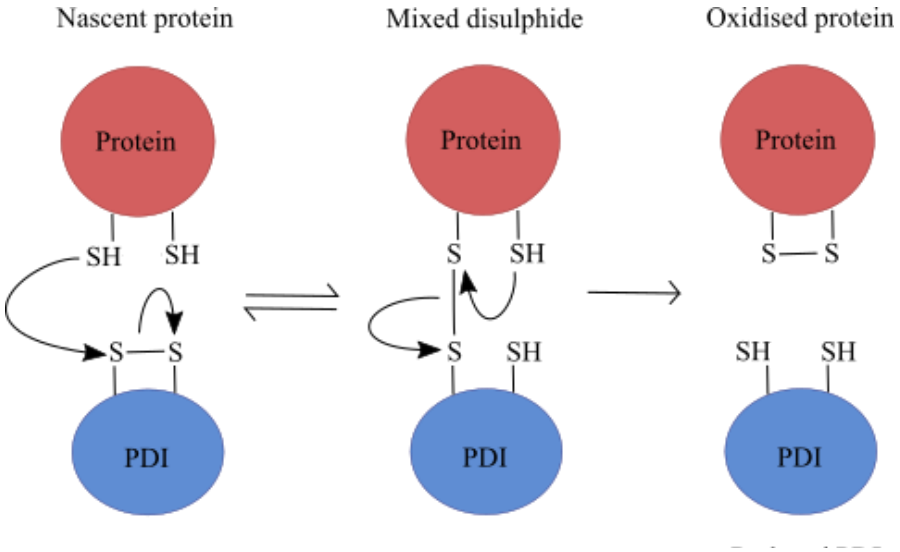

Figure 13. **A schematic showing the actions of peptidyl-prolyl cis/trans isomerases (PPIs) and protein disulphide isomerases (PDIs) during protein folding.**

Isomerisation is catalysed by PPIs in the ER. PPIs function to change proline residues from the *cis* confirmation to the *trans* confirmation in the nascent chain, allowing for proper protein folding (**A.**). The formation of disulphide bonds during protein folding are catalysed by PDIs. A disulphide bond is a covalent bond formed when two free thiol residues on a cysteine amino acid are oxidised (**B.**). First, a cysteine residue in the substrate protein is deprotonated. This thiol-disulphide exchange forms a reactive thiolate anion that acts as a disulphide acceptor and attacks the disulphide in the donor, the PDI. A transient mixed disulphide is formed between the enzyme and the structure. The disulphide donor is then reduced by protonation, and a disulphide bond forms between the cysteine residues in the substrate protein. Isomerisation follows the same basic mechanism with repeated rounds of oxidation and reduction except no net exchange occurs between the PDI donor and the substrate acceptor.

1.7.3 The unfolded protein response (UPR)

Despite the wide range of chaperones and enzymes that aid in protein folding, some proteins misfolded and aggregate in the ER. If attempts at folding fail the misfolded protein is retrotranslocated into the cytoplasm where it is targeted for proteasomal degradation in a process called ER-associated degradation (ERAD) (Brodsky, 2007). However, if the misfolded proteins cannot be retrotranslocated, they are sectioned into double membrane autophagosomes that bud off from the ER and fuse with a lysosome for degradation (Bernales et al., 2007, Ishida et al., 2009).

The accumulation of misfolded proteins within the ER lumen initiates a highly conserved process known as the unfolded protein response (UPR) (Figure 14) (Chakrabarti et al., 2011). The UPR initially acts in a pro-survival manner to refold or degrade the accumulated protein; however, if the stress on the ER is not returned to physiological levels, the UPR activates a pro-apoptotic signaling cascade by inducing C/EBP homologous protein (CHOP)-dependant/-independent cascades (Ma et al., 2002, Szegezdi et al., 2006).

The UPR is initiated by the ER lumen resident chaperone BIP dissociating from three transmembrane bound receptors and binding to the exposed hydrophobic residues on the unfolded protein. This results in the activation of the signalling pathways of the transmembrane bound receptors protein kinase RNA-like ER kinase (PERK), inositol-requiring enzyme 1 (IRE-1) and activating transcription factor (ATF) 6, with the ultimate aim to decrease protein translation, degrade the misfolded protein and ultimately promote cell death. Studies have shown that different types of stress initiate the UPR pathways. For example, a change in intracellular calcium levels results in high activation of IRE1 and PERK, whereas ATF6 signalling is induced by protein load (DuRose et al., 2006, Maiuolo et al., 2011).

IRE1, a type 1 transmembrane protein, is evolutionarily the oldest branch of the UPR and is found in both lower eukaryotes and higher animals whereas PERK and ATF6 are only found in higher animals (Wu et al., 2014). The IRE1 pathway is crucial for cell viability as *Ire1* and its downstream signalling protein, *X-box binding protein 1* (*Xbp1)*-null mice are embryonic lethal (Urano et al., 2000). IRE1 exists in two isoforms, the highly conserved and ubiquitous alpha isoform and the beta isoform that is only found in gut epithelium (Bertolotti et al., 2001). The IRE1 transmembrane receptor contains a cytoplasmic domain that possesses Serine/Threonine kinase and

endoribonuclease activity. BIP dissociation from the luminal domain of IRE-1α leads to homodimerisation and activation of its ribonuclease activity via autophosphorylation. Active IRE-1 then cleaves a 26-nucleotide intron sequence from unspliced XBP1 (XBP1u) messenger RNA (mRNA). This leads to a translational frame shift producing XBP1 (XBP1s); a 54 kDa protein comprising 376 amino acids rather than the 261 amino acid Xbp1u isoform of 33 kDA. The unspliced form is highly unstable and as of yet functions are still not clarified (Yoshida et al., 2006, Vidal and Hetz, 2013, Chen et al., 2014a). Spliced XBP1 is active as a member of the cyclic adenosine monophosphate **(**cAMP) responsive element-binding protein (CREB)/ATF basic leucine zipper (bZIP) family of transcription factors and migrates to the nucleus where it binds the promoters and up-regulates genes encoding chaperones, PDIs and genes encoding the proteins of ERAD (Lee et al., 2003, Acosta-Alvear et al., 2007). Studies have shown that the kinase domain is involved in activating JUN N-terminal kinase (JNK) signalling through recruiting TRAF2 (Urano et al., 2000). It is postulated that this regulates autophagy and apoptosis however the result of activating JNK signalling is not fully understood (Yoneda et al., 2001, Zhao et al., 2013). Interestingly, the role of XBP1 is not restricted to folding and degrading misfolded proteins. Studies have shown that XBP1 plays a role in differentiation and in the hypoxia induced hypoxia-inducible factor 1α (HIF1α) pathway (Chen et al., 2014c). This suggests that the roles of IRE1-XBP1 are much more diverse than their role in the classical UPR.

PERK is a type 1 transmembrane protein that like IRE1, binds to BIP via its ER luminal domain and its cytoplasmic domain exerts serine/threonine kinase activity. Following BIP dissociation from PERK, it is found to homodimerise, leading to autophosphorylation and activation of Serine/Threonine kinase domain. PERK then phosphorylates and inactivates the alpha subunit of eukaryotic translation initiation factor 2α (eIF2α) required for mRNA 5' capping and 80s ribosomal activity. This leads to the reduction of global protein synthesis, thus reducing the load on the ER (Harding et al., 1999). Interestingly the inactivation of eIF2α also facilitates the translation of ATF4 a member of the CREB/ATF family (Lu et al., 2004). ATF4 binds a cAMP response element in the promoters of target genes increasing the expression of protein folding chaperones. The activation of PERK signalling pathway is controlled by CHOP as CHOP induces the transcription of GADD34 which dephosphorylates eIF2α and restores protein synthesis (Marciniak et al., 2004).

ATF6, type 2 90kda transmembrane protein, consists of an ER luminal domain that binds BIP and a cytoplasmic domain of a bZip transcription factor. AFT6 plays a minor role in maintaining the general ER homeostasis as *Atf6*-null mice display no developmental phenotype at birth (Wu et al., 2007). Dissociation of BIP from ATF6 allows for interactions between ATF6 and the COPII vesicular complex (Schindler and Schekman, 2009). ATF6 then translocates to the Golgi apparatus where it undergoes cleavage by site-1 and site-2 proteases (Ye et al., 2000, Shen et al., 2002). It is postulated that ATF6 is held in the ER due to interactions with the ER resident lectin chaperone, calreticulin. Following its deglucosylation, it is unable to bind calreticulin and so is transported to the Golgi apparatus (Hong et al., 2004). Following cleavage, the cytosolic portion of ATF6 then acts as a 50 kDa transcription factor, $ATF6_{50}$, moving to the nucleus and binding to ER stress-responsive cis-acting elements (ERSE) and unfolded protein response elements (UPRE) in the promoters of target genes encoding chaperones and genes involved in ERAD and apoptosis (Adachi et al., 2008).

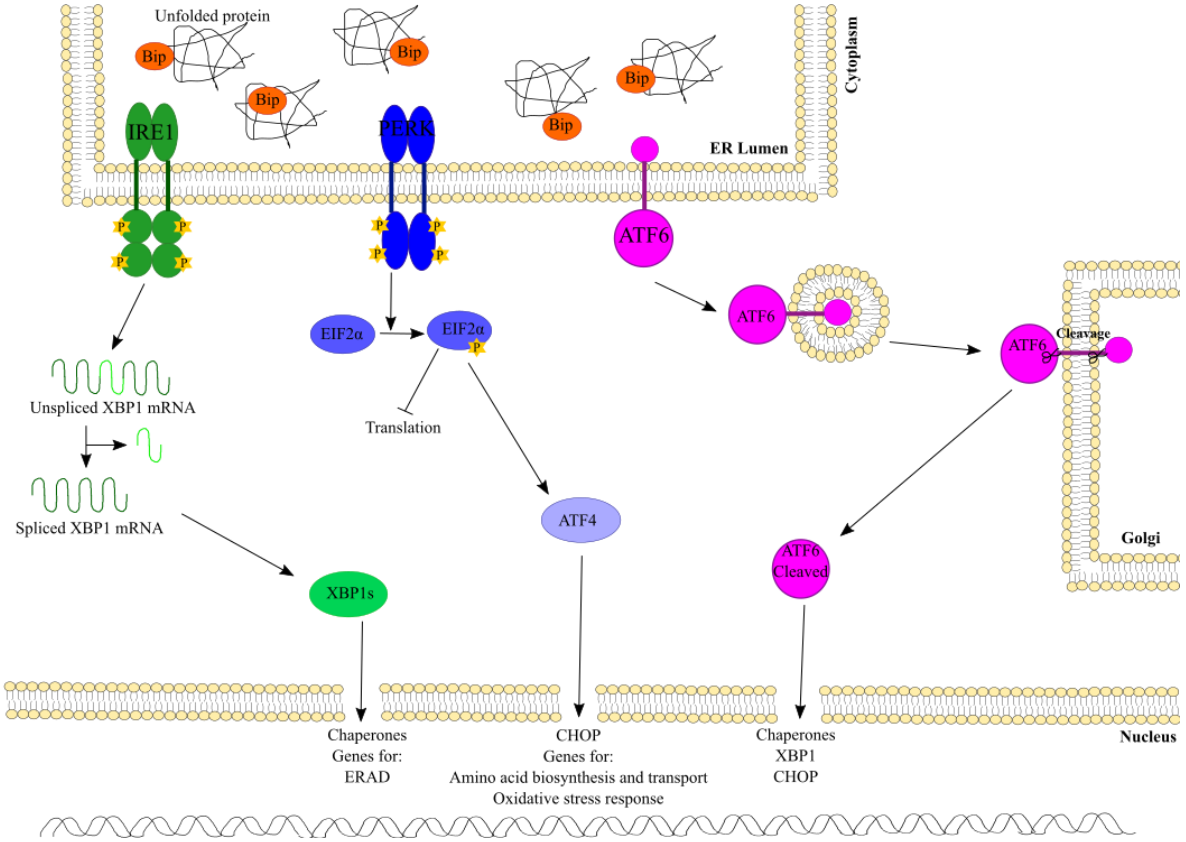

Figure 14. **The unfolded protein response.**

The accumulation of misfolded proteins within the ER lumen initiates the UPR. Misfolded proteins are recognised by BIP, that dissociates from three transmembrane bound receptors and binds to the exposed hydrophobic residues on the unfolded protein. This results in the activation of the signalling pathways of the transmembrane bound receptors PERK, IRE1 and ATF6 with the ultimate aim to cease translation, degrade the misfolded protein and promote cell death.

1.7.4 The UPR in skeletal development and homeostasis

The process of endochondral ossification requires the formation of a cartilage precursor by chondrocytes and its conversion to bone by osteoblasts. The bone is continually modified throughout life through the combined actions of osteocytes, osteoblasts and osteoclasts. Besides its function in ER quality control of protein folding, the UPR has also been implicated in the maturation of highly secretory skeletal cells. Cells of the skeletal system including chondrocytes osteoblasts and osteoclasts have adopted the classical UPR not only to fold proteins but also to aid in cell differentiation and ultimately skeletal growth.

1.7.4.1 The UPR and cartilage development

Besides maintaining cellular homeostasis, several pathways of the UPR have also been implicated in cartilage development (Figure 15). BBF2 human homolog on chromosome 7 (BBF2H7)/cAMP responsive element binding protein 3 like 2 (CREB3L2) is a transmembrane receptor and a novel homolog of ATF6 (Kondo et al., 2007). Like ATF6, BBF2H7/CREB3L2 undergoes proteolytic cleavage in the Golgi by site-1 and site-2 proteases. This results in an N-terminal fragment that translocates to the nucleus where it is active as a transcription factor. BBF2H7/CREB3L2 is ubiquitously expressed; however, its expression is highest in proliferating chondrocytes of the growth plate. Unsurprisingly, the expression of BBF2H7/CREB3l2 is induced by SOX9, the master regulator of chondrogenesis (Hino et al., 2014). *Creb3l2*-null mice have significantly shorter bones with a reduced cartilage matrix and a disrupted growth plate in which columnar localisation of chondrocytes is impaired indicating a role in skeletogenesis (Saito et al., 2009). Moreover, the ER in *Creb3l2*-null chondrocytes is extended due to the aggregation of matrix proteins resulting in disrupted protein export. Studies show a decreased expression of SEC2A, a protein subunit of the COPII complex that controls vesicle budding from the ER in the protein secretory pathway in the *Creb3l2*-null mice, resulting in a defect in export of matrix proteins affecting cartilage development.

Following cleavage in the Golgi the N-terminal fragment of BBF2H/CREB3L2 acts as a transcription factor. Unexpectedly it was shown that the C-terminal fragment of BBF2H/CREB3L2 binds to IHH and PTHrP, and facilitates their interaction, thus

enhancing proliferation (Saito et al., 2014). Taken together, these findings indicate that BBF2H7/CREB3L2 plays a role in skeletal development.

ATF4 is also plays a role in skeletal development and *Atf4*-null mice displayed reduced chondrocyte proliferation and delayed hypertrophic mineralisation resulting in a short-limb dwarfism (Wang et al., 2009). Wang *et al.* also showed that ATF4 is a transcription factor for *Ihh* and treatment of *Atf4*-null mice with purmorphamine, an antagonist for Smoothened, rescued the skeletal phenotype of these mice.

XBP1 has been shown to play a minor role in cartilage development as chondrocyte-specific *Xbp1* knockout mice exhibited shorter long bones at 2 week of age, with a reduction in length of 13 % compared to controls (Wang et al., 2009). Interestingly, these mice displayed mild decrease in proliferation and a reduction in the size of the hypertrophic zone. The exact role of XBP1 is not known; however, the ablation of XBP1 in a mouse model for multiple epiphyseal dysplasia bearing the V194D mutation aggravates the phenotype (Pirog *et al.*, Unpublished data).

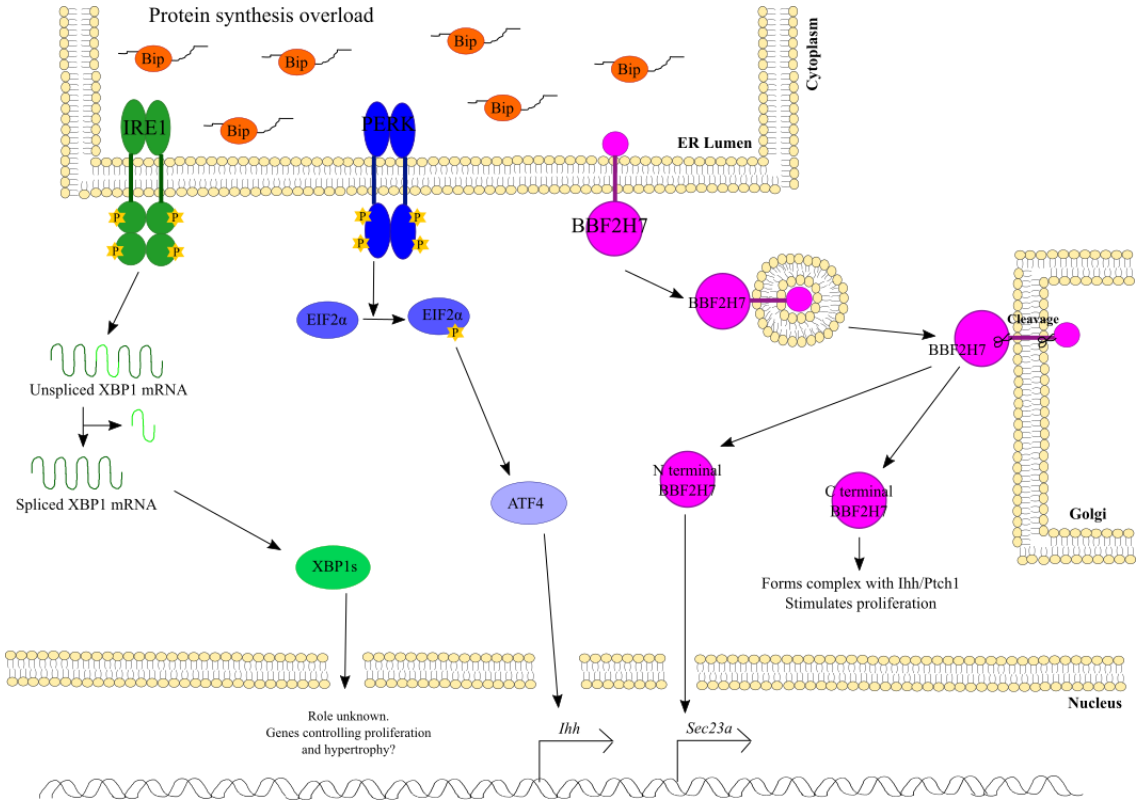

Figure 15. **The unfolded protein response in chondrogenesis.**

The UPR has been implicated in cartilage development. For example, following cleavage in the Golgi of BBF2H7/CREB3L2, a homolog of ATF6, the N-terminal fragment of acts as a transcription factor, upregulating the vesicular protein SEC23A. Interestingly, it was shown that the C-terminal fragment of BBF2H7/CREB3L2 binds to IHH and PTHrP, facilitating their interaction and enhancing chondrocyte proliferation. ATF4 was also found to induce the expression of *Ihh.* Finally, XBP1 plays a role in chondrogenesis however the precise role of XBP1 is not understood.

1.7.4.2 The UPR and osteoblastogenesis

A novel role for the UPR has also been found in osteoblastogenesis (Figure 16). *In vitro* assays have shown that BMP2 stimulation results in the upregulation of the transcription factors, RUNX2 and osterix, stimulating osteoblastogenesis (Tohmonda et al., 2011). RUNX2 levels reach a peak 24 hours after stimulation. This induces the expression of osteoblast markers such as type I collagen, a marker of early differentiation. The levels of osterix peak at 72 hours. Interestingly the levels of several ER stress proteins such as XBP1 and BIP increase at 24 hours and peak at 48 hours. This suggests that RUNX2 expression is induced prior to stress and the expression of osterix is a result from ER stress.

To IRE1α -XBP1 pathway plays a role in in osteoblast differentiation as mouse embryonic fibroblasts (MEFs) derived from *IRE1α*-null mice did not differentiate into osteoblasts following BMP2 stimulation and subsequently the levels of RUNX2 and osteoblast specific markers were reduced. Gene silencing of *Xbp1* in wild type MEFs also showed impaired osteoblast differentiation. Gene silencing of *Traf2* however did not affect osteoblastogenesis confirming that XBP1 downstream of IRE1 plays a crucial role in osteoblastogenesis (Urano et al., 2000). Moreover, XBP1 was found to bind highly conserved binding sites on the *Osterix* promoter (Tohmonda et al., 2011).

PERK signalling has also been implicated in osteoblast maturation as *Perk*-null mice display osteopenia due to a reduction in bone formation activity and less osteoblasts (Wei et al., 2008). Additionally, there was a significant reduction in the expression of mature osteoblast makers including ALP, IBSP, osteocalcin and type I collagen in osteoblasts. As there was no significant difference in the levels of osteopontin an early marker of osteoblast differentiation, suggesting that PERK is required for osteoblast maturation. Type I collagen was also found to be upregulated by cAMP-responsive element-binding protein 3-like protein 1 (OASIS), an ATF6 homolog (Murakami et al., 2011a).

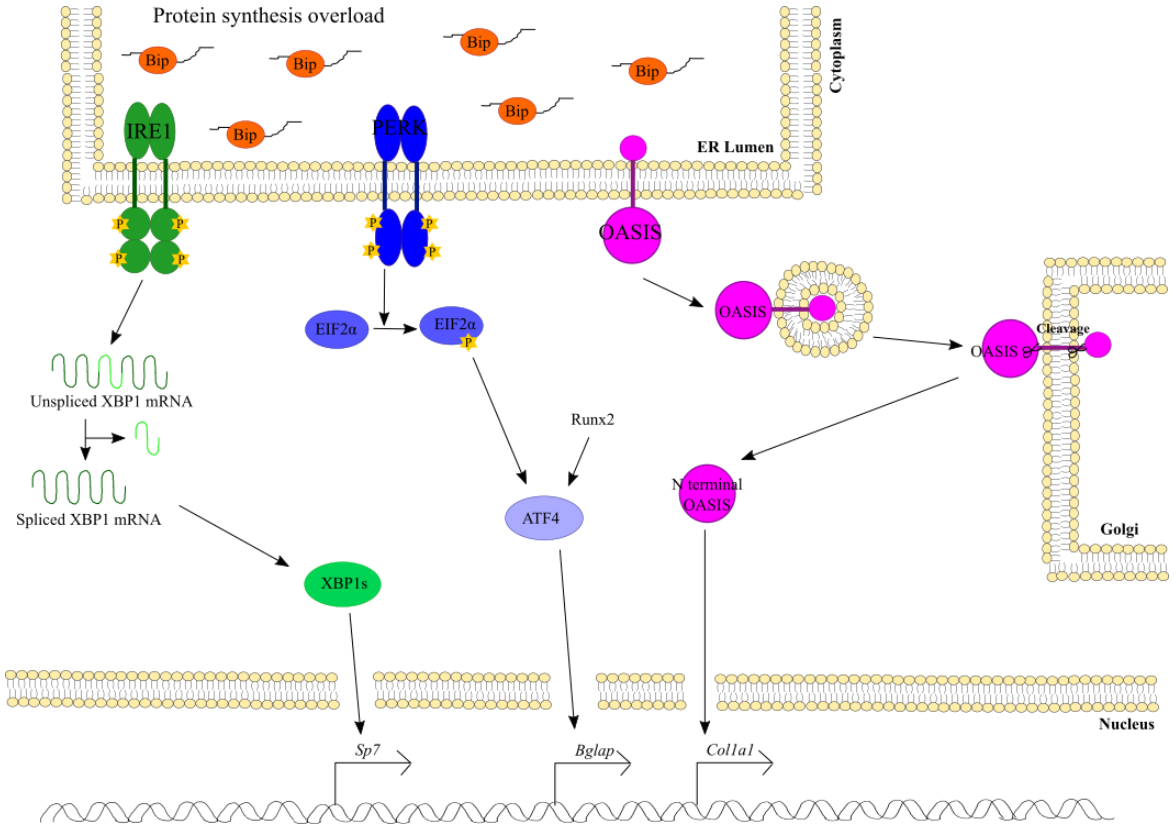

Figure 16. **The unfolded protein response and osteoblastogenesis.**

A novel role for the UPR has also been shown in osteoblastogenesis. Signalling through the IRE1α-XBP1 pathway results in upregulation of *Sp7,* a transcription factor that drives osteoblastogenesis. Signalling via the PERK pathway results in the upregulation of osteoblast specific genes including *Bglap* that encodes osteocalcin. Finally, an ATF6 homolog OASIS has also been shown to play a role in osteogenesis by stimulating the expression of Collagen I.

1.7.4.3 The UPR and osteoclastogenesis

The UPR also plays a central role in osteoclast differentiation (Figure 17). For example, the splicing of XBP1 is upregulated following stimulation with RANKL (Tohmonda et al., 2015). Additionally, inhibition of IRE1α and silencing of the *Xbp1* genes were shown to inhibit osteoclastogenesis. The most strongly induced transcription factor following stimulation of pre-osteoclasts is nuclear factor of activated T-Cells 1 (NFATc1), a master transcription factor for osteoclastogenesis. Following RANKL stimulation, Ca^{2+} oscillation is enchanced by activated RANK and provides an ER stress situation promoting the expression of NFATc1 via a calcineurin-dependant mechanism. Interestingly the IRE1α-XBP1 pathway is a potent stimulator of NFATc1 expression, with spliced XBP1 binding to the NFATc1 promoter, coupling RANKL signalling to osteoclast differentiation.

ATF4 is also important for osteoclastogenesis and was found to directly induce NFATc1 expression by binding directly to its promoter. Osteoclast precursors null for *Atf4* expression do not differentiate into TRAcP positive multinucleated cells (Cao et al., 2010). The expression of ATF4 was shown to primarily be regulated by the colony stimulating factor 1 (CSF1) receptor activation and signalling via PI3K-AKT signalling pathway. ATF4 is also stimulated by PERK-eIF2α following RANKL stimulation and an ER imbalance resulting from calcium ion outflow from the ER.

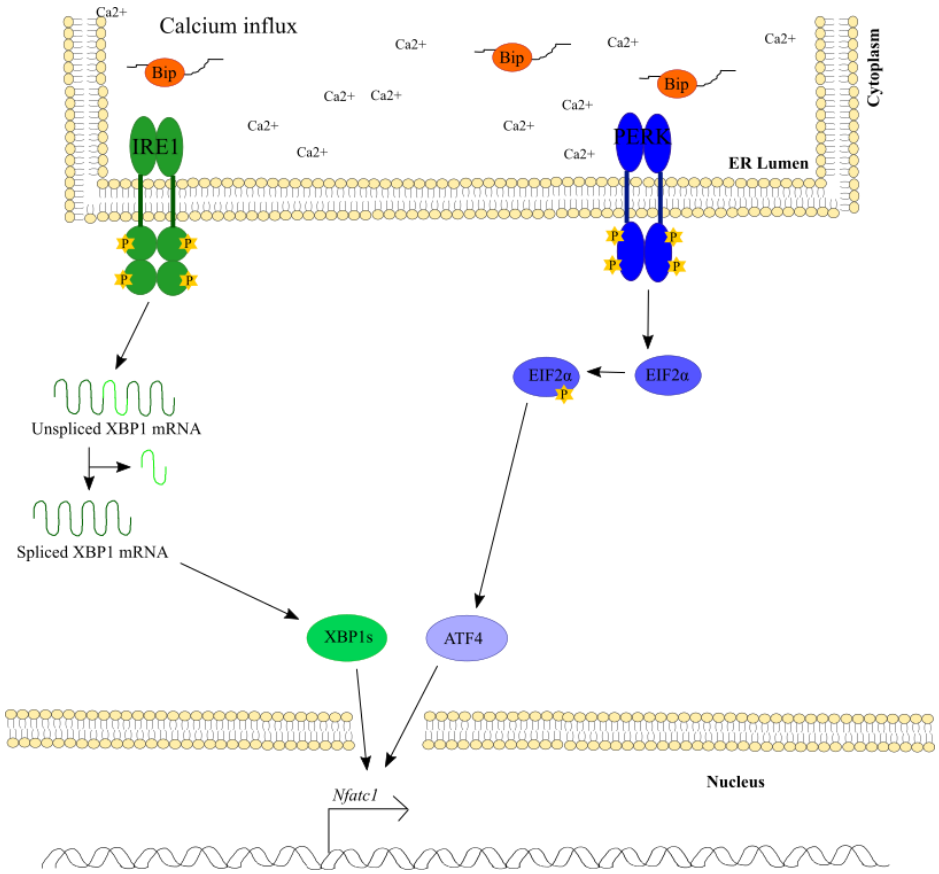

Figure 17. **The unfolded protein response and osteoclast differentiation.**

The unfolded protein response has been implicated as playing a role in osteoclastogenesis. Following stimulation with RANKL, signalling via PERK and the splicing of Xbp1 is upregulated. Spliced XBP1 and ATF6 then translocate to the nucleus where they act as transcription factors for *Nfatc1*, the master regulator of osteoclastogenesis.

1.7.5 The UPR and skeletal dysplasia

The evolutionarily conserved process of the UPR is crucial for cell differentiation; however, it has also been shown to play a key role in a range of diseases including a heterogeneous group of diseases known as skeletal dysplasias (Ozcan et al., 2006, Lin et al., 2008, Rajpar et al., 2009, Nundlall et al., 2010). Individually these diseases are rare and phenotypes are grouped by clinical presentation, ranging from mild to severe and lethal diseases that affect the osseous skeleton. Skeletal dysplasias are characterised by disproportionate short stature and malformations/deformations of the skeleton with a disrupted growth plate.

Pseudoachondroplasia (PSACH) and multiple epiphyseal dysplasia (MED) are two genetically and clinically heterogenous diseases that form a disease spectrum ranging from mild MED resulting from mutations in the extracellular matrix proteins matrilin-3 and type IX collagen to more severe forms of MED and PSACH resulting from mutations in cartilage oligomeric matrix protein (COMP) (Figure 18) (Briggs et al., 1995, Muragaki et al., 1996, Paassilta et al., 1999, Chapman et al., 2001).

Mutations in the *MATN3* gene lead to a less severe chondrodysplasia, MED. The first two mutations identified in *MATN3* that result in MED were V194D and R121W, two mutations in the von Willebrand factor A (vWFA) domain of matrilin-3 (Chapman et al., 2001). Separate studies have shown that mutant matrilin-3 is retained within the ER *in vitro* and *in vivo* (Cotterill et al., 2005, Otten et al., 2010, Leighton et al., 2007, Suleman et al., 2012). The retention of misfolded mutant matrilin-3 leads to ER stress and the initiation of UPR characterised by an upregulation of BIP, calreticulin as well as several PDIs. Prolonged stress by this mutant protein reduces chondrocyte proliferation and dysregulates apoptosis

Metaphyseal chondrodysplasia type Schmid (MSDS) is a mild short limb dwarfism that results from mutations in *COL10A1*. Except for two mutations that affect the signal peptide cleavage site, all mutations that cause MCDS lay in the non-collagenous NC1 domain, a domain that is responsible for collagen fibril trimerisation (Bateman et al., 2005). *In vivo* studies of MCDS have indicated that intracellular retention of type X Collagen results in an increase in ER stress in hypertrophic chondrocytes with increased expression of BIP and CHOP and increased splicing of XBP1 (Tsang et al., 2007).

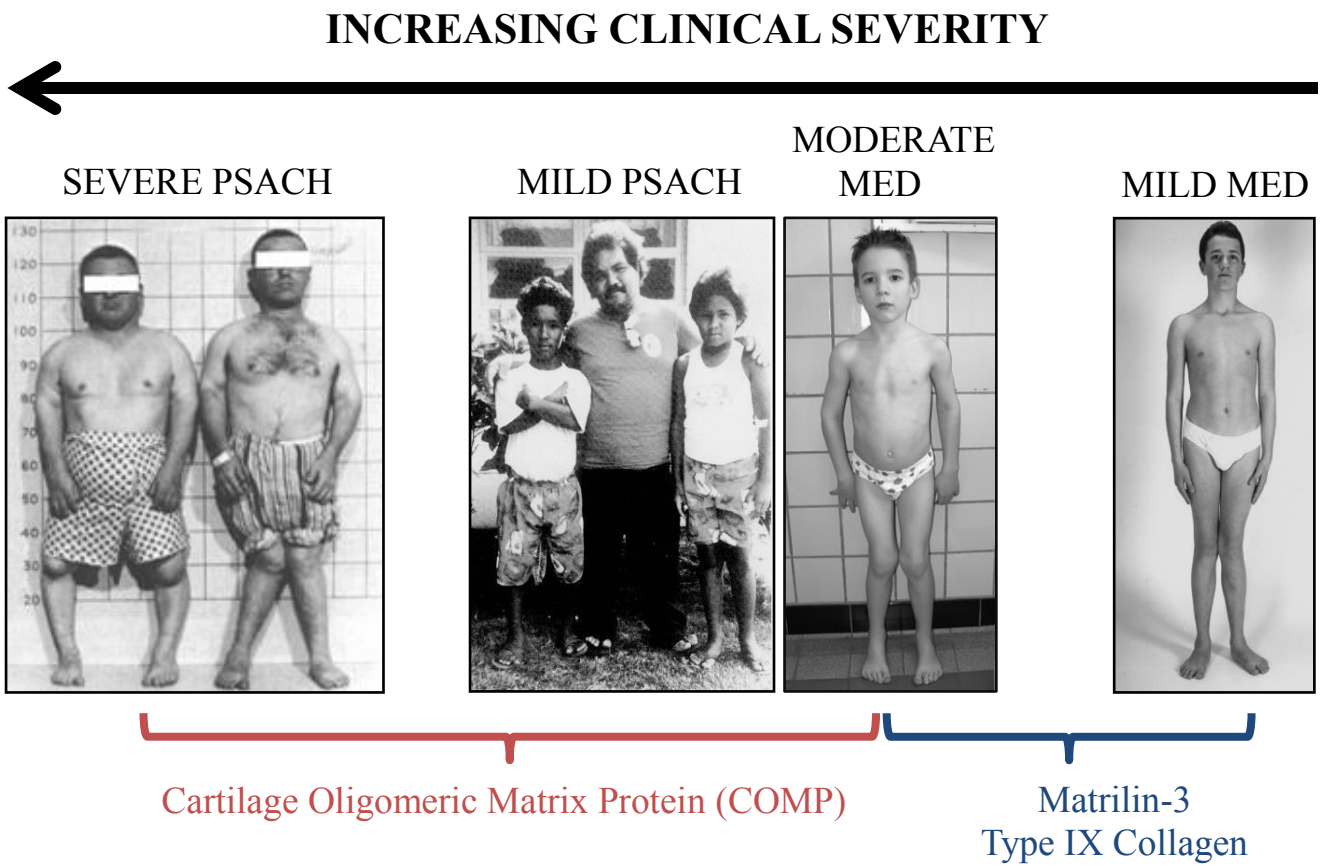

Figure 18. **Pseudoachondroplasia and Multiple Epiphyseal Dysplasia.**

Skeletal dysplasias are characterised by disproportionate short stature and malformations and deformations of the skeleton with a disrupted growth plate.Pseudoachondroplasia (PSACH) and multiple epiphyseal dysplasia (MED) are two genetically and clinically heterogenous diseases that form a disease spectrum ranging from mild MED resulting from mutations in the extracellular matrix proteins Matrilin-3 and type IX collagen to more severe forms of MED and PSACH resulting from mutations in cartilage oligomeric matrix protein (COMP).

1.8 The Cysteine rich with EGF-like domains (CRELD) family of proteins

Rupp *et al.* first identified the CRELD family of proteins comprising of CRELD1 and its homolog CRELD2 (Rupp et al., 2002). CRELD1 and CRELD2 share 51 % similarity in sequence and are multidomain proteins containing EGF-like and Calcium-binding EGF-like domains as well as a unique and highly conserved Tryptophan-Aspartic Acid (WE) domain. This unique WE domain is the region of greatest similarity between the family members with a 55 % identical nucleic acid sequence.

The main difference between CRELD1 and CRELD2 is that CRELD1 contains two type II transmembrane domains at the C-terminus of the protein indicating that CRELD1 is anchored to membranes. CRELD2 on the other hand does not this domain and is secreted into the extracellular space suggesting a functional divergence between the family members.

1.8.1 CRELD1

CRELD1 is the first member of the CRELD family of proteins and has been identified as an integral membrane component where it plays a role in cell adhesion (Rupp et al., 2002). This evolutionarily conserved protein plays important roles during development and the ablation of *Creld1* results in embryonic lethality between E11 and E11.5.

During embryogenesis CRELD1 is expressed in soft tissues including the brain and the heart. CRELD1 plays crucial roles in heart development with mutations in *CRELD1* associated with atrioventricular septal defects (AVSD) (Robinson et al., 2003, Zatyka et al., 2005, Alcantara-Ortigoza et al., 2015).

During heart development CRELD1 regulates the function of calcineurin, a calcium and calmodulin dependant protein phosphatase (Mass et al., 2014). It has been postulated that CRELD1 exerts its effect by bringing the β-subunit of calcineurin through its unique WE domain as the deletion of the WE domain using a nonapeptide impaired this interaction. The binding of CRELD1 to calcineurin leads to the dephosphorylation of NFATc1, allowing it to translocate to the nucleus where it induces the expression of genes required for heart development. Additionally CRELD1 was

shown to play a role in VEGF signalling, as *Creld1*-null cells do not respond to VEGF stimulation (Mass et al., 2014, Redig et al., 2014).

Interestingly CRELD1 can also modulate the pro-apoptotic properties of reticulon-3 (RTN3) (Xiang and Zhao, 2009). Studies have shown that CRELD1 recruits RTN3 from its subcellular location in the ER to the plasma membrane, reducing apoptosis induced by RTN3.

It has previously been suggested that CRELD1 is an ER stress-inducible gene. However, a recent study has shown that following thapsigargin treatment the expression of CRELD1 was not increased unlike CRELD2 (Mass et al., 2014). Additionally, unlike the promoter of *CRELD2*, the promoter of *CRELD1* does not contain an ERSE, a hallmark of ER stress-inducible genes.

1.8.2 CRELD2

CRELD2 is a 69-kDa glycoprotein encoded by *CRELD2* localised predominantly in the ER and Golgi due to an imperfect C-terminal KDEL sequence (Oh-hashi et al., 2009). Studies have shown that CRELD2 is also spontaneously secreted (Oh-hashi et al., 2011). In adult tissue CRELD2 is expressed in the thyroid gland, the pancreas, the lungs, the liver, male reproductive organs, the trachea and smooth muscle (Maslen et al., 2006). During mouse embryonic development, *Creld2* is expressed in the early long bones and ribs, the developing skull, the lungs and the pancreas at E14.5 (Figure 19A).

CRELD2 is a multidomain protein comprising EGF-like and calcium-binding EGF-like domains as well as a unique and highly conserved tryptophan-aspartic acid (WE) domain (Maslen et al., 2006). *CRELD2* also undergoes alternative splicing in humans and so far 5 isoforms of varying numbers of EGF-like domains have been identified (Figure 19B) (Maslen et al., 2006). In mice, however, only one isoform has been identified. Interestingly, the only isoform expressed by human chondrocytes is 77 % similar to the amino acid sequence of the mouse isoform (Cheung *et al.,* Unpublished data).

The precise function of CRELD2 is largely unknown, however, several roles have been identified in protein folding and trafficking through studies of the nicotinic

acetylcholine receptor (nAChR) α4 and β2 subunits (Ortiz et al., 2005). *CRELD2* has also been identified as an ER stress-inducible gene upon treatment of the Neuro2α cell line with thapsigargin (Oh-hashi et al., 2009). Importantly, the promoter of the *CRELD2* contains an AFT6 response element. In ER stress situations CRELD2 is also secreted from the ER, potentially due to an imperfect KDEL sequence and possible out-competition for KDEL receptors by other ER resident chaperones containing a perfect KDEL sequence (Hartley et al., 2013). Extracellular CRELD2 has a different glycosylation pattern however its exact role outside the cell is unknown (Oh-hashi et al., 2011).

Recently studies by Hartley *et al.* have identified *Creld2* as an ER stress-inducible gene in the pathology of skeletal dysplasia as it is upregulated in a mouse model of MED and MCDS (Hartley et al., 2013). These diseases are characterised by sort-limb dwarfism and a disrupted growth plate due to retention of mutant protein within the ER, leading to an ER stress response. Substrate-trapping experiments have shown that CRELD2 acts as a putative PDI due to an N-terminal CxxC motif with potential substrates identified as matrilin-3, laminin 5 β3, type VI collagen and thrombospondin 1, all of which contain many disulphide bonds (Hartley et al., 2013). Perhaps this suggests a specialised form of the UPR initiated by unfolded proteins with many unpaired cysteine residues.

Interestingly, a novel role for *Creld2* has also been identified in the context of skeletal development as it is upregulated in BMP9 stimulated osteogenic differentiation of MSCs due to SMAD1/6/5 binding directly to its promoter (Zhang et al., 2013b).

A.

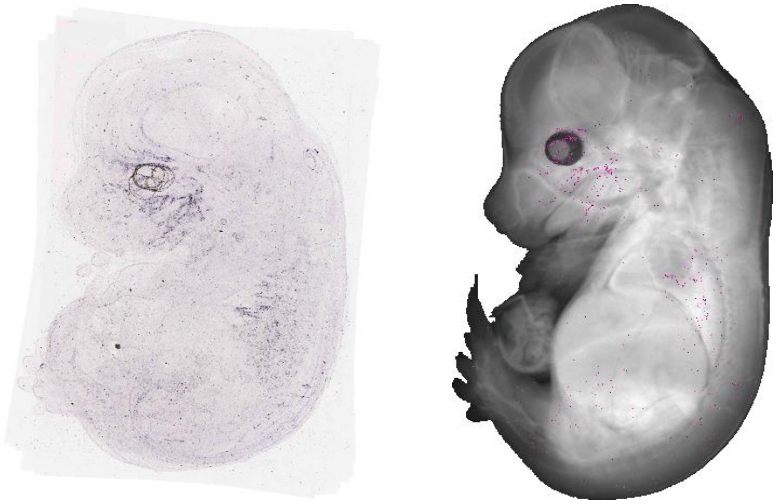

B.

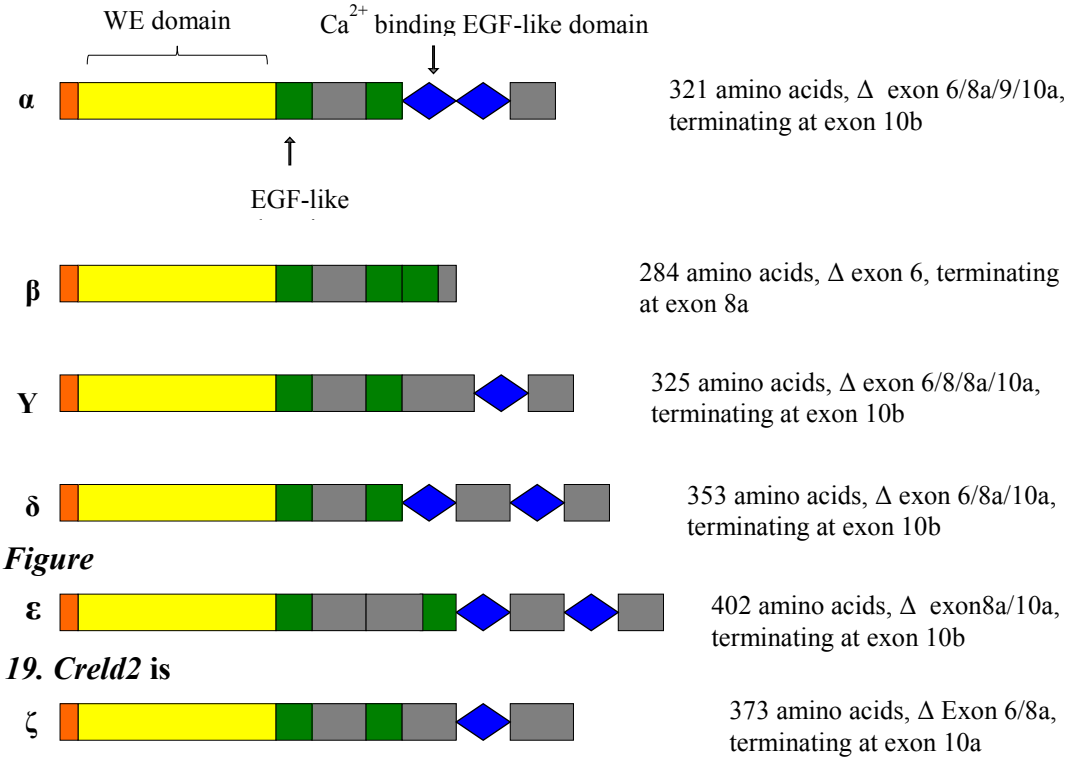

Figure

***19. Creld2* is**

expressed in the developing skeleton and undergoes alternative splicing in humans to produce 5 isoforms.

During mouse embryonic development *Creld2* is expressed in the early long bones and ribs, the developing skull, the lungs and the pancreas at E14.5 (**A.**). *CRELD2* undergoes alternative splicing in humans to produce 5 isoforms (**B.**). Each isoform contains a unique WE domain (yellow box) and varying numbers of EGF-like domains (green box) and calcium binding EGF-like domains (blue diamond). Unknown domains are identified by grey boxes. Despite 5 isoforms identified in humans, only one has been identified in the mouse. *Adapted from: (Maslen et al., 2006)*

1.9 Project aims

Studies to date have provided some insight into the role of the novel ER-stress inducible molecular chaperone gene *CRELD2* (Ortiz et al., 2005, Oh-hashi et al., 2009). However, despite the expression of *Creld2* in embryonic skeletal tissues, no transgenic mouse models have been generated to study its role in the skeleton *in vivo*. The work presented here is the first study to deep phenotype *Creld2* cartilage-specific and bone specific knockout mouse models in order to investigate the role of CRELD2 in chondrocytes and mature osteoblasts. This study was therefore important for establishing the mechanistic link between CRELD2 and skeletal development and homeostasis.

The specific aims of the research presented in this thesis were as follows:

1. **To characterise the skeletal development of *Creld2* cartilage-specific knockout mice**

   CRELD2 is expressed in the developing skeleton during mouse embryonic development and is upregulated in the context of skeletal dysplasias that result from the accumulation of misfolded protein within the ER producing a UPR (Maslen et al., 2006, Hartley et al., 2013). It therefore is hypothesised that the ablation of this protein will impair skeletal development. The skeletal pathology of *Creld2* cartilage-specific knockout mice was analysed using various morphometric and histological techniques with work focusing on the epiphyseal growth plate.

2. **To analyse bone homeostasis in *Creld2* bone-specific knockout mice**

   CRELD2 has been postulated to play a role in mesenchymal stem cell BMP9-induced osteogenic differentiation (Zhang et al., 2013a). It is therefore hypothesised that that ablation of *Creld2* in osteoblasts will result in impaired osteoblast activity and therefore affect bone homeostasis. The bone pathology of *Creld2* bone-specific knockout mice was therefore analysed using various morphometric and histological techniques to analyse bone structure and cellular parameters of bone.

3. **To investigate the molecular cell pathology and dysregulated pathways following the ablation of CRELD2 in chondrocytes and mature osteoblasts**

As CRELD2 functions as a molecular chaperone and putative PDI, it is hypothesised that the ablation of CRELD2 will result in impaired protein folding and have implications on the integrity of chondrocytes and osteoblasts (Hartley et al., 2013). Several histological techniques were therefore used to investigate the effect of the deletion of *Creld2* on chondrocyte and osteoblast function. The expression of differentially expressed genes in knockout cells was analysed by OMICs techniques in order to deduce the dysregulated pathways contributing to the skeletal pathologies in knockout mice.

Chapter 2. Materials and methods

Chapter 2. Materials and methods

2.1 Materials

All chemicals came from **Sigma-Aldrich** unless otherwise stated.

The sources of the antibodies used are outlined in Appendix D.

Thapsigargin, Protein A Sepharose®, Anti-V5 tag antibody (Agarose), Fluoroshield mounting media with DAPI were supplied by **Abcam**.

AbD Serotec supplied the donkey serum.

Molecular sieves 4A 2-12 mesh were obtained from **ACROS Organics™**.

The Agilent RNA 6000 Nano kit was supplied by **Agilent.**

Power SYBR® Mastermix was acquired from **Applied Biosciences**.

10X Biomix™ Red and Hyperladder™ 100 bp came from **Bioline**.

The 0.1 M sodium cacodylate buffer was supplied by the **Electron Microscopy Research Services Unit at Newcastle University**.

Primers were obtained from **Eurofins Genomics.**

Yeast, agar, tryptone, xylene and paraffin wax with added polymers (melting point 62 ºC) came from **Fisher Scientific**.

Vivaspin® 500 MWCO 5,000 Da centrifugal concentrators and Cell Proliferation Labelling Reagent (Bromodeoxyuridine (BrdU) were bought from **GE Healthcare**.

REVERT™ Total protein stain came from **LI-COR®**.

Active basic aluminum oxide 60 and 0.22 μm Millex-GP Syringe Filter Units came from **Merck Millipore**.

Histo-clear® came from **National Diagnostics**.

Ethylenediaminetetraacetic acid (EDTA), 5-bromo-4-chloro-3-indolyl-β-D-galactopyranoside (X-Gal), DeadEnd™ Fluorometric TUNEL System, proteinase K,

The ReliaPrep™ RNA Tissue and Cell Miniprep Systems, GoScript™ Reverse Transcription System, restriction enzymes were obtained from **Promega**.

Qiagen supplied the QIAquick PCR Purification Kit, the QIAquick Gel Extraction Kit and the QIAGEN Plasmid Midi Kit.

Recombinant mouse RANKL, recombinant mouse MCSF, the Mouse TRANCE/RANKL/TNFSF11 Quantikine ELISA Kit and the MOUSE Osteoprotegerin/TNFSF11B Quantikine ELISA Kit were purchased from **R&D systems**.

The Pierce bicinchoninic acid kit, 4.0-12.0 % NuPAGE® Bis-Tris precast gels, Wheat Germ Agglutinin Alexa Fluor™ 594 Conjugate, OCT, Lipofectamine® 2000, Gibco® Geneticin® Selective Antibiotic, HistoMount™ mounting solution, GIBCO® Hank's Balanced Salt Solution, GIBCO® Dulbecco's Phosphate-Buffered Saline no calcium no magnesium, GIBCO® Dulbecco's Modified Eagle Medium (DMEM) high glucose high pyruvate, GIBCO® DMEM/F-12 Media-GlutaMAX™-I, GIBCO® Minimum Essential Medium Eagle Alpha Modification (MEMα) nucleosides no ascorbic acid, GIBCO® Opti-MEM® I Reduced-Serum Medium, Gibco® Penicillin-Streptomycin (10,000 U/mL), Gibco® MEM Non-Essential Amino Acids, Gibco® Fetal Bovine Serum, qualified E.U.-approved South America origin and Gibco® 0.05 % Trypsin-EDTA, T4 DNA ligase and the DH5α™ competent cells were supplied by **Thermo Fisher Scientific**.

Vectamount™ AQ mounting media was obtained from **Vector Laboratories**.

Acetic acid, ethanol (EtOH) and methanol, hydrochloric acid (HCl) were purchased from **VWR**.

2.2 Generation, maintenance and characterisation of the mouse models

2.2.1 Generation of the mouse models

2.2.1.1 Origin of mouse models

Conditional knockout mouse models were previously generated by Dr Sarah Edwards (University of Manchester).

Briefly, *Creld2*-targeted mouse embryonic stem cell clones, *Creld2*$^{tm1a(EUCOMM)Hmgu}$, were obtained from the European Conditional Mouse Mutagenesis Programme (EUCOMM) and were used to generate chimeras, which were bred onto the C57BL/6J background. The *Creld2* targeting construct contains both FRT and LoxP sites for *Flp* and *Cre* recombination respectively (Figure 20A.). In order to knockout *Creld2* expression, mice heterozygous for this targeting construct were crossed with *Actin-flp* mice generating offspring with the conditional *Creld2* allele (Figure 20B.). These mice were then bred onto mice expressing the *Cre* transgene to generate *Creld2* conditional knockout mice by *Cre recombination* resulting in the deletion of exons 3-5 in *Creld2*. (Figure 20C.)

In order to generate conditional knockout mice, *Cre* expression was driven under specific promoters. To generate cartilage-specific and bone-specific knockout mice *Cre* expression was driven under the *Collagen Type II Alpha I Chain* (*Col2-Cre*) or *Osteocalcin* (*OC-Cre*) promoters respectively. This successfully knocks out *Creld2* expression at the translational level as shown previously using a global *Cre* mouse (Figure 20F, Sarah Edwards, Unpublished data.). Knockout mice were analysed either against *Creld2 wt/wt; Cre* + or *Creld2 fl/fl; Cre*- control mice for each strain.

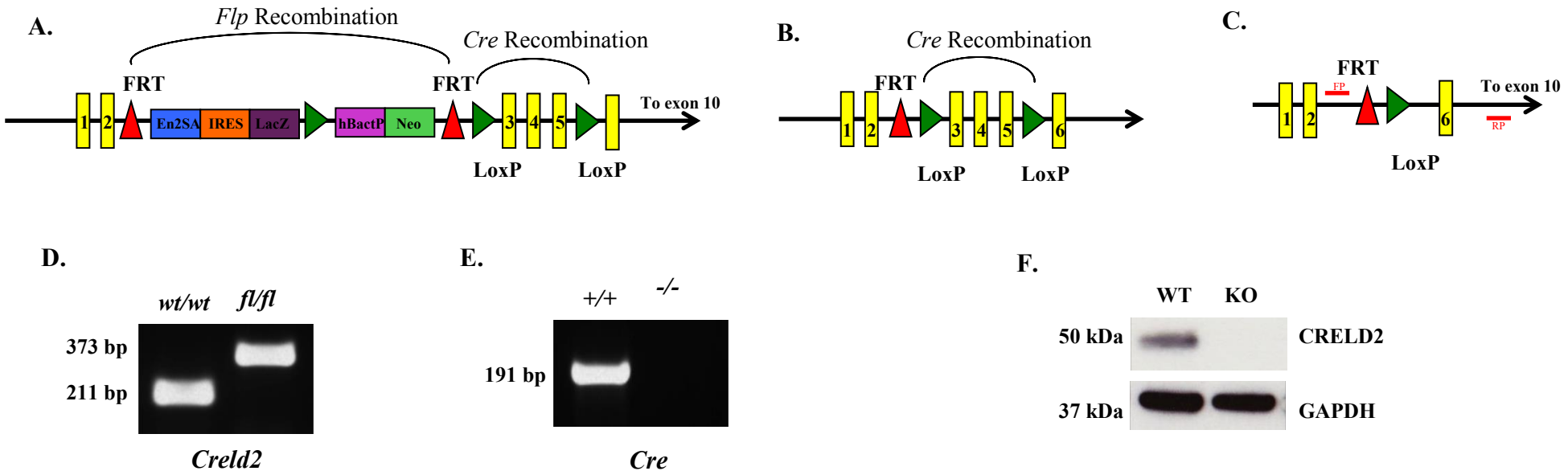

Figure 20. **Breeding strategy for the *Creld2* knockout mice.**

Creld2-targeted mouse stem cells were used to generate chimeras, which were bred onto the C57BL/6 background (**A**.). In order to knockout *Creld2* expression, mice heterozygous for this targeting construct were crossed with *Actin-flp* mice, resulting in Flp-FRT recombination and the generation of offspring with the conditional *Creld2* allele (**B**.). These mice were then bred onto *Cre* expressing mice to generate *Creld2* knockout mice by Cre-LoxP recombination resulting in the deletion of exons 3-5 in *Creld2.* The position of the forward (FP) and reverse (RP) genotyping primers are shown by the red lines (**C**.). *Creld2*$^{fl/fl}$ mice are identified by a band at 373 base pairs and *Creld2*$^{wt/wt}$ mice are identified by a band at 211 base pairs (**D**.*).* A separate PCR was then carried out to determine *Cre* genotype due to the presence or absence of a band at 191 base pairs (**E**.). CRELD2 is successfully knocked-out by *Cre* recombination as shown by the western blot of liver tissue from a global *Creld2* knockout mouse line (Image courtesy of Dr Sarah Edwards) (**F.**).

2.2.1.2 Animal husbandry

Mice were housed in ventilated cages in the Functional Genomics Unit (FGU) at Newcastle University where they experienced a 12 hour light-dark cycle and obtained food *Ad libitum.* All protocols were carried out according to Directive 2010/63/EU of the European Parliament, under project licence 60/4525. Local ethical approval was provided under The Animals (Scientific Procedures) Act (ASPA) 1986.

2.2.2 Genotyping the mouse models

2.2.2.1 HotSHOT DNA extraction

Ear or tail biopsies were incubated in 75 μL alkaline lysis buffer pH 12 for 30 minutes at 95 °C. Samples were then cooled to 4 °C and incubated for a further 10 minutes in order to extract genomic DNA via the HotSHOT method. Following this incubation, 75 μL neutralising buffer pH 5 was added to each sample. Prior to use in PCR reactions, samples were centrifuged full speed for 2-3 minutes. To accurately determine the concentration of genomic DNA samples a Nanodrop® 1000 spectrophotometer was used. The Nanodrop® was blanked with a 50:50 solution of alkaline buffer : neutralising buffer. All solutions are outlined in Appendix A.

2.2.2.2 Genotyping PCR

A typical PCR reaction mix contained 2x Biomix™ Red and 10 pmol of forward and reverse primers (Appendix B). Genomic DNA at a concentration of 150 – 300 ng/μL was added to each reaction. 18 MΩ dH2O was added to a final reaction volume of 20 μL. PCR reactions were carried out on a Labnet International MultiGene OptiMax thermal cycler. (For cycling conditions, see Appendix B).

Mice were genotyped using primers designed to analyse the presence of the *Cre* gene and to amplify a region in the *Creld2* gene (Appendix B).

2.2.2.3 Agarose gel electrophoresis

Agarose gel electrophoresis was carried out to analyse DNA fragment sizes. Samples were separated on a 1.5-2.0 % (w/v) agarose gel in 1x Tris-Base, acetic acid and EDTA (TAE) buffer (Appendix A). 5 μL of Hyperladder™ 100 bp DNA ladder was used for size estimation of the DNA products. Ethidium bromide was used as the intercalating agent and was added to the molten gel at a concentration of 0.5 μg/mL, allowing for visualisation of DNA bands under UV light. Samples were electrophoresed at 110 V for 30 minutes before visualisation on a on a Bio-Rad Gel Doc System.

2.2.3 Characterising Cre expression using a Cre reporter mouse strain

Female mice that genotyped positive for the *Cre* transgene were bred onto the gene trap ROSA 26 (R26R) reporter mouse strain. These mice are homozygous for the *Gtrosa26*^{tm1Sor} targeted mutation consisting of a bacterial *β-galactosidase* gene flanked by two *loxP* sites. When bred with a *Cre* expressing strain, a DNA fragment that prevents transcription of the *lacZ* gene is removed and *lacZ* is expressed in the tissues expressing Cre recombinase. These mice can therefore be used to analyse the tissue expression pattern of the *Cre* transgene as β-galactosidase activity can therefore be assayed using X-gal, with activity marked by a blue stain.

2.2.3.1 LacZ staining of whole mount embryos and tissues

Col2-Cre embryos at embryonic stage 12.5 were dissected from pregnant *Col2-Cre* positive females that had been bred with an R26R male. Embryos were fixed for 15 minutes in fixing solution containing formaldehyde and glutaraldehyde at a final concentration of 2.0 % and 0.2 % (v/v) respectively.

One week old limbs from R26R;*Col2Cre+* and R26R;*OC-Cre+* mice were harvested and fixed in 10 % neutral buffered formalin solution (containing 4 % formaldehyde) for 4 hours at room temperature.

Following fixing the samples were washed twice at room temperature gently shaking in lacZ staining wash buffer containing 0.01 % sodium deoxycholate (v/v) and 0.02 % (v/v) Nonidet™ P-40. Embryos/Limbs were then placed in lacZ staining

solution containing 1 mg/ml (v/v) X-Gal and stained overnight in a humidified darkened chamber at 37 °C. After 24 hours the embryos/tissues were washed twice 1x PBS and fixed in 10 % neutral buffered formalin solution (containing 4 % formaldehyde) overnight. Samples were incubated in 1 % formaldehyde solution for long-term storage. All solutions are outlined in Appendix A.

Stained embryos (heterozygous for the *Gtrosa26*^{tm1Sor} targeted mutation and positive for the *Cre* transgene) were imaged using a Zeiss Axioplan2 bright field microscope before being embedded in OCT. Prior to embedding, limbs were decalcified by gentle agitation in 20 % EDTA pH 7.4 (Appendix A) for 3 days at room temperature.

Specimens were sectioned at 10 μm sections using Leica CM1860 Cryostat. Sections were then counterstained with eosin for 30 seconds before being dehydrated through a series of ethanol concentrations (50 %, 70 %, 90 % and 100 %). Slides were incubated in Histo-Clear® and mounted in HistoMount™ mounting solution and imaged using a Zeiss Axioplan2 bright field microscope.

2.3 Morphometric analysis of knockout mice

2.3.1 Whole body weights

Mice at 3, 6 and 9 weeks were anesthetised with isoflurane prior to weighing. Whole body weights were measured and allowed for monitoring of the growth rate. The average weight for each genotype at each time point and the subsequent standard error of the mean (SEM) was calculated in order to generate growth curves. A Student's unpaired *t*-test carried out using the online GraphPad tool was used to determine any significant difference in weight between the genotypes at the three time points.

2.3.2 Bone measurements

Mice at 3, 6 and 9 weeks were anesthetised using isoflurane and X-rayed using the Faxiton X-ray radiography system at 23 kV for 5 seconds. Raw data files were opened in the ImageJ 1.50c software and bone measurements (tibia, femur, inner canthal distance (ICD) and skull) were carried out using the measure tool (Measurements are outlined in Figure 21A). Intramembranous ossification was analysed by the ICD and the length of the skull. Endochondral ossification was analysed by the length of the tibiae and femurs. Average measurements of the right and left tibia and femur were calculated per mouse.

In order to visualise and analyse skull plates, 3-week-old skulls were stained with alcian blue and alizarin red to stain cartilage and mineralised bone respectively. First, skulls were dissected and fixed in 95 % ethanol for 48 hours. The skulls were then cleaned free from soft tissue and incubated in alcian blue staining solution (Appendix A) for 24 hours. Skulls were then fixed for a second time in 95 % ethanol for 48 hours. Soft tissue was digested from the skull with 1 % potassium hydroxide and the skulls were stained with alizarin red staining solution (Appendix A) for 24 hours. Skulls were then imaged using a Zeiss KL1500 LCD microscope. Images were opened in the ImageJ 1.50c software and measurements of skull plates were made (Measurements are outlined in Figure 21B). To statistically analyse the data obtained from bone measurements, a Student's unpaired *t*-test was carried out using the online GraphPad tool and the subsequent SEM was calculated.

A.

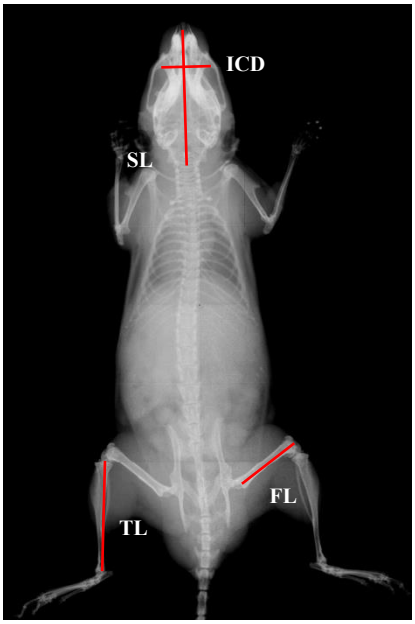

Measurements

1) ICD : Inner Canthal Distance

2) SL : Skull Length

3) FL : Femur Length

4) TL : Tibia Length

B.

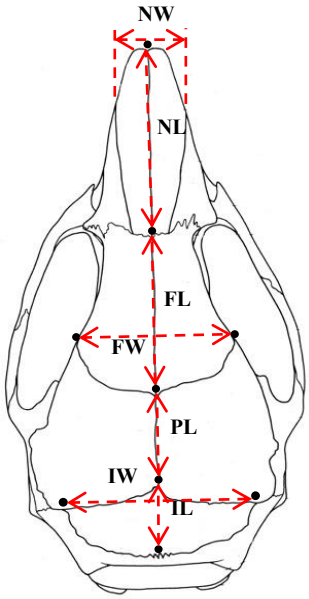

Measurements

1) NW : Nasal Bone Width

2) NL : Nasal Bone Length

3) FW : Frontal Bone Width

4) FL : Frontal Bone Length

5) PL : Parietal Bone Length

6) IW : Interparietal Bone Width

7) IL : Interparietal Bone Length

Figure 21. **Method for measuring bones and skull plates.**

Mice at 3, 6 and 9 weeks were X-rayed and bone measurements were made. The lengths of the tibia and femur were used to analyse endochondral ossification and intramembranous ossification was analysed by the length of the skull and the inner canthal distance (**A**.). To visualise skull plates, 3-week skulls were stained with alizarin red and alcian blue and measurements of the different skull plates, including measurements of the nasal bone, the frontal bone, the parietal bone and the Interparietal bone were made (**B**.).

2.3.3 Quantative bone morphology by micro-computed tomography (μCT)

2.3.3.1 Dissection and fixation of bones for μCT

Mice at 3, 6 or 9 weeks were sacrificed by cervical dislocation or carbon dioxide exposure according to Schedule 1 of the ASPA 1986. Hind limbs were sprayed with 70 % ethanol and the skin was removed around the circumference of the hip joint. The head of femur was then dislocated from the hip socket and removed from the mouse. The foot was removed from the ankle joint and the soft tissue removed. The femur and tibia were then separated, allowing for analysis of the tibia.

Following dissection, tibiae were fixed in 10 % neutral buffered formalin (containing 4.% formaldehyde) for 24 hours before being stored in 70 % ethanol in H_2O for long-term storage, until analysis by μCT.

2.3.3.2 X-Ray micro-computed tomography (μCT)

To analyse tibial bone structure, tibial bones from mice at 3, 6 and 9 weeks were subjected to μCT analysis. All scans were performed using the Sky Scan 1174v2 μCT machine in the Bone Biopathy lab ran by Professor Anna Teti at the University of L'Aquila (Italy). Bone specimens were placed in a sample vial filled with 70 % ethanol that was fixed to the rotating stage of the μCT X-ray chamber. Multiple 2D image projections were obtained with a rotation step of 0.3 ° and a spatial resolution of 6.74 nm. X-rays were obtained at 50 kV and 800 mA. 2D images for each bone were stacked and reconstructed using the NRecon (v1.6.4.1) programme producing a reconstructed 3D bone image.

2.3.3.3 Bone architecture analysis from 3D μCT images

The CTAn (v.1.16) programme was used to analyse the bone architecture from the reconstructed 3D bone images. In order to analyse trabecular bone, the region of interest (ROI) was set to analyse trabecular bone in a depth of 1000 μm, 675 μm from the top of the tibial growth plate. In order to analyse the cortical bone of the tibial shaft, the ROI was set at to analyse cortical bone in a depth of 675 μm, 3500 μm from the top of the tibial growth plate. If bones differed in size, these parameters were adjusted to

take size difference into account. For example, average tibial length from male *Creld2* cartilage-specific knockout mice was significantly smaller than control mice by 12.22 % and so the ROI parameters (depth and distance from the growth plate) were adjusted accordingly and reduced by 12.22 %. Reconstruction parameters were consistent between all samples and the higher and lower grey thresholding values were set at 62 and 255 respectively.

Results were subjected to statistical analysis using the Student's unpaired *t*-test carried out using the online GraphPad tool to determine differences in the bone structural parameters between control and knockout mice.

2.4 Histological and ultrastructural analysis of the cartilage growth plate

2.4.1 Tissue preparation for histological analysis of cartilage

Knee joints were dissected from 3-week-old mice as outlined previously. Joints were fixed for 24 hours at 4 °C in 4 % formaldehyde (histological staining) or 95 % ethanol; 5 % acetic acid (immunohistochemical (IHC) staining). In order to decalcify bones, limbs were immersed in 20 % (w/v) EDTA pH 7.4 (Appendix A) for two weeks with gentle agitation at room temperature.

Following decalcification, knee joints were washed with water before being processed overnight in a Thermo Scientific™ STP 120 Spin Tissue Processor (Appendix C). Tissue samples were then embedded in paraffin blocks and allowed to set over night.

Wax blocks were placed at -20 °C prior to sectioning. Legs were sectioned using a Thermo Scientific™ HM 355S automatic microtome to 6 μm sections (histology and immunohistochemistry) and 20 μm (immunohistochemical staining for cilia analysis using the Nikon A1R confocal microscope). Wax sections were fixed onto positively charged slides at 60 °C on a hot plate for 1 minute and left to air dry over night. Slides were matched and growth plates from 3 mice per genotype were analysed.

2.4.2 Hematoxylin and eosin (H&E) staining

Sectioned formaldehyde-fixed limb specimens were dewaxed in xylene and processed for H&E staining using the Thermo Scientific ™ Linestat™ Slide Stainer.

Briefly, slides were rehydrated through a series of decreasing ethanol concentrations (100 %, 90 %, 70 % and 50 %), followed by a rinse in tap water. Slides were then immersed in filtered Harris modified haematoxylin for 20 seconds before being rinsed in water. To remove excess stain, slides were then incubated for 20 seconds in 1 % acid alcohol (Appendix A) followed by a water rinse, retaining nuclear staining only. Slides were then incubated in filtered Alcoholic eosin Y for 20 seconds, staining the cytoplasm, and rinsed in water to remove excess stain. Following staining, slides were then dehydrated through increasing concentrations of ethanol (50 %, 70 %, 90 %, 100 %) and placed in xylene before being mounted using Vectamount™ AQ

mounting media. Once dry sections were imaged using a Zeiss Axioplan2 bright field microscope.

2.4.3 Toluidine blue staining

Toluidine blue staining of the cartilage growth plate was used to analyse sulphated proteoglycans. Sectioned formaldehyde-fixed limb specimens were dewaxed in xylene and processed for toluidine blue staining using the Thermo Scientific ™ Linestat™ Slide Stainer.

First, sections were rehydrated to water through a series of decreasing ethanol concentrations as described previously. Slides were then incubated in 0.04 % toluidine blue pH 3.75 (Appendix A) for 40 seconds. To remove excess stain, slides were rinsed twice in water before being incubated in Nuclear Fast Red solution for 20 seconds to counterstain the nuclei. Following two rinses in tap water, sections were dehydrated in 90 % and 100 % ethanol for 20 seconds each incubation, placed in xylene and mounted using Vectamount™ AQ mounting media. Once dry, sections were imaged using a Zeiss Axioplan2 bright field microscope.

2.4.4 Picrosirius red staining

Collagen fibrils within the cartilage growth plate were visualised using picrosirius red staining. Under polarised light, picrosirius red staining enhances the birefringence of collagen and collagen fibrils appear red, orange, yellow or green depending on the thickness of the fibril, decreasing in thickness from red to green.

For picrosirius red staining, the slides were dewaxed in xylene then taken to distilled water through a series of decreasing ethanol concentrations as outlined previously. The slides were then incubated in Harris modified haematoxylin for 20 minutes. Excess stain was removed by washing slides in running tap water for 20 minutes. Picrosirius red stain was then applied to sections and incubated for 1 hour. Slides were then washed in two changes of 0.5 % (v/v) acidified water and dehydrated through three changes of 100 % ethanol. The alcohol was then cleared by immersing the slides in xylene and samples were mounted using Vectamount™ AQ mounting media.

Once dry, sections were imaged at 200x magnification using transmitted polarised light with a Leica DM2700 P polarising microscope.

2.4.5 Immunohistochemistry

3-week-old legs were fixed, decalcified, processed, embedded and sectioned as described previously. Sections were dewaxed in xylene and dehydrated through a decreasing ethanol series (100 %, 90 %, 70 %, 50 %) and washed in water. To unmask epitopes, sections were incubated in 0.2 % (w/v) bovine hyaluronidase in 1x phosphate buffered saline (PBS) at 37 °C in a humidified chamber for 30 minutes. Slides were then washed in 1x PBS, incubated in 0.2 % (v/v) Triton-X for 5 minutes and 20 µg/mL proteinase K in 1x PBS for 5 minutes at room temperature, washing with 1x PBS in between unmasking steps. Samples were blocked in donkey serum in a 1 % (w/v) bovine serum albumin (BSA) solution in 1x PBS solution for 1 hour at room temperature. Sections were then incubated overnight at 4 °C in primary antibodies diluted in 1x PBS (Appendix D). Slides were then washed in 1 % BSA/1x PBS and incubated at room temperature with secondary antibodies diluted in donkey serum/1 % BSA. Slides were washed in 1x PBS before being dehydrated in increasing ethanol concentrations and mounted in Fluoroshield Mounting Media with DAPI. All solutions are outlined in Appendix A. Antibody dilutions are outlined in Appendix D.

Slides were imaged on a Zeiss Axioimager 2 microscope at 200x magnification using the DAPI and corresponding AlexaFluor™ filter sets.

In order to analyse primary cilia of chondrocytes in the growth plate, an anti-acetylated tubulin primary antibody was used on 20 nm sections. Following immune labelling, sections were imaged using a Nikon A1R confocal microscope. Overlapping sequential images were taken at 630x magnification and the images were reconstructed into a 3D chondron. The length of primary cilia were analysed using the ImageJ Skeleton Tool in the ImageJ 1.50c software. Cilia were analysed on matched slides from 3 mice per genotype. A Student's unpaired *t*-test was then carried out using the online GraphPad tool and statistical significance was given as $p<0.05$.

2.4.6 Bromodeoxyuridine (BrdU) labelling

3-week-old mice were injected subcutaneously with BrdU labelling reagent according to weight (0.1 ml per 10 g). Two hours after injection, mice were sacrificed by cervical dislocation according to Schedule 1 of the ASPA 1986. Limbs were fixed for immunohistochemistry, decalcified, processed, embedded and sectioned as outlined previously.

Immunohistochemistry was preformed to detect BrdU labelled cells. Briefly, slides were dewaxed in xylene then rehydrated to water through a decreasing ethanol series (100 %, 90 %, 70 %, 50 %). To unmask antigens, slides were incubated in 4.0 M hydrochloric acid for 15 minutes. Slides were then placed in 0.1 M borate buffer for 5 minutes to stop the reaction. Slides were then blocked donkey serum in a 1 % (w/v) bovine serum albumin (BSA) solution 1x PBS solution for 1 hour at room temperature and immunohistochemical process continued as outlined previously using an anti-BrdU primary antibody (Appendix D). Slides were mounted using the Fluoroshield Mounting Media with DAPI and allowed to dry in a dark box overnight. Slides were then imaged on a Zeiss Axioimager 2 microscope at 200x magnification using the DAPI and AlexaFluor™488 filter sets. Images were tiled and stitched using the Zen 2 software.

Raw images were opened in Fiji (ImageJ), colour channels were split and images were converted to grey scale. BrdU positive cells were counted using the Watershed Segmentation algorithm on the Fiji program and expressed as a percentage of total cells within the proliferative zone.

Analysis was performed on 3 matched slides per mouse, from 3 mice per genotype. A Student's unpaired *t*-test carried out using the online GraphPad tool and statistical significance was given as $p<0.05$.

2.4.7 Terminal deoxynucleotidyl transferase deoxyuridine triphosphate (dUTP) nick end labelling (TUNEL) assay

The DeadEnd™ Fluorometric TUNEL System was used to analyse cell death on formaldehyde fixed samples. The TUNEL assay was performed according to manufacturer's instructions. First slides were dewaxed in xylene and rehydrated through a series of decreasing ethanol concentrations as outlined previously. Samples were

incubated in 0.85 % sodium chloride (w/v) for 5 minutes then washed twice in 1x PBS. Specimens were fixed in 4 % methanol-free formaldehyde (v/v) in 1x PBS for 15 minutes at room temperature then washed twice again in 1x PBS. For Antigen unmasking a citric buffer pH 6 boil was performed. This was a deviation from the protocol that uses proteinase K to unmask antigens as proteinase k treatment has been shown to result in false positives due to the release of endogenous endonucleases (Stähelin et al., 1998). Samples were allowed to equilibrate to room temperature for 30 minutes before being washed again in 1x PBS, followed by a second fixing step in 4 % methanol-free formaldehyde (v/v) in 1x PBS. Samples were washed again in 1x PBS and incubated in equilibration buffer for 10 minutes at room temperature. Specimens were then incubated in labelling solution at 37 °C in a humidified chamber for 60 minutes as outlined in the manufacturer's instructions. Labelling was terminated by immersion of the slides in 2x saline sodium citrate (SSC) buffer. Samples were then washed and dehydrated through a series of ethanol concentrations and mounted in Fluoroshield Mounting Media with DAPI. All solutions are outlined in Appendix A.

Once dry, slides were imaged on a Zeiss Axioimager 2 microscope at 200x magnification using the DAPI and the AlexaFluor™488 filter sets. Images were tiled and stitched using the Zen 2 software.

Raw images were opened in Fiji, colour channels were split and images were converted to grey scale. TUNEL positive cells from each zone were counted using the Watershed Segmentation program in the Fiji program and were expressed as a percentage of total cells within the each zone (resting zone, proliferative one and hypertrophic zone).

Analysis was performed on 3 matched slides per mouse, from 3 mice per genotype. A Student's unpaired *t*-test carried out using the online GraphPad tool and statistical significance was given as $p<0.05$.

2.4.8 Transmission electron microscopy (TEM) for ultrastructural analysis of the growth plate

Tibial cartilage from one week old pups was dissected and fixed in overnight in 2 % (v/v) glutaraldehyde in 0.1 M sodium cacodylate buffer at 4 °C. The following

protocol was then performed by the Electron Microscopy Research Services Unit at Newcastle University.

Cartilage samples were then washed three times in 0.1 M sodium cacodylate buffer for 30 minutes each wash, then fixed a second time for 1 hour at room temperature in 2 % (w/v) osmium tetroxide in distilled water. Tissues were then rinsed twice in water and immersed in 2 % uranyl acetate for 2 hours, and rinsed twice again in water before being washed with 25 %, 50 %, 75 % acetone for 30 minutes each wash. Samples were then incubated in two changes of 100 % acetone, for 1 hour each wash and embedded using the TAAB epoxy resin kit according to manufacturers specification. To allow for resin to fully penetrate the tissues, samples were incubated in 100% resin for 2 days. Tibial cartilage samples were then placed in a mould and resin was polymerised overnight at 60 °C.

Following embedding, samples were sectioned to ultrathin sections of 70 nm using a diamond knife on a Leica EM UC7 ultramicrotome, stretched with chloroform and mounted onto Pioloform-filmed copper grids. Prepared grids were the stained with 2 % aqueous uranyl acetate and lead citrate solution.

Grids were then photographed using a Phillips CM100 Transmission Electron Microscope.

2.5 Bone histomorphometry

2.5.1 Tissue preparation for histological analysis of bone

Bones were dissected as previously described and subjected to μCT analysis. Following μCT, bones were dehydrated through a series of ethanols (70 %, 90 %, 100 %), placed in methyl methacrylate (MMA) Embedding Solution 1 and incubated overnight at 4 °C. Bones were transferred to MMA Embedding Solution 2 for a further 24 hours at 4 °C before being embedded in MMA Embedding Solution 3. Polymerisation of MMA was aided by immerging samples in water for at 4 °C for 48 hours.

Samples were cut to 5 μM sections on a Thermo Scientific™ HM 355S automatic microtome using a Shandon™ tungsten carbide D-profile knife. To aid in cutting a cutting solution was applied to the cutting surface of the tissue. Following collection of sections onto positively charged slides, stretching solution was applied to sections and incubated for 5 minutes. This was repeated three times before slides were cover slipped with plastic coverslips, sandwiched together and held firmly with G-clamps. Slides were placed at 62 °C in an oven for 72 hours to ensure sections stuck to the slides. All solutions are outlined in Appendix A.

2.5.2 Von Kossa staining

In order to analyse calcification of bone by histology, von Kossa/van Geison staining was performed. Slides were first deplastified with 2-methoxyethyl-acetate (AME) before being rehydrated in decreasing concentrations of ethanol (100 %, 90 %, 70 %, 50 %). Slides were then incubated in a 1 % (w/v) silver nitrate for 10 minutes before being washed for 10 minutes in deionised water. To reduce the silver nitrate, sections were then incubated in a sodium formamide solution for 5 minutes. Slides were then washed in tap water for 10 minutes. To remove unreacted silver nitrate, slides were incubated in 5 % sodium thiosulphate. Following a 10 minute wash in tap water, specimens were then dehydrated through an increasing ethanol series (50 %, 70 %, 90 %, 100 %) and cleared in xylene before being mounted in Vectamount™ AQ mounting media. All solutions are outlined in Appendix A.

Slides were then imaged using a bright field camera on a Zeiss Axioimager 2 microscope at a magnification of 200x. Images were tiled and stitched using the Zen 2 software.

An area of length 300 μM, 100 μM from the bottom of the growth plate, was analysed. Analysis was performed on matched sections from 5 mice per genotype. A Student's unpaired *t*-test carried out using the online GraphPad tool and statistical significance was given a $p<0.05$.

2.5.3 Toluidine blue staining for analysis of osteoblasts

In order to analyse osteoblasts on trabecular bone surface, bones were stained with toluidine blue. Sections were first deplastified in AME and rehydrated in a decreasing ethanol series as outlined previously. Bone sections were then stained with 1 % toluidine blue pH 4.5 for 2 minutes. Slides were washed with water to remove excess stain, dehydrated in an increasing ethanol series as outlined previously and placed in xylene prior to mounting with Vectamount™ AQ mounting media. All solutions are outlined in Appendix A.

Bones were imaged using a bright field camera on a Zeiss Axioimager 2 microscope at a magnification of 200x. Images were tiled and stitched using the Zen 2 software.

Osteoblasts were analysed in an area of length 300 μM, 100 μM from the bottom of the growth plate. Analysis was performed on matched sections from 5 mice per genotype. A Student's unpaired *t*-test carried out using the online GraphPad tool and statistical significance was given a $p<0.05$.

2.5.4 Tartrate-resistant acid phosphatase (TRAcP) staining for analysis of osteoclasts

To analyse osteoclasts, a TRAcP stain was performed. The bones were deplastified in AME and rehydrated in ethanol as described above. 1.125 mL of TRAcP solution 2 was added to 112.5 mL of preheated TRAcP solution 1. Slides were then placed in this solution and incubated at 37 °C for 45 minutes. Before the end of the 45-minute incubation, 2.25 mL of TRAcP solution 3 was mixed with 2.25 mL of TRAcP

solution 4 by inversion and left to sit for 2 minutes. This solution was then added to a second staining pot of preheated solution 1. Slides were incubated in this solution for ten minutes. Slides from all replicates were stained at the same time to standardise staining. Slides were then mounted in CC/Mount™ tissue mounting medium. All solutions are outlined in Appendix A.

Bones were imaged immediately using a bright field camera on a Zeiss Axioimager 2 microscope at a magnification of 200x. Images were tiled and stitched using the Zen 2 software.

Osteoclasts were analysed in an area of length 300 μM, 100 μM from growth plate. Analysis was performed on matched sections from 5 mice per genotype. A Student's unpaired *t*-test carried out using the online GraphPad tool and statistical significance was given a $p<0.05$.

2.5.5 Dynamic histomorphometry

2.5.5.1 In vivo alizarin complexone/calcein lablleling

In order to analyse the dynamic properties of bone, mice were restrained and injected in the intraperitoneal cavity 1-week prior and 1 day prior to sacrifice with 30 mg/kg alizarin complexone and 20 mg/kg calcein in 2 % (w/v) sodium bicarbonate pH 7.4 solution respectively. All mice were euthanised at 9 weeks of age by cervical dislocation according to Schedule 1 procedures of the ASPA 1986. Tibial bones were then harvested and fixed in 4 % formaldehyde. These bones were then processed, embedded and sectioned as outlined previously.

2.5.5.2 Analysis of dynamic parameters of bone

Slides were deplastified in AME and rehydrated through a series of ethanol concentrations as described previously. Samples were then mounted in Canada balsam mounting media and imaged on a Zeiss Axioimager 2 microscope using the Alizarin complexone (Excitation and emission wavelengths: 495/515 nm) and calcein (Excitation and emission wavelengths: 530-560/580 nm) filter sets. Images were tiled and stitched using the Zen 2 software.

An area of length 300 μM, 100 μM from the bottom of the growth plate, was analysed. Analysis was performed on matched sections from 5 mice per genotype. The bone surface (BS), mineralising surface (MS), mineral appositional rate (MAR) and bone formation rate (BFR) was calculated for each mouse. The mineral appositional rate defines the linear rate of bone formation and is calculated by the average distance between the labels divided by the interval between labelling. The bone formation rate describes the amount of new bone formed per unit of time per unit of bone surface and is calculated by dividing the MAR by the mineralising surface (the length of double labelling/bone surface). A Student's unpaired *t*-test was carried out using the online GraphPad tool and statistical significance was given a $p<0.05$.

2.6 Primary cell extraction, culture and analysis

2.6.1 Extraction and culture of primary chondrocytes

Primary chondrocytes were isolated following digestion of 5-day-old costal and tibial cartilage with collagenase IA. First, costal and tibial cartilage is dissected from the bone and incubated in 2.5 mg/mL collagenase IA chondrocyte digest solution (Appendix A) at 37 °C for 45 minutes to remove soft tissue. Tissues were then scraped clean of soft tissue and incubated in a fresh aliquot of collagenase IA solution for 3-4 hours at 37 °C, vortexing every 30 minutes.

To isolate chondrocytes, the collagenase solution was then transferred to a 50 mL falcon tube, pipetted several times to dissociate the cells from the digested cartilage and passed through a cell strainer. Chondrocyte growth media, which contains 10% fetal bovine serum (FBS) was then passed through the cell strainer to quench the action of collagenase. Primary chondrocytes were then pelleted by centrifugation at 500 g for 5 minutes. The chondrocyte cell pellet was washed in PBS followed by a further centrifugation step at 500 g for 5 minutes. Chondrocyte number per mL was determined using FastRead 102 disposable counting slides. Primary chondrocytes were subsequently plated accordingly for experimental use and cultured in an incubator at 37 °C, 5 % carbon dioxide in chondrocyte growth media (Appendix E).

2.6.2 Extraction and culture of primary osteoblasts

Primary osteoblasts were isolated from 1-week-old neonatal calvarias by sequential enzymatic digestion of the bone matrix (Bakker and Klein-Nulend, 2012). First, calvariae were dissected from skulls and placed in osteoblast digest solution containing 1 mg/mL collagenase IV and 2.5 mg/mL trypsin (Appendix A). Calvariae were then incubated at 37 °C with gentle agitation for 15 minutes (Digest 1). Digest solution was then removed and calvariae were washed with Hank's buffered saline solution (HBSS). Following sequential enzymatic digestion osteoblasts were released from the bone matrix. Calvariae were then incubated in fresh digest solution at 37 °C with gentle agitation for 30 minutes (Digest 2). Cells from digest 2 were pelleted by centrifugation at 500 g for 5 minutes. The cell pellet was resuspended in bone cell growth media (Appendix E) and cultured in an incubator at 37 °C, 5 % carbon dioxide. Calvariae were incubated in fresh digest solution at 37 °C with gentle agitation for 45

minutes (Digest 3). Cells from digest 3 were pelleted by centrifugation at 500 g for 5 minutes. The cell pellet was resuspended in bone cell growth media (Appendix E) and cultured in an incubator at 37 °C, 5 % carbon dioxide. Growth media was changed after 3 hours in culture to avoid contaminating cells adhering to plastic.

After 24 hours in culture osteoblasts were trypsonised and osteoblast number per mL was calculated. Primary osteoblasts were subsequently plated accordingly for experimental use (T25 flask: 0.5 x 10^6 cells, 6-well plate: 0.3 x 10^6 cells) and cultured in an incubator at 37 °C, 5 % carbon dioxide in bone cell growth media.

For osteoclastogenesis, osteoblast conditioned media was used. In order to collect conditioned media, osteoblasts were cultured in serum-free bone cell growth media for 72 hours. The media was then collected and filtered using a 0.22 μm filter and frozen at -80 °C until required. The osteoblast-conditioned media was then diluted in a 50:50 ratio with bone cell media prior to use.

2.6.3 Extraction and differentiation of pre-osteoclasts

Primary osteoclast precursors were isolated as outlined by Marino *et al.* (Marino et al., 2014). Briefly, primary osteoclast precursors were isolated from the bone marrow of 1-week-old neonatal hind limbs and fore limbs by homogenisation of the long bones. First, the fore limbs and the hind limbs were dissected from mice and cleaned free of soft tissue. The bones were then finely chopped in Dulbecco's phosphate-buffered saline (DPBS) using a sterile scalpel and the bone marrow was mechanically isolated from the bone by repeated pipetting. This process was repeated 5 times and the medium containing hematopoietic and stromal cells was collected each time and combined. The cell suspension was filtered through a Corning® 70 μm nylon cell strainer and pelleted by centrifugation at 300 g for 3 minutes and resuspended in DPBS containing 2 % (v/v) FBS. The bone marrow mononuclear cell fraction was separated from blood using Histopaque®-1077. In brief, 10 mL of the cell suspension was layered over 10 mL Histopaque®-1077 solution and centrifuged for 15 minutes at 200 g. The sample was then layered into two phases with erythrocytes and granulocytes sedimenting at the bottom and the bone marrow mononuclear cells at the interphase between the two layers. The bone marrow mononuclear cells were then pelleted by centrifugation at 200 g for 5 minutes and resuspended in bone cell growth media (Appendix E) supplemented

with 30 ng/mL MCSF. Cells were cultured in an incubator at 37 °C, 5 % carbon dioxide for 3 days with no disturbance.

After 3 days the monolayer was washed 3 times with DPBS, scraped in ice cold DPBS and centrifuged at 300 g for 3 minutes. The osteoclast precursor number per mL was calculated and cells were subsequently plated accordingly for experimental use (12-well plate: 0.1 x 10^6 cells) and cultured in an incubator at 37 °C, 5 % carbon dioxide in bone cell growth media supplemented with 30 ng/mL MCSF.

To analyse the effect of primary osteoblast conditioned media on osteoclastogenesis, pre-osteoclasts were isolated following the above protocol and after 24 hours in culture, the media was replaced with osteoblast-conditioned media supplemented with 30 ng/mL MCSF and 100 ng/µL RANKL to differentiate osteoclast precursors into mature osteoclasts. Media was then changed every two days for one week.

2.6.4 Lysate collection and western blotting

To collect protein lysates, cells in monolayer were washed three times with PBS. 1x RIPA buffer was then added to the cells that were immediately scraped from the flask and kept on ice for 15 minutes. The cells were then lysed by exchanging the eppendorf between liquid nitrogen until frozen and a water bath at 37 °C until defrosted, followed by thorough vortexing. To remove cellular debris, samples were centrifuged at 20,000 g for 10 minutes at 4°C and supernatant collected. Protein concentration in the cell lysates were then determined using the Pierce™ bicinchoninic acid assay (BCA) Assay kit according to manufacturer's instructions.

Protein expression in cell lysates was analysed by western blotting. Briefly, samples containing 50 ng of protein were made to a total of 25 µL in 5x sodium dodecyl sulphate (SDS)-PAGE sample buffer containing 0.05 M Dithiothreitol (DTT) (for reducing conditions) (Appendix A). Samples were denatured at 95 °C for 5 minutes before being loaded into a 4-12 % NuPAGE® Bis-Tris precast gel alongside a Precision Plus Protein™ dual colour protein marker. The gel was electrophoresed in MES SDS-PAGE running buffer for 50 minutes at 200 V. Proteins were then electroblotted onto a nitrocellulose membrane in 1x transfer buffer for 1 hour at 30 V. To confirm equal loading of the gel and the efficiency of transformation, the membrane was stained with

LI-COR® REVERT™total protein stain according to manufacturers instructions. To prevent non-specific antibody binding the membrane was then blocked for one hour in a 3 % (w/v) solution of semi-skimmed powdered milk in 1x PBS-T. The membrane was then incubated overnight in the required concentration of primary antibody in a 3 % (w/v) powdered milk/PBS-T solution at 4 °C. The primary antibody solution was removed from the membrane and the membrane washed three times for 5 minutes in 1x PBS-T. The membrane was then incubated at room temperature with the appropriate LI-COR® IRDye® 800W secondary antibody in a 5 % (w/v) powdered milk/PBS-T solution for 1 hour. This incubation was followed by three 15 minute washes in PBS-T in order to remove excess secondary antibody before being imaged on the LI-COR® Odyssey CLx Imaging System. Densitometric analysis of the fluorescent protein bands was performed using the ImageJ 1.50c software and protein levels were presented relative to the protein loading. All buffers and solutions are outlined in Appendix A. Antibody dilutions are outlined in Appendix D.

2.6.5 Enzyme-linked immunosorbent assay (ELISA)

In order to analyse the expression of secreted OPG and RANKL in osteoblast conditioned media, an enzyme-linked immunosorbent assay was performed using the Mouse RANKL Quantikine ELISA kit and the Mouse Ostoprotegerin Quantikine ELISA kit from R&D systems as outlined in manufacturer's instructions.

Prior to analysis by ELISA, osteoblast conditioned media was concentrated using the Vivaspin® 500 MWCO 5,000 Da centrifugal concentrators. To concentrate, media was centrifuged in a fixed-angle centrifuge at 4 °C for 30 minutes at 15,000 g.

2.7 Immunocytochemistry

Primary chondrocytes were extracted as per the protocol outlined in Methods: "2.6.1. Extraction and culture of primary chondrocytes." Following extraction chondrocytes were seeded into Nunc® Lab-Tek® Chamber Slide™ at a concentration of 2.0 x 10^4 cells per well and cultured for 48 hours in chondrocyte growth media. After 48 hours, media was aspirated from the chondrocytes and monolayer was washed in DPBS. To fix cells, monolayer was incubated in 10 % neutral buffered formalin solution (containing 4 % formaldehyde) for 10 minutes at room temperature. The fixative was then removed and monolayer was washed twice in DPBS.

To analyse the localisation of CRELD2 within primary chondrocytes, immunocytochemistry was performed. First, to label the cell membrane cells were incubated with 5 µg/mL Wheat Germ Aggultinin AlexaFluor™647 conjugate for 10 minutes. Cells were then washed three times in 1x PBS. Chondrocytes were incubated in 0.5 % (v/v) Triton-X for 5 minutes to permeabilise the cells and then washed three times in 1x PBS. Cells were blocked for 1 hour in 10 % (v/v) donkey serum in 1x PBS at room temperature. The primary chondrocytes were then incubated in primary antibodies diluted in 1x PBS (Appendix D) for 1 hour at room temperature. Cells were then washed three times in 1x PBS before being incubated with secondary antibodies diluted in 10 % donkey serum (v/v) in 1x PBS for 1 hour at room temperature. The primary cells were washed in 1x PBS and mounted in Fluoroshield mounting media with DAPI. All solutions are outlined in Appendix A. Antibody dilutions are outlined in Appendix D.

Cells were then imaged using a Nikon A1R confocal microscope at a magnification of 630x.

2.8 Analysis of gene expression

2.8.1 Ribonucleic acid (RNA) extraction

Whole knee joints were dissected from 5 day old mice and frozen at -80 °C until required. To extract total RNA, the cartilaginous joints were flash-frozen in liquid nitrogen and placed in a cooled stainless steel vial containing a cooled stainless steel ball and frozen BL + TG buffer (Buffer contains: 4 M Guanidine thiocyanate, 0.01 M Tris (pH 7.5), 2 % 1-Thioglycerol. Supplied by the Promega ReliaPrep™ RNA Tissue Miniprep System). The joints were then homogenised using a Satoris Mikro-dismembrator S, shaking for 1 minute at 2000 RPM. Subsequently, RNA was extracted from the powdered tissue using the ReliaPrep™ RNA Tissue Miniprep System from Promega according to manufacturer's instructions. Resulting RNA was eluted in RNase free water.

RNA was also extracted from primary cells. Briefly, cells were trypsonised and pelleted by centrifugation at 1000 g for 5 minutes. Pellets were then snap-frozen in liquid nitrogen and frozen at -80 °C until required. To extract RNA from the cell pellet the ReliaPrep™ RNA Cell Miniprep System from Promega was used according to manufacturer's protocol. The resulting RNA was eluted in RNase free water.

The concentration and integrity of the extracted RNA was assessed using the Agilent RNA 6000 Nano chip according to the Agilent 2100 Bioanalyzer protocol. The RNA integrity number (RIN) was evaluated based on the 28S to 18S rRNA ratio by the software as a measure of RNA degradation, with a RIN of 1 being the most degraded and 10 being the most intact profile (Figure 22).

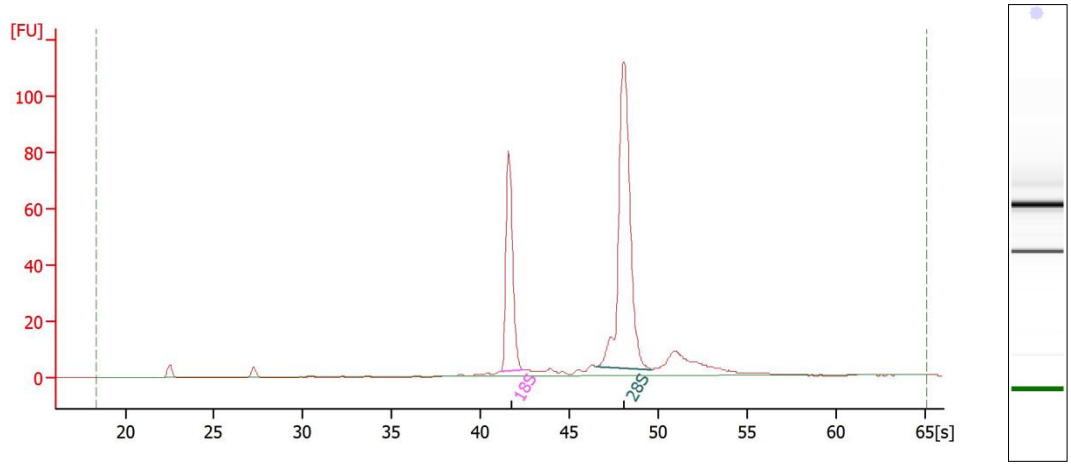

RIN 10.0

***Figure 22*. RNA integrity profiles from the Agilent 2100 Bioanalyzer.**

The Agilent 2100 Bioanalyzer is used to analyse the integrity of RNA through the generation of an electropherogram and a gel picture. The electropherogram gives an accurate quantification of RNA integrity based on the ration between the peak at 18S and 28S. With degradation there is a decrease in the ratio between the two ribosomal peaks and the baseline between the peaks increases. Several smaller bands are also seen on the gel picture if the RNA quality is low. From these results the Bioanalyzer generates a RIN number for the sample, with 1 being the most degraded and 10 being the most intact.

2.8.2 RNA sequencing (RNA-seq)

Extracted RNA from joint cartilage and extracted osteoblasts were analysed by RNA-seq. RNA from the cartilage of 2 mice per litter was pooled into one sample and RNA from osteoblasts was pooled from 6+ mice per litter. A total of 3 samples from 3 different litters per genotype was sent to GATC Biotech at a concentration of 1 μg total RNA with a RIN ≥ 8.

RNA was sequenced and analysed by GATC Biotech. Quality control statistics for samples are outlined in Appendix B. Briefly, RNA sequencing reads were aligned to the mouse reference genome using Bowtie generating genome/transcriptome alignments. TopHat was used to identify exon-exon splice junctions of the initial alignment. Then Cufflinks was used to identify and quantify the transcripts from the processed RNA-seq alignment assembly. Following this, Cuffmerge merged the identified transcripts to full-length transcripts and annotates the transcripts based on given annotations. Finally the merged transcripts from the two samples were compared using Cuffdiff to determine differential expression levels with a measure of significance between the samples. Several RNA-seq hits were confirmed by quantitative real time polymerase chain reaction (PCR) (qPCR) (Appendix B).

2.8.3 Reverse transcription polymerase chain reaction (RT-PCR) and quantitative polymerase chain reaction (qPCR)

cDNA was synthesised from the extract RNA using the GoScript™ Reverse Transcription System according to manufacturer's protocol. RNA was first combined with Oligo$(dt)_{15}$ and random primers, heated to 70 °C for 5 minutes then immediately placed on ice. This mix was used in the reverse transcription reaction mix to generate cDNA. 200 ng of osteoclast RNA, 250 ng of chondrocyte RNA and 800 ng of osteoblast RNA was used to generate cDNA in a final reaction volume of 20 μL containing 3.0 mM magnesium chloride, 0.5 μg Oligo$(dt)_{15}$ primers, 0.5 μg random primers, 1x GoScript™ reaction buffer, 20 units Recombinant RNasin® ribonuclease inhibitor and GoScript™ reverse transcriptase. Reverse transcription reactions were carried out on a Labnet International MultiGene OptiMax thermal cycler. Samples were incubated at 25 °C for 5 minutes, 42 °C for 1 hour and 70 °C for 15 minutes to anneal, extend and

inactivate the reverse transcriptase respectively. RNA was removed following the incubation with 1 µL RNase H for 20 minutes at 37 °C.

Quantitatve real time PCR (qPCR) was performed using the Power SYBR® Green method as outlined in manufacturer's instructions. A typical qPCR reaction mix contained Power SYBR® green and 10 pmol of forward and reverse primers (Appendix B). cDNA made directly from RT-PCR was added to each reaction (4 µL cDNA made from osteoclast RNA, 2 µL cDNA made from chondrocyte RNA, 1.5 µL cDNA made from osteoblast DNA). 18 MΩ dH2O was added to a final reaction volume of 50 µL. PCR reactions were carried out on a Bio-Rad DNA engine Peltier Thermal Cycler. (For cycling conditions, see Appendix B). Samples were ran in duplicate on each plate and the level of cDNA was normalised to the level of three housekeeping genes. The housekeeping genes used for osteoclast qPCR analysis were *Actb* (encoding β-actin), *B2m* (encoding β-2-Microglobulin) and *Hmbs* (encoding Hydroxymethylbilane Synthase) whereas the internal control genes used for osteoblast qPCR analysis were *Actb*, *Hmbs* and *Hprt1* (encoding Hypoxanthine Phosphoribosyltransferase 1) (Stephens et al., 2011). For chondrocyte qPCR analysis the housekeeping genes analysed were *18s*, *Hmbs* and *Gapdh* (encoding glyceraldehyde-3-phosphate dehydrogenase). Using the Opticon Monitor 3.1 programme, a C_T value was obtained for each sample and expressed as $2^{-\Delta CT}$ to determine gene expression relative to housekeeping genes (Table 1). The average fold expression value for each gene and the subsequent SEM was calculated. A Student's unpaired *t*-test carried out using the online GraphPad tool was used to determine any significant difference gene expression between the two genotypes.

Table 1. **Steps to calculate ΔΔCT analysis.**

Step	Calculation
1	Calculate the difference between Tested knockout and Housekeeping knockout (ΔCT Experimental) and Tested control and Housekeeping control (ΔCT Control)
2	Calculate ΔΔCT by the difference between ΔCT Experimental and ΔCT Control
3	Calculate $2^{-\Delta\Delta CT}$ to obtain expression fold change

2.9 Analysis of CRELD2 binding partners

2.9.1 Transfection and culture of ATDC5 cells with V5 tagged WT CRELD2

A V5-tagged wild type CRELD2 cDNA construct in pcDNA™3.1 (+) was previously generated by Dr Sarah Edwards (University of Manchester). This construct was used to overexpress V5-tagged CRELD2 in cartilage-like (SW1353) cells in order to identify binding partners of CRELD2. SW1353 cells were cultured in monolayer in the appropriate growth media until 70-80% confluent in an incubator at 37 °C, 5 % carbon dioxide. Cells were then transfected with 6 μg plasmid DNA using the Lipofectamine® 2000 transfection reagent in Opti-MEM® serum free media for 24 hours according to manufacturer's instructions. Media was then replaced with the appropriate growth media containing 450 ng/mL Geneticin® to select for transfected cells and obtain a stable cell line. To determine the optimum concentration of Geneticin® required for selection a kill curve was performed in which cells were grown in a range of Geneticin® concentrations and the lowest concentration in which all cells were dead within a week was selected.

Selecting media was replaced every 2-3 days for 14 days. Cultures were then maintained in the appropriate growth media containing 100 ng/mL Geneticin® and were passaged upon reaching confluency. The compositions of the growth medias are outlined in Appendix E.

2.9.2 Crosslinking and co-Immunoprecipitation (Co-IP)

Media was aspirated from V5-tagged CRELD2 transfected cells and protein-protein interactions were cross-linked by incubation in 1.0 mM dithiobis(succinimidyl propionate) (DSP) (Appendix A) for 10 minutes at room temperature. The reaction was stopped upon the addition of Tris-HCl pH 7.5 added to a final concentration of 20 mM and the incubation for 15 minutes at room temperature. The monolayer was then washed twice in water and cell lysates collected using 1x RIPA buffer (Appendix A). Cells in 1x RIPA buffer were immediately scraped from the flask and incubated at 4 °C under constant agitation for 30 minutes. To remove cellular debris, samples were centrifuged at 20,000 g for 10 minutes at 4°C and supernatant collected. Protein concentration in the cell lysates were then determined using the Pierce™ BCA Assay

kit according to manufacturer's instructions. Cross-linking was confirmed by western blotting as outlined in Methods: "2.6.4. Lysate collection and western blotting." (Appendix D).

Lysates were pre-cleared with 5 % (v/v) protein A Sepharose for 30 minutes at 4 °C with gentle rotation. Protein A Sepharose was then removed by centrifugation at 1000 g for 5 minutes at 4 °C. 40 µL anti-V5 agarose from Abcam was added to an eppendorf and pelleted by centrifugation at 10000 g for 30 seconds. The supernatant was removed and agarose beads were washed 5 times in 1x PBS. 500 µg protein lysate was added to the anti-V5 agarose beads and incubated overnight at 4°C under gentle agitation to allow binding of V5-tagged CRELD2 protein complexes to the agarose beads. The cell lysate was then removed and the resin was washed 4 times with 1 mL 1x RIPA. After the final wash the supernatant was removed. 25 µL 2x SDS buffer (Appendix A) was added to the resin and samples were incubated at 100 °C for 5 minutes to dissolve the agarose beads. Prior to electrophoresis, samples were vortexed and centrifuges briefly for 5 seconds. In order to identify binding partners of V5-tagged CRELD2 by Co-IP using anti-V5 agarose beads, untransfected SW1353 lysates were used as a control for the coimmunoprecipitation.

2.9.3 Mass-Spectrometry

Samples were loaded into a 4-12 % NuPAGE® Bis-Tris precast gel and electrophoresed for 4 minutes at 200 V to allow the samples to enter the gel. The gel was then incubated in InstantBlue™ protein staining solution (Appendix A) for 1 hour with constant agitation at room temperature. The protein bands were excised from the gel, submerged in water and placed at 4 °C overnight. Gel slices were then dehydrated in 100 % (v/v) acetonitrile and dried using a Savant™ DNA 120 SpeedVac™ concentrator and sent to the Biological Mass Spectrometry unit at The University of Manchester ran by Dr David Knight.

At the Mass Spectrometry Unit, dried gel pieces were reduced with 10 mM dithiothreitol and alkylated with 55 mM iodoacetamide. Gel pieces were then washed alternately with 25 mM ammonium bicarbonate followed by acetonitrile. This was repeated, and the gel pieces dried by vacuum centrifugation. Samples were digested with trypsin overnight at 37 °C. Digested samples were then analysed by LC-MS/MS

using an UltiMate® 3000 Rapid Separation LC coupled to a Thermo Fisher Scientific Orbitrap Elite™ mass spectrometer. Peptide mixtures were separated using a gradient from 92 % of 0.1 % formic acid in water and 8 % of 0.1 % formic acid in acetonitrile to 67% of 0.1% formic acid in water and 33 % of 0.1% formic acid in acetonitrile, in 44 min at 300 nL min^{-1}, using a 75 mm x 250 μm i.d. 1.7 □M BEH C18, analytical column from Waters. Peptides were selected for fragmentation automatically by data dependant analysis. Data produced were searched using Mascot (Matrix Science UK), against the UniProt database (version 2011-05) with taxonomy of *Mus musculus* selected. Data were validated using the Scaffold software (Proteome Software).

Chapter 3. Phenotyping the *Creld2* cartilage-specific knockout mouse model

Phenotyping the *Creld2* cartilage-specific knockout mouse model

3.1 Introduction

Creld2 has previously been identified as a genotype-specific ER stress inducible gene implicated in the pathogenesis of skeletal dysplasias caused by mutations in matrilin-3 and type X collagen (Hartley et al., 2013). The function of *Creld2* is largely unknown despite putative roles being described in protein folding and trafficking (Ortiz et al., 2005). The precise role of *Creld2* in cartilage however is not understood. The purpose of this study was therefore to investigate the role of *Creld2* in skeletal development *in vivo* using a *Creld2* cartilage-specific conditional knockout mouse model ($Creld2^{Cart\Delta Ex3\text{-}5}$).

In order to analyse the phenotype of the *Creld2* cartilage-specific knockout mouse model, a variety of morphometric and histological techniques were employed. The phenotyping strategy included:

- Morphometric studies in which the weights of mice at 3, 6 and 9 weeks were analysed to determine if the deletion of *Creld2* in chondrocytes affected size.
- Bone measurements were taken from whole body radiographs at 3, 6 and 9 weeks to assess the effect of the knockout of *Creld2* in chondrocytes on specific bone elements formed by intramembranous and endochondral ossification.
- Skulls from 3-week-old mice were dissected and stained with alizarin red and alcian blue for better visualisation of skull plates. This allowed for measurements of skull plates to be taken to assess the effect of the targeted deletion of *Creld2* in chondrocytes on skull development.
- Histological analysis of 3-week joints was performed to analyse differences between the growth plates of control and knockout mice.
- Growth plates were also analysed by immunohistochemistry to determine the localisation of key extracellular matrix structural proteins following the ablation of *Creld2* in cartilage.

- Transmission electron microscopy (TEM) was used to assess any differences between the growth plates of 1-week-old control and knockout mice at the ultrastructural level.
- μCT scanning was employed to assess the effect of the ablation of *Creld2* in chondrocytes on bone structure at 3 weeks of age.

3.2 *Col2Cre* is expressed in the developing cartilage but absent from bone

In the transgenic *Col2Cre* expressing mouse, the *Col2a1* promoter drives the expression of *Cre recombinase*. Crossing these mice with mice homozygous for the *Gtrosa26*^{tm1Sor} targeted mutation (R26R mice) allowed for analysis of the pattern of *Cre* expression.

Expression of *Col2Cre* in transgenic mice was restricted to chondrogenic tissues in the developing mouse embryo at E12.5 (Figure 23A). X-gal staining was observed in the developing long bones, the spinal column, the thoracic cage and the chondrogenic regions of the developing skull but was not in soft tissues for example the liver or heart. X-gal staining in 1-week growth plates was observed in chondrocytes of the growth plate and the perichondrium, but was absent from bone (Figure 23B).

Since the expression of the *Col2Cre* transgene is restricted to cartilaginous tissues, it is therefore a useful and reliable method of manipulating gene expression in chondrocytes alone.

A.

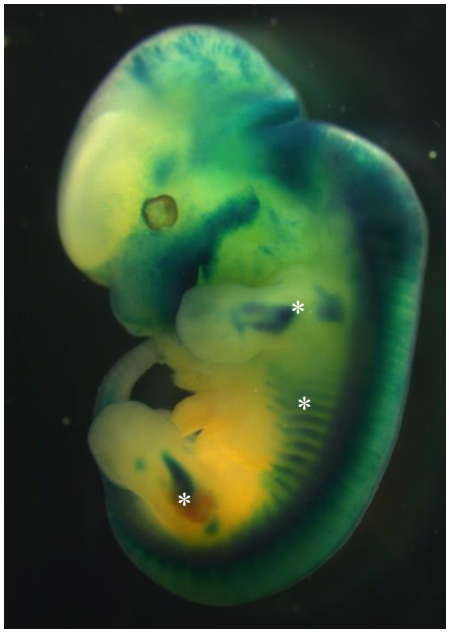

B.

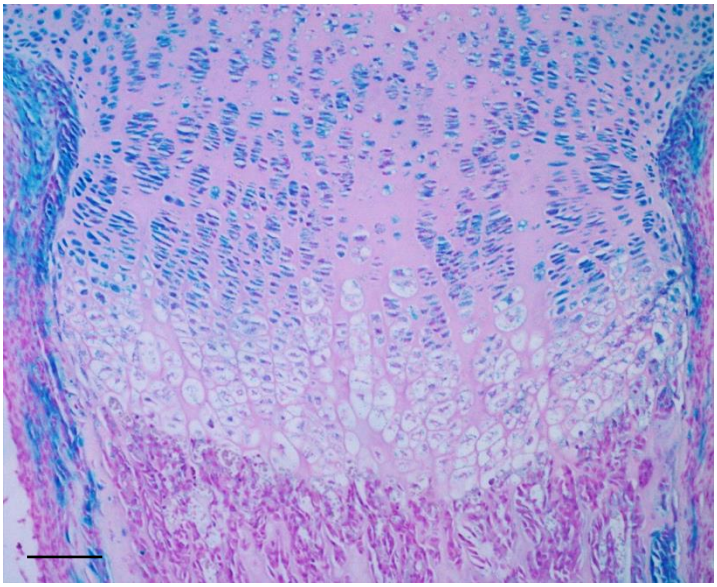

Figure 23. **The expression of the *Col2Cre* transgene is restricted to cartilaginous tissues and absent from bone.**

To analyse the expression pattern of *Col2Cre*, mice expressing the *Col2Cre* transgene were crossed with the R26R reporter mouse strain. β-galactosidase activity was examined using X-Gal with activity indicated by a blue stain. *Col2Cre* expression was restricted to cartilaginous tissues (denoted by *) during mouse embryonic development at E12.5 (**A.**). In growth plates from 3-week old mice *Col2Cre* expression was observed in the cartilage growth plate and the perichondrium but absent from bone (**B.**). (Images representative of n=3 mice, Scale bar 100 μm).

3.3 The chondrocyte specific deletion of CRELD2 results in abnormal skeletal growth

Creld2 cartilage-specific knockout mice and control mice were weighed at 3, 6 and 9 weeks and measurements were used to chart growth over this time period (Figure 24A & 24B). *Creld2*$^{CartΔEx3\text{-}5}$ mice grow significantly slower at 3 and 6 weeks than control mice (Figure 2C and D). Male knockout mice were 17.4 % ($p<0.005$) lighter at 3 weeks and 9.2 % ($p<0.05$) lighter at 6 weeks than age matched control mice, and female knockout mice were lighter than age matched controls by 12.1 % ($p<0.05$) and 12.6 % ($p<0.05$) at 3 and 6 weeks respectively (Figure 24 C & 24D). At 9 weeks however the body weights of mice were comparable as knockout mice were fed on a soaked diet due to overgrown incisors that required cutting weekly.

Bone lengths were measured in order to study the effect of the ablation of *Creld2* in chondrocytes on bone development and the impact on endochondral and intramembranous ossification. To assess the effect of the deletion of *Creld2* on endochondral ossification the lengths of the femur and tibia were used and the inter-canthal distance was used as a measure of intramembranous ossification.

Creld2$^{CartΔEx3\text{-}5}$ mice appeared smaller than their age matched controls at 3, 6 and 9 weeks of age (Figure 25 and 26). Endochondral ossification was disrupted in both male and female knockout mice since the long bones were significantly shorter in mutant mice at all time points examined. In males, the average femur length was shorter at 3, 6 and 9 weeks by 15.4 %, 14.0 % and 11.0 % ($p<0.005$ for all ages) respectively (Figure 27A). The femurs of females were also smaller at all time points by 15.4 %, 10.2 % and 11.3 % respectively ($p<0.005$ for all ages) (Figure 28A). Tibiae were shorter and males displayed a 12.3 %, 12.2 % and 8.7 % ($p<0.005$ for all ages) reduction in tibia length at 3, 6 and 9 weeks respectively (Figure 27B). In females, tibiae were also significantly shorter by 11.2 %, 8.2 % and 7.1 % ($p<0.005$ for all ages) at 3, 6 and 9 weeks relative to age-matched controls (Figure 28B).

In contrast, intramembranous ossification was unaffected in male and female *Creld2*$^{CartΔEx3\text{-}5}$ mice as the ICD was unchanged between genotypes at all time points (Figure 27C & Figure 28C).

Interestingly both male and female mice had significantly shorter skulls at 3, 6 and 9 weeks. Male skulls were 9.3 %, 6.5 % and 5.7 % ($p<0.005$, $p<0.05$, $p<0.005$)

shorter and female skulls were 8.5 % 6.4 % and 4.8 % ($p<0.005$, $p<0.005$, $p<0.05$) shorter at 3, 6 and 9 weeks respectively (Figure 27D & Figure 28D).

To further analyse the effect of the deletion of *Creld2* on skull development 3-week skulls were stained with alcian blue and alizarin red to visualise and analyse the skull plates (Figure 29A). Interestingly, skeletal preperations of the skulls revealved that knockout mice displayed malloclusion that occurs following a disalingment of the maxillary and mandibular teeth resulting in overgrown incisors (Figure 29A). Skull plates were comparable between the genotypes however the nasal bone length was significantly reduced by 9.6 % in knockout mice (Figure 29B).

A.

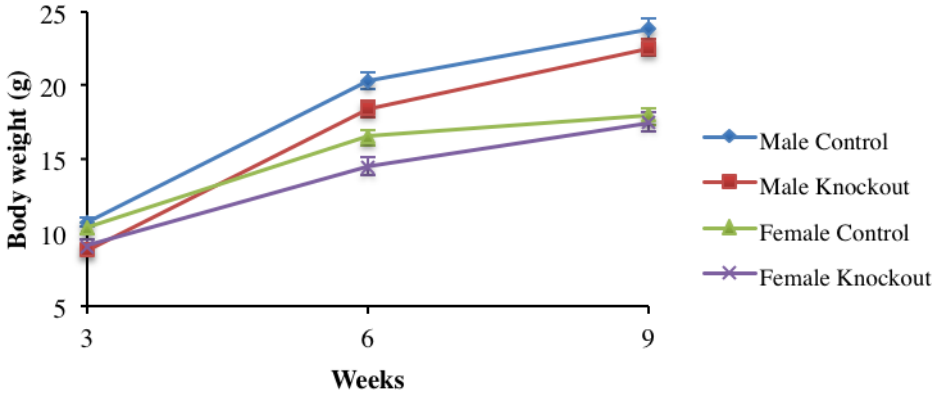

B.

		Average body weight (g) ± SEM		
		3 Weeks	6 Weeks	9 Weeks
Males	**Control**	10.71 ± 0.31	20.30 ± 0.56	23.86 ± 0.66
	Knockout	8.85 ± 0.28**	18.44 ± 0.56*	22.58 ± 0.59
Females	**Control**	10.35 ± 0.36	16.59 ± 0.34	18.00 ± 0.45
	Knockout	9.10 ± 0.45*	14.50 ± 0.63*	17.50 ± 0.65

C.

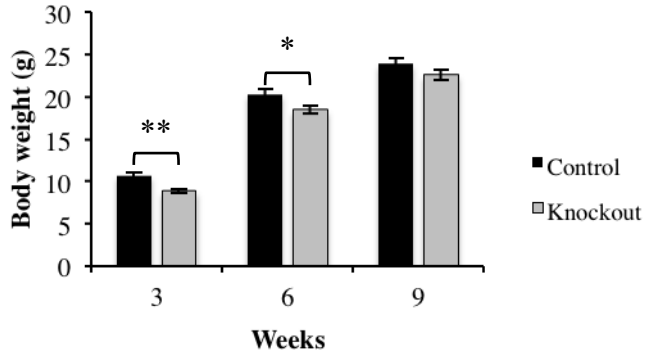

D.

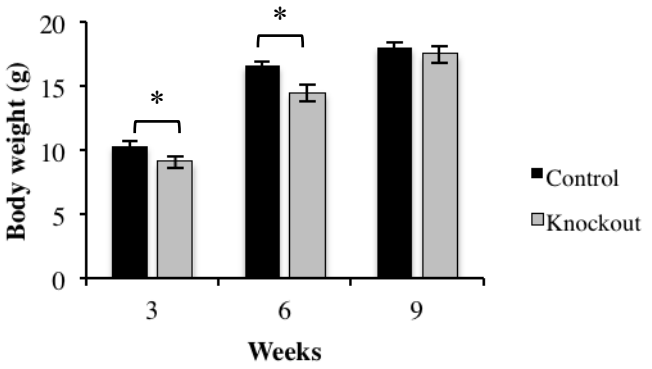

***Figure 24. Creld2* cartilage-specific knockout mice are significantly smaller than age matched controls.**

The growth of male and female mice was charted over 9 weeks. Both male and female knockout mice grew slower than control mice (**A.**). Table presenting the numerical data that is shown in the graphs (**B.**). Knockout males were significantly smaller at 3 and 6 weeks but are not significantly smaller at 9 weeks of age (**C.**). Knockout females were significantly smaller at 3 and 6 weeks but are not significantly smaller at 9 weeks of age (**D.**). (SEM = standard error of the mean, * $p<0.05$, ** $p<0.005$, unpaired t-test, $n>10$ per genotype at all ages). western blot of liver tissue (**F**.).

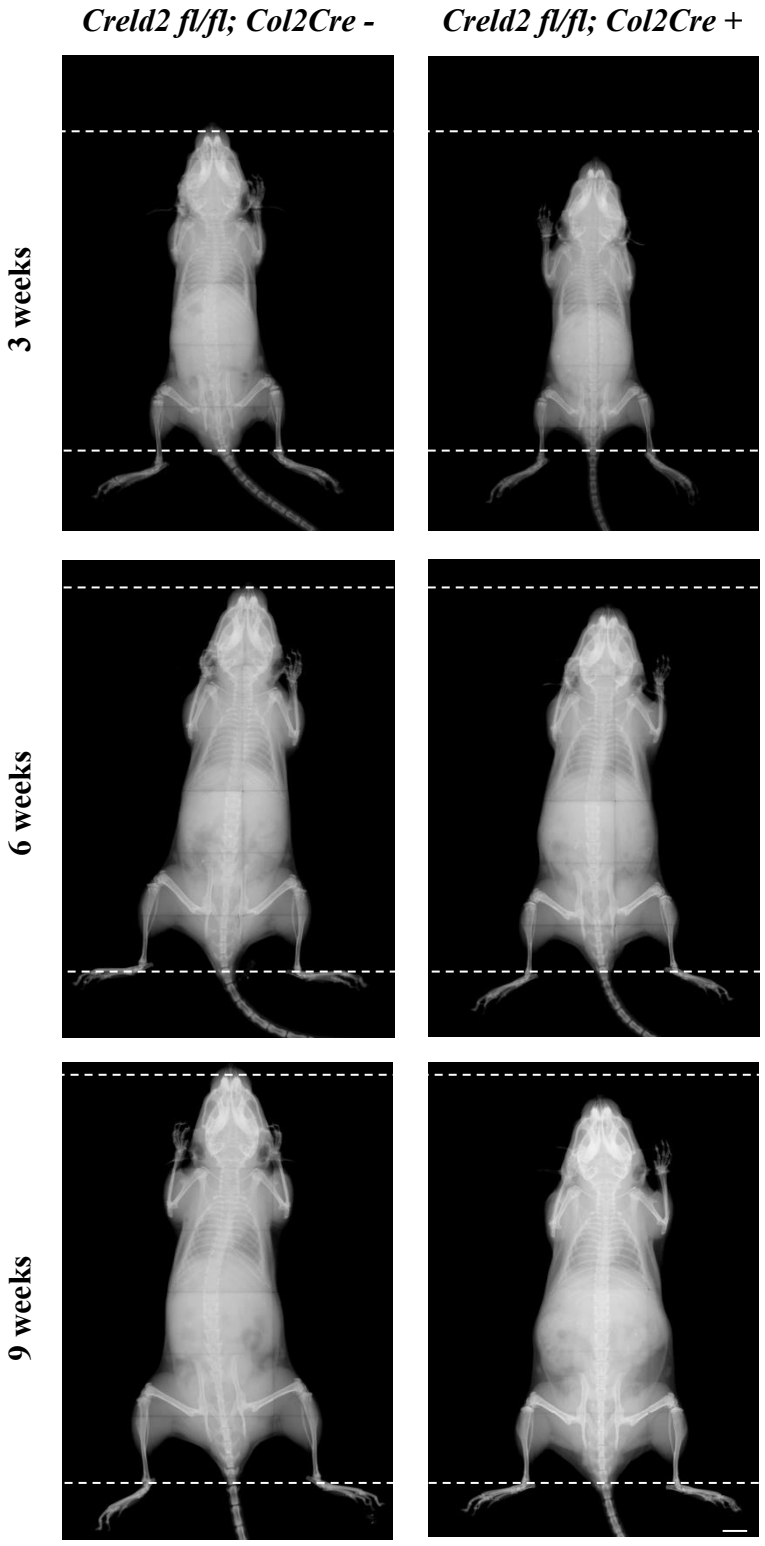

Figure 25. **Radiographs of male mice at 3, 6 and 9 weeks.**

To study the skeletal phenotype following the ablation of *Creld2* in cartilage radiographs were taken. Male *Creld2*$^{CartΔEx3\text{-}5}$ mice appeared shorter at 3, 6 and 9 weeks. (Images representative of n>10 mice at all ages per genotype, Scale bar 5 mm).

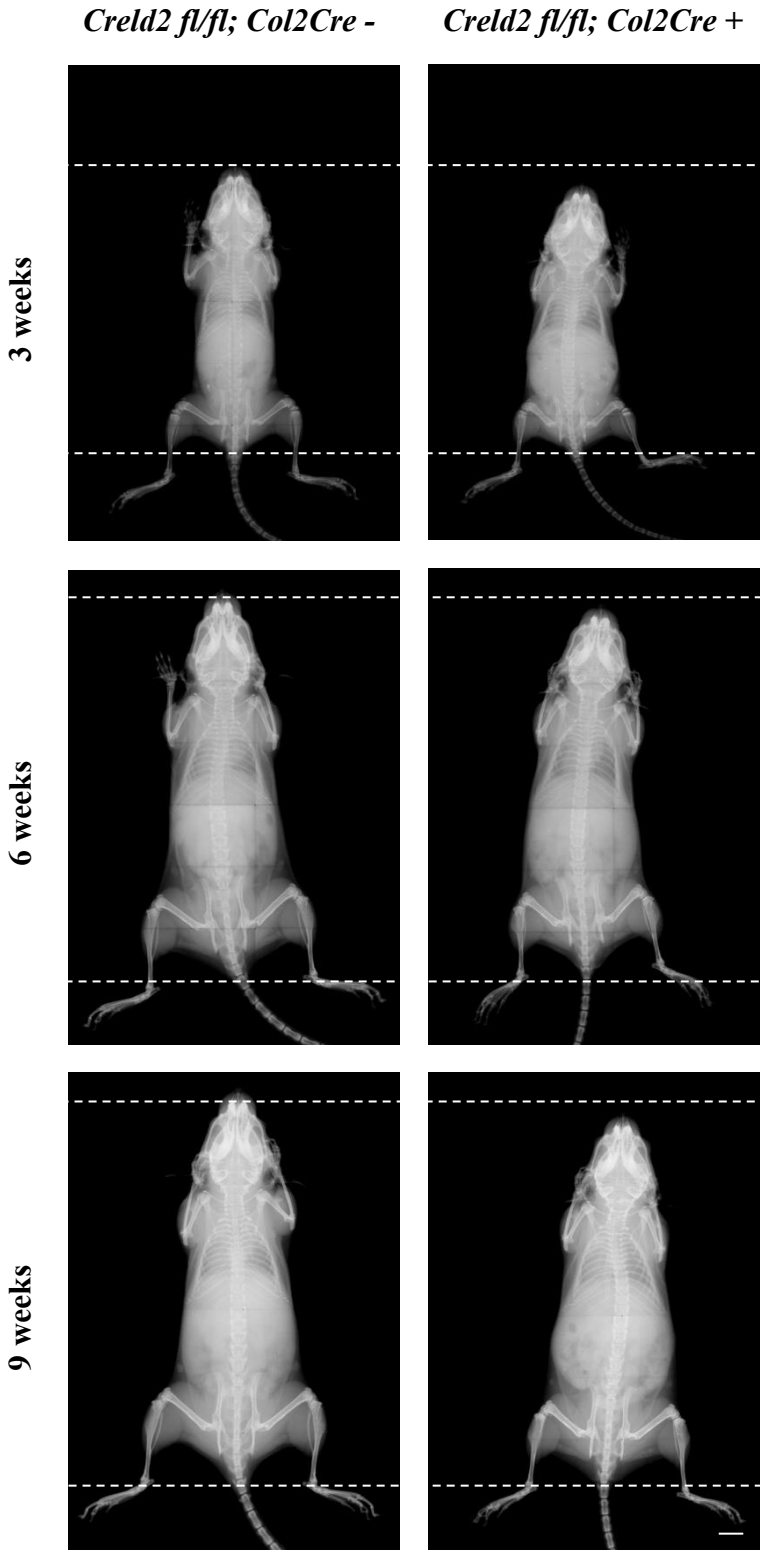

Figure 26. **Radiographs of female mice at 3, 6 and 9 weeks of age.**

To study the skeletal phenotype following the ablation of *Creld2* in cartilage, radiographs were taken at defined ages. Female *Creld2*$^{CartΔEx3\text{-}5}$ mice appeared shorter at 3, 6 and 9 weeks. (Images representative of n>10 mice at all ages per genotype, Scale bar 5 mm).

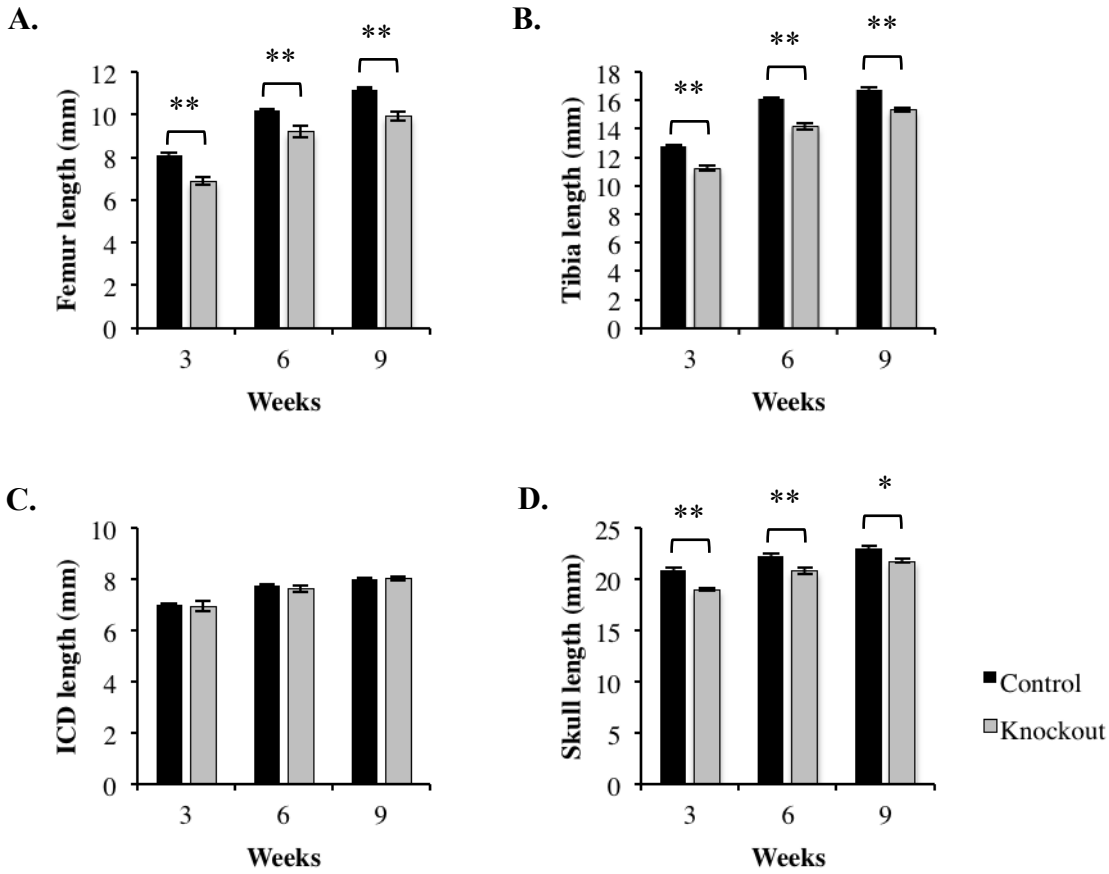

		Bone length (mm) ± SEM		
		3 Weeks	6 Weeks	9 Weeks
Femur	Control	8.11 ± 0.37	10.21 ± 0.30	10.84 ± 0.53
	Knockout	6.87 ± 0.53**	8.78 ± 0.58**	9.66 ± 0.45**
Tibia	Control	12.77 ± 0.40	16.13 ± 0.29	16.78 ± 0.93
	Knockout	11.21 ± 0.77**	14.17 ± 0.71**	21.75 ± 0.80**
ICD	Control	6.99 ± 0.28	7.31 ± 0.27	7.99 ± 0.20
	Knockout	6.93 ± 0.20	7.64 ± 0.45	8.01 ± 0.30
Skull	Control	20.92 ± 1.06	22.27 ± 0.92	23.05 ± 0.93
	Knockout	18.98 ± 0.74**	20.82 ± 1.03*	21.75 ± 0.80**

Figure 27. **Male *Creld2* cartilage-specific knockout mice are shorter than age matched controls.**

Mice were X-rayed and lengths of the femur, tibia, ICD and skull lengths were measured at 3, 6 and 9 weeks of age. Knockout mice had significantly shorter femurs (**A.**) and tibiae (**B.**) at all time points, with a reduction in lengths of 11.0 % and 8.7 % respectively at 9 weeks of age. There was no significant difference in the ICD lengths (**C.**), but interestingly, there was a significant reduction in the skull length (**D.**) of the knockout mice compared to age matched controls, with knockout skulls 5.7 % shorter than controls. Numerical data presented in graphs shown in the table. (SEM = standard error of the mean, * $p<0.05$, ** $p<0.005$, unpaired t-test, $n>10$ at each age per genotype).

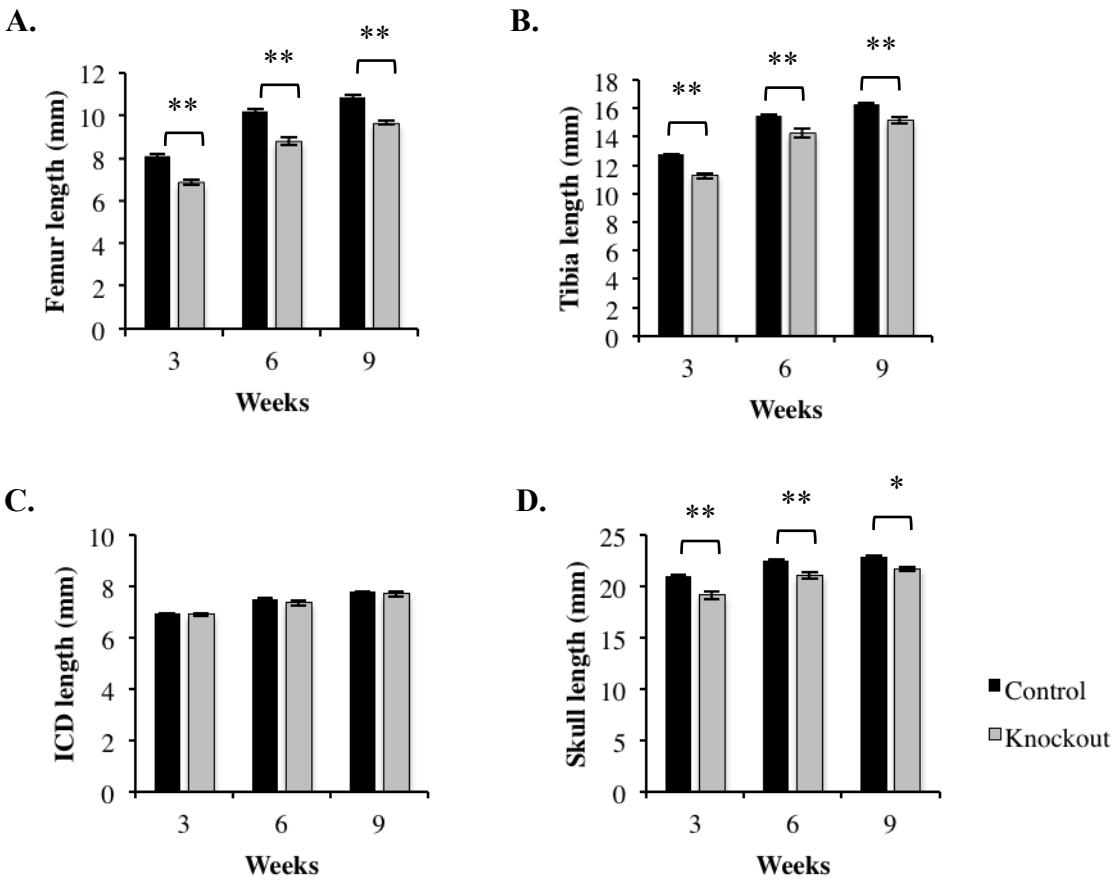

		Bone length (mm) ± SEM		
		3 Weeks	6 Weeks	9 Weeks
Femur	Control	8.11 ± 0.07	10.22 ± 0.04	11.19 ± 0.05
	Knockout	6.87 ± 0.18**	9.18 ± 0.25**	9.92 ± 0.21**
Tibia	Control	12.37 ± 0.11	15.52 ± 0.07	16.28 ± 0.07
	Knockout	11.30 ± 0.24**	14.25 ± 0.32**	15.13 ± 0.26**
ICD	Control	6.92 ± 0.05	7.52 ± 0.03	7.78 ± 0.06
	Knockout	6.92 ± 0.05	7.39 ± 0.11	7.73 ± 0.09
Skull	Control	20.95 ± 0.18	22.54 ± 0.13	22.82 ± 0.27
	Knockout	19.17 ± 0.32**	21.10 ± 0.35**	21.74 ± 0.24**

Figure 28. **Female *Creld2* cartilage-specific knockout mice are shorter than age matched controls.**

Mice were X-rayed and lengths of the femur, tibia, ICD and skull lengths were measured at 3, 6 and 9 weeks of age. Knockout mice had significantly shorter femurs (**A.**) and tibiae (**B.**) at all time points, with a reduction in lengths of 11.3 % and 7.1 % respectively at 9 weeks. There was no significant difference in the ICD lengths (**C.**), but interestingly, there was a significant reduction in the skull length (**D.**) of the knockout mice compared to age matched controls, with knockout skulls 4.8 % shorter than controls. Numerical data presented in graphs shown in the table. (SEM = standard error of the mean, * $p<0.05$, ** $p<0.005$, unpaired t-test, $n>10$ at each age per genotype).

A.

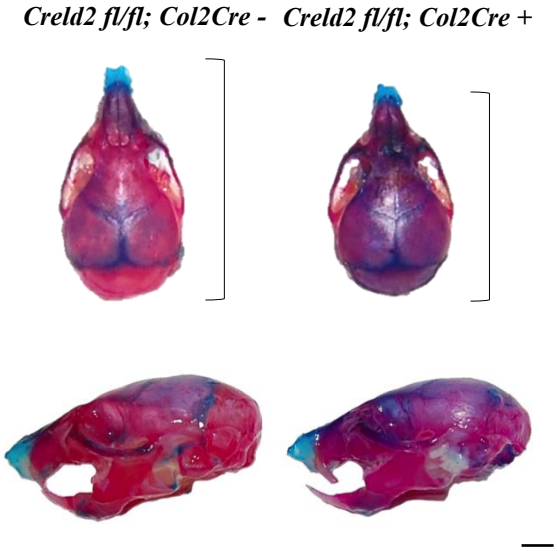

B.

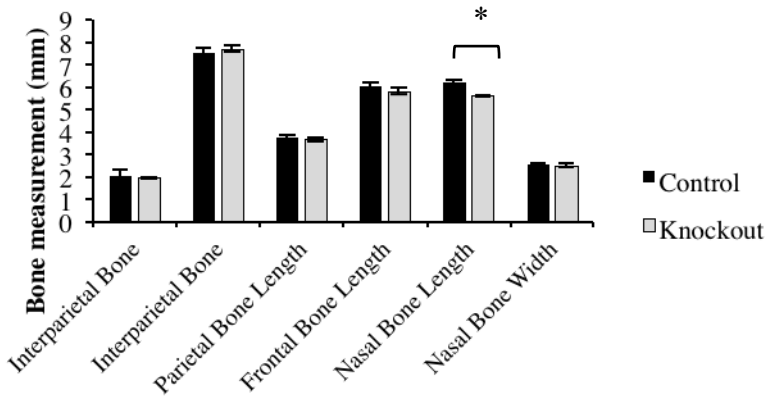

		Measurement (mm) ± SEM at 3 weeks
Interparietal Bone Length	**Control**	2.07 ± 0.22
	Knockout	1.97 ± 0.03
Interparietal Bone Width	**Control**	7.51 ± 0.23
	Knockout	7.68 ± 0.14
Parietal Bone Length	**Control**	3.76 ± 0.11
	Knockout	3.66 ± 0.08

		Measurement (mm) ± SEM at 3 weeks
Frontal Bone Length	**Control**	7.08 ± 0.18
	Knockout	6.89 ± 0.17
Nasal Bone Length	**Control**	6.20 ± 0.12
	Knockout	5.60 ± 0.04*
Nasal Bone Width	**Control**	2.58 ± 0.02
	Knockout	2.50 ± 0.09

Figure 29. **The length of the nasal bone in *Creld2* cartilage-specific knockout mice is significantly shorter than control mice.**

Skulls from 3-week males were stained with alcian blue and alizarin red to allow analysis of the skull plates. Interestingly, staining showed that knockout mice displayed maloclussion which led to overgrowth of the incisors (**A.**). There were no differences in the sizes of the skull plates between genotypes, however the length of the nasal bone was significantly reduced by 9.6 % in knockout mice (**B.**). Numerical data presented in graph shown in the table. (SEM = standard error of the mean, * $p<0.05$, unpaired t-test, n=3 per genotype, Scale bar 2.5 mm).

3.4 Deletion of CRELD2 affects growth plate organisation and chondrocyte morphology

In order to analyse the morphological changes in the growth plate following the ablation of *Creld2,* H&E staining was performed. The control growth plate displayed an ordered structure with a distinct boundary between the proliferative and hypertrophic zone (Figure 30). In the proliferative zone, chondrocytes were flattened in shape and organised into longitudinal columns perpendicular to the axis of bone growth. In the hypertrophic zone, chondrocytes swell in size as observed by enlarged lacunae and the growth plate terminates with the zone of calcification and the formation of bone.

Unlike the ordered structure of the control growth plate, knockout growth plates were disrupted and chondrocytes were morphologically different (Figure 30). The proliferative zone was characterised by large acellular regions (denoted by *) and abnormally large and rounded chondrocytes that did not arrange into the regular columns that were observed in the control mice (Box 1.). Cells were also present deep within the zone of calcification in the knockout growth plates (Box 2.).

Interestingly the lengths of the proliferative zone and the hypertrophic zone in the growth plates of 3-week old knockout male mice were significantly reduced by 5.9 % and 18.4 % (both $p<0.05$) respectively compared to age-matched control mice (Figure 31).

To analyse individual chondrons at the ultrastructural level, tibia growth plates from 1-week-old mice were studied by electron microscopy. Due to technical difficulties, TEM could not be performed on 3-week old cartilage as the decalcification process affects the structure of the tissue.

As outlined with H&E staining, the proliferative zone of the control growth plate was highly ordered with chondrocytes dividing and orienting into longitudinal columns, known as chondrons (Figure 32A & 32B). The proliferative zone of the knockout growth plate however appeared irregular and chondrocytes were morphologically abnormal (Figure 32C). Chondrocytes were misaligned and did not organise into regular columns, instead they were arranged perpendicular to the axis of bone growth. Chondrocytes were also irregular in shape. Unlike the control growth plate that contained flattened proliferative chondrocytes in chondrons, proliferative chondrocytes in the knockout growth plate were rounder in shape (Figure 32D). Large rounded cells

were also present in the knockout growth plates that appeared independent of the chondrons (Figure 32E).

In the hypertrophic zone of the control growth plate, some cellular remnants were observed in the lacunae of the chondrocyte (Figure 33A). In the hypertrophic zone of the knockout growth plate flattened chondrocytes, similar to the morphology of the proliferative zone, were observed on the border of the zone of calcification (Figure 33B & 33C).

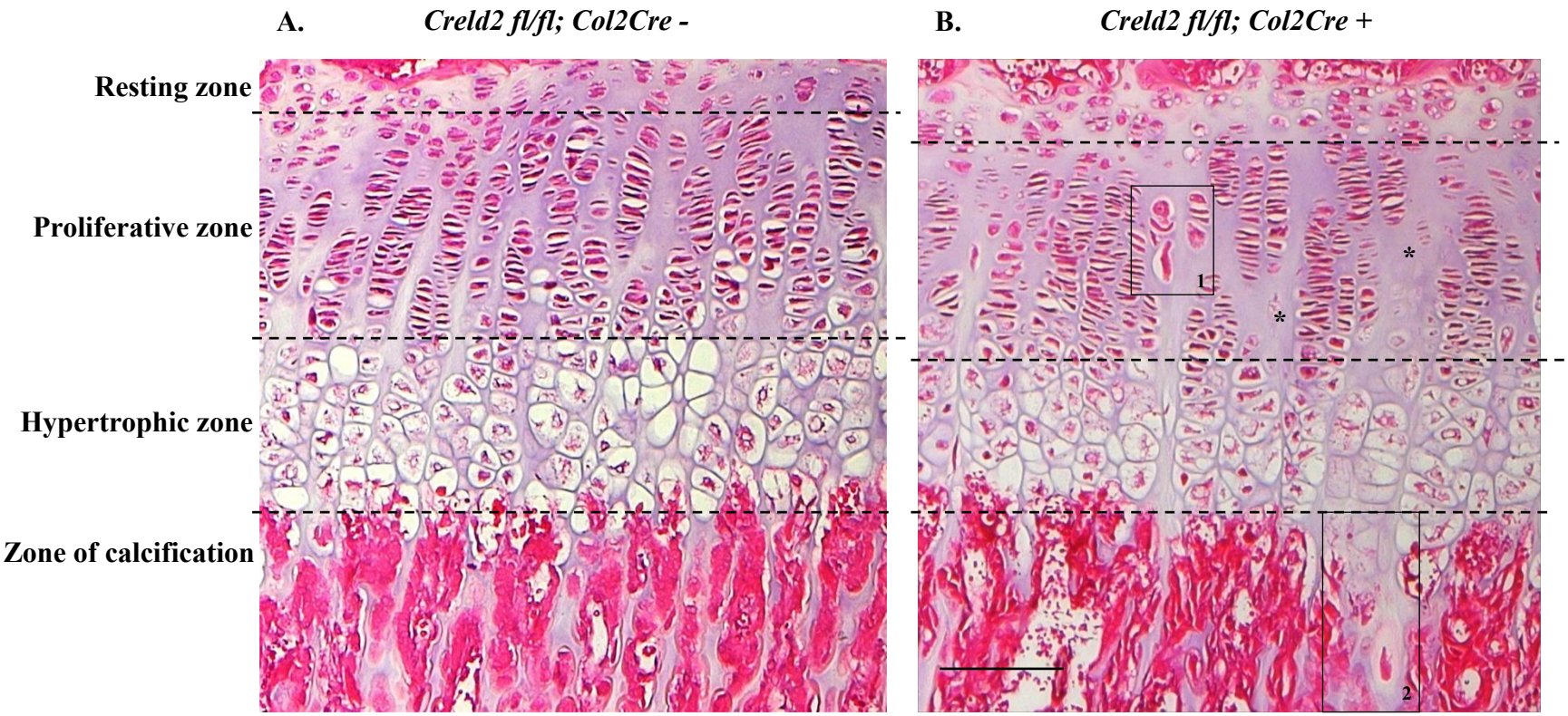

***Figure 30. Creld2* cartilage-specific knockout mice display a disrupted growth plate with abnormal chondrocyte morphology.**

Tibial growth plates from 3-week old mice were stained with hematoxylin and eosin to visualise growth plate morphology. Control growth plates were highly ordered with clearly distinguishable zones (**A.**). Growth plates from *Creld2*$^{CartΔEx3\text{-}5}$ mice were disrupted with morphologically abnormal chondrocytes (**B.**). The knockout growth plates were characterised by large acellular regions (indicated with *) and abnormally large and rounded chondrocytes in the proliferative zone (Box 1). Cells were also present deep within the zone of calcification (Box 2). Dashed lines indicate zone boundaries. (Images are representative of n= 3 matched sections from 3 unrelated male mice per genotype, Magnification x100, Scale bar 100 μm).

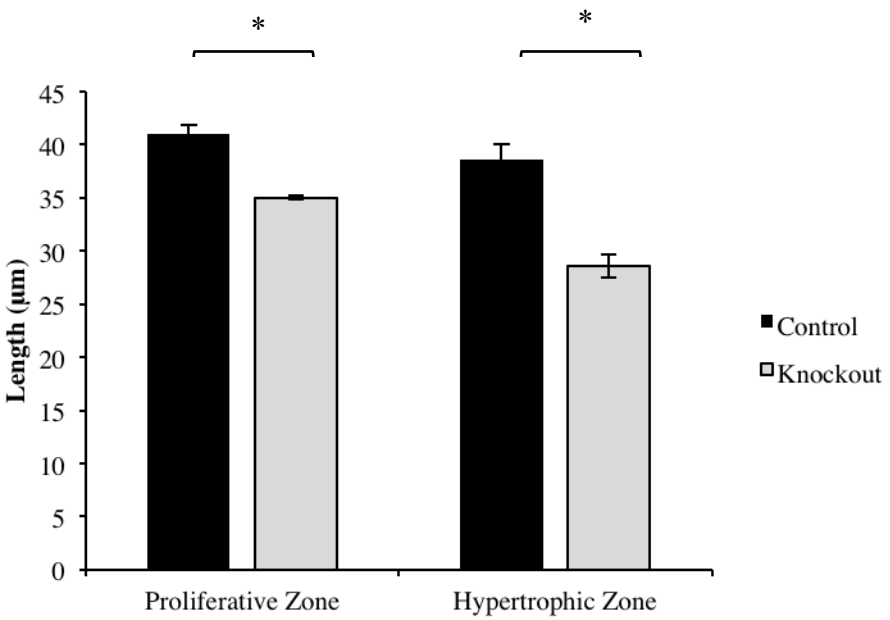

	Proliferative zone length (µm) ± SEM	Hypertrophic zone length (µm) ± SEM
Control	40.97 ± 0.84	35.00 ± 1.40
Knockout	38.57 ± 0.30*	28.57 ± 1.06*

Figure 31. **The length of the proliferative zone and the hypertrophic zone is significantly reduced in *Creld2* cartilage-specific knockout mice.**

Tibia growth plates from 3-week old mice were stained with H&E and the lengths of the proliferative and hypertrophic zone were measured. The lengths of the proliferative zone and the hypertrophic zone were significantly reduced in the knockout mice by 5.9 % and 18.4 % respectively. Numerical data presented in graph is shown in the table. (SEM = standard error of the mean, * $p<0.05$, unpaired t-test, n=39 matched sections from 3 unrelated male mice per genotype).

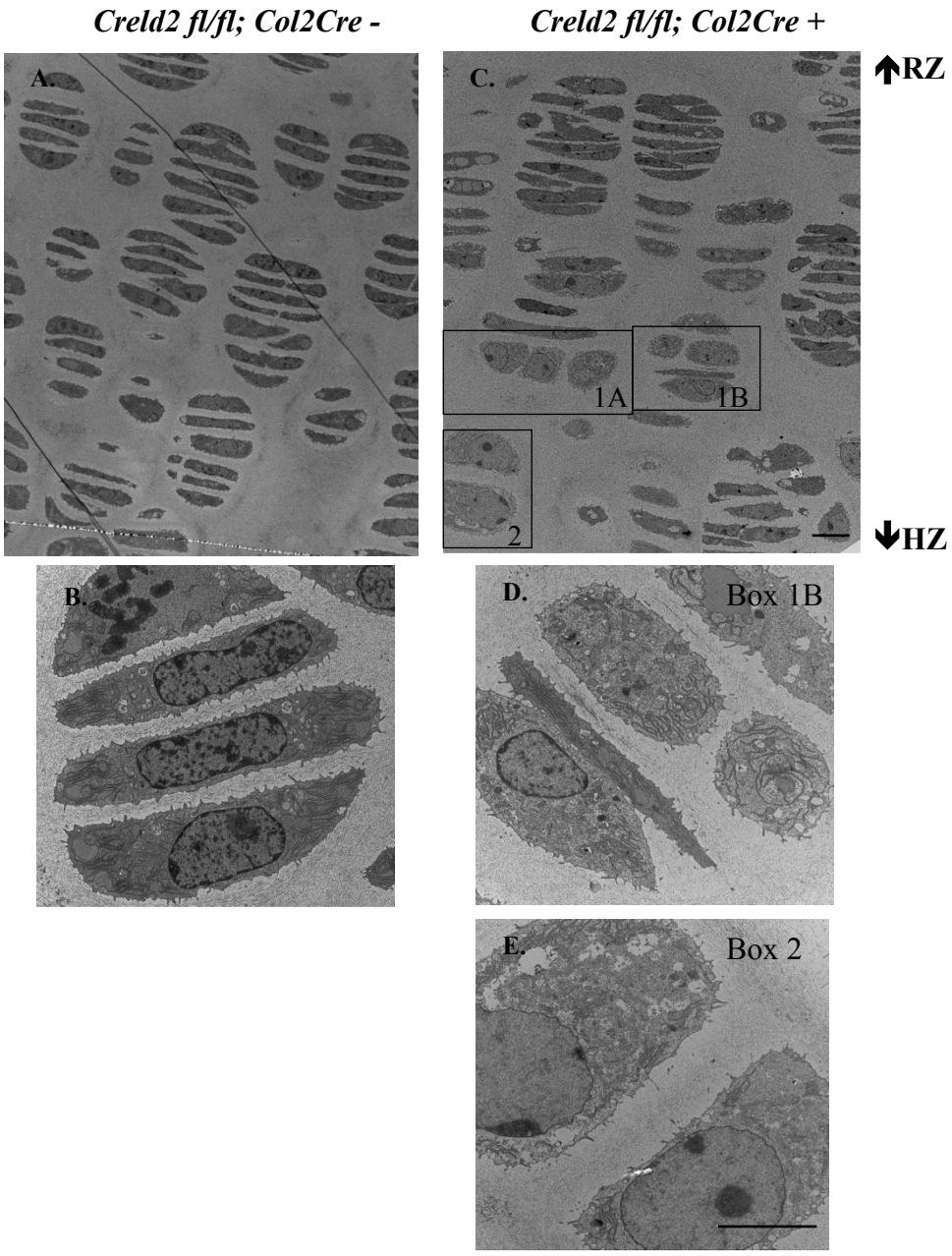

Figure 32. **The growth plates of *Creld2* cartilage-specific knockout mice are characterised by a disrupted proliferative zone containing abnormal chondrocytes.**

1-week-old tibiae were analysed by transmission electron microscopy to investigate individual chondrons in the proliferative zone at the ultrastructural level. The proliferative zone of the control growth plate was highly organised with chondrocytes arranging into longitudinal columns (**A.**). A magnified chondron is shown in (**B.**). The knockout growth plate was disorganised with disrupted chondrons (**C.** Box 1B. Magnified in **D.**) and large rounded cells (**C.** Box 2. Magnified in **E.**) (RZ= resting zone, HZ= hypertrophic zone. Images are representative of n=2 males per genotype, Magnification x620 (A. C.) x4600 (B. D. E.), Scale bar 10 μm).

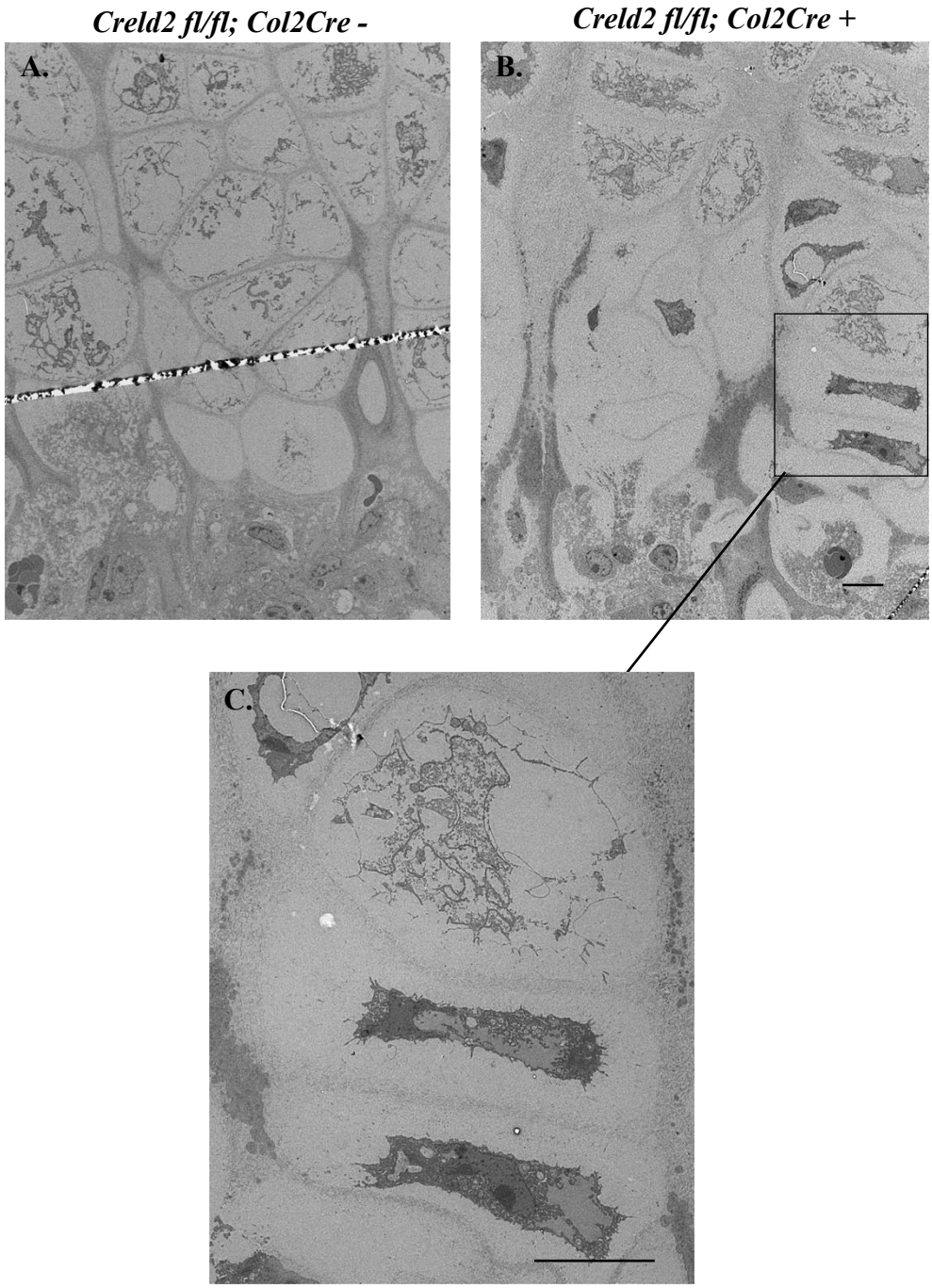

Figure 33. **The growth plates of *Creld2* cartilage-specific knockout mice contain abnormal hypertrophic chondrocytes.**

1-week-old tibiae were analysed by transmission electron microscopy to analyse ultrastructurally the cells of the growth plate. Some remnants of cellular material are present in the hypertrophic zone of the control growth plate (**A.**). The hypertrophic zone of the knockout growth plate flattened chondrocytes that do not appear to be dying are present (**B.**, magnified in **C.**) (Images are representative of n=2 males per genotype, Magnification x620 (A. B.) x4600 (C.), Scale bar 10 μm).

3.5 Deletion of CRELD2 does not alter the expression or localisation of cartilage extracellular matrix proteins

To study the effect of the ablation of *Creld2* on the localisation of key structural components of the cartilage ECM, immunohistochemical staining of three-week-old tibial growth plates was performed.

Matrilin-3 has been previously shown to interact with CRELD2 intracellularly *in vitro* (Hartley et al., 2013). It was therefore important to analyse the expression pattern of matrilin-3 following the deletion of *Creld2* in cartilage. At 3 weeks of age, comparable uniform extracellular staining for matrilin-3 was observed in both the knockout and control growth plates (Figure 34).

Aggrecan staining was localised evenly throughout the cartilage ECM of the growth plates and was comparable across the genotypes at 3 weeks of age (Figure 12). Toluidine blue staining was used to analyse the sulphation status of the cartilage matrix. No differences in staining intensities were seen between the cartilage of knockout and control mice; thus, sulphation of proteoglycans was not affected following the deletion of *Creld2* in chondrocytes (Figure 34).

The expression levels of cartilage structural collagens, such as types II, X and I collagen were also analysed by IHC (Figure 35). Type II collagen was distributed evenly throughout the growth plate and staining was comparable between knockout and control growth plates. Control growth plates displayed the characteristic staining for type X collagen, a marker of hypertrophy, since extracellular staining was restricted to the hypertrophic zone where the growth plate terminates. The same characteristic staining was observed in growth plates from *Creld2*$^{CartΔEx3\text{-}5}$ mice; however, the area of expression of type X collagen appears was reduced by 28.5 % compared to age matched controls which correlated with the finding that the knockout mice display a reduction in the size of the hypertrophic zone (Appendix D). The expression of type I collagen, the main fibrous protein in bone, was analysed by IHC. The trabecular bone directly under the cartilage growth plate in knockout mice displayed reduced staining of type I collagen compared to age matched controls.

The localisation of proteins in the ECM was therefore not affected following the ablation of *Creld2* in chondrocytes, however the staining intensities of several structural collagens appeared to be reduced in knockout mice.

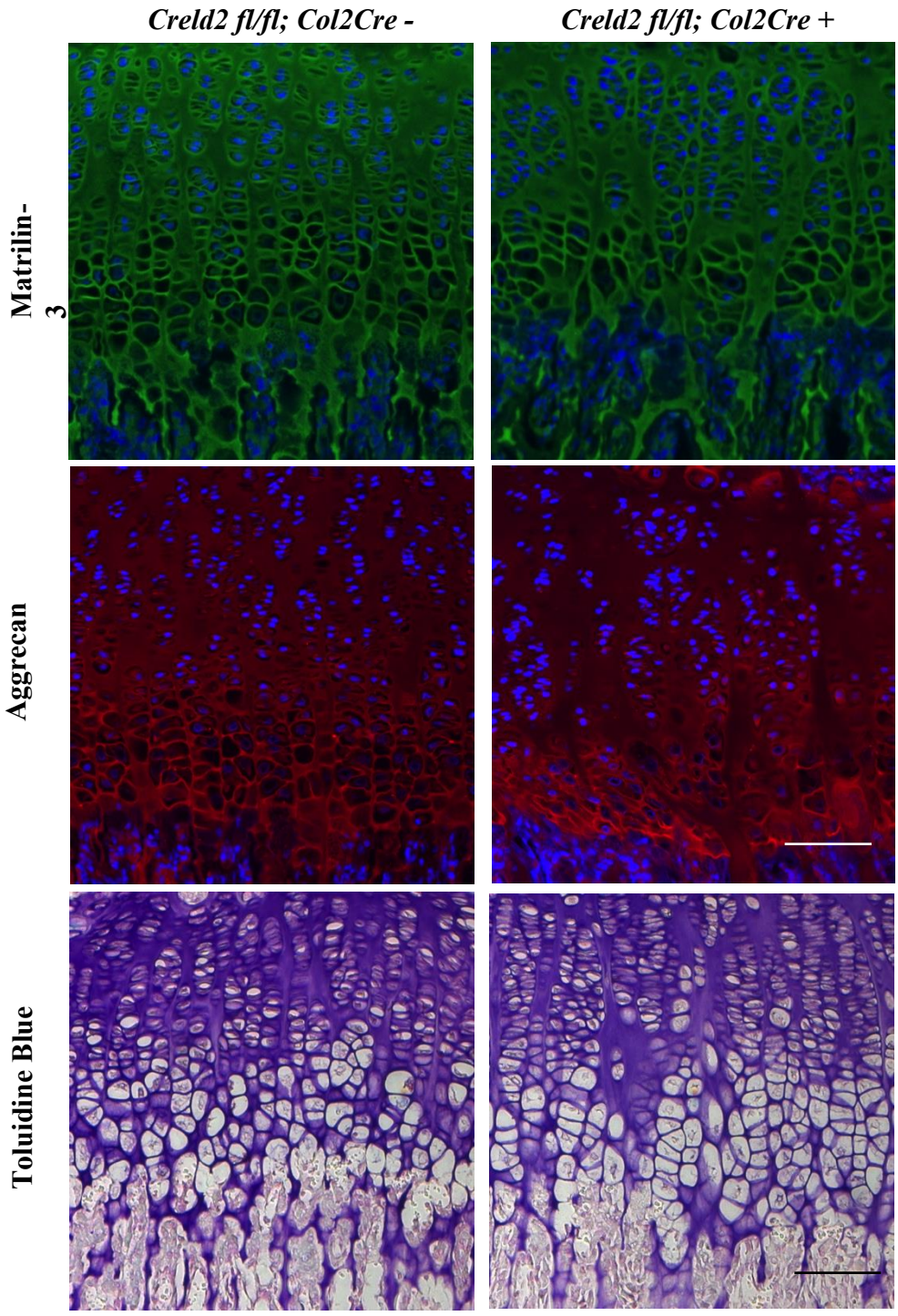

Figure 34. **The ablation of *Creld2* in chondrocytes does not affect the expression of matrilin-3 or sulphated proteins including aggrecan.**

Tibial growth plates from 3-week old mice were analysed by immunohistochemistry to visualise the expression of ECM structural components matrilin-3 and aggrecan detected in the green and red channel respectively. The nuclei were counterstained with DAPI (blue staining). Staining of the knockout and control growth plates was comparable and displayed an even extracellular distribution of matrilin-3 and aggrecan. Sulphation was also comparable between the genotypes as observed by toluidine blue staining. (Images are representative of n= 3 matched sections from 3 unrelated male mice per genotype, Magnification x100, Scale bar 100 μm).

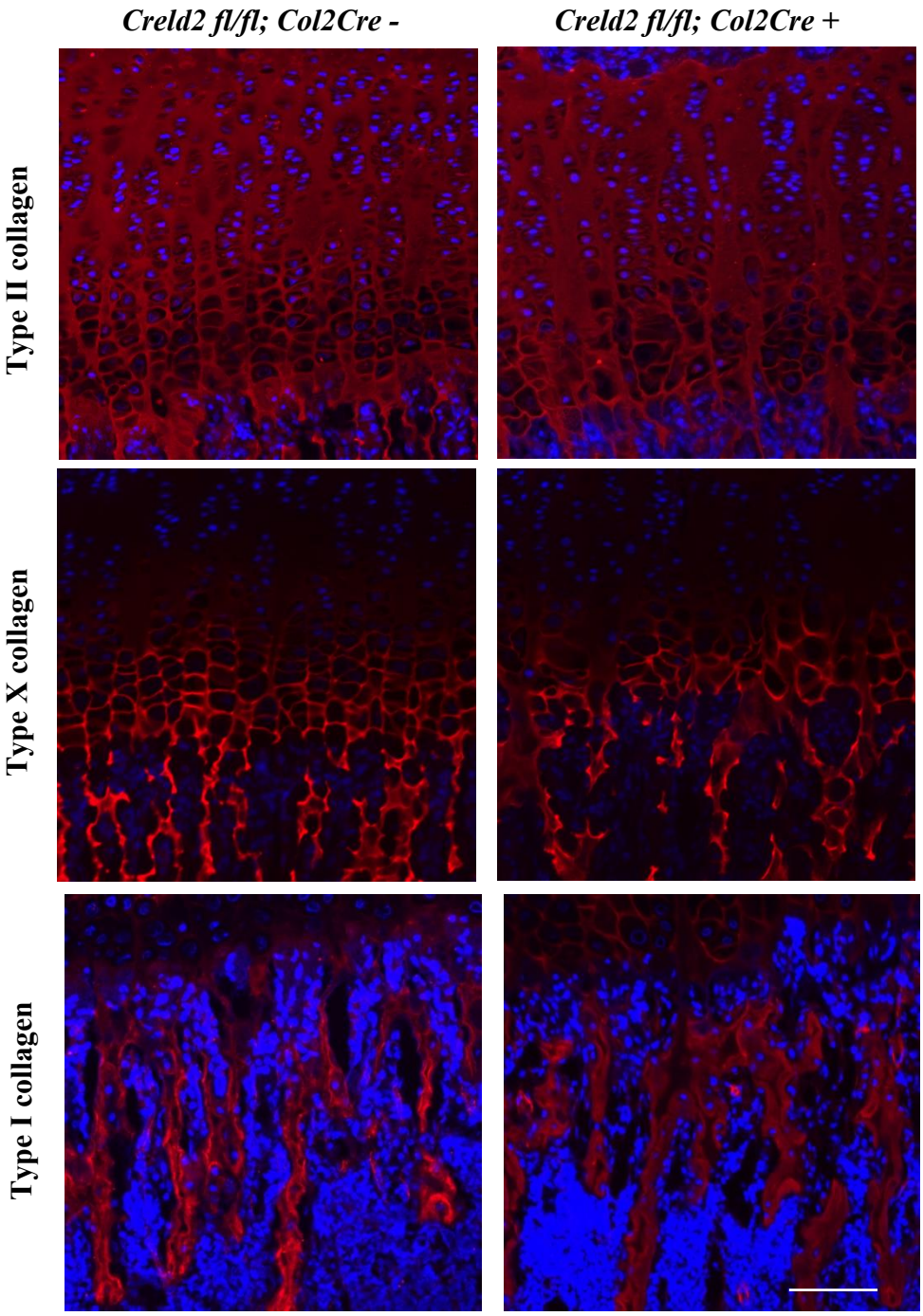

Figure 35. **The ablation of *Creld2* in chondrocytes has no effect on type II collagen expression but reduces type X collagen and type I collagen expression.**

Tibial growth plates from 3-week old mice were analysed by immunohistochemistry to visualise the expression of the structural proteins; types II, X and I collagen, all of which were detected in the red channel. Nuclei were counterstained with DAPI (blue staining). Staining for type II collagen was comparable between the genotypes and was expressed throughout the growth plate. The zone of type X collagen expression was reduced in the knockout growth plates compared to age matched controls. The staining intensity of type I collagen in bone appeared reduced in knockout bone compared to age matched controls. (Images are representative of n= 3 matched sections from 3 unrelated male mice per genotype, Magnification x100, Scale bar 100 μm).

3.6 Ablation of CRELD2 results in altered collagen fibril deposition in the hypertrophic zone of the growth plate

Since the area of type X collagen expression appeared reduced in the growth plates of *Creld2*$^{Cart\Delta Ex3\text{-}5}$ mice, the ECM architecture surrounding the chondrocytes in the hypertrophic zone of 1-week tibial growth plates was analysed ultrastructurally using transmission electron microscopy.

The pericellular matrix of the hypertrophic zone of 1-week-old control growth plates contained more electron dense appearing collagen fibrils. In contrast, the hypertrophic pericellular matrix of 1-week-old knockout growth plates contained less fibrillar material and individual fibrils were not as clearly visible (Figure 36).

The hypertrophic interterritorial matrix of the control growth plate was a densely packed random network of long collagen fibrils. In knockout mice the hypertrophic interterritorial matrix was morphologically different as the matrix appeared sparser and individual fibrils were both smaller and unidirectional (Figure 36).

To analyse fibril thickness picrosirius red staining was used. Picrosirius red enhances the birefringence of collagen and under polarised light collagen fibrils appear red, orange yellow or green depending on the thickness of the fibril. Initial observations revealed that three-week-old knockout growth plates appeared to have thinner collagen fibrils in the hypertrophic zone and the trabecular bone, which was demonstrated by more fibrils that exhibit green and yellow polarising colours (Figure 37).

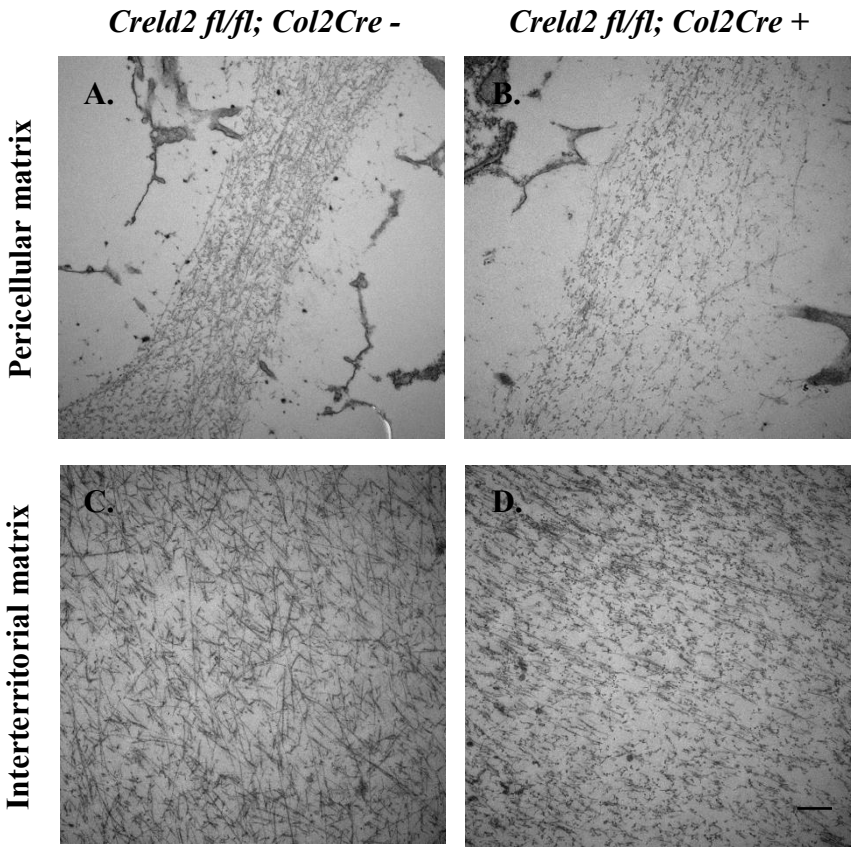

Figure 36. **The growth plates of *Creld2* cartilage-specific knockout mice have altered collagen fibril deposition in the hypertrophic zone.**

To analyse the extracellular matrix architecture at the ultrastructural level of 1-week tibial growth plates, transmission electron microscopy was used. The hypertrophic pericellular (**A.**) and interterritorial (**C.**) matrix of the control growth plate contained more electron dense collagen fibrils. The pericellular (**B.**) and interterritorial (**D.**) matrix in the hypertrophic zone of the knockout growth plates are morphologically different with less fibrillar content. (Images are representative of n=2 males per genotype, Magnification x4600, Scale bar 500 nm).

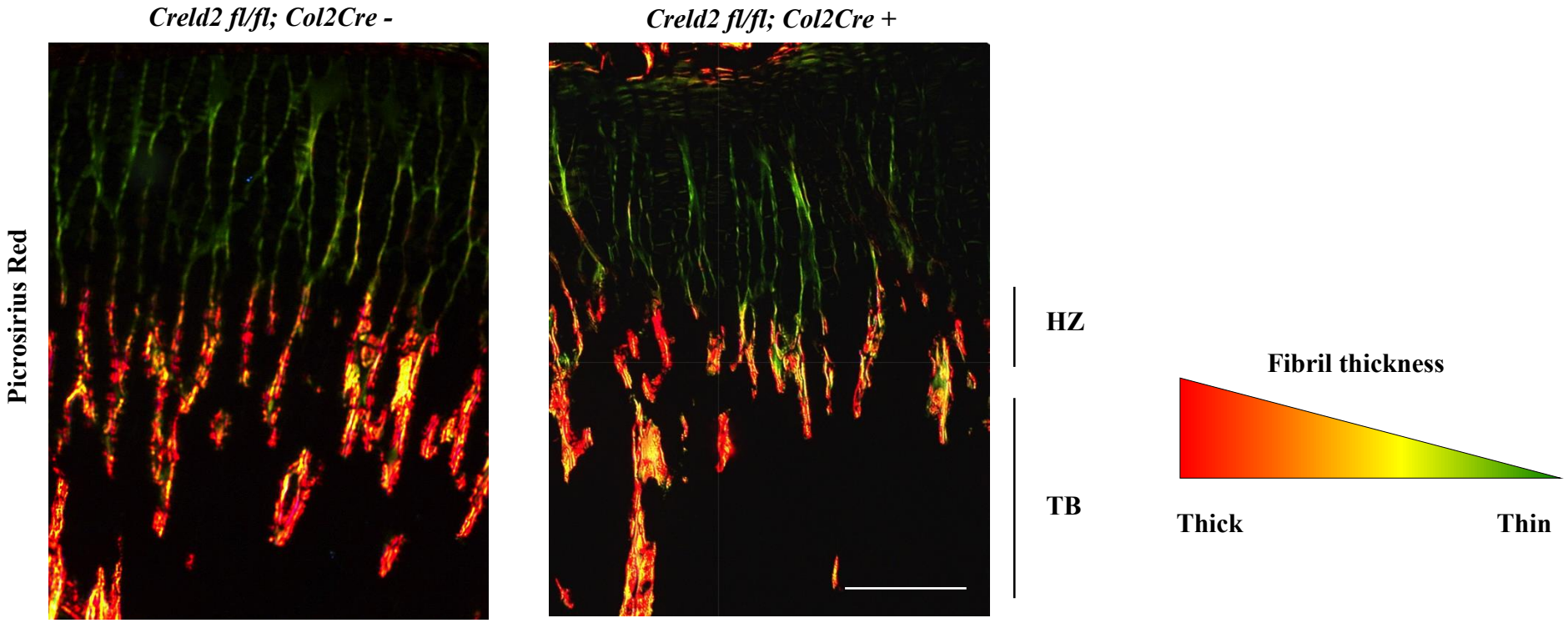

***Figure 37. Creld2* cartilage-specific knockout mice have thinner collagen fibrils in the hypertrophic zone of the growth plate.**

To analyse collagen fibril thickness tibial growth plates from 3-week-old mice were stained with picrosirius red. Under polarised light collagen fibrils stained with picrosirius red appear red, orange yellow or green depending on the thickness of the fibril, decreasing in thickness from red to green. Knockout growth plates appear to have thinner collagen fibrils in the hypertrophic zone and the trabecular bone, as there are more fibrils that exhibit green and yellow polarising colours. (HZ = Hypertrophic zone, TB = Trabecular bone. Images are representative of n=2 males per genotype, Magnification x200, Scale bar 200 μm).

3.7 Chondrocyte specific knockout of CRELD2 in the growth plate impairs trabecular bone formation

To assess trabecular and cortical bone architecture, 3D μCT scanning of 3-week-old male tibiae was performed. Trabecular bone was analysed under the epiphyseal growth plate of the proximal tibia and cortical bone was analysed in the tibia midshaft.

Tibiae of *Creld2*$^{CartΔEx3\text{-}5}$ mice appeared much smaller than their age matched controls on reconstructed μCT images (Figure 38). Interestingly, the secondary centre of ossification in knockout tibiae was also much smaller, consistent with an epiphyseal dysplasia and delayed bone growth. In addition, there also appeared to be a reduction in the width of the tibiae in knockout mice.

From the μCT images trabecular bone microarchitecture was analysed at 3 weeks of age. Knockout mice had significantly less trabecular bone with a reduction of 27.5 % ($p<0.05$) compared to age-matched controls (Figure 39A) and trabecular number was also significantly reduced by 25.0 % ($p<0.05$) (Figure 39B). In contrast, knockout bone displayed a 12.1 % ($p<0.05$) reduction in trabecular separation due to the reduced width of the knockout tibia (Figure 39C). Trabecular thickness was not significantly affected in the knockout tibia compared to control tibia (Figure 39D). Trabecular pattern factor is a parameter used to measure bone microarchitecture and is inversely proportional to trabecular connectivity. Interestingly, the trabecular pattern factor of knockout bones was 31.6 % ($p<0.005$) higher compared to age matched controls (Figure 39E).

No significant difference was found in cortical porosity between the genotypes (Figure 40), suggesting that the defect in bone directly results from a defect in the growth plate.

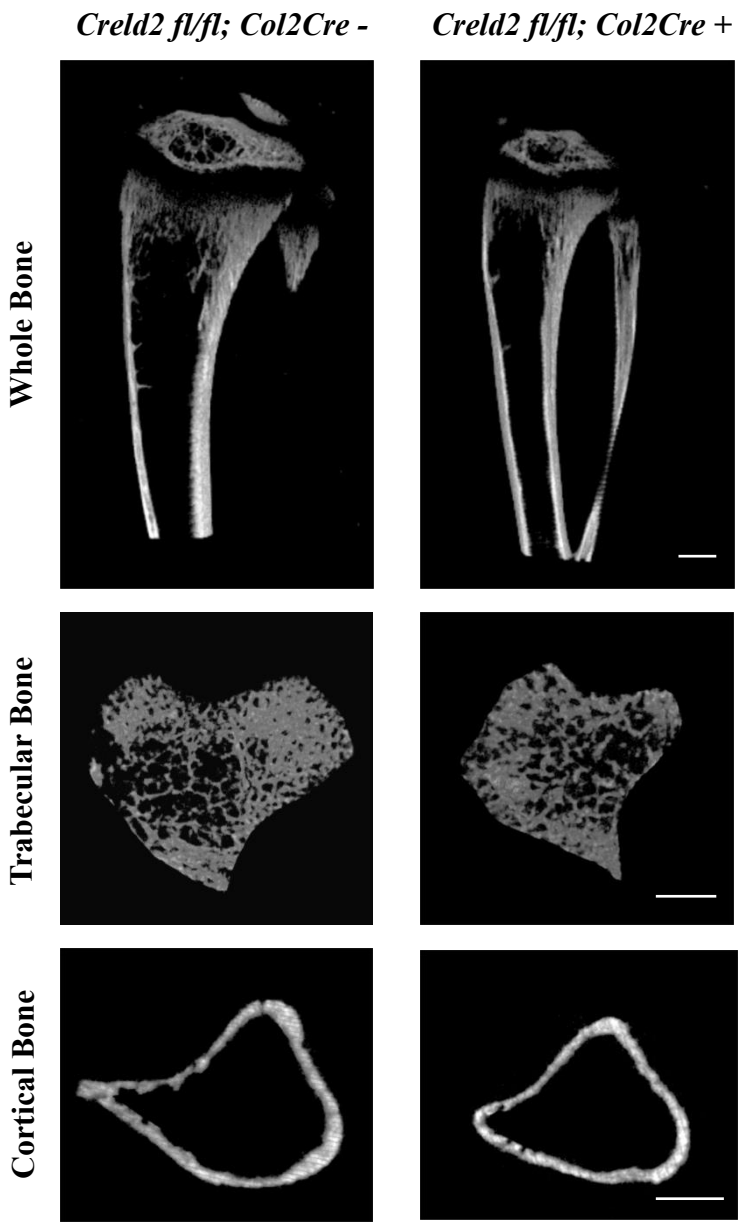

Figure 38. **Reconstructed µCT images of 3-week tibia.**

To study the effect of *Creld2* deletion in chondrocytes on bone, 3-week male tibiae were scanned and analysed using µCT. Male *Creld2*$^{CartΔEx3\text{-}5}$ mice have smaller, thinner tibia with a smaller secondary centre of ossification shorter (Images representative of n=5 mice per genotype, Scale bar = 500 µm).

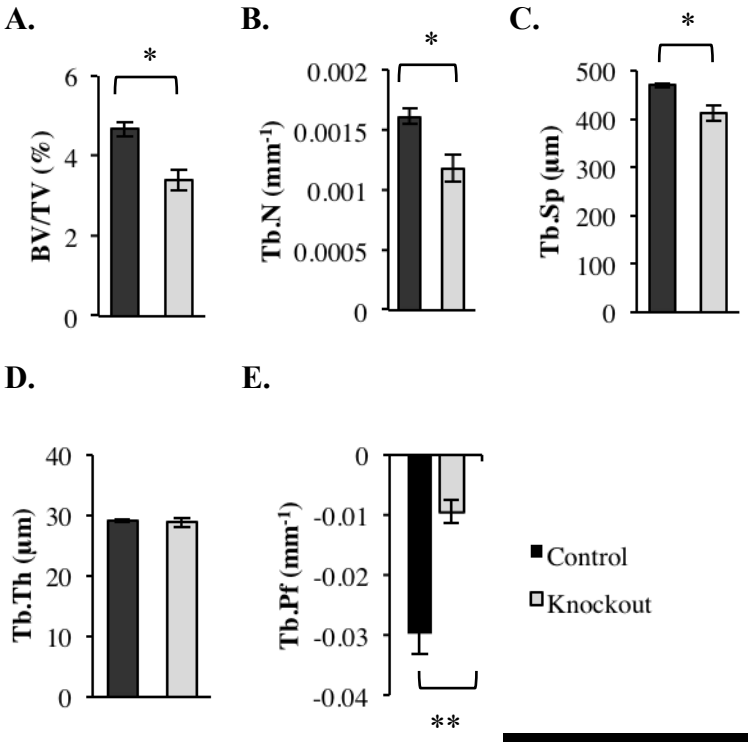

		Measurement ± SEM
Percentage Bone Volume (%)	**Control**	4.66 ± 0.17
	Knockout	3.38 ± 0.26*
Trabecular Number (mm^{-1})	**Control**	0.0016 ± 0.000071
	Knockout	0.0012 ± 0.00015*
Trabecular Spacing (µm)	**Control**	468.43 ± 4.77
	Knockout	411.74 ± 15.31*
Trabecular Thickness (µm)	**Control**	29.00 ± 0.23
	Knockout	28.77 ± 0.70
Trabecular Pattern Factor (mm^{-1})	**Control**	-0.030 ± 0.0033
	Knockout	-0.0095 ± 0.0019**

Figure 39. **Male *Creld2* cartilage-specific knockout mice have altered trabecular bone compared to age matched controls.**

To assess trabecular architecture, 3D µCT imaging of 3-week male tibiae was performed and bone volume, trabecular parameters were analysed. Knockout mice had significantly less trabecular bone (**A.**), with a reduction of 27.5 % at 3 weeks. Trabecular number (**B.**) and trabecular separation (**C.**) was also significantly reduced by 25.0 and 12.1 % respectively, however, there was no significant difference in the trabecular thickness (**D.**). Trabecular pattern factor (**E.**), the inverse index of connectivity, was significantly increased by 31.6 % in knockout mice compared to age matched controls. Numerical data presented in graphs shown in the table. (BV/TV = Percentage bone volume, Tb.N = Trabecular number, Tb.Sp = Trabecular spacing, Tb.Th = Trabecular thickness, Tb.Pf = Trabecular pattern factor, SEM = standard error of the mean, * $p<0.05$, ** $p<0.005$, unpaired t-test, n=5 mice per genotype).

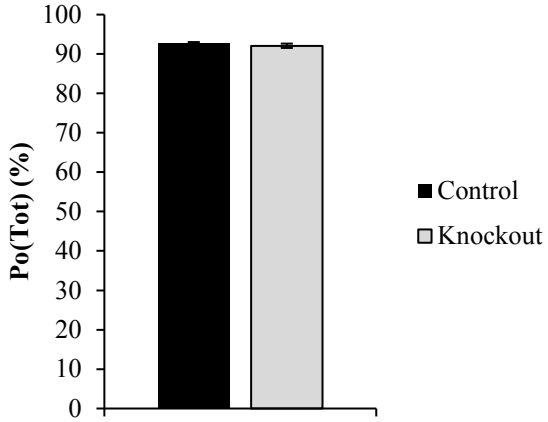

	Total porosity (%) ± SEM
Control	92.78 ± 0.24
Knockout	92.09 ± 0.55

Figure 40. **There is no significant difference in cortical bone porosity between *Creld2* cartilage-specific knockout mice and age matched controls.**

To assess cortical architecture, 3D μCT imaging of 3-week male tibiae was performed and cortical porosity was analysed. There was no significant difference in tibial cortical porosity between knockout and control mice at 3 weeks. Numerical data presented in graphs shown in the table. (Po(Tot) = Cortical porosity, SEM = standard error of the mean, unpaired t-test, n=5 mice per genotype).

3.8 Summary

The aim of this chapter was to characterise the skeletal phenotype of a *Creld2* cartilage-specific knockout mouse model using a variety of morphometric and histological techniques.

Analysis of the skeletal phenotype revealed that *Creld2*$^{CartΔEx3\text{-}5}$ mice display disproportionate short stature with the long bones significantly shorter in male and female mice at 3, 6 and 9 weeks. For example, the lengths of the tibia were reduced by 8.7 % and 7.1 % in 9-week male and female knockout mice respectively. These mice did not however exhibit a hip deformity that is often seen in mice with chondrodysplasia (Piróg-Garcia et al., 2007, Suleman et al., 2012). The nasal bone, which grows by endochondral ossification of the cartilaginous synchondroses in the skull, was 9.6 % shorter in 3-week knockout mice (Wealthall and Herring, 2006). Interestingly, *Creld2*$^{Cart\,ΔEx3\text{-}5}$ mice exhibited maloclussion that occurs when the incisor teeth are overgrown due to the disalignment of the mandibular and maxillary teeth. Therefore these mice required their teeth to be cut weekly and so were fed on a soaked diet. At 3 weeks, knockout mice were significantly lighter than control mice, however, by 9 weeks weights were comparable between the genotypes and this could be due to being fed a soaked diet.

Creld2$^{CartΔEx3\text{-}5}$ mice also displayed a disrupted growth plate with altered chondrocyte morphology. The length of the proliferative zone in knockout growth plates was significantly reduced by 5.9 % compared to control mice. The length of the hypertrophic zone was also significantly shorter, with a decrease of 18.4 % in knockout growth plates. The growth plates of *Creld2*$^{CartΔEx3\text{-}5}$ mice also exhibited abnormal chondrocyte morphology. Unlike the ordered structure of the control growth plates, the knockout growth plates contained large areas of hypocellularity in both the proliferative and hypertrophic zones. In the proliferative zone there were large misaligned chondrocytes that did not arrange into longitudinal chondrons parallel to the axis of bone growth. In the hypertrophic zone of the control growth plate chondrocytes were dying and there appeared to be some remnants of cellular material. In contrast, flattened chondrocytes that appeared to have the phenotype of proliferative chondrocytes were identified in the hypertrophic zone of knockout growth plates and cells were alse retained within the bone scaffold. This indicated a possible delay in chondrocyte maturation in the growth plates of knockout mice.

Interestingly, the growth plate pathology observed in *Creld2*$^{CartΔEx3-5}$ mice bears some similarities to other mouse models of chondrodysplasia (Table 2). For example, *Creld2* knockout growth plates are similar to those of *Comp* T585M and D469 mice as growth plates from these mice also display large areas of hypocellularity with the inclusion of large misaligned chondrocytes in the proliferative zone (Piróg-Garcia et al., 2007, Suleman et al., 2012). The growth plates from *Creld2*$^{CartΔEx3-5}$ mice also bear a resemblance to the growth plates from *Xbp1* cartilage-specific knockout mice that are characterised by large regions of hypocellularity and the inclusion of large rounded cells in the proliferative zone that do not arrange into the typical longitudinal chondrons (Cameron et al., 2015).

Table 2. **Similarities between the growth plate pathology of *Creld2* cartilage-specific knockout mice (*Creld2* $^{CartΔEx3-5}$) and the growth plates of other mice with a chondrodysplasia phenotype.**

Mouse model	Hypocellularity	Misaligned proliferative chondrocytes	Reference
Creld2 $^{CartΔEx3-5}$	✓	✓	N/A
Col2-Tg^{rdw}	✓	×	(Gualeni et al., 2013)
Comp T585M	✓	✓	(Piróg-Garcia et al., 2007)
Comp D469del	✓	✓	(Suleman et al., 2012)
Matn3 V194D	×	✓	(Leighton et al., 2007, Suleman et al., 2012)
Xbp1^{CartΔEx2}	✓	✓	(Cameron et al., 2015)

Creld2 has been shown to be upregulated in skeletal dysplasias that arise from mutations in matrilin-3 and type X collagen, but not from mutations in COMP. Mutations in matrilin-3 and type X collagen result in the mutant protein accumulating in the ER resulting in an unfolded protein response (Hartley et al., 2013). It is postulated that CRELD2 can act as a PDI because it has been shown to interact with proteins such as matrilin-3 that contain disulphide bonds (Hartley et al., 2013). This current study shows that following the ablation of *Creld2* in chondrocytes there is no retention of matrilin-3. This suggests that there are other mechanisms involved in folding and trafficking matrilin-3 to the cartilage extracellular matrix of the growth plate.

The distribution of major structural proteins were unaffected in the growth plates of *Creld2*$^{CartΔEx3-5}$ mice. Type II collagen staining was comparable between the genotypes, however, knockout mice displayed diminished staining of type X collagen in

the hypertrophic zone and type I collagen in trabecular bone suggesting that the ablation of *Creld2* in chondrocytes potentially results in a defect in chondrocyte maturation and subsequent bone formation.

Ultrastructural analysis of the growth plate by transmission electron microscopy showed that the hypertrophic architecture of the cartilaginous extracellular matrix in knockout growth plates was also disrupted. The hypertrophic pericellular and interterritorial matrix was morphologically different in the knockout mice as the growth plates contained less fibrillar content. In addition, smaller unidirectional fibrils were observed in the interterritorial matrix.

To assess trabecular and cortical architecture, 3D μCT imaging of 3-week male tibiae was performed. *Creld2*$^{CartΔEx3\text{-}5}$ appeared to be smaller with a smaller secondary centre of ossification. Analysis of the trabecular bone showed that there was a reduction of 27.5 % in trabecular bone volume in *Creld2*$^{CartΔEx3\text{-}5}$ mice. Interestingly, there was no significant difference in cortical bone architecture suggesting that the effect of the ablation of *Creld2* in chondrocytes on bone arises from the disrupted growth plate and the turnover of cartilage to trabecular bone.

This is the first study to deep phenotype a cartilage-specific knockout of *Creld2*. The data presented here suggests a novel and important role for CRELD2 in cartilage. In summary, morphological and histochemical analyses showed that knockout mice displayed a distinctive chondrodysplasia phenotype characterised by disproportionate short statue, a disrupted cartilage growth plate with abnormal chondrocyte morphology and a resulting bone defect.

Chapter 4. Phenotyping the *Creld2* bone-specific knockout mouse model

Chapter 4. Phenotyping the *Creld2* bone-specific knockout mouse model

4.1 Introduction

Creld2 is a novel ER stress inducible gene expressed in mouse embryonic skeletal tissues. Several studies have identified CRELD2 as playing a role in protein folding and trafficking, however, the function of CRELD2 is largely unknown. Interestingly, a novel role has been identified for *Creld2* in mesenchymal stem cell BMP9-induced osteogenic differentiation (Zhang et al., 2013a). The precise role of *Creld2* in bone however is not understood. The purpose of this study was to investigate the role of *Creld2* in bone homeostasis *in vivo* using a *Creld2* bone-specific conditional knockout mouse *(Creld2*$^{Bone\Delta Ex3\text{-}5}$*)*, in which *Creld2* was knocked out in mature osteoblasts using the Cre-LoxP system, with *Cre* expression driven by the *Osteocalcin* promoter.

A number of morphometric and histological techniques were employed to analyse indepth the phenotype of the *Creld2* bone-specific knockout mouse model. The phenotyping strategy included:

- Morphometric studies in which the weights of mice at 3, 6 and 9 weeks were measured to determine if the deletion of *Creld2* in mature osteoblasts affected skeletal growth.
- Bone length measurements were taken from whole body radiographs to assess the effect of the knockout of *Creld2* on intramembranous and endochondral ossification.
- μCT scanning was also used to assess the effect of the ablation of *Creld2* on trabecular and cortical architecture.
- Histological assessment of bone phenotype, including quantitative analysis of cellular parameters, was performed to analyse differences between knockout and control bone.

4.2 The osteoblast-specific deletion of CRELD2 is not important for promoting skeletal growth

In the transgenic *Osteocalcin (OC)-Cre* expressing mouse, the *Osteocalcin* promoter drives *Cre* expression. The *OC-Cre* mouse was generated in Dr Thomas Clement's lab (John Hopkins University, USA.). Preliminary characterization of *OC-Cre* expression by Zhang *et al.* has shown that *OC-Cre* expression was initiated during mouse embryonic development at E17.5 and was restricted to cells of the osteoblast lineage (Zhang et al., 2002a).

Crossing these mice with a R26R reporter mouse strain allowed for the verification of the pattern of *OC-Cre* expression in 1-week limbs by X-gal staining. The expression of the *OC-Cre* transgene was restricted to cells lining the bone of 1-week joints (Figure 41). X-gal staining was therefore observed in osteoblasts but was not detected in chondrocytes of the cartilaginous growth plate.

As the expression of the *OC-Cre* transgene is restricted to cells of the osteoblast lineage, the *OC-Cre* transgene is therefore both a reliable and useful tool for manipulating gene expression in mature osteoblasts.

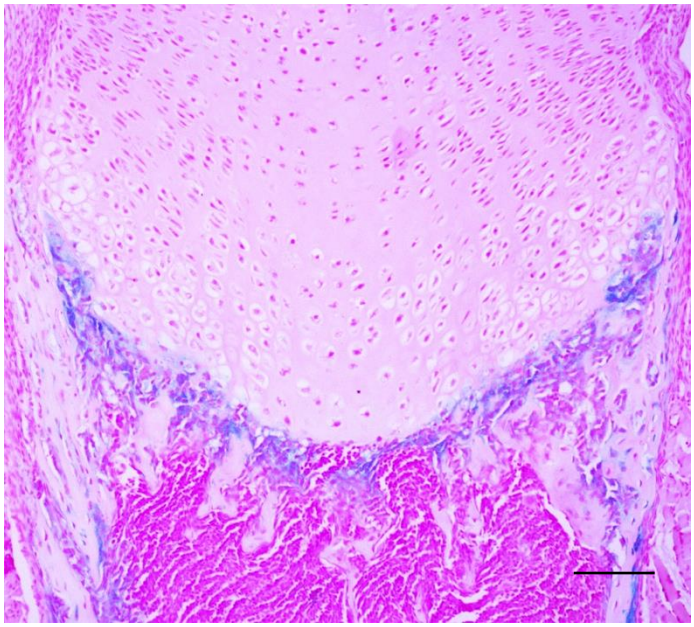

Figure 41. **The expression of the *OC-Cre* transgene is restricted to bone and is absent from chondrocytes in the cartilage growth plate.**

To analyse the expression pattern of *OC-Cre*, *OC-Cre* expressing mice were crossed with the R26R reporter mouse strain. β-galactosidase activity was examined using X-Gal, with activity indicated by a blue stain. In 3-week growth plates, *OC-Cre* expression was observed in osteoblasts lining the bone and absent from the cartilage growth plate. As the expression of the *OC-Cre* transgene is restricted to cells of the osteoblast lineage tissues, it is therefore a useful and reliable method of manipulating gene expression in mature osteoblasts. (Images representative of n=3 mice, Scale bar 100 μm).

4.3 The osteoblast specific deletion of CRELD2 is important for promoting postnatal skeletal growth

Creld2$^{Bone\Delta Ex3\text{-}5}$ and control mice were weighed at 3, 6 and 9 weeks and measurements were used chart growth over time (Figure 42A & 42 B). There was no significant difference between the weights of knockout and control male and female mice at 3 and 6 weeks of age. However, by 9 weeks of age male knockout mice were significantly lighter than control mice with a reduction in weight of 5.2 % ($p<0.05$) (Figure 42C). There was no significant difference in the weights of female mice at this time point (Figure 42D).

To study the effect of the ablation of *Creld2* in mature osteoblasts on endochondral and intramembranous bone development individual bone lengths were measured. By 9 weeks of age there appeared to be no obvious difference between the sizes of control and knockout mice (Figure 43). Endochondral ossification was unaffected in male and female knockout mice at 3 and 6 weeks as average lengths of the femur and tibia were comparable between the genotypes (Figure 43A & 43B and Figure 44A & 44B). However, by 9 weeks of age long bones were significantly shorter in knockout mice compared to age matched controls. In male mice the average length of the femur was 3.8 % ($p<0.05$) shorter and the average length of the tibias showed a reduction of 2.7% ($p<0.05$) relative to control mice (Figure 43B & 43C). Female mice also displayed shorter long bones at 9 weeks, with a 3.2 % and 1.8 % ($p<0.05$) reduction in average femur and tibia length respectively when compared to control mice (Figure 44B & 44C). Since endochondral ossification was unaffected at early ages but significantly disrupted by 9 weeks, this suggested that the ablation of *Creld2* in mature osteoblasts impairs bone growth but not bone development.

Intramembranous ossification was unaffected in both male and female *Creld2*$^{Bone\Delta Ex3\text{-}5}$ mice as the ICD and the skull lengths were comparable between genotypes at all time points (Figure 43C & 43D and Figure 44C & 44D). knockout mice.

A.

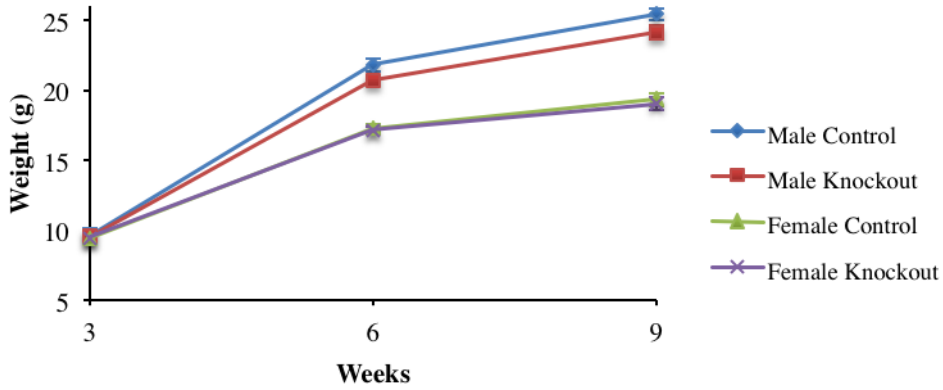

B.

		Average body weight (g) ± SEM		
		3 Weeks	6 Weeks	9 Weeks
Males	**Control**	9.61 ± 0.53	21.79 ± 0.47	25.42 ± 0.40
	Knockout	9.61 ± 0.19	20.72 ± 0.34	24.11 ± 0.47*
Females	**Control**	9.42 ± 0.32	17.26 ± 0.33	19.38 ± 0.34
	Knockout	9.47 ± 0.18	17.12 ± 0.28	19.02 ± 0.50

C.

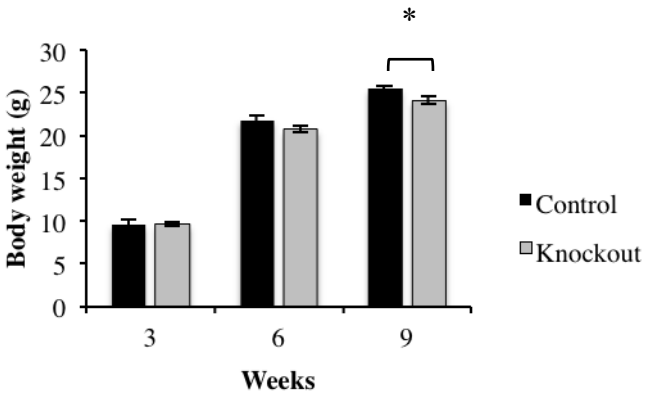

D.

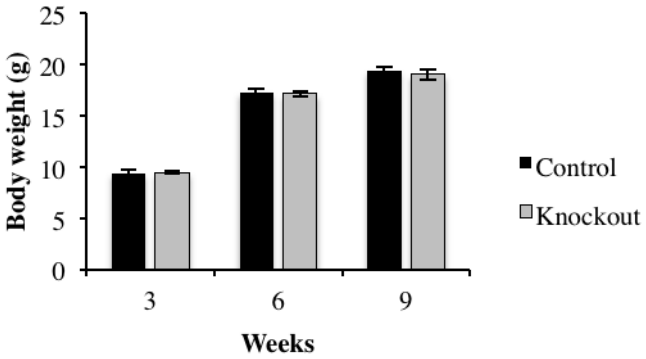

***Figure 42. Creld2* bone-specific knockout mice are not significantly smaller than age matched controls.**

The growth of male and female mice was charted over 9 weeks. There was no significant difference in the rate of growth of male and female knockout mice relative to control mice (**A.**). A table showing numerical data that is presented in the graphs (**B.**). Knockout males were not significantly smaller at 3 and 6 but were significantly lighter at 9 weeks (**C.**). There was no significant difference in size between knockout and control females at 3, 6 and 9 weeks (**D.**). (SEM = standard error of the mean, * $p<0.05$, ** $p<0.005$, unpaired t-test, $n>10$ per genotype at all ages.

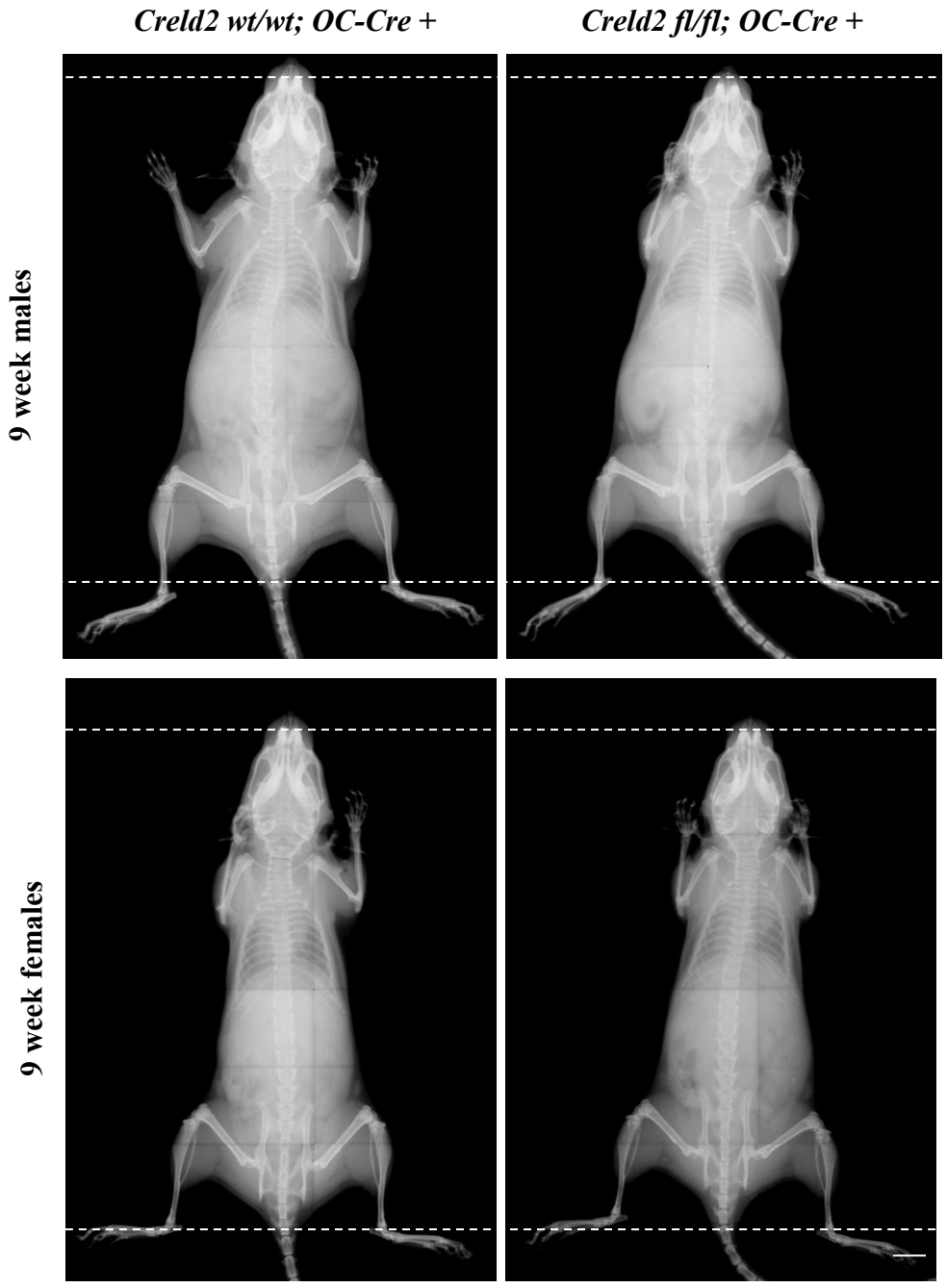

Figure 43. **Radiographs of male and female mice at 9 weeks.**

To study the skeletal phenotype following the ablation of *Creld2* in bone, radiographs were taken. There appeared to be no difference in the overall size of mice at 9 weeks however long bones appeared shorter in *Creld2*$^{Bone\Delta Ex3\text{-}5}$ mice. (Images representative of n>10 mice at all ages per genotype, Scale bar 5 mm).

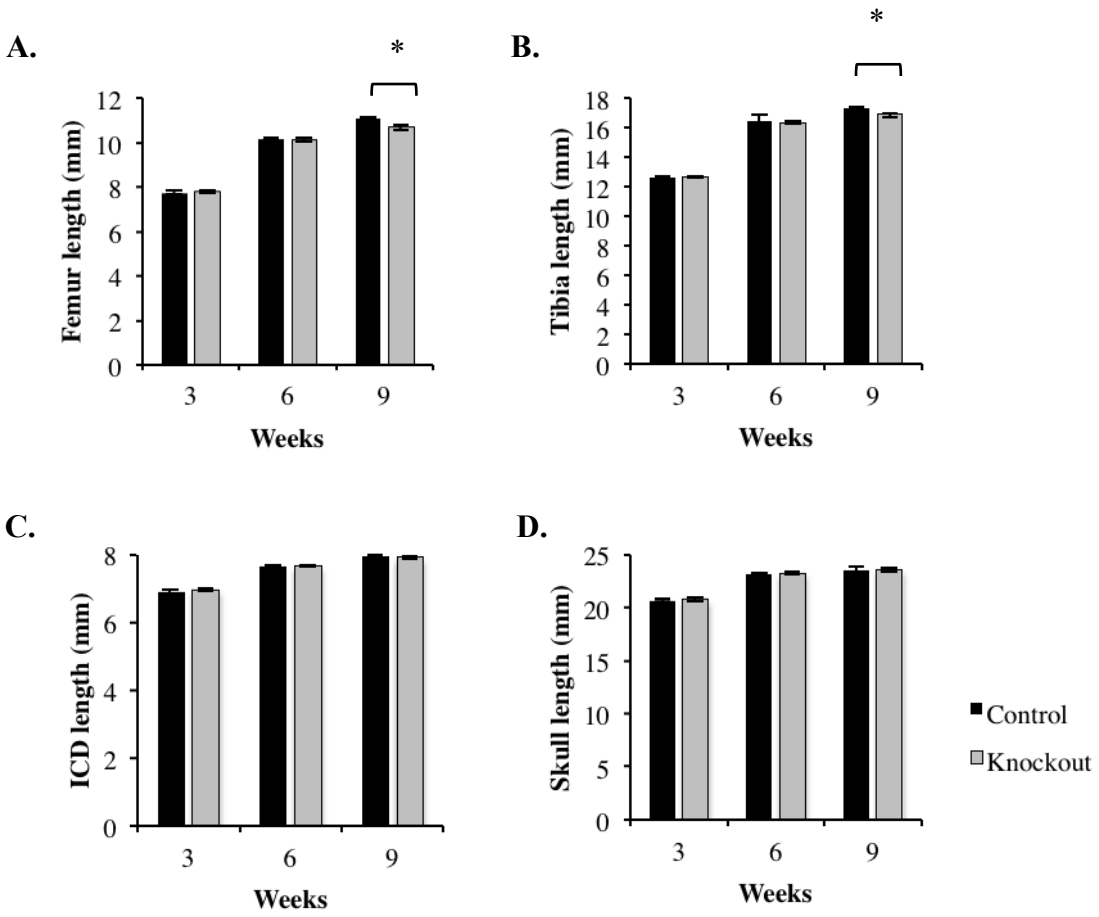

		Bone length (mm) ± SEM		
		3 Weeks	6 Weeks	9 Weeks
Femur	**Control**	7.74 ± 0.09	10.17 ± 0.07	11.09 ± 0.07
	Knockout	7.78 ± 0.06	10.14 ± 0.08	10.67 ± 0.11*
Tibia	**Control**	12.56 ± 0.17	16.46 ± 0.41	17.31 ± 0.07
	Knockout	12.64 ± 0.05	16.31 ± 0.10	16.87 ± 0.12*
ICD	**Control**	6.90 ± 0.06	7.65 ± 0.03	7.97 ± 0.03
	Knockout	6.96 ± 0.02	7.66 ± 0.04	7.82 ± 0.04
Skull	**Control**	20.64 ± 0.21	23.12 ± 0.11	23.60 ± 0.25
	Knockout	20.78 ± 0.13	23.27 ± 0.16	23.58 ± 0.20

Figure 44. **By 9 weeks of age *Creld2* bone-specific knockout male mice have significantly shorter long bones than age matched controls.**

Mice were X-rayed and lengths of the femur, tibia, ICD and skull lengths were measured at 3, 6 and 9 weeks. There was no significant difference in bone lengths between knockout and control mice at both 3 and 6 weeks. Interestingly, by 9 weeks knockout mice displayed a 3.8 % and 2.7 % reduction in lengths of the femur (**A.**) and tibia (**B.**) respectively compared to age matched controls. At 9 weeks however lengths of the ICD (**C.**) and the skull (**D.**) were comparable between genotypes. Numerical data presented in graphs shown in the table. (SEM = standard error of the mean, * $p<0.05$, unpaired t-test, $n>10$ at each age per genotype).

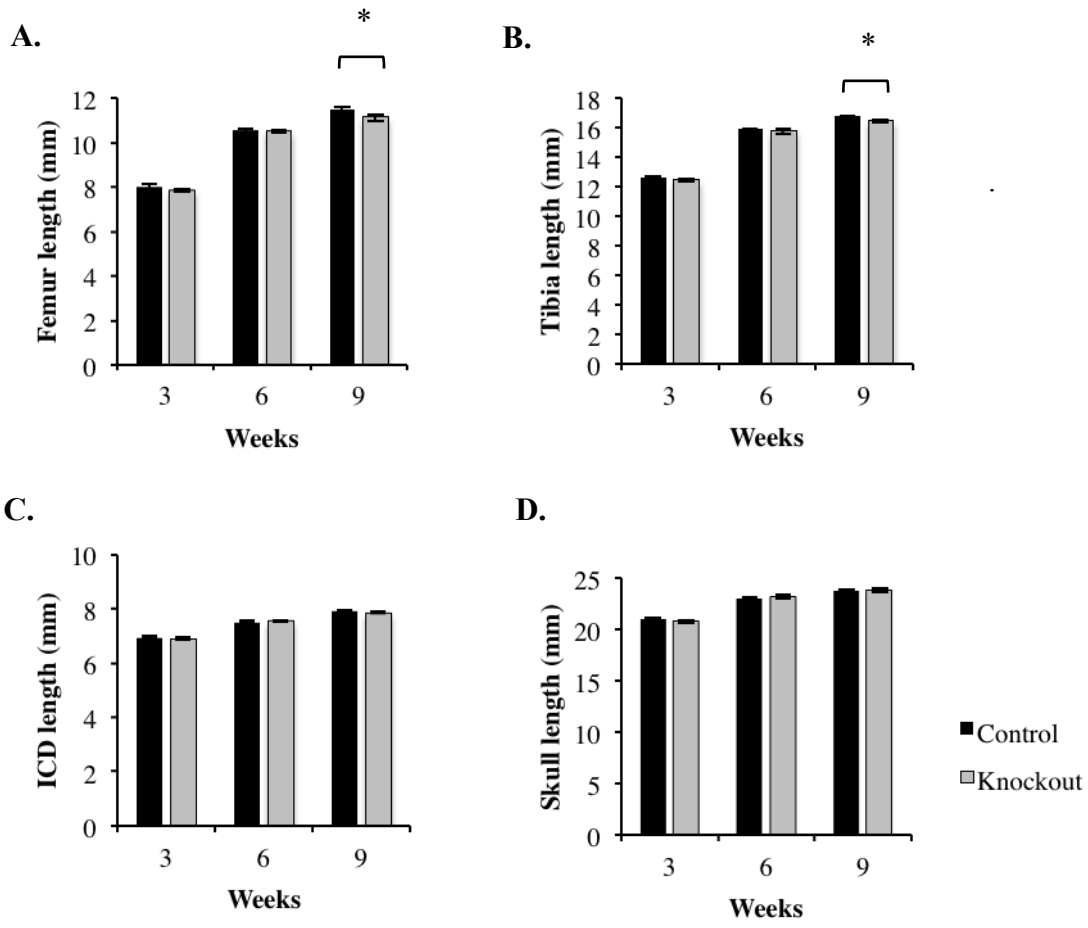

		Bone length (mm) ± SEM		
		3 Weeks	6 Weeks	9 Weeks
Femur	**Control**	8.02 ± 0.10	10.55 ± 0.07	11.50 ± 0.10
	Knockout	7.85 ± 0.06	10.50 ± 0.05	11.13 ± 0.13*
Tibia	**Control**	12.57 ± 0.12	15.87 ± 0.08	16.75 ± 0.07
	Knockout	12.46 ± 0.08	15.75 ± 0.18	16.45 ± 0.10 *
ICD	**Control**	6.95 ± 0.06	7.52 ± 0.04	7.90 ± 0.04
	Knockout	6.89 ± 0.05	7.55 ± 0.03	7.85 ± 0.05
Skull	**Control**	20.96 ± 0.17	23.03 ± 0.14	23.70 ± 0.17
	Knockout	20.78 ± 0.18	23.18 ± 0.20	23.86 ± 0.18

Figure 45. **By 9 weeks of age *Creld2* bone-specific knockout female mice have significantly shorter long bones than age matched controls.**

Mice were X-rayed and lengths of the femur, tibia, ICD and skull lengths were measured at 3, 6 and 9 weeks. There was no significant difference in bone lengths between knockout and control mice at both 3 and 6 weeks. Interestingly, by 9 weeks knockout mice displayed a 3.2 % and 1.8 % reduction in lengths of the femur (**A.**) and tibia (**B.**) respectively compared to age matched controls. At 9 weeks however lengths of the ICD (**C.**) and the skull (**D.**) were comparable between genotypes. Numerical data presented in graphs shown in the table. (SEM = standard error of the mean, * $p<0.05$, unpaired t-test, $n>10$ at each age per genotype).

4.4 The deletion of CRELD2 in osteoblasts results in an osteopenic phenotype with reduced bone volume

To evaluate the effects of the targeted deletion of *Creld2* in mature osteoblasts on trabecular and cortical bone microarchitecture, individual tibial bones from *Creld2*$^{BoneΔEx3\text{-}5}$ mice at 3, 6 and 9 weeks were imaged by 3D μCT. Images were reconstructed into a 3D volumetric structure from which bone structural parameters were analysed. Trabecular bone was analysed under the epiphyseal growth plate of the proximal tibia whilst cortical bone was analysed in the tibia midshaft.

μCT images of control and knockout tibiae suggest that *Creld2*$^{BoneΔEx3\text{-}5}$mice appear to have less trabecular bone (Figure 45). In depth analysis of bone microarchitecture showed that *Creld2*$^{BoneΔEx3\text{-}5}$ female mice have significantly less trabecular bone in the proximal tibia relative to control mice, with a reduction of 30.1 %, 36.9 % and 29.2 % (all $p<0.005$) at 3, 6 and 9 weeks respectively (Figure 46A). There were also significantly less trabeculae in knockout tibiae at all age groups with trabecular number reduced by 29.4 %, 38.6 % and 27.5 % ($p<0.005$, $p<0.005$, $p<0.05$) (Figure 46B). Knockout tibiae also displayed thinner trabeculae, which were 4.1 %, 3.3 % and 4.0 % ($p<0.05$, $p<0.005$, $p<0.05$) thinner than trabeculae in control mice at 3, 6 and 9 weeks (Figure 46C). This corresponds to a significant increase in trabecular spacing in knockout tibiae, with an increase of 8.0 %, 6.4 % and 5.8 % ($p<0.005$, $p<0.05$, $p<0.05$) relative to age matched controls at 3, 6 and 9 weeks of age (Figure 46D).

In order to study cortical bone structure of knockout tibiae, cortical porosity was analysed. Tibiae from *Creld2*$^{BoneΔEx3\text{-}5}$ mice displayed an increase in cortical porosity with an increase of 1.2 %, 1.1 % and 1.4 % ($p<0.005$, $p<0.005$, $p<0.05$) compared to age matched controls at 3, 6 and 9 weeks of age (Figure 47).

The bone phenotype observed by μCT scanning was confirmed using Von Kossa staining. Von Kossa staining was used to quantify mineralisation as a black precipitate forms when silver ions react with the phosphate of mineralised bone (Figure 48A-D). Counterstaining with Van Geison allowed for visualisation of the unmineralised bone known as osteoid that appears pink following staining. Concurrent with the results from μCT scanning, *Creld2*$^{BoneΔEx3\text{-}5}$ female mice had significantly less trabecular bone, with a reduction of 19.7 % compared to age matched controls (Figure 48E). Interestingly, there was also a 47.3 % significant decrease in osteoid surface in *Creld2*$^{BoneΔEx3\text{-}5}$ mice

relative to control mice (Figure 48F). *Creld2* bone-specific knockout mice therefore display an osteopenic phenotype with reduced bone density.

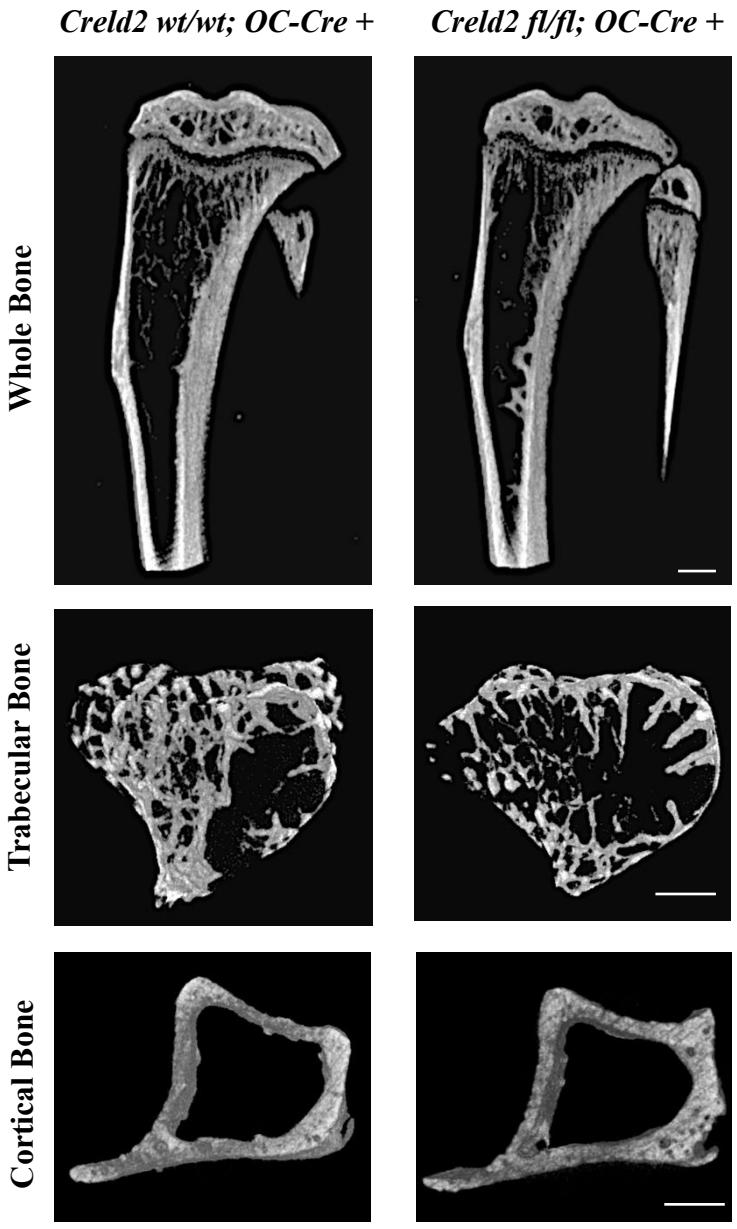

Figure 46. **Reconstructed µCT images of a 9 week old tibias.**

To study the effect of *Creld2* deletion in osteoblasts on bone microarchitecture, 3, 6 and 9 week old female tibiae were scanned and analysed using µCT imaging. Initial observations of the 3D µCT images of control and knockout tibiae suggest that *Creld2*$^{Bone\Delta Ex3\text{-}5}$ mice appear to have less trabecular bone (Images representative of n=10 mice per genotype, Scale bar 500 µm. Male mice showed same phenotype, data not shown).

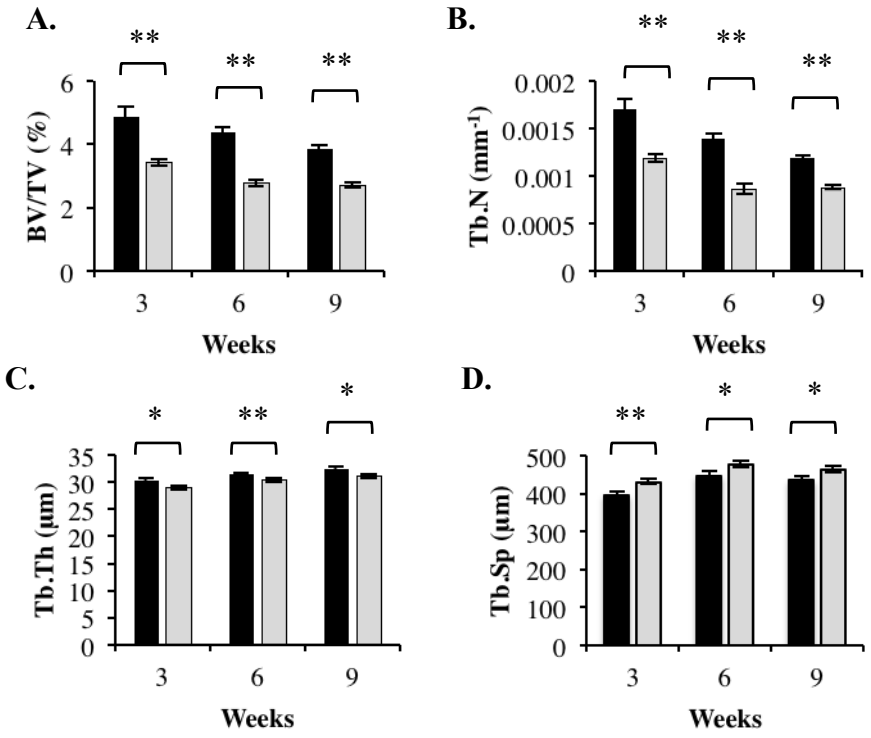

		Measurement ± SEM		
		3 Weeks	6 Weeks	9 Weeks
Percentage Bone Volume (BV/TV) (%)	**Control**	4.88 ± 0.30	4.39 ± 0.13	3.84 ± 0.11
	Knockout	3.41 ± 0.12**	2.77 ± 0.12**	2.72 ± 0.08**
Trabecular Number (Tb.N) (mm^{-1})	**Control**	0.0017 ± 0.00010	0.0014 ± 0.000044	0.0012 ± 0.000027
	Knockout	0.0012 ± 0.000040**	0.00086 ± 0.000053**	0.00087 ± 0.00030**
Trabecular Thickness (Tb.Th) (µm)	**Control**	30.18 ± 0.42	31.39 ± 0.26	32.42 ± 0.52
	Knockout	28.95 ± 0.27*	30.37 ± 0.37**	31.12 ± 0.33*
Trabecular Spacing (Tb.Sp) (µm)	**Control**	396.13 ± 8.29	446.89 ± 11.11	435.99 ± 10.33
	Knockout	430.57 ± 6.86**	477.39 ± 8.63*	462.99 ± 8.39*

Figure 47. **Female *Creld2* bone-specific knockout mice have significantly less trabecular bone with altered microarchitecture compared to age matched control mice.**

To assess trabecular architecture 3D µCT imaging of female tibiae was performed. Knockout mice had significantly less trabecular bone (**A.**) relative to control mice with reductions of 30.1 %, 36.9 % and 29.2 % at 3, 6 and 9 weeks of age. Trabecular number (**B.**) was also significantly reduced in knockout mice at all ages by 29.4 %, 38.6 % and 27.5 % respectively. A significant reduction of 4.1 %, 3.3 % and 4.0 % was also seen for trabecular thickness (**C.**). Trabecular spacing (**D.**) was subsequently increased in knockout mice with significant increases of 8.0 %, 6.4 % and 5.8 % at 3, 6 and 9 weeks of age. Numerical data presented in graphs shown in the table. (BV/TV = Percentage bone volume, Tb.N = Trabecular number, Tb.Sp = Trabecular spacing, Tb.Th = Trabecular thickness, Tb.Pf = Trabecular pattern factor, SEM = standard error of the mean, * $p<0.05$, ** $p<0.005$, unpaired t-test, $n>10$ mice per genotype. Male mice showed the same phenotype, data not shown).

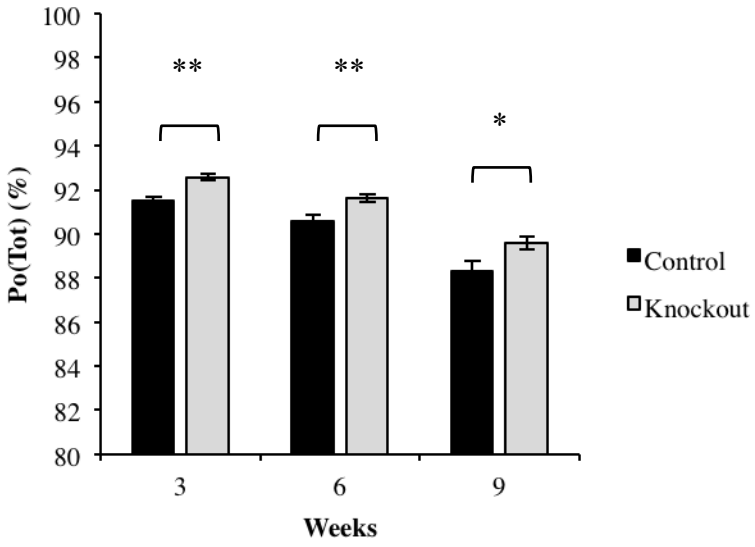

	Total porosity (%) ± SEM		
	3 Weeks	**6 Weeks**	**9 Weeks**
Control	91.49 ± 0.22	90.60 ± 0.26	88.33 ± 0.11
Knockout	92.57 ± 0.15**	91.60 ± 0.17**	89.60 ± 0.30*

Figure 48. **Tibial cortical bone is significantly more porous in female *Creld2* bone-specific knockout mice than age matched controls.**

To assess cortical architecture 3D micro-computed tomography (μCT) imaging of tibias from female mice at 3, 6 and 9 weeks of age was performed and cortical porosity was analysed. *Creld2*$^{Bone\Delta Ex3\text{-}5}$ mice display an increase in cortical porosity of the trabecular bone with increases of 1.2 %, 1.1 % and 1.4 % at 3, 6 and 9 weeks of age relative to age matched controls. Numerical data presented in graphs shown in the table. (Po(Tot) = Cortical porosity, SEM = standard error of the mean, * $p<0.05$, ** $p<0.005$,unpaired T-Test, n>10 mice per genotype. Male mice showed same phenotype, data not shown).

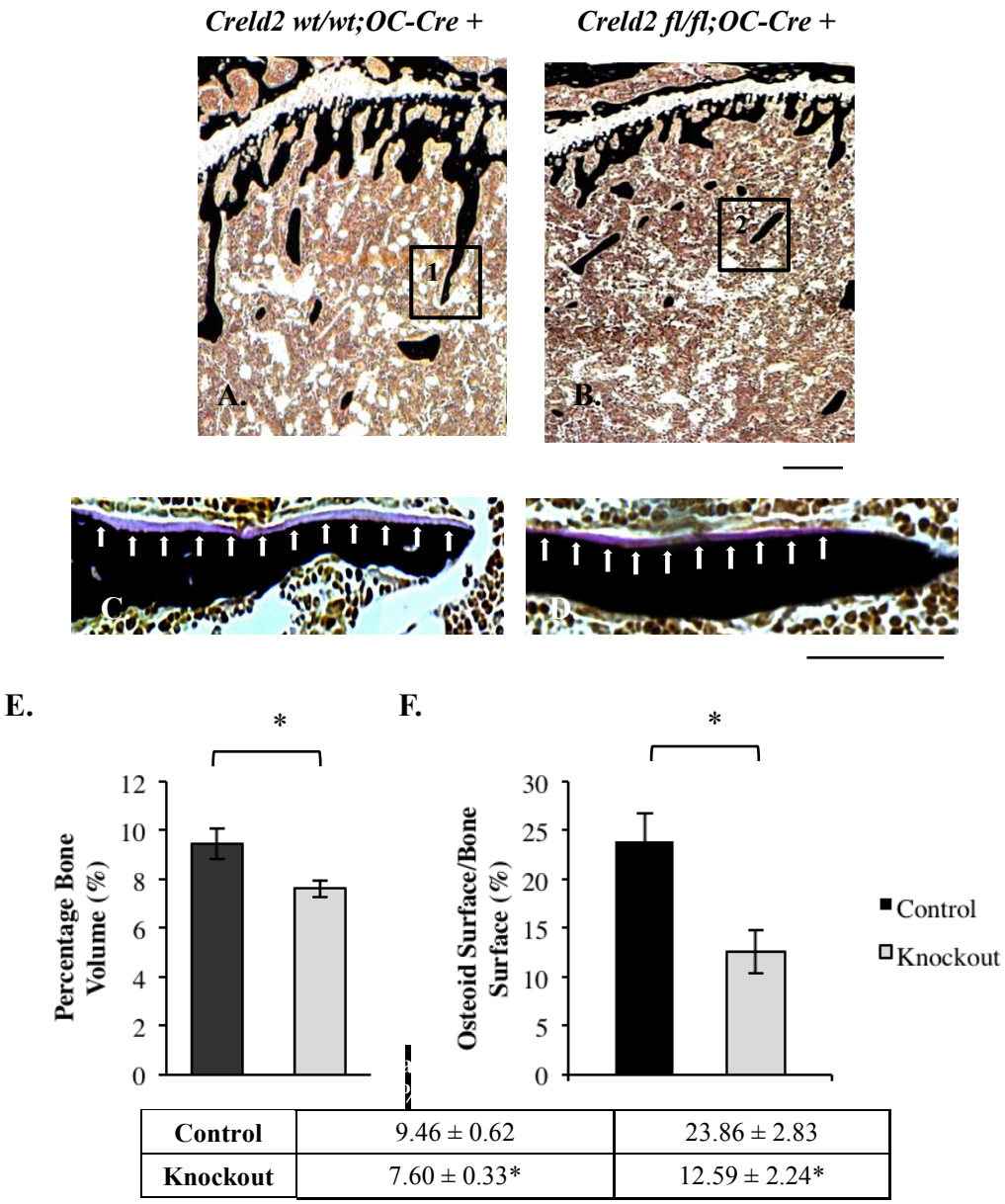

Control	9.46 ± 0.62	23.86 ± 2.83
Knockout	7.60 ± 0.33*	12.59 ± 2.24*

***Figure 49. Creld2* bone-specific knockout mice display a reduction in bone volume with a decrease in osteoid.**

To assess bone volume and the percentage of unmineralised bone, female tibial sections were stained with Von Kossa/Van Geison (**A.** & **B.**). Magnified images showing osteoid presented in (**C.** & **D.**). (Box 1 magnified in **C.**, Box 2 magnified in **D.**) *Creld2*$^{Bone\Delta Ex3\text{-}5}$ mice display a significant reduction of 19.7 % in the percentage trabecular bone (**E.**) relative to control mice. Interestingly, there was also a 47.3 % significant decrease in osteoid surface (**F.**) in *Creld2*$^{Bone\Delta Ex3\text{-}5}$ mice relative to control mice. Numerical data presented in graphs shown in the table. (The newly forming bone, the osteoid, is stained pink and outlined by white arrows. SEM = standard error of the mean, * $p<0.05$, unpaired t-test, n=5 mice per genotype, Scale bar 50 µm. Male mice showed same phenotype, data not shown).

4.5 The knockout of CRELD2 expression in osteoblasts disrupts bone cell homeostasis and results in a decreased number of osteoblasts and an increased number of osteoclasts

To investigate the effect of knocking out *Creld2* in mature osteoblasts at a cellular level, histological staining was performed to visualise osteoblasts and osteoclasts on the trabecular bone surface.

To analyse the impact of *Creld2* deletion on osteoblast numbers tibial sections were stained with toluidine blue and the number of active osteoblasts per bone surface was analysed (Figure 50A-50D). Analysis of knockout bone revealed a 25.7 % ($p<0.05$) reduction in the number of active osteoblasts per bone surface relative to control mice at 9 weeks of age (Figure 50E)

Histochemical staining of tibial sections for TRAcP allowed an assessment of osteoclast number and erosion surface (Figure 51A). Interestingly, knockout mice displayed a dramatic increase in osteoclast number per bone surface, with an increase of 53.3 % ($p<0.005$) compared to control mice (Figure 51B). Subsequently a 59.4 % ($p<0.005$) increase in erosion surface was also observed in 9 week old knockout mice (Figure 51C).

Despite the targeted deletion of *Creld2* in mature osteoblasts, the lack of *Creld2* in osteoblasts indirectly affects osteoclastogenesis. As such, these data suggest a disruption to cellular communication and homeostasis between osteoblasts and osteoclasts.

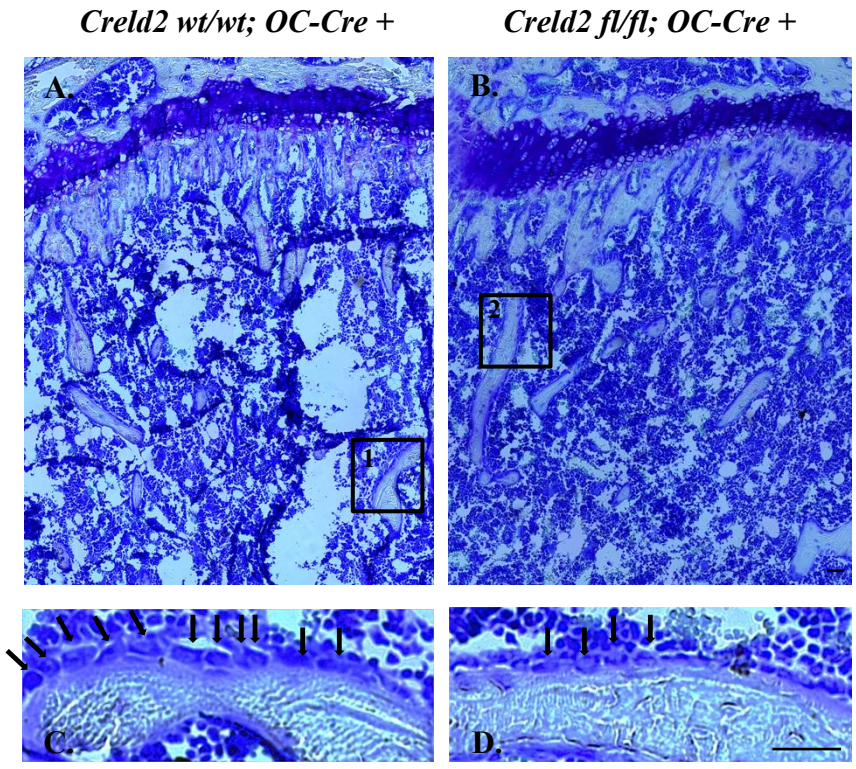

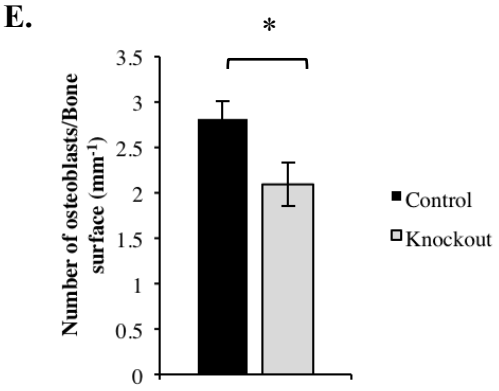

	Number of osteoblasts/Bone Surface (mm^{-1})± SEM
Control	2.81 ± 0.19
Knockout	2.09 ± 0.23*

***Figure 50. Creld2* bone-specific knockout mice display a reduction in the number of active osteoblasts compared to control mice.**

To assess osteoblast number, female tibial sections were stained with toluidine blue and the number of active osteoblasts per bone surface was counted (**A.** & **B.**). Magnified images showing osteoblasts presented in (**C.** & **D.**). (Box 1 magnified in **C.**, Box 2 magnified in **D.**). *Creld2*$^{Bone\Delta Ex3\text{-}5}$ mice display a significant reduction of 25.7 % in the number of active osteoblasts (**E.**) per trabecular bone surface relative to control mice. Numerical data presented in graphs shown in the table. (Osteoblasts indicated by black arrow. SEM = standard error of the mean, * $p<0.05$, unpaired t-test, n=5 mice per genotype, Magnification x200, Scale bar 50 μm. Male mice showed same phenotype, data not shown.).

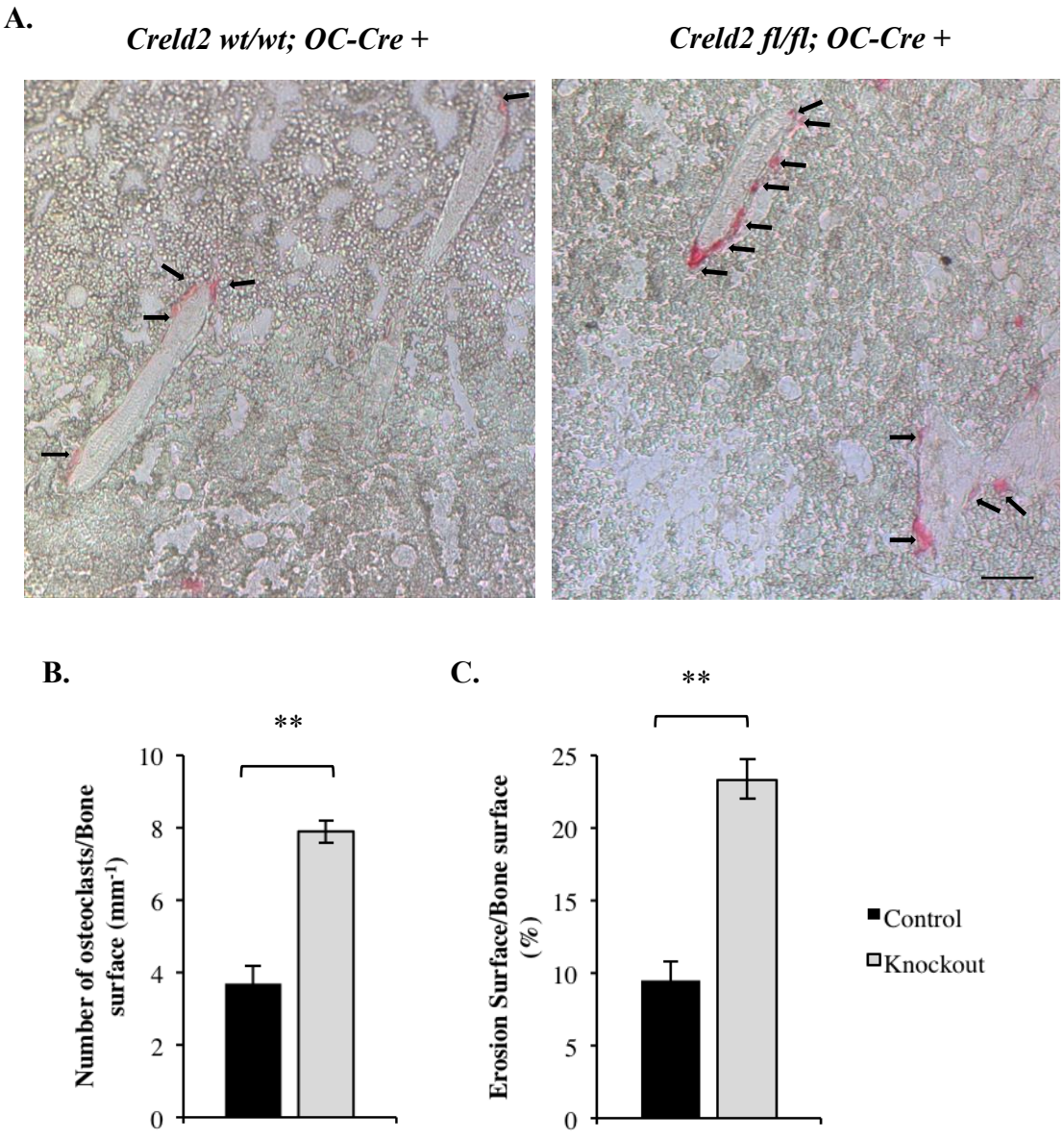

	Number of osteoclasts/Bone Surface (mm^{-1}) ± SEM	Erosion Surface/Bone Surface (%) ± SEM
Control	3.68 ± 0.52	9.46 ± 1.34
Knockout	7.88 ± 0.29**	23.33 ± 1.35**

***Figure 51. Creld2* bone-specific knockout mice display a dramatic increase in the number of osteoclasts and subsequent erosion of surface compared to control mice.**

Histochemical staining of female tibial sections for TRAcP allowed an assessment of osteoclast number and erosion surface (**A.**). *Creld2*$^{Bone\Delta Ex3\text{-}5}$ mice display a significant increase of 53.3 % in the number of osteoclasts per trabecular bone surface (**B.**) relative to control mice. Subsequent erosion surface (**C.**) was also dramatically increased in knockout mice by 59.4 %. Numerical data presented in graphs shown in the table. (Osteoclasts indicated by black arrow. SEM = standard error of the mean, ** $p<0.005$, unpaired t-test, n=5 mice per genotype, Scale bar 50 μm. Male mice showed same phenotype, data not shown.).

4.6 Summary

The aim of this chapter was to characterise the skeletal phenotype of a *Creld2* bone-specific knockout mouse model using a variety of morphometric and histological techniques.

Creld2$^{Bone\Delta Ex3\text{-}5}$ mice had a normal skeletal phenotype at 3 and 6 weeks of age with no differences in bone lengths between control and knockout mice. However, knockout mice displayed a progressive phenotype with shorter long bones by 9 weeks of age. For example the lengths of the tibiae were reduced by 1.7 % and 1.8 % in 9-week male and female knockout mice respectively. Weights were comparable between the genotypes at 3 and 6 weeks. By 9 weeks, *Creld2*$^{Bone\Delta Ex3\text{-}5}$ male mice were significantly lighter than control mice with a decrease in body weight of 5.2 % relative to age matched controls potentially due to a progressive decrease in bone mineral density.

To assess the effects of the targeted *Creld2* deletion in mature osteoblasts on trabecular and cortical bone microarchitecture, tibiae from *Creld2*$^{Bone\Delta Ex3\text{-}5}$ mice at 3, 6 and 9 weeks were imaged by 3D μCT. Analysis of the bone phenotype revealed that the *Creld2*$^{Bone\Delta Ex3\text{-}5}$ mice displayed an osteopenic phenotype with reduced bone density. For example, by 9 weeks trabecular bone volume was significantly reduced in knockout mice, with a decrease of 29.2 % relative to age matched controls. Similar patterns of cortical bone loss was also observed in knockout mice, with an increase of 1.4 % in cortical porosity of 9 week knockout bones relative to control mice.

Interestingly, physiological ER stress has been shown to play a role in active osteoblasts as cuboidal osteoblasts lining the bone have been shown to express BIP and PDI. PERK signalling is also important in bone formation as *Perk* global knockout mice exhibit postnatal growth retardation and osteoporosis (Zhang et al., 2002b). In a murine model for osteoporosis, osteoblasts show diminished expression of the ER molecular chaperones BIP and PDI suggesting that the folding capacity of osteoblasts for secreted proteins is diminished and could result in decreased bone formation (Hino et al., 2010). It is postulated that CRELD2 functions as a putative protein disulphide isomerase due to C-terminal CxxC motifs and therefore could play a role in the aiding the folding and trafficking of proteins stabilised by disulphide bonds (Hartley et al., 2013). It can therefore be postulated that the osteopenic phenotype observed in the bone-specific *Creld2* knockout mice could result from reduced bone formation.

The bone phenotype observed by μCT scanning was confirmed using Von Kossa staining. Like the phenotype observed with μCT scanning, *Creld2*$^{Bone\Delta Ex3\text{-}5}$ female mice have significantly less percentage trabecular bone. Interestingly, there was also a 47.3 % significant decrease in the percentage of unmineralised bone called osteoid in *Creld2*$^{Bone\Delta Ex3\text{-}5}$ mice relative to control mice. As there was not a significant increase in osteoid, this suggests that the low bone mass is not related to a defect in mineralization, but perhaps due to a disruption to osteoid formation.

Physiological ER stress signalling has been shown to play a role in bone formation. The expression pattern of OASIS, a transcription factor similar to ATF6, was found to overlap with the expression of components of osteoid including osteonectin, osteopontin and type I collagen (Nikaido et al., 2001). Furthermore, the deletion of *Oasis* in mice resulted in growth retardation and severe osteopenia due to a reduction in bone formation and a decrease in *Col1a1* expression (Murakami et al., 2009, Murakami et al., 2011b). *Creld2* is a downstream target of ATF6 and this could therefore explain the milder phenotype observed in *Creld2*$^{Bone\Delta Ex3\text{-}5}$ mice (Oh-hashi et al., 2009).

The pathogenesis of osteopenia can result from an increase in active osteoclasts, a decrease in the number of active osteoblasts or a combination of the two. To analyse if the defect in bone density resulted from a disruption to bone cells, the number of active osteoblasts and osteoclasts were analysed by histological staining. Interestingly, there was a 25.7 % reduction in the number of active osteoblasts in knockout bones. In addition there was a dramatic increase in osteoclast number in knockout bone with an increase of 53.3 % relative to control mice.

The global knockouts of *Perk* and *Oasis* both show that there is a reduction in the number of bone forming osteoblasts (Wei et al., 2008, Murakami et al., 2009). However in *Oasis* -/- mice osteoclast number was unaffected and in *Perk* -/- mice osteoclast function was impaired. These results presented here indicate that the osteopenic skeletal phenotype of *Creld2*$^{Bone\Delta Ex3\text{-}5}$ mice is due to the inhibition of osteoblast maturation and the indirect stimulation of osteoclastogenesis. This outlines that CRELD2 potentially plays a role in osteoblast differentiation, however unlike the role of other ER stress signalling proteins, CRELD2 also indirectly regulates osteoclast differentiation.

This is the first study to deep phenotype a bone-specific knockout of *Creld2*. The data presented here suggests a novel and important role for CRELD2 in bone. In

summary, the morphological and histochemical analyses showed that *Creld2*$^{Bone\Delta Ex3\text{-}5}$ mice display an osteopenic phenotype characterised by a lower bone density. This is potentially due to a disruption in osteoblast/osteoclast communication and homeostasis since knockout mice display a reduction in the number of active osteoblasts and a dramatic increase in the number of osteoclasts.

Chapter 5. Investigating the role of *Creld2* in skeletal development

Chapter 5. Investigating the role of *Creld2* in skeletal development

5.1 Introduction

The work presented in Chapter 3 has shown that *Creld2* cartilage-specific knockout mice display disproportionate short stature with a disrupted growth plate. The aim of this chapter was therefore to investigate the role of this putative PDI in cartilage and deduce its function in both development and postnatal longitudinal bone growth.

In order to analyse the mechanism that resulted in the pathology of *Creld2*$^{Cart\Delta Ex3\text{-}5}$ mice outlined in Chapter 3, a variety of histological and OMICS techniques were employed. Specifically:

- The temporal and spatial regulation of chondrocyte proliferation and apoptosis at the chondro-osseous boundary is the main driving force of endochondral ossification. Growth plate chondrocyte apoptosis and proliferation was therefore analysed to provide a mechanistic link between the lack of CRELD2 in chondrocytes and the reduction in long bone growth observed in the knockout mice.
- Work presented in Chapter 3 showed that *Creld2*$^{Cart\Delta Ex3\text{-}5}$ mice display a reduction in trabecular bone volume. The switch between cartilage and bone during endochondral ossification is controlled by angiogenesis (Gerber et al., 1999). The expression of a vascular marker was therefore analysed by immunohistochemistry in order to identify differences in angiogenesis following the ablation of CRELD2. In addition, histological analysis of osteoblasts was performed to analyse if the number of trabecular osteoblasts was affected in *Creld2*$^{Cart\Delta Ex3\text{-}5}$ mice.
- Primary cilia play an important role in the regulation of growth plate structure and function (de Andrea et al., 2010). Immunohistochemistry was employed to determine the organisation of primary non-motile cilia on proliferative chondrocytes and to give a measure of cell polarity in the growth plate.

- RNA-sequencing was performed to compare the transcriptome of knockout mice with control mice and identify genes and pathways affected following the ablation of *Creld2* in chondrocytes.
- Studies show that CRELD2 is spontaneously secreted from cells (Oh-hashi et al., 2011). Immunocytochemistry was performed to confirm the subcellular localisation of CRELD2 in chondrocytes
- Finally, to deduce the role of CRELD2 in chondrocytes, CRELD2 binding partners were identified by Co-IP. The function of these proteins may be impaired following the knockout of *Creld2* expression and could result in the phenotype outlined in Chapter 3.

5.2 The deletion of CRELD2 in chondrocytes disrupts proliferation and survival

To assess chondrocyte proliferation chondrocytes were labelled *in vivo* for 2 hours with BrdU. A total of 9 sections per mouse from 3 unrelated mice per genotype were analysed. As the length of the proliferative zone in knockout growth plates was significantly smaller, this may have corresponded to a reduced total number of cells. Therefore, the number of BrdU-labelled proliferating cells was expressed as a proportion of the total number of cells in the proliferative zone. Overall, *Creld2*$^{Cart\Delta Ex3\text{-}5}$ mice displayed a 19.0 % ($p<0.05$) reduction in the number of proliferating cells with 9.6 % of cells labelled in the proliferative zone compared to 11.7 % in age matched controls (Figure 52).

Chondrocyte apoptosis was assessed by a TUNEL assay. A total of 9 sections per mouse from 3 unrelated mice per genotype were analysed. The numbers of TUNEL positive cells were counted in each of the three zones, resting, proliferative and hypertrophic, and were presented as a proportion of the total number of cells in each zone. Control mice displayed TUNEL positive cells almost exclusively in the hypertrophic zone with 0.06 %, 0.03 % and 0.35 % in the resting, proliferative and hypertrophic zones respectively (Figure 53). In contrast, apoptosis was detected in all zones of the knockout growth plates with 1.92 %, 0.24 % and 1.30 % in the resting, proliferative and hypertrophic zones respectively (Figure 53). This corresponded to a 32.0-fold ($p<0.05$), 8.0-fold ($p<0.05$) and 3.7-fold ($p<0.005$) significant increase in apoptosis in the three growth plate zones.

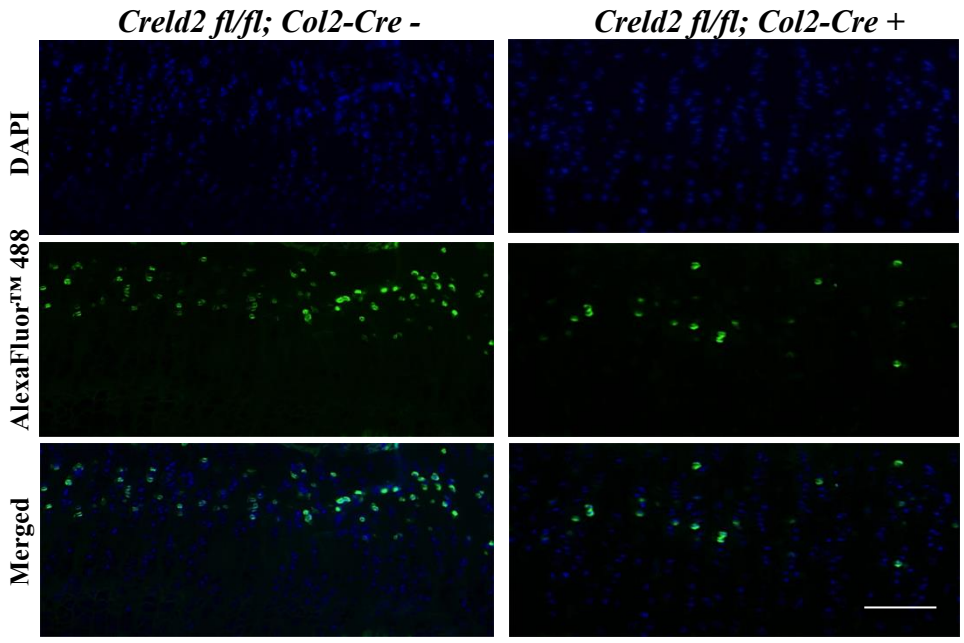

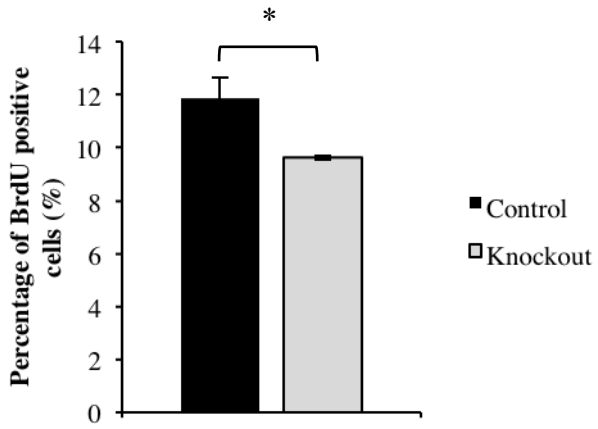

	Percentage BrdU positive cells (%) ± SEM
Control	11.86 ± 0.77
Knockout	9.61 ± 0.07*

Figure 52. **The knockout of *Creld2* in cartilage disrupts chondrocyte proliferation.**

Immunohistochemistry using an anti-BrdU antibody was performed to assess chondrocyte proliferation. BrdU positive cells were detected using an AlexaFluor™ 488 secondary antibody (green) and the nuclei of chondrocytes were counterstained with DAPI (blue). BrdU positive cells in the proliferative zone of the growth plate were calculated as a percentage of the total number of cells in the proliferative zone. *Creld2*$^{CartΔEx3\text{-}5}$ mice displayed a 19.0 % significant reduction in the percentage number of proliferating cells compared to age matched controls. Numerical data presented in graphs are shown in the table. (SEM = standard error of the mean, * $p<0.05$, unpaired t-test, n=3 matched sections from 3 locations throughout the growth plate. Sections were from 3 male mice from 3 different litters per genotype, Scale bar 100 μm).

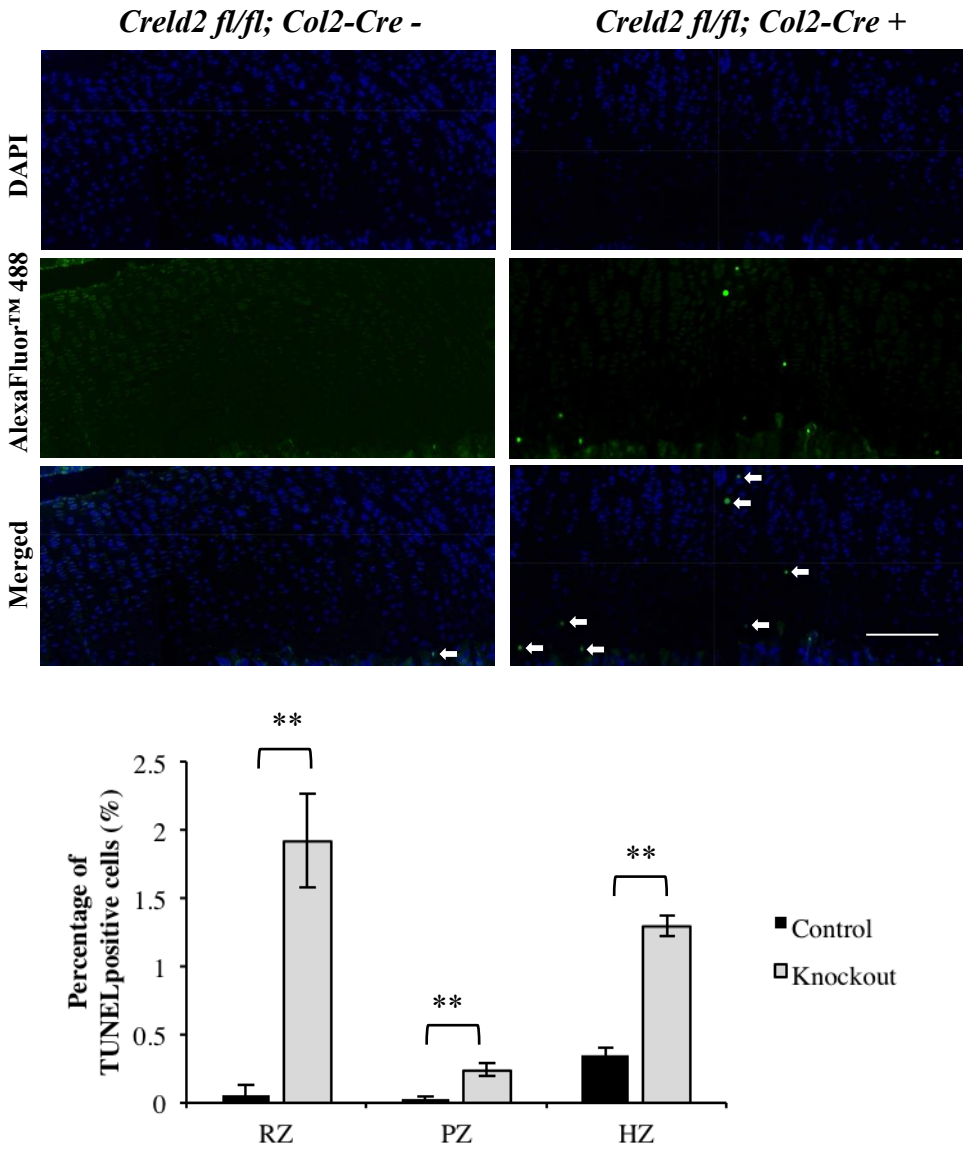

	Percentage TUNEL positive cells (%)± SEM		
	Resting Zone	Proliferative Zone	Hypertrophic Zone
Control	0.062 ± 0.062	0.03 ± 0.01	0.35 ± 0.044
Knockout	1.92 ± 0.35	0.25 ± 0.045	1.30 ± 0.078

Figure 53. **The knockout of *Creld2* in cartilage affects chondrocyte survival.**

Terminal apoptosis was analysed by TUNEL assay. Apoptotic labelled cells fluoresced in the AlexaFluor™ 488 channel (green) and the nuclei of cells were counterstained with DAPI (blue). TUNEL positive cells were almost exclusively observed in the hypertrophic zone of control growth plates at the cartilage/bone boundary. In knockout mice, apoptosis was observed throughout the growth plate with a 32.0, 8.0 and 3.7 increase in the resting, proliferative and hypertrophic zones, respectively. Numerical data presented in graphs are shown in the table. (TUNEL positive cells fluoresce green and are indicated by white arrows. RZ = Resting zone, PZ = proliferative zone, HZ = hypertrophic zone, SEM = standard error of the mean, * $p<0.05$, unpaired t-test, n=3 matched sections from 3 locations throughout the growth plate. Sections were from 3 male mice from 3 different litters per genotype Scale bar 100 μm).

5.3 The knockout of CRELD2 expression in chondrocytes results in impaired angiogenesis and a reduction in the number of trabecular osteoblasts

As *Creld2*$^{Cart\Delta Ex3\text{-}5}$ mice displayed a significant reduction in trabecular bone with altered trabecular architecture, histological staining was performed to investigate differences in angiogenesis and the number of trabecular osteoblasts under the growth plate.

To investigate angiogenesis, immunohistochemistry was performed using an anti-podocalyxin antibody. Podocalyxin is a sialoglycoprotein present in endothelial cells and can be used as a vascular lumen marker (Horvat et al., 1986). Control growth plates displayed the characteristic staining for podocalyxin, with staining restricted to the vascular invasion front at the chondro-osseous junction. The same characteristic staining was observed in growth plates from *Creld2*$^{Cart\Delta Ex3\text{-}5}$ mice; however, the intensity of staining appeared to be diminished suggesting that angiogenesis was impaired in knockout mice (Figure 54).

To analyse the impact of the targeted deletion of *Creld2* in chondrocytes on osteoblast number, tibial sections were stained with toluidine blue and the number of active osteoblasts per bone surface was analysed (Figure 55A-55D). Interestingly, analysis of knockout bone revealed a 44.0 % ($p<0.05$) reduction in the number of active osteoblasts per bone surface at 3 weeks of age relative to control mice (Figure 55E).

These results therefore suggest that the ablation of *Creld2* in chondrocytes potentially disrupts endochondral ossification either due to impaired angiogenesis or by disrupting osteoblast differentiation.

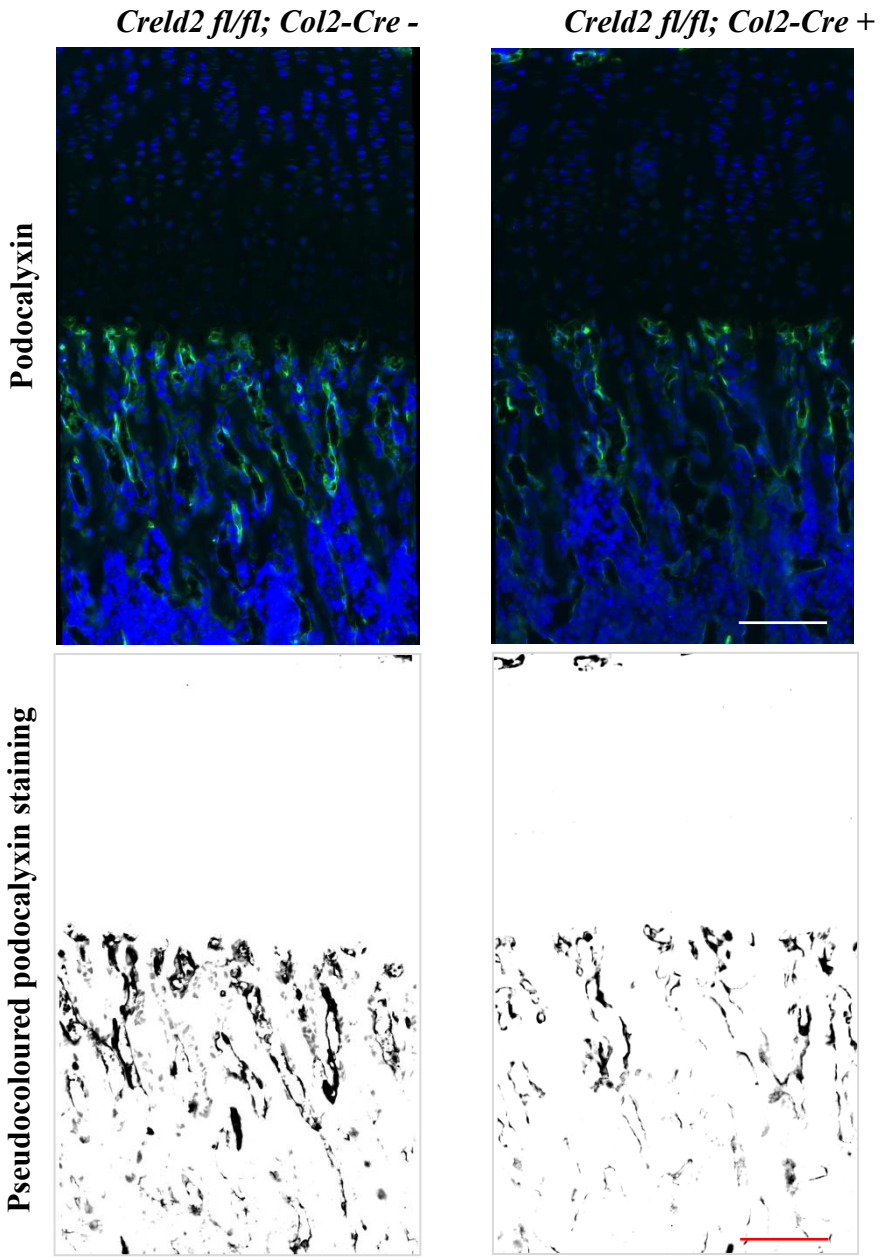

Figure 54. **The expression of the vascular marker podocalyxin is reduced in *Creld2* cartilage-specific knockout growth plates.**

Tibial growth plates from 3-week old mice were analysed by immunohistochemistry to visualise the expression of the endothelial marker podocalyxin which was detected using an AlexaFluor™ 488 secondary antibody (green). Nuclei were counterstained with DAPI (blue). Staining of podocalyxin appeared to be less intense in the knockout growth plates indicating that angiogenesis at the chondro-osseous junction is impaired. Podocalyxin staining was pseudocoloured to aid in visualisation of staining intensities (Images are representative of n= 3 matched sections from 3 male mice from 3 different litters per genotype, Magnification X100, Scale bar 100 μm).

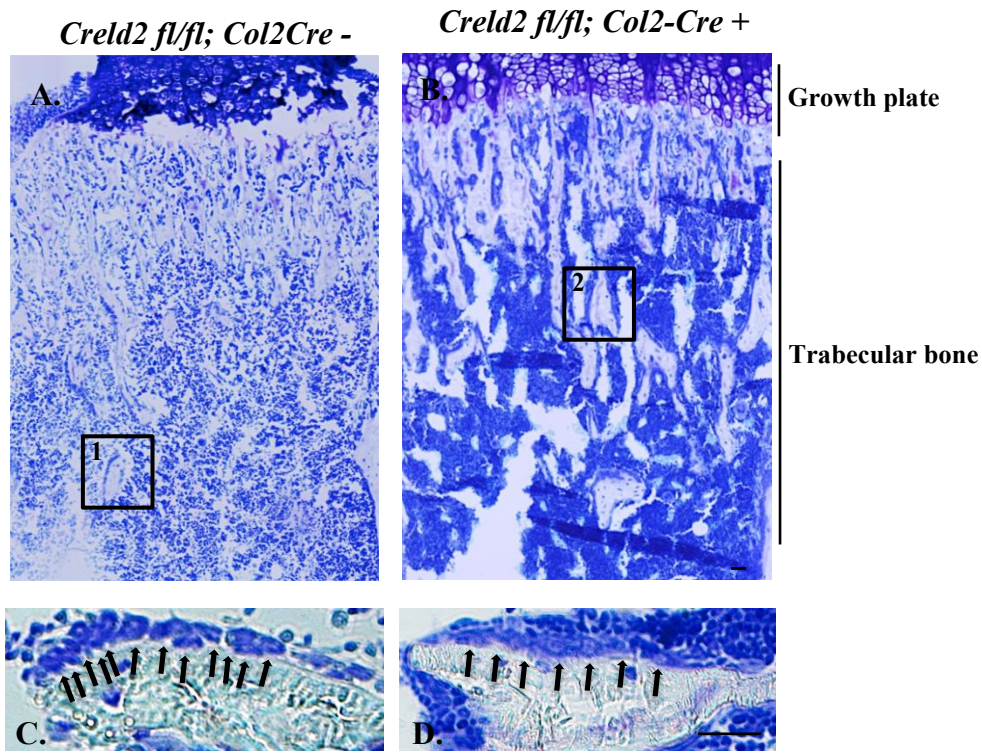

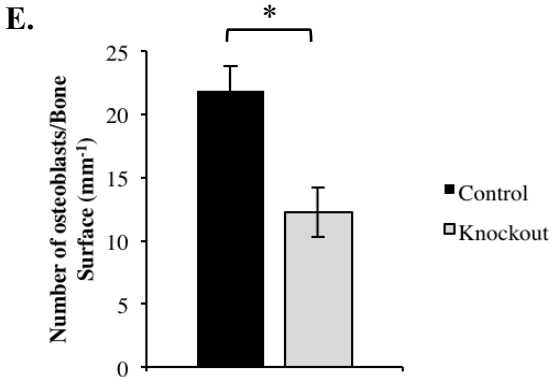

	Number of osteoblasts/Bone Surface (mm^{-1}) ± SEM
Control	21.89 ± 1.87
Knockout	12.25 ± 1.97*

***Figure 55. Creld2* cartilage-specific knockout mice display a reduction in the number of osteoblasts compared to control mice.**

To assess osteoblast number tibial sections were stained with toluidine blue and the number of active osteoblasts per bone surface was counted (**A.** & **B.**). Magnified images showing osteoblasts presented in (**C.** & **D.**). (Box 1 magnified in **C.**, Box 2 magnified in **D.**). *Creld2*$^{Cart\Delta Ex3\text{-}5}$ mice displayed a significant reduction of 44.0% in the number of active osteoblasts per trabecular bone surface relative to control mice (**B.**). Numerical data presented in graphs shown in the table. (Osteoblasts indicated by black arrow. SEM = standard error of the mean, * $p<0.05$, unpaired t-test, n= 3 mice per genotype, Scale bar 50 μm).

5.4 The ablation of CRELD2 disrupts cilia organisation

The central skeleton of primary cilia contains 9 microtubule pairs that are enriched in acetylated α-tubulin (Ruhlen and Marberry, 2014). Therefore chondrocyte primary cilia were visualised immunohistochemically using an anti-acetylated α-tubulin antibody (Figure 56A-56D). A total of 3 sections from 3 mice per genotype were analysed.

At 3 weeks of age the primary cilia of chondrocytes in the proliferative zone of *Creld2*$^{Cart\Delta Ex3\text{-}5}$ mice were significantly shorter by 24.0 % ($p<0.05$) with the average length of knockout cilia being 0.98 μm compared to 1.29 μm in age matched controls (Figure 56E).

The organisation of primary non-motile cilia on chondrocytes reflects the polarity of the chondrocytes (de Andrea et al., 2010). In the proliferative zone, chondrocyte primary cilia orientate parallel to the axis of bone growth and point either towards the epiphysis or metaphysis (de Andrea et al., 2010). In the proliferative zone of *Creld2*$^{Cart\Delta Ex3\text{-}5}$ mice, 29.6 % of primary cilia were aligned incorrectly and were perpendicular to the axis of bone growth. This was a 1.8-fold increase relative to control mice that showed only 11.8 % of primary cilia were perpendicular to the axis of bone growth (Figure 56F).

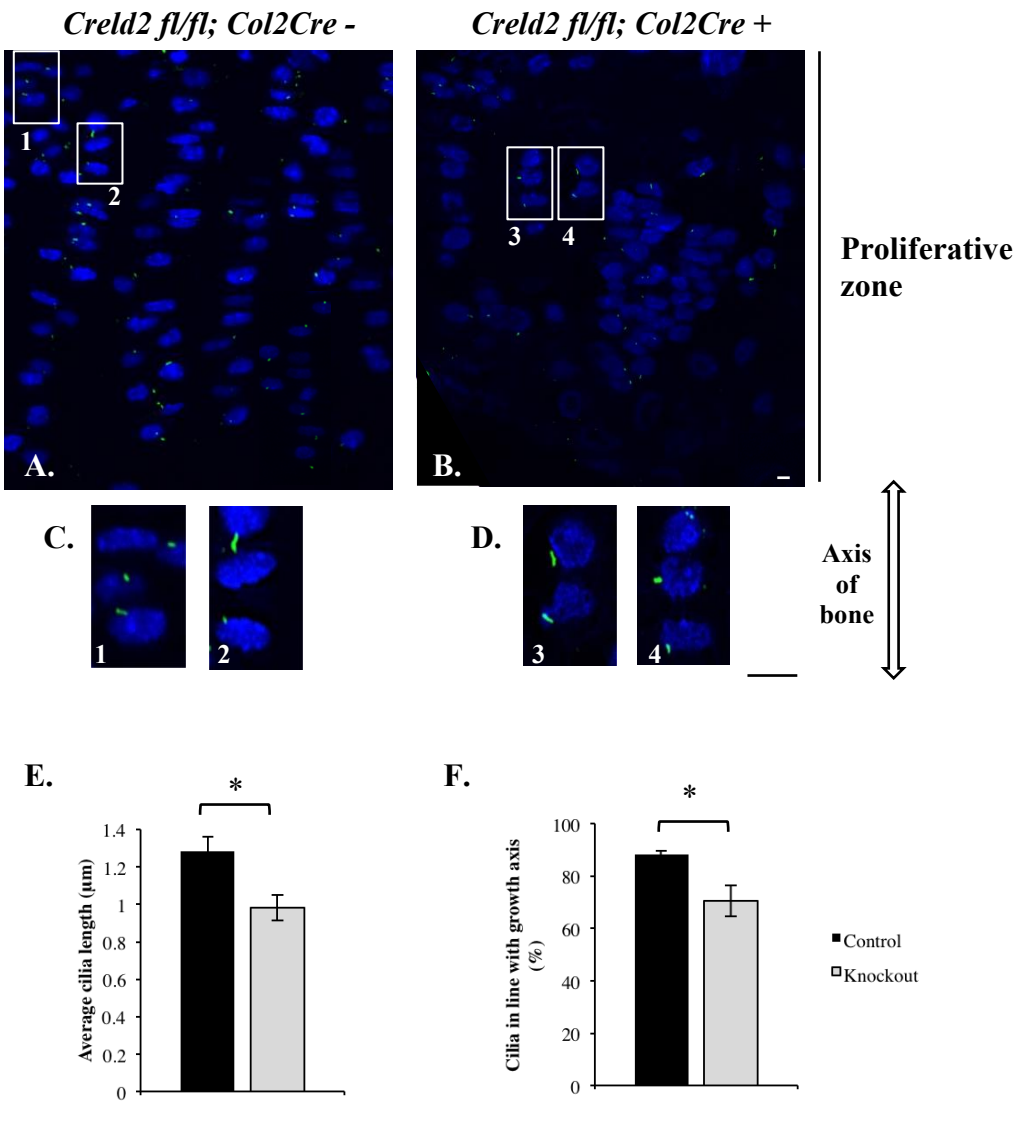

	Average cilia length (µm) ± SEM	Cilia in line with growth axis (%) ± SEM
Control	1.29 ± 0.07	88.20 ± 1.47
Knockout	0.98 ± 0.07*	70.41 ± 6.00*

Figure 56. **The organisation of primary cilia implies loss of chondrocyte polarity in the growth plates of *Creld2* cartilage-specific knockout mice.**

Chondrocyte primary non-motile cilia were analysed using an anti-acetylated α-tubulin antibody that was detected using an AlexaFluor™488 secondary antibody (green). The nuclei were counterstained with DAPI (blue). Representative Z-stack images are shown in (**A.** & **B.**). Magnified images showing cilia are presented in (**C.** & **D.**). (Box 1 and 2 magnified in **C.**, Box 3 and 4 magnified in **D.**). Primary cilia present on proliferating chondrocytes in the knockout growth plates were significantly shorter with a reduction of 24.0 % relative to controls (**E.**). There were also significantly less cilia in line with the axis of bone growth in the knockout growth plate, with a decrease of 20.2 %, implying a loss of polarity for proliferative chondrocytes (**F.**). Numerical data presented in graphs shown in the table. (Images are representative of n= 3 matched sections from 3 male mice from 3 different litters per genotype, Scale bar 5 µm, Magnification X630).

5.5 Transcriptome profiling indicates *Creld2* is important for the differentiation of chondrocytes

RNA-sequencing was performed to obtain a quantitative and unbiased list of differentially expressed genes that contribute to the phenotype of *Creld2*$^{Cart\Delta Ex3\text{-}5}$ mice. RNA was extracted from 5-day-old knee joint cartilage and sent to GATC Biotech for next generation sequencing. The transcriptome of *Creld2*$^{Cart\Delta Ex3\text{-}5}$ mice was compared against that of control mice in order to generate a gene expression profile of genes and genetic pathways that are directly affected by the knockout of *Creld2*.

5.5.1 Quality control check of RNA prior to RNA sequencing

In order to generate an accurate gene expression prolife by RNA sequencing the integrity of the RNA needed to be high. Following RNA extraction, the quality of the RNA was assessed using an Agilent 2100 Bioanalyzer. The electropherograms and gel-like images provided by the Bioanalyzer showed that there is some level of RNA degradation as there are several smaller peaks and bands on the electropherograms and gel-like images respectively (Figure 57). The RIN numbers assigned by the software for the control samples were >8.0 so passed quality control checks at GATC Biotech. The RIN numbers for the knockout samples were lower, ranging from 6.8 – 7.6. The degradation of the RNA was minimal and samples still passed the quality control checks at GATC Biotech and were therefore used for subsequent RNA sequencing.

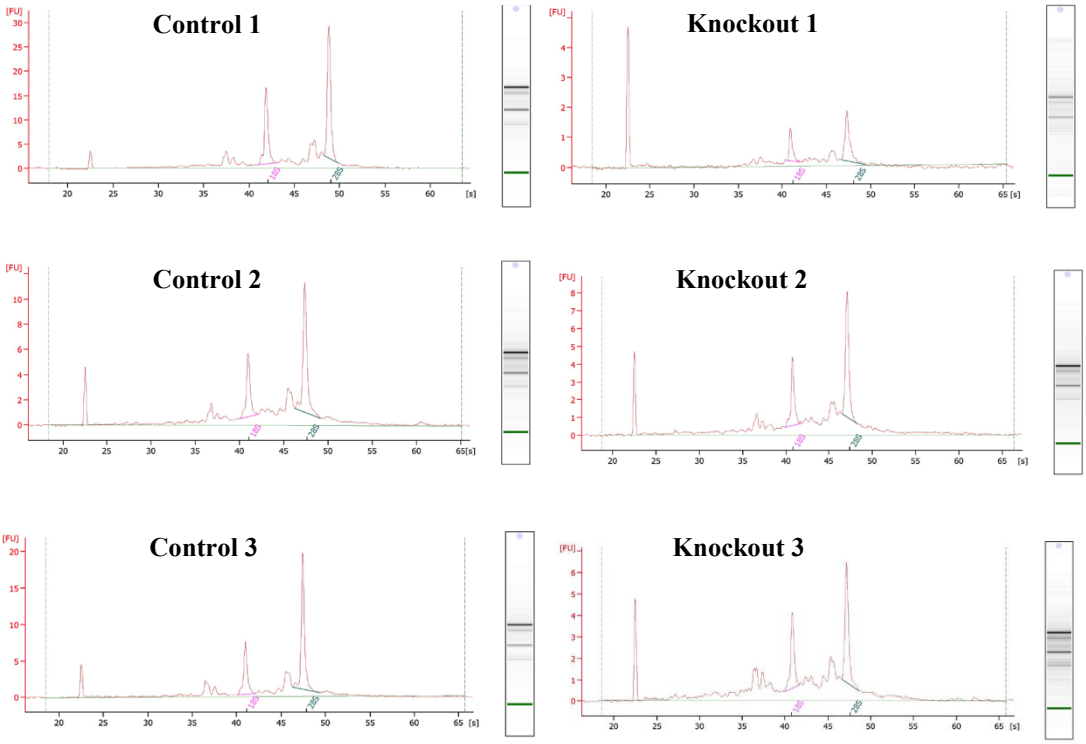

Sample	RIN	Quality control passed (GATC)
Control 1	8.2	Yes
Control 2	8.0	Yes
Control 3	8.0	Yes
Knockout 1	7.3	Yes
Knockout 2	6.8	Yes
Knockout 3	7.6	Yes

Figure 57. **Analysis of RNA integrity from cartilage knee joints.**

The Agilent 2100 Bioanalyzer was used to assess the integrity of RNA samples prior to RNA sequencing. The first peak on the electropherogram indicates the marker and the following two peaks denote the 18S and 28S RNA. Other peaks present are a result of RNA degradation. The gel-like images of intact RNA show two clear bands denoting the 18S and 28S ribosomal subunits. Other bands indicate RNA degradation. All the RINs were above 6 and passed quality control at GATC Biotech. The samples (n=3 per genotype) were subsequently used for RNA sequencing to generate a transcriptome profile of mice.

5.5.2 Identification of potential candidate pathways affected by the ablation of Creld2 in chondrocytes

Following the ablation of *Creld2* in chondrocytes, 181 genes were differentially expressed (Figure 58). 64.6 % of these genes (117 genes) were upregulated while only 35.4 % of genes (64 genes) were downregulated in *Creld2*$^{Cart\Delta Ex3\text{-}5}$ mice relative to control mice.

As *Creld2* has been identified as an ER-stress inducible gene it was interesting to see if any genes of the UPR were differentially expressed following the knockout of *Creld2* in chondrocytes. However, there were no significant differences in fold change of any genes related to ER stress in knockout chondrocytes.

The list of significantly differentially expressed genes were analysed by the online bioinformatics software DAVID that clusters genes according to gene ontology. The web server REViGO was then used to summarise the list of GO terms, removing redundant GO terms therefore providing a general overview of the biological changes occurring as a result of the knockout of *Creld2* (Supek et al., 2011). The REViGO summary of the enriched GO terms is outlined in Table 3.

When the differentially expressed genes in *Creld2*$^{Cart\Delta Ex3\text{-}5}$ mice were clustered, the top cluster included genes involved in cell adhesion. The summarised gene clusters comprised of genes with ubiquitous functions as well as genes specific to skeletal development. Interestingly, genes involved in cell cycle arrest, inhibition of cell proliferation and apoptotic processes were differentially expressed in knockout mice. For example, *Cdkn1a* that is involved in modulating cell proliferation by inhibiting the cell cycle was upregulated by 4-fold (Harper et al., 1995). Differentially expressed genes were also clustered into genes involved in apoptotic processes and negative regulation of proliferation. *Fas*, which stimulates apoptosis primarily by activating a cascade of caspase enzymes, was upregulated by 1.8-fold (Scaffidi et al., 1998).

Genes involved in embryonic skeletal system development were also differentially expressed. For example, *Bmp7* was downregulated whereas *Fgf9* was upregulated. Differentially expressed genes also included *Mmp13,* encoding a marker of hypertrophic chondrocytes, which was downregulated by 2.2-fold in *Creld2*$^{Cart\Delta Ex3\text{-}5}$ mice. Genes were also clustered into groups involved in osteoblast differentiation and ossification. Genes such as *Cyr61* that stimulates BMP and WNT-dependant osteoblast

differentiation and *Bmp7* that enhances osteoblast differentiation and is involved in calcium matrix mineralisation were found to be downregulated by 2.0-fold and 1.5-fold respectively (Si et al., 2006, Shen et al., 2010, Su et al., 2010). Genes involved in cell migration were also differentially expressed. *Sema3e* inhibits the migration of osteoblasts and was also found to be significantly upregulated by 1.9-fold in *Creld2*$^{Cart\Delta Ex3\text{-}5}$ mice (Hughes et al., 2012).

The invasion of blood vessels in the growth plate allows osteoblasts to move into the developing bone and form bone on the cartilage template (Maes et al., 2010). Differentially expressed genes in *Creld2*$^{Cart\Delta Ex3\text{-}5}$ mice clustered into genes involved in the negative regulation of angiogenesis, for example, *Thbs2,* that negatively regulates angiogenesis by binding the anti-angiogenic receptor CD36 on epithelial cells, was upregulated by 1.5-fold (Simantov et al., 2005).

Genes also clustered into those involved in cell signalling. Several genes involved in the response to FGF and TNF, two signalling pathways that mediate chondrocyte differentiation and maturation, were differentially expressed. For example *Irf1,* stimulated by FGF and TNF, was upregulated by 1.5-fold and functions to inhibit cell growth (Kirchhoff et al., 1993). Genes involved in canonical WNT signalling were also differentially expressed. This included the significant reduction in expression of *Wnt4* (by 1.5-fold), a gene that encodes a canonical WNT protein that accelerates chondrocyte maturation (Hartmann and Tabin, 2000). Conversely, several genes that encode proteins that stimulate *Wnt* expression were upregulated. For example, *Fgf9* and was found to be significantly upregulated by 2.1-fold.

Several interesting genes that were differentially expressed between knockout and control mice are outlined in Table 4. Taken together these results suggest that the knockout of *Creld2* in chondrocytes results in a defect in chondrocyte differentiation and results in reduced bone formation.

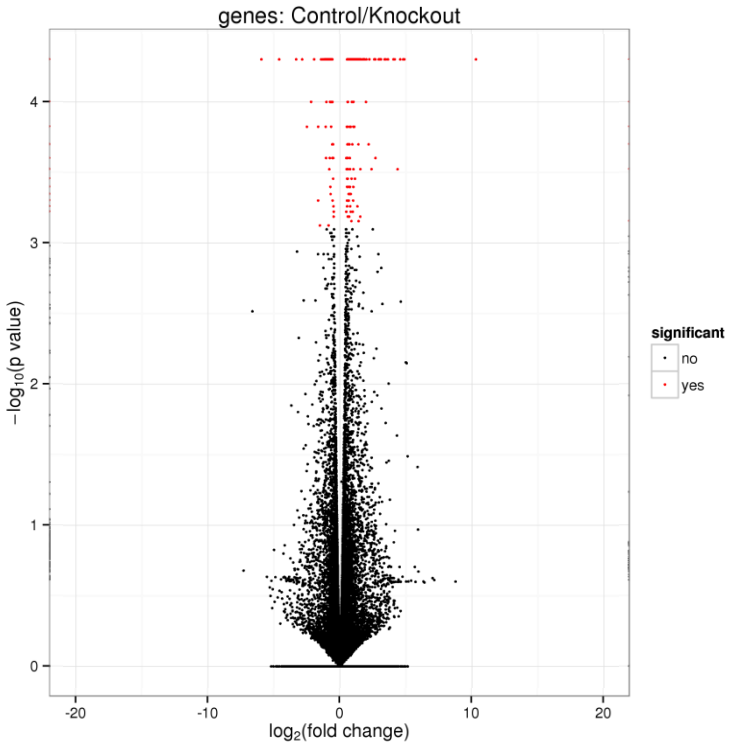

Number of genes	
Upregulated	**Downregulated**
177	64

Figure 58. **181 genes were found to be differentially expressed in *Creld2* cartilage-specific knockout mice relative to control mice.**

A volcano plot of statistical significance against fold-change between *Creld2*$^{CartΔEx3\text{-}5}$ mice and control mice, demonstrating significant differentially expressed genes. 181 genes were differentially expressed between the two genotypes. 117 genes (64.6 %) were found to be upregulated while only 64 genes (35.4 %) were downregulated in *Creld2*$^{CartΔEx3\text{-}5}$ mice.

Table 3. **REViGO summary of the significantly enriched gene ontology terms for the differentially expressed genes observed in *Creld2* cartilage-specific knockout mice.**

GO:ID	Go term	p value
GO:0007155	Cell adhesion	6.50E-07
GO:0046813	Receptor-mediated virion attachment to host cell	6.20E-04
GO:0010628	Positive regulation of gene expression	9.00E-04
GO:0001649	Osteoblast differentiation	1.10E-03
GO:0030198	Extracellular matrix organization	1.20E-03
GO:0007050	Cell cycle arrest	1.50E-03
GO:0071774	Response to fibroblast growth factor	1.50E-03
GO:0001503	Ossification	3.10E-03
GO:0001666	Response to hypoxia	3.80E-03
GO:0048048	Embryonic eye morphogenesis	4.50E-03
GO:0006171	cAMP biosynthetic process	4.70E-03
GO:0019933	cAMP-mediated signaling	4.70E-03
GO:0006915	Apoptotic process	6.20E-03
GO:0051924	Regulation of calcium ion transport	6.40E-03
GO:0045471	Response to ethanol	7.20E-03
GO:0051384	Response to glucocorticoid	7.50E-03
GO:0048706	Embryonic skeletal system development	1.00E-02
GO:2001241	Positive regulation of extrinsic apoptotic signaling pathway in absence of ligand	1.00E-02
GO:0001822	Kidney development	1.10E-02
GO:0007193	Adenylate cyclase-inhibiting G-protein coupled receptor signaling pathway	1.10E-02
GO:0043388	Positive regulation of DNA binding	1.10E-02
GO:0045429	Positive regulation of nitric oxide biosynthetic process	1.10E-02
GO:0016477	Cell migration	1.40E-02
GO:0048468	Cell development	1.40E-02
GO:0006936	Muscle contraction	1.50E-02
GO:0002376	Immune system process	1.80E-02
GO:0008285	Negative regulation of cell proliferation	1.80E-02
GO:0006874	Cellular calcium ion homeostasis	2.00E-02
GO:0010629	Negative regulation of gene expression	2.00E-02
GO:0035860	Glial cell-derived neurotrophic factor receptor signaling pathway	2.00E-02
GO:0071307	Cellular response to vitamin K	2.00E-02
GO:1904761	Negative regulation of myofibroblast differentiation	2.00E-02
GO:0007267	Cell-cell signaling	2.20E-02
GO:0014850	Response to muscle activity	2.30E-02
GO:0008284	Positive regulation of cell proliferation	2.50E-02
GO:0030574	Collagen catabolic process	2.50E-02
GO:0001816	Cytokine production	2.70E-02
GO:0009612	Response to mechanical stimulus	2.70E-02
GO:0071260	Cellular response to mechanical stimulus	2.70E-02
GO:0071356	Cellular response to tumour necrosis factor	2.70E-02

GO:0008584	Male gonad development	2.90E-02
GO:0030201	Heparan sulphate proteoglycan metabolic process	3.10E-02
GO:0030325	Adrenal gland development	3.10E-02
GO:0090263	Positive regulation of canonical WNT signaling pathway	3.20E-02
GO:0007569	Cell aging	3.80E-02
GO:0016525	Negative regulation of angiogenesis	3.80E-02
GO:0006812	Cation transport	3.90E-02
GO:0030324	Lung development	3.90E-02
GO:0030308	Negative regulation of cell growth	4.00E-02
GO:0007249	I-kappaB kinase/NF-kappaB signaling	4.30E-02

Table 4. **Twenty differentially expressed genes in *Creld2* cartilage-specific knockout mice.**

Gene Symbol	Gene Title	log2(Fold Change)	q value	Subcellular locations	Function
Bglap	Osteocalcin	**3.39**	5.44E-03	Extracellular	Binds calcium and hydroxyapatite and comprises 1-2 % of total bone protein. Pro-osteoblastic and regulates bone mineralisation.
Cdkn1a	Cyclin Dependent Kinase Inhibitor 1A	**2**	5.44E-03	Cytoplasm, nucleus	Regulates the cell cycle by inhibiting cell cycle progression upon interaction with G1 cyclin/cyclin dependant kinase complexes and proliferating cell nuclear antigen.
Lmna	Lamin A/C	**1.32**	3.78E-02	Extracellular, cytoskeleton, nucleus, cytosol	Plays a role in nuclear assembly, the organisation of chromatin and nuclear membrane dynamics, providing a framework for the nuclear envelope. Required for development, osteoblastogenesis and bone formation.
Fgf9	Fibroblast Growth Factor 9	**1.08**	1.41E-02	Extracellular	Important role in development, differentiation, cell proliferation and migration.
Sema3e	Semaphorin 3E	**0.92**	5.44E-03	Extracellular	Promotes focal adhesion disassembly. Regulates angiogenesis and inhibits adhesion of endothelial cells to the extracellular matrix.
Zak	Mitogen-Activated Protein Kinase Kinase Kinase 20	**0.92**	5.44E-03	Cytoplasm, nucleus	Stress-activated pro-apoptotic component of a protein kinase signalling pathway. Plays a role in regulating the S and G2 cell cycle checkpoint upon phosphorylation of CHEK2.
Fas	Fas Cell Surface Death Receptor	**0.81**	1.41E-02	Cell membrane, extracellular	Mediates apoptosis by caspase-8 proteolytic activation that initiates the subsequent cascade of caspase enzymes.

Fat4	FAT Atypical Cadherin 4	**0.68**	5.44E-03	Cell membrane	A calcium-dependant protein that plays a role in adhesion and maintaining planar cell polarity.
Irf1	Interferon Regulatory Factor 1	**0.61**	1.00E-02	Cytoplasm, nucleus	Regulates a variety of cellular responses including cell differentiation and proliferation, the cell cycle, inflammation, the immune response and cell death.
Itga2	Integrin Subunit Alpha 2	**0.6**	3.53E-02	Cell membrane	Acts as a receptor for extracellular matrix proteins including collagen. Plays a role in modulating collagen and collagenase gene expression and organisation of the matrix. Mediates cell-cell and cell-matrix adhesion connecting to the cytoskeleton and a variety of signaling molecules.
Thbs2	Thrombospondin 2	**0.54**	2.07E-02	Extracellular	Mediates cell-cell and cell-matrix interactions. Regulates angiogenesis as ligand for the anti-angiogenic receptor CD36.
Wnt4	Wnt Family Member 4	**-0.56**	3.53E-02	Extracellular	Role in development. Regulates cell fate.
Bmp7	Bone Morphogenic Protein 7	**-0.57**	2.07E-02	Extracellular	Induces bone and cartilage formation. Plays a role in bone homeostasis.
Panx3	Pannexin 3	**-0.67**	5.44E-03	Cell membrane	Structural component of the gap junctions and the hemichannels. Panx3 regulates both chondrocyte and osteoblast differentiation via the activation of intracellular Ca^{2+} signaling pathways
Ctgf	Connective Tissue Growth Factor	**-0.77**	5.44E-03	Extracellular	Mitoattractant secreted by vascular endothelial cells. Promotes differentiation and proliferation of chondrocytes. Mediates cell adhesion.
Fgf11	Fibroblast Growth Factor 11	**-0.78**	2.07E-02	Extracellular	Unknown function. Postulated to be involved in the differentiation and function of the nervous system.

Mmp9	Matrix Metallopeptidase 9	**-0.94**	5.44E-03	Extracellular	Regulates matrix remodelling. Regulates angiogenesis in hypertrophic zone of the cartilage growth plate.
Cyr61	Cysteine Rich Angiogenic Inducer 61	**-0.99**	5.44E-03	Extracellular	Promotes cell adhesion, proliferation, chemotaxis and angiogenesis.
Ibsp	Bone Sialoprotein	**-1.03**	5.44E-03	Extracellular	Part of the mineralised bone matrix where it binds hydroxyapatite. Potentially plays a role in cell-matrix attachment.
Mmp13	Matrix Metallopeptidase 13	**-1.13**	5.44E-03	Extracellular	Plays a role in cartilage degradation, bone development and ossification. Also plays a role in tissue remodelling and wound healing potentially by a mechanism involving cleavage and activation of TGFβ1 and degradation of CTGF.

5.6 CRELD2 localises to exosomes in chondrocytes

Immunocytochemistry was performed to assess the subcellular localisation of CRELD2 in primary chondrocytes. CRELD2 was found to localise to compartments of the trafficking pathway as it co-localised with the ER marker Heat shock protein 90kDa beta member 1 (Also known as GRP94) and the Golgi marker Golgi apparatus protein 1 (GLG1) (Figure 59). Interestingly, the expression of CRELD2 was not localized solely to the ER and the Golgi apparatus but in fact co-localised with the tetraspanin exosomal marker Cluster of differentiation (CD) 81. This correlates with previous data that identified the presence of CRELD2 in murine serum (Dr Peter Bell, unpublished data).

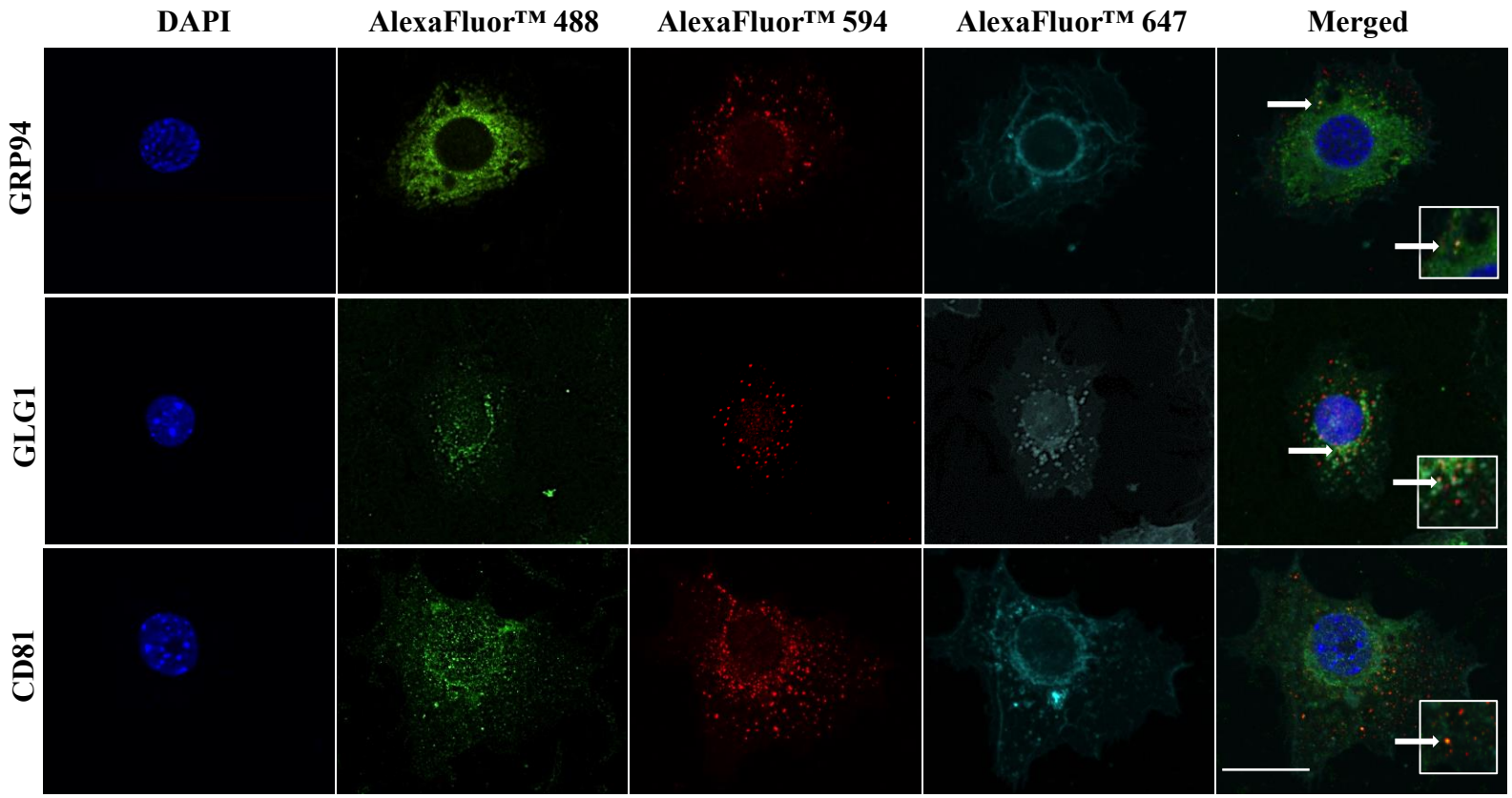

Figure 59. **CRELD2 localises to exosomes in chondrocytes.**

The intracellular localisation of CRELD2 in wild type knee chondrocytes was analysed by immunocytochemistry. Nuclei were counterstained with DAPI (blue) and cell membrane was labelled with Wheat Germ Agglutinin AlexaFluor™647 conjugate (pseudocoloured light blue). GRP94, GLG1 and CD81 were detected using an AlexaFluor™ 488 secondary antibody (green) and CRELD2 was detected using an AlexaFluor™ 594 secondary antibody (red). CRELD2 was found to colocalise with GRP94 (ER marker), GLG1 (Golgi marker) and CD81 (exosomal marker) with colocalisation indicated by shades of yellow. (Colocalisation magnified in white boxes and highlighted with white arrow. Images are representative of primary chondrocytes extracted from two separate extractions, Magnification X630, Scale bar 20.0 μm).

5.7 CRELD2 plays a role in the folding, processing and trafficking of proteins

To elucidate the role of CRELD2 in chondrocytes, putative CRELD2 binding partners were identified by Co-IP in the SW1353 chondrocyte-like cell line. V5-tagged CRELD2 was overexpressed in SW1353 cells and proteins were crosslinked using the amine-reactive crosslinker DSP to preserve binding interactions. Overexpression of V5-tagged CRELD2 and crosslinking of the binding partners were confirmed by western blotting with a V5-specific antibody (Appendix D). Co-IP was performed on lysates from 3 separate transfections using anti-V5 agarose beads and untransfected SW1353 cell lysates were used as a control for the Co-IP. LC-MS/MS was performed to generate a detailed global list of potential CRELD2 binding partners that might be impaired in *Creld2* knockout chondrocytes, contributing to the phenotype of the mice outlined in Chapter 3.

LC-MS/MS was performed to generate a detailed global list of potential CRELD2 binding partners that might be impaired in *Creld2* knockout chondrocytes, contributing to the phenotype of the mice outlined in Chapter 3.

The Scaffold™ programme was used to validate the protein identifications generated from LC-MS/MS. Binding partners were identified as proteins that coimmunoprecipitated with V5-tagged CRELD2 but were absent from the proteins identified in untransfected lysates. Proteomic investigation by mass spectrometry revealed 59 proteins, outlined in Table 5, which precipitated with V5-tagged wild type CRELD2 in SW1353 cells.

V5-precipitated protein complexes revealed that CRELD2 bound to many proteins including proteins involved in translation and several chaperones and folding enzymes involved in the folding and processing of nascent proteins (Figure 60). For example, CRELD2 co-precipitated with ribosomal subunit proteins such as ribosomal protein L15 (RPL15) that comprises part of the translocon. CRELD2 also precipitated with proteins in the oligosaccharyltransferase (OST) complex that catalyses the co-translational glycosylation of the nascent proteins. CRELD2 was also found to bind chaperones involved in folding proteins such as BIP and calreticulin, and to several PDIs that catalyse the formation of disulphide bonds that stabilise protein folding.

Protein complexes involved in the processing of collagen fibrils were also found to precipitate with CRELD2 therefore outlining a potential role for CRELD2 in collagen

processing. For example, serpin family H member 1 (SERPINH1), a collagen-specific molecular chaperone precipitated with CRELD2 as did Procollagen-lysine,2-oxoglutarate 5-dioxygenase enzymes (PLOD1, PLOD2 and PLOD3) that form hydroxylysine residues in collagen proteins enhancing the stability of intermolecular collagen cross-links.

CRELD2 was also found to precipitate with protein complexes involved in vesicular trafficking, such as coatomer proteins such as coatomer protein subunit alpha (COPA), coatomer subunit gamma-1 (COPG1) and transmembrane P24 trafficking protein 9 (TMED9). These protein have been implicated with COPI coatomer dependant retrograde transport and also with COPI-mediated anterograde transport, binding to exocytic vesicular proteins (Orci et al., 1997). Additionally, CRELD2 also precipitated with proteins such as EH domain-containing protein 4 (EHD4) that is involved in endosomal trafficking.

Several extracellular and transmembrane proteins also precipitated with CRELD2. These included the adhesion proteins thrombospondin (TSP) 1, cysteine-rich angiogenic-inducer 61 (CYR61) and LRP1. As CRELD2 functions as a putative PDI, it can be hypothesised that CRELD2 assists in their folding, maturation and transport though the secretory pathway.

Table 5. **Putative binding partners of CRELD2 in chondrocytes.**

Protein symbol	Protein name	UniProt ID	Total spectra counts			Subcellular location	Function
			Exp 1	Exp 2	Exp 3		
APMAP	Adipocyte plasma membrane-associated protein	APMAP_MOUSE	2	2	2	Extracellular	Plays a role in adipogenesis.
ASPH	Aspartyl/asparaginyl beta-hydroxylase	A2AL85_MOUSE	2	3	4	Extracellular	An enzyme involved in hydroxylating of aspartic acid and arginine residues in the epidermal growth factor-like domains of proteins.
BIP	78 kDa glucose-regulated protein	GRP78_MOUSE	77	77	76	Endoplasmic reticulum, extracellular, nucleus	Molecular chaperone.
CALR	Calreticulin	B2MWM9_MOUSE	21	20	20	Cytosol, endoplasmic reticulum, extracellular, nucleus	Molecular chaperone.
CHID1	Chitinase domain-containing protein 1	A0A0R4J058_MOUSE	2	2	3	Endosome, extracellular, Golgi apparatus, lysosome, nucleus	Saccharide- and lipopolysaccharide-binding protein.
CKAP4	Cytoskeleton-associated protein 4	CKAP4_MOUSE	11	11	9	Cell membrane, cytoskeleton, cytosol, endoplasmic reticulum, extracellular, nucleus	Anchors endoplasmic reticulum to microtubules.
COL6A3	Collagen alpha-3 (VI) chain	A0A087WS16_MOUSE	6	9	8	Endoplasmic reticulum, extracellular	A connective tissue protein that binds extracellular matrix proteins organizing the matrix.

COPA	Coatomer subunit alpha	COPA_MOUSE	4	3	3	Cytosol, endoplasmic reticulum, extracellular, Golgi apparatus	Part of a complex involved in vesicular protein trafficking in secretory pathway.
COPG1	Coatomer subunit gamma-1	COPG1_MOUSE	4	2	3	Cytosol, Golgi apparatus	Part of a complex involved in vesicular protein trafficking in secretory pathway.
CPA4	Carboxypeptidase A4	CBPA4_MOUSE	3	4	3	Extracellular	An exopeptidase that catalyses the release of carboxy-terminal amino acids.
CRELD2	Cysteine-rich with epidermal growth factor-like domain protein 2	CREL2_MOUSE	28	35	33	Endoplasmic reticulum, extracellular, Golgi apparatus	Putative PDI.
CYR61	Cysteine-Rich Heparin-Binding Protein 61	CYR61_MOUSE	3	10	4	Extracellular	Promotes cell proliferation, chemotaxis, angiogenesis and cell adhesion through extracellular interactions.
DDOST	Dolichyl-diphosphooligosaccharide--protein glycosyltransferase 48 kDa subunit	OST48_MOUSE	5	7	8	Cell membrane, endoplasmic reticulum, lysosome	Part of an N-oligosaccharyl transferase complex that adds high mannose oligosaccharides to the Asn-X-Ser/Thr motif on nascent polypeptide chains.
DNAJB11	DnaJ homolog subfamily B member 11	DJB11_MOUSE	4	4	6	Endoplasmic reticulum	Molecular chaperone.
DNAJC10	DnaJ homolog subfamily C member 10	DJC10_MOUSE	4	5	7	Endoplasmic reticulum	Co-chaperone that catalyses the removal of non-native disulphide bonds. Also found to promote apoptosis under pathological ER stress conditions.
DNAJC3	DnaJ homolog subfamily C member 3	DNJC3_MOUSE	6	3	3	Endoplasmic reticulum, extracellular, lysosome	Co-chaperone. Inhibits the phosphorylation of EIF2A.

EHD4	EH domain-containing protein 4	EHD4_MOUSE	2	2	2	Endosome, extracellular, nucleus	ATP- and membrane-binding protein that probably controls membrane reorganisation/tubulation upon ATP hydrolysis. Plays a role in early endosomal transport.
EOGT	Epidermal growth factor domain-specific O-linked N-acetylglucosamine transferase	EOGT_MOUSE	5	5	5	Endoplasmic reticulum	An enzyme that catalyses the transfer of N-acetylglucosamine to serine/threonine residues of extracellular proteins.
ERO1A	Endoplasmic Reticulum Oxidoreductase 1-like protein alpha	ERO1A_MOUSE	8	8	5	Endoplasmic reticulum	An oxidoreductase enzyme involved in disulphide bond formation. Reoxidises PDI allowing it to carry out additional rounds of disulphide bone formation. Also implicated in ER stress and stimulates CHOP-dependant apoptosis.
ERP19	Thioredoxin domain-containing protein 12	TXD12_MOUSE	2	2	2	Endoplasmic reticulum	Similar activity to PDI.
ERP29	Endoplasmic reticulum resident protein 29	ERP29_MOUSE	2	2	2	Endoplasmic reticulum, extracellular	Part of the PDI family but does not function as a PDI. Potential role in the processing of secretory proteins in the ER.
ERP44	Endoplasmic reticulum resident protein 44	ERP44_MOUSE	5	5	5	Endoplasmic reticulum, extracellular	PDI.
GANAB	Alpha glucosidase 2 alpha neutral subunit	A1A4T2_MOUSE	11	13	11	Endoplasmic reticulum, extracellular	Plays a role in protein folding, cleaving glucose resides from immature glycoproteins.
GRP94	94 KDa Glucose-Regulated Protein	ENPL_MOUSE	92	89	100	Cytosol, endoplasmic reticulum, extracellular, nucleus	Molecular chaperone.
GT251	Procollagen galactosyltransferase 1	GT251_MOUSE	11	8	9	Endoplasmic reticulum	Transfers galactose moieties to hydroxylysine residues of collagen and mannose binding lectin.

HYOU1	Hypoxia upregulated protein 1	HYOU1_MOUSE	36	34	37	Endoplasmic reticulum, extracellular	May act as a molecular chaperone facilitating protein folding.
LAMB1	Laminin B1 subunit 1	B9EKB0_MOUSE	15	7	8	Extracellular	Laminins are composed of 3 non-identical chains: α, β and γ. Laminin plays a wide variety of roles including cell adhesion, differentiation, migration, signaling and organisation of cells.
LAMC1	Laminin subunit gamma-1	F8VQJ3_MOUSE	20	13	13	Extracellular	Laminins are composed of 3 non-identical chains: α, β and γ. Laminin plays a wide variety of roles including cell adhesion, differentiation, migration, signaling and organisation of cells.
LMAN1	Endoplasmic Reticulum-Golgi Intermediate Compartment Protein 53	LMAN1_MOUSE	4	5	4	Endoplasmic reticulum, extracellular, Golgi apparatus	Cargo receptor for glycoprotein transport.
LRP1	Low density lipoprotein receptor-related protein 1	A0A0R4J0I9_MOUSE	13	6	15	Cell membrane, cytosol, lysosome, nucleus	A receptor that is involved in a wide variety of cellular processes, including intracellular signaling, lipid homeostasis, and clearance of apoptotic cells.
MANF	Mesencephalic astrocyte-derived neurotrophic factor	Q3TMX5_MOUSE	4	4	4	Cytosol, endoplasmic reticulum, extracellular, nucleus	Molecular chaperone.
MOGS	Mannosyl-oligosaccharide glucosidase	MOGS_MOUSE	3	3	3	Endoplasmic reticulum, extracellular	First enzyme in the N-linked oligosaccharide-processing pathway. This enzyme cleaves the distal glucose residue in the oligosaccharide precursor.
MYDGF	Myeloid-derived growth factor	MYDGF_MOUSE	3	3	2	Endoplasmic reticulum, extracellular	Unknown function.
NOMO1	Nodal modulator 1	NOMO1_MOUSE	5	8	6	Endoplasmic reticulum	May antagonize Nodal signalling.

P3H1	Prolyl 3-hydroxylase 1	A2A7Q5_MOUSE	5	5	5	Endoplasmic reticulum, extracellular	An enzyme that catalyses the formation of 3-hydroxyproline in X-Pro-Gly sequences in collagen proteins.
P4HA2	Prolyl 4-Hydroxylase Subunit Alpha 2	Q5SX74_MOUSE	11	16	17	Cytosol, endoplasmic reticulum	An enzyme that catalyses the formation of 4-hydroxyproline in X-Pro-Gly sequences in collagen proteins.
P4HB	Protein disulphide-isomerase	PDIA1_MOUSE	24	27	32	Cell membrane, extracellular, endoplasmic reticulum	PDI.
PDIA4	Protein disulphide-isomerase A4	A0A0R4J0Z1_MOUSE	22	22	21	Cytosol, endoplasmic reticulum, extracellular, nucleus	PDI.
PDIA6	Protein disulphide-isomerase A6	PDIA6_MOUSE	19	18	15	Cytosol, endoplasmic reticulum, extracellular	PDI.
PLOD1	Procollagen-lysine,2-oxoglutarate 5-dioxygenase 1	PLOD1_MOUSE	14	18	17	Endoplasmic reticulum, extracellular	Forms hydroxylysine resides in X-Lys-Gly sequences in collagen proteins. These residues are critical for aiding the stability of the intermolecular collagen cross-links.
PLOD2	Procollagen-lysine,2-oxoglutarate 5-dioxygenase 2	E9Q718_MOUSE	8	9	11	Endoplasmic reticulum, extracellular	Forms hydroxylysine resides in X-Lys-Gly sequences in collagen proteins. These residues are critical for aiding the stability of the intermolecular collagen cross-links.
PLOD3	Procollagen-lysine,2-oxoglutarate 5-dioxygenase 3	PLOD3_MOUSE	10	10	7	Endoplasmic reticulum, Golgi apparatus, extracellular	Forms hydroxylysine resides in X-Lys-Gly sequences in collagen proteins. These residues are critical for aiding the stability of the intermolecular collagen cross-links.
POFUT2	GDP-fucose protein O-fucosyltransferase 2	B2RV73_MOUSE	4	5	7	Endoplasmic reticulum, Golgi apparatus	An enzyme that catalyses the attachment of fucose through an O-glycosidic linkage to a conserved Ser/Thr residue.

PPIB	Peptidyl-prolyl *cis*-trans isomerase B	PPIB_MOUSE	14	10	10	Extracellular, nucleus	PPI.
RPL15	Ribosomal protein L15	E9QAZ2_MOUSE	2	4	2	Cytosol, extracellular, nucleus	Component of the 60S ribosomal subunit.
RPN1	Dolichyl-diphosphooligosaccharide--protein glycosyltransferase subunit 1	Q3U900_MOUSE	10	10	10	Cytosol, endoplasmic reticulum, extracellular	Part of an N-oligosaccharyl transferase complex that adds high mannose oligosaccharides to the Asn-X-Ser/Thr motif on nascent polypeptide chains.
RPN2	Dolichyl-diphosphooligosaccharide--protein glycosyltransferase subunit 2	Q3U505_MOUSE	2	3	3	Endoplasmic reticulum	Part of an N-oligosaccharyl transferase complex that adds high mannose oligosaccharides to the Asn-X-Ser/Thr motif on nascent polypeptide chains.
S15A	40S ribosomal protein S15a	Q5M9M4_MOUSE	6	4	4	Cytosol, extracellular	Component of the 40S ribosomal subunit.
SEP15	Selenoprotein F	A0A0R4J0K1_MOUSE	2	2	2	Extracellular	May be involved in the redox reaction associated with the formation of disulphide bonds.
SERPH	Serpin family H member 1	Q3TJK3_MOUSE	2	5	5	Endoplasmic reticulum, extracellular	Collagen-specific molecular chaperone.
SLC2A1	Solute carrier family 2, facilitated glucose transporter member 1	GTR1_MOUSE	2	3	2	Cell membrane, cytoskeleton, extracellular	Glucose transporter.
STT3A	Dolichyl-diphosphooligosaccharide-protein glycosyltransferase subunit STT3A	Q3TG02_MOUSE	5	5	5	Endoplasmic reticulum	The catalytic subunit of the N-oligosaccharyl transferase complex that adds high mannose oligosaccharides to the Asn-X-Ser/Thr motif on nascent polypeptide chains.

STT3B	Dolichyl-diphosphooligosaccharide--protein glycosyltransferase subunit STT3B	A0A0R4J0D3_MOUSE	4	4	3	Endoplasmic reticulum	The catalytic subunit of the N-oligosaccharyl transferase complex that adds high mannose oligosaccharides to the Asn-X-Ser/Thr motif on nascent polypeptide chains.
SUMF2	Sulphatase Modifying Factor 2	Q0VDW5_MOUSE	3	2	2	Endoplasmic reticulum	An enzyme that catalyses the hydrolysis of sulphate esters in the sulphatase leading to its activation.
TMED9	Transmembrane P24 Trafficking Protein 9	Q3TFU8_MOUSE	2	2	2	Endoplasmic reticulum, extracellular, Golgi apparatus	Involved in vesicular protein trafficking in early secretory pathway.
TMX3	Thioredoxin Related Transmembrane Protein 3	TMX3_MOUSE	2	3	3	Endoplasmic reticulum	PDI.
TSP1	Thrombospondin 1	Q3TR40_MOUSE	7	8	4	Cell membrane, endoplasmic reticulum, extracellular	Adhesive glycoprotein that mediates cell-to-cell and cell-to-matrix interactions. Plays a role in angiogenesis. Also has a role in ER-stress due to its interaction with ATF6.
TXNDC5	Thioredoxin domain-containing protein 5	E9PXX7_MOUSE	4	5	6	Endoplasmic reticulum, extracellular, lysosome	PDI.
UGGT1	UDP-glucose:glycoprotein glucosyltransferase 1	UGGG1_MOUSE	15	14	13	Endoplasmic reticulum, extracellular	Recognises misfolded glycoproteins and reglucosylates the N-glycans near the misfolded part of the protein. This is then recognized by calreticulin for refolding or degradation.

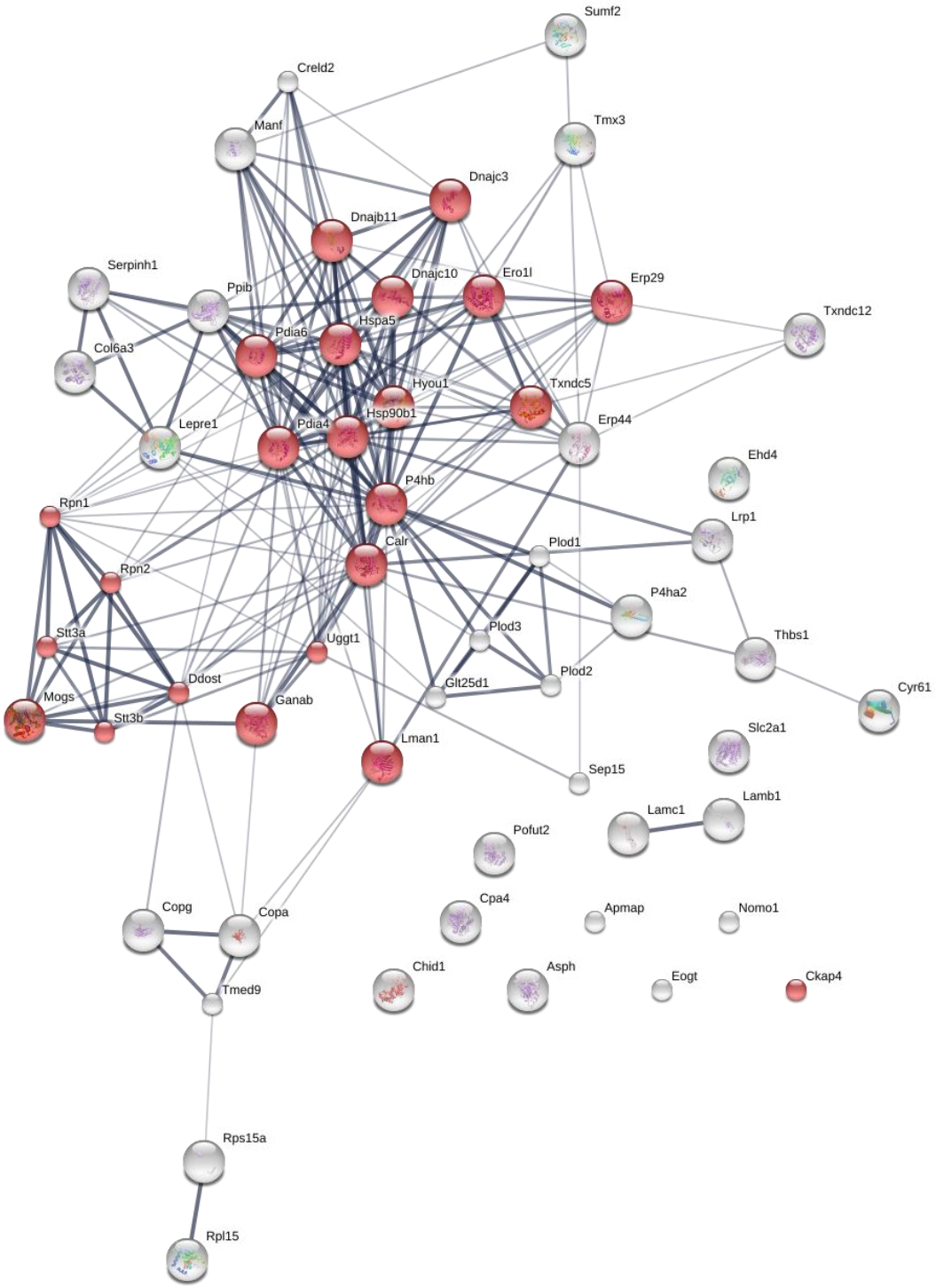

Figure 60. **CRELD2 binds complexes involved in protein folding.**

The online STRING database was used to analyse the interactions between CRELD2 binding proteins (Szklarczyk et al., 2017). CRELD2 was found to bind to protein complexes involved in protein folding. For example, CRELD2 precipitated with HSPA5/BIP, HSP90B/GRP94 and CALR that chaperone protein folding and enzymes involved in glycosylation such as DDOST, RPN1 and RPN2. (CRELD2 binding partners involved in protein folding are highlighted in red. Line thickness indicates strength of interaction.).

5.8 Discussion

The studies presented in this chapter focused on the underpinning mechanism that resulted in the pathology *Creld2*$^{Cart\Delta Ex3\text{-}5}$ mice described in Chapter 3.

Impaired chondrocyte survival and proliferation

The growth pathology outlined in Chapter 3 revealed that *Creld2*$^{Cart\Delta Ex3\text{-}5}$ mice display a disorganised growth plate characterised by large areas of hypocellularity within the proliferative zone. These regions of hypocellularity may correspond either to a decrease in chondrocyte proliferation or an increase in chondrocyte apoptosis.

Several mouse models of chondrodysplasias have shown reduced chondrocyte proliferation and dysregulated apoptosis within the mutant growth plates (Table 6) (Leighton et al., 2007, Piróg-Garcia et al., 2007, Suleman et al., 2012, Cameron et al., 2015). The data presented here revealed that the ablation of *Creld2* in chondrocytes results in a reduction in chondrocyte proliferation and an increase in apoptosis consistent with a generic growth plate dysplasia. Apoptotic cells were detected in the resting, proliferative and hypertrophic zones of the *Creld2*$^{Cart\Delta Ex3\text{-}5}$ growth plate and apoptosis was increased by 32.0-fold, 8.0-fold and 3.7-fold respectively.

Interestingly, the increase in apoptosis observed in the resting zone of *Creld2*$^{Cart\Delta Ex3\text{-}5}$ mice was much more severe than that observed in the targeted models of chondrodysplasia. In mouse models of chondrodysplasia, mutant protein is expressed by chondrocytes in the proliferative zone of the growth plate and apoptosis in this zone is subsequently increased. As the percentage of cells undergoing apoptosis is highest in the resting zone of *Creld2*$^{Cart\Delta Ex3\text{-}5}$ mice, this indicates that the deletion of *Creld2* has a pathological effect on chondrocytes at the early stages of maturation. This suggests that CRELD2 modulates pathways early in differentiation and the lack of CRELD2 triggers chondrocyte apoptosis. It can therefore be hypothesised that CRELD2 is required for the differentiation and survival of chondrocytes and could explain the reduction in the lengths of the proliferative and hypertrophic zones observed in knockout growth plates.

CRELD2 lies downstream of XBP1 in the IRE1 branch of the UPR (Cameron et al., 2015). *In vivo* studies have shown that chondrocyte proliferation was also significantly reduced in *Xbp1*$^{Cart\Delta Ex3\text{-}5}$ mice. This suggests that XBP1 potentially

modulates chondrocyte proliferation via CRELD2. In contrast, apoptosis was unaffected in *Xbp1*-null growth plates suggesting that cell death does not contribute to the skeletal phenotype seen in the *Xbp1* mutant mice, contrary to what was observed for *Creld2*$^{CartΔEx3\text{-}5}$ mice therefore suggesting CRELD2 can also function independently of XBP1 signalling.

Table 6. **Summary of proliferative and apoptotic changes in mouse models of chondrodysplasias.**

Mouse model	Decrease in proliferation	Increase in apoptosis	Reference
Creld2 $^{CartΔEx3\text{-}5}$	19.00 %	Resting: 32-fold, Proliferative: 8-fold, Hypertrophic: 3.7-fold	This study
Comp T585M	24.00 %	Resting: 2.5-fold, Proliferative: 12-fold,	(Piróg-Garcia et al., 2007)
Comp D469del	17.00 %	Proliferative: 90-fold, Hypertrophic: 5-fold	(Suleman et al., 2012)
Matn3 V194D	16.00 %	Not dysregulated. Hypertrophic: 40 % increase	(Leighton et al., 2007, Suleman et al., 2012)
Xbp1^{CartΔEx2}	20.0 %	Unaffected	(Cameron et al., 2015)

Due to the presence of N-terminal C-XX-C motifs in CRELD2 sequence it was postulated that CRELD2 functions as a protein folding chaperone, specifically, a PDI (Hartley et al., 2013). Interestingly, *in vivo* studies show that the deletion of another PDI, *Pdia3*, leads to an impairment of long bone growth (Linz et al., 2015). PDIA3 null mice were characterised by an increase in apoptosis and a reduction in proliferation similar to the findings in *Creld2*$^{CartΔEx3\text{-}5}$ mice. However, the UPR was stimulated in *Pdia3*-null chondrocytes but was not changed following the ablation of *Creld2* as no genes involved in the UPR were differentially expressed in *Creld2*$^{CartΔEx3\text{-}5}$ mice.

Disrupted bone formation

The results presented in Chapter 3 outline an important role for CRELD2 in skeletal growth as *Creld2*$^{Cart\Delta Ex3\text{-}5}$ mice were characterised by disproportionate short stature indicating that CRELD2 may play a role in skeletal development. Interestingly, the lack of *Creld2* expression in chondrocytes also resulted in a reduction in trabecular bone mass.

Several studies have identified a reduction in bone mass following an ablation of gene expression in chondrocytes. For example, an ablation of *Osterix* in chondrocytes result in a disrupted growth plate with a reduction in the height of the hypertrophic zone and in a reduction in trabecular bone mass similar to the phenotype observed in *Creld2*$^{Cart\Delta Ex3\text{-}5}$ mice (Cheng et al., 2013). Furthermore, the cartilage-specific knockouts of the WNT co-receptors *Lrp5* and *Lrp6* also result in low bone mass (Schumacher et al., 2016).

It has been postulated that the effect of a chondrocyte-specific gene knockout on bone mass could be attributed to the leaky expression of the *Col2-Cre* transgene (Schumacher et al., 2016). However, the work presented in Chapter 3 showed that the only cells expressing *Col2-Cre* in the studied models were chondrocytes and cells of the perichondrium. The expression of *Col2-Cre* was absent from osteoblasts and therefore the bone-related phenotype of *Creld2*$^{Cart\Delta ex3\text{-}5}$ mice is likely a direct consequence of the chondrocyte knockout of *Creld2.*

Within the growth plates of *Creld2*$^{Cart\Delta ex3\text{-}5}$ mice, there appeared to be a delay in chondrocyte differentiation or reprogramming to an immature cell type since the chondrocytes in hypertrophic zone had adopted a proliferative morphology. Furthermore, chondrocytes were abnormally present deep within the zone of calcification. As hypertrophic chondrocytes trigger angiogenesis allowing access for osteoblasts to deposit bone on the mineralised cartilage scaffold, a defect in chondrocyte maturation could lead to a defect in angiogenesis and subsequently result in less mature osteoblasts on the trabecular bone under the growth plate (Maes et al., 2010). The work presented here showed reduced intensity of staining for the vascular marker podocalyxin in *Creld2*$^{Cart\Delta ex3\text{-}5}$ mice suggesting impaired angiogenesis.

Trabecular bone mass was reduced in *Creld2*$^{Cart\Delta ex3\text{-}5}$ mice; however, the cortical bone was unaffected. This suggests that the defect in trabecular bone is a direct

consequence of the growth plate defect. As it has been proposed that up to 60 % of osteoblasts are derived from terminal growth plate chondrocytes, a delay in chondrocyte differentiation could result in delayed transdifferentiation of chondrocytes into osteoblasts (Zhou et al., 2014). Interestingly, the work outlined in this chapter revealed that the osteoblast number on trabecular bone surface was significantly reduced (by 44.0 %) in *Creld2*$^{CartΔex3\text{-}5}$ mice. This could be due to the impairment of angiogenesis or due to a defect in terminal chondrocyte transdifferentiation. Further studies are required to investigate these findings.

Loss of growth plate polarity

Through the use of transgenic mouse models of ciliary proteins, it has been shown that the primary cilia play a role in skeletal patterning and endochondral ossification (Zhang et al., 2003, Haycraft et al., 2007, McGlashan et al., 2007, Song et al., 2007, Haycraft and Serra, 2008). The columnar organisation of chondrocytes in the proliferative zone may be controlled by cilia and disruptions to cilia result in growth plate defects such as a disruption to cellular morphology and a lack of columnar organisation (Song et al., 2007).

The work presented in this thesis showed that the average length of primary cilia in the proliferative zone of knockout growth plates was significantly shorter. Furthermore, organisation of primary cilia defines the polarity of the cell as all cilia align in one axis and point either towards the epiphysis or the metaphysis (de Andrea et al., 2010). There was also a significant reduction in the cilia aligned within the correct axis in *Creld2*$^{CartΔEx3\text{-}5}$ mice indicating that both ciliary organisation and polarity was impaired. β1-integrin conditional knockout mice displayed a similar phenotype to *Creld2*$^{CartΔex3\text{-}5}$ mice, with abnormal rounded proliferative chondrocytes and impaired columnar organisation (Aszodi et al., 2003). A disruption to intraflagellar transport resulting from the deletion of Kinesin family member 3A (*Kif3a*) in chondrocytes also caused a similar growth plate pathology to *Creld2*$^{CartΔEx3\text{-}5}$ mice with misaligned rounded chondrocytes in the proliferative zone (Koyama et al., 2007). This suggests that overall the cilia-controlled rotation of chondrocytes in these mouse models was impaired.

The work presented in this chapter demonstrated that the organisation of chondrocyte primary non-motile cilia of *Creld2*$^{CartΔEx3\text{-}5}$ mice was disrupted and

suggested that the chondrocytes had lost correct polarity. This indicated that CRELD2 may either play a direct role in cilia organisation or the impaired cilia could be a secondary effect of an ECM or signalling defect, potentially due to its function in protein folding and trafficking. Overall these data suggest that chondrocyte differentiation and maturation were affected potentially as a result of ciliary defects due to the knockout of *Creld2* in chondrocytes.

Cellular response to the deletion of *Creld2* in chondrocytes

The main aim of this study was to investigate the mechanism that underpinned the skeletal pathology outlined in Chapter 3, following the ablation of *Creld2* in chondrocytes. RNA-sequencing analysis was performed to identify novel candidate genes and pathways that could contribute to the phenotype of $Creld2^{Cart\Delta ex3\text{-}5}$ mice.

It was postulated that CRELD2 plays a role in the classical UPR and it was found to be an ER-stress inducible gene in skeletal dysplasia resulting from the retention of mutant matrilin-3 (Hartley et al., 2013). Interestingly, CRELD2 was found to bind to BIP and act in a putative chaperone complex important for protein folding (Hartley et al., 2013). Therefore, it could be speculated that ablation of CRELD2 would lead to dysregulated compensatory expression of other UPR and ER stress genes. For example, the knockout of BIP led to an upregulation of GRP94 and PDI *in vivo* (Wang et al., 2010). Additionally, the cartilage-specific knockout of *Manf* (a gene encoding Mesencephalic Astrocyte derived Neurotrophic Factor (MANF) also known as Arginine-rich, mutated in early-stage tumors (ARMET), another ER-stress inducible gene upregulated in a mouse model of skeletal dysplasia), lead to an upregulation of several UPR molecular chaperones (Hartley et al., 2013, Bell *et al.* unpublished data). However, the RNA-seq data presented here did not show any evidence of an increased UPR and/or an increase in the expression of ER stress genes such as *Hspa5*, *Hsp90b* and *Pdia4*.

During skeletal development and growth, major signalling pathways act together to control chondrocyte differentiation and maturation, from proliferation to hypertrophy, thus promoting endochondral ossification (Kozhemyakina et al., 2015). The data presented in this chapter suggested a role for CRELD2 in promoting chondrocyte maturation within the epiphyseal growth plate, as several dysregulated genes in

Creld2$^{Cart\Delta ex3\text{-}5}$ mice function to inhibit chondrocyte differentiation, proliferation and maturation (Table 7).

Table 7. **Dysregulated genes in *Creld2* cartilage-specific knockout mice that lead to the inhibition of chondrocyte differentiation, proliferation and maturation.**

Gene	log2(Fold Change)	q value	Contribution to skeletal pathology of *Creld2* cartilage-specific knockout mice	Reference
Fgf9	**1.08**	1.41E-02	Delays chondrocyte maturation	(Garofalo et al., 1999)
Wnt4	**-0.56**	3.53E-02	Delays hypertrophy	(Hartmann and Tabin, 2000, Lee and Behringer, 2007)
Panx3	**-0.67**	5.44E-03	Delays hypertrophy	(Oh et al., 2015)
Ctgf	**-0.77**	5.44E-03	Delays chondrocyte proliferation	(Ivkovic et al., 2003)
Cyr61	**-0.99**	5.44E-03	Delays chondrocyte maturation	(Zhang et al., 2016)
Ibsp	**-1.03**	5.44E-03	Delays chondrocyte proliferation	(Bouleftour et al., 2014)

Fibroblast growth factor 9 (FGF9) plays an important role in skeletal development (Su et al., 2014). *In vivo* studies have shown a role for FGF9 in promoting chondrocyte differentiation and maturation during development as *Fgf9*-null mice were characterised by disproportionate short stature but with normal limb patterning (Colvin et al., 2001). Interestingly, FGF9 plays different roles at different stages of limb development and growth, and the overexpression of *Fgf9* in chondrocytes also results in a dwarfism due to reduced chondrocyte proliferation, impaired columnar organisation of proliferative chondrocytes and impaired terminal differentiation (Garofalo et al., 1999). This phenotype shares some similarities with the phenotype of *Creld2*$^{Cart\Delta ex3\text{-}5}$ mice and interestingly *Fgf9* was found to be upregulated in *Creld2*$^{Cart\Delta ex3\text{-}5}$ cartilage. This suggests that CRELD2 may exert its role in chondrocyte maturation through modulation of FGF9 expression. Moreover, the ablation of *Creld2* in chondrocytes also resulted in a reduction in the expression of several other genes encoding important signalling

proteins such as WNT4 that promotes maturation and terminal differentiation of growth plate chondrocytes *in vivo* and *in vitro* (Hartmann and Tabin, 2000, Lee and Behringer, 2007).

CYR61/CCN1 and connective tissue growth factor (CTGF/CCN2) are two secreted proteins that regulate cell matrix interactions by binding to a wide range of extracellular proteins including IGF1, TGFβ, BMPs, MMPs, TSP proteins as well as receptors such as integrins and LRP1 (Holbourn et al., 2008). The CCN proteins play important roles in skeletal development and chondrocyte maturation, and double knockout mice exhibit severe global dysplasia with delayed ossification affecting both the appendicular and axial skeleton and the knockout of *Ctgf* leads to a very severe chondrodysplasia phenotype due to a disruption in chondrocyte maturation (Mo et al., 2002, Ivkovic et al., 2003, Hall-Glenn et al., 2009, Katsube et al., 2009). CYR61 alone plays a minor role in skeletal development and the cartilage-specific knockout of *Cyr61* does not display skeletal defects, however, it has been shown to promote chondrogenesis *in vitro* (Wong et al., 1997a). Furthermore, an overexpression of *Cyr61* or *Ctgf* enhances chondrocyte maturation *in vitro* (Nakanishi et al., 2000, Zhang et al., 2016). Interestingly, both *Cyr61* and *Ctgf* were downregulated following the ablation of *Creld2* in chondrocytes, providing further evidence that the knockout of CRELD2 impairs chondrocyte differentiation and maturation *in vivo*.

Expression of several hypertrophic markers, such as *Mmp13* and *Mmp9*, was downregulated in $Creld2^{Cart\Delta ex3\text{-}5}$ cartilage. These genes encode metalloproteinases that play an important role in matrix remodelling, allowing for vascular invasion and the formation of bone (Vu et al., 1998, Nagai and Aoki, 2002). In addition, the extracellular matrix glycoprotein TSP2 that regulates cell-matrix interactions and inhibits proliferation and angiogenesis was upregulated in knockout mice (Armstrong et al., 2002, Simantov et al., 2005). *Sema3e,* encoding Semaphorin 3E (SEMA3E) was also upregulated in knockout cartilage. The overexpression of *Sema3e* in embryos results in inhibition of vessel growth and, interestingly, SEMA3E can also inhibit osteoblast migration *in vitro* (Hughes et al., 2012). These findings correlate with impaired angiogenesis in $Creld2^{Cart\Delta ex3\text{-}5}$ mice which could in turn result in the reduction of the number of osteoblasts beneath the growth plate.

Proliferation and cell survival were disrupted following the ablation of *Creld2* in chondrocytes and several genes that contribute to this process were identified in the

RNAseq analysis. Interestingly, *Cdkn1a* encoding the anti-proliferative Cyclin Dependent Kinase Inhibitor 1A (alternatively known as $p21^{Waf1/Cip1}$) was upregulated in $Creld2^{CartΔex3\text{-}5}$ cartilage. The p21 protein is a potent regulator of the cell cycle that regulates the progression at G1/S transition by binding to and inhibiting cyclin/cyclin dependent kinase complexes (Harper et al., 1995). Another gene upregulated in knockout cartilage was *Irf1,* encoding the transcription factor interferon regulatory factor 1 (IRF1). This protein plays a role in inhibiting cell growth by regulating the cell cycle partly through the upregulation of p21 upon direct interaction with its promoter (Coccia et al., 1999). IRF1 inhibits proliferation and stimulates apoptosis through the activation of caspase proteins (Tamura et al., 1995, Suk et al., 2001, Bouker et al., 2005). Another interesting gene upregulated in knockout chondrocytes was *Lmna* encoding the nuclear scaffold protein lamin A/C. Studies have shown that the intracellular accumulation of lamin A/C is associated with osteoarthritis and overexpression of *Lmna in vitro* inhibits mesenchymal stem cell chondrogenesis potentially via disrupting the oxidative stress response (Attur et al., 2012, Mateos et al., 2013). Overexpression of LMNA was also found to inhibit proliferation by upregulating p21 and induces apoptosis via caspase activation (Attur et al., 2012). Numerous genes that also stimulate apoptosis, such as *Fas* and *Zak,* were also upregulated in $Creld2^{CartΔex3\text{-}5}$ cartilage. Overall theses data suggest that proliferation and apoptosis were affected following the ablation of *Creld2* in chondrocytes potentially as a downstream effect of impaired differentiation.

Cilia organisation and cellular polarity was disrupted in $Creld2^{CartΔex3\text{-}5}$ cartilage. Interestingly, *Fat4* was upregulated in the knockout chondrocytes. Studies have shown that the protocadherin FAT Atypical Cadherin 4 (FAT4) localises to the primary cilia and plays a role in controlling the proliferation and polarity of pre-chondrogenic mesenchyme during vertebral development; however, its role in mature chondrocytes is unknown (Saburi et al., 2008, Mao et al., 2016). The upregulation of *Fat4* in $Creld2^{CartΔex3\text{-}5}$ mice could therefore result in the disrupted polarity of proliferative chondrocytes in knockout growth plates. Primary cilia project into the ECM and interact with matrix molecules via a number of receptors including integrins (Ruhlen and Marberry, 2014). *Itga2* encoding the integrin alpha 2 subunit was upregulated in $Creld2^{CartΔex3\text{-}5}$ mice. This misexpression of an integrin subunit could result in altered matrix interaction and affect chondrocyte activity. For example, the misexpression of

integrin α5β1 resulted in accelerated maturation of chondrocytes in the developing skeleton (Garciadiego-Cazares et al., 2004).

In summary, RNA sequencing provided a detailed insight into the role of CRELD2 in chondrocytes and generated original data suggesting a novel and important role for CRELD2 in chondrocyte differentiation and maturation.

The potential role of CRELD2 in chondrocytes

To understand how this putative PDI regulates chondrocyte differentiation and maturation, an important aim of the study was to identify binding partners of CRELD2 by mass spectrometry. Interestingly, the mass spectrometry data presented in this thesis suggest that CRELD2 plays a role in protein folding and trafficking. It is important to note that not all proteins identified by mass spectrometry bind directly to CRELD2 and several proteins have likely been pulled down as part of a larger complex. Moreover, binding partners of CRELD2 could be proteins that are important for the processing of CRELD2 itself.

CRELD2 was found to co-precipitate with 40S ribosomal protein S15A (S15A) and ribosomal protein L15 (RPL15) that encode proteins of the 40S and 60S ribosomal subunits respectively. This could result from binding during the translation of CRELD2 or alternatively suggests that CRELD2 aids in assembling the translation machinery at the ER. As proteins are translated they are co-translationally translocated into the ER lumen by the translocon. Interestingly, CRELD2 was found bound to several components of the membrane protein complex, the oligosaccharyltransferase (OST), that catalyses the addition of N-linked glycans to the to the asparagine-X-serine/threonine motif on the nasent polypeptide chain, including the catalytic subunits STT3A/B and the non-catalytic subunit DDOST (Stanley, 2016). Additionally, CRELD2 precipitated with proteins downstream of the OST involved processing and folding N-linked glycoproteins including mannosyl-oligosaccharide glucosidase (MOGS), dolichyl-diphosphooligosaccharide--protein glycosyltransferase subunit 1 (RPN1), Calreticulin, UGGT1, selenoprotein F (SEP15), alpha glucosidase 2 alpha neutral subunit (GANAB) and ER-Golgi intermediate compartment protein 53 (LMAN1) (Stanley, 2016). Moreover, CRELD2 was found to bind to guanine diphosphate-fucose protein O-fucosyltransferase 2 (POFUT2), an enzyme that catalyses the addition of O-linked fucose residues to serine/threonine residues in thrombospondin

repeats. As CRELD2 is glycosylated these data could result from processing of CRELD2 itself or perhaps suggest that CRELD2 forms part of a protein complex controlling N-linked glycan folding and processing in the ER and vesicular trafficking from the ER to the Golgi apparatus (Oh-hashi et al., 2011).

CRELD2 was also found to bind a variety of other chaperones within the ER that aid in protein folding, such as BIP, GRP94, hypoxia upregulated protein 1 (HYOU1) and PDIs that form a complex with DNAJ proteins to promote protein folding. Furthermore, CRELD2 bound endoplasmic reticulum oxidoreductase 1-like protein alpha (ERO1A) that is known to activate PDIs. Since CRELD2 functions as a putative PDI the binding of CRELD2 to ERO1A could activate its PDI activity. Interestingly, CRELD2 was also found in a complex with the novel chaperone, MANF/ARMET.

CRELD2 co-precipitated with several proteins involved in the processing of collagen molecules suggesting a role for CRELD2 in collagen folding and maturation. These included SERPINH1, a collagen specific molecular chaperone and procollagen-lysine,2-oxoglutarate 5-dioxygenase (PLOD) 1, PLOD2, PLOD3, prolyl 3-hydroxylase 1 (P3H1) and prolyl 4-hydroxylase aubunit apha 2 (P4HA2) that modify the collagen protein allowing for proper folding to be achieved.

Since CRELD2 acts as a putative PDI it comes as no surprise that it binds protein folding chaperones within the ER. However, unlike other proteins that are resident in the ER, CRELD2 does not contain a perfect KDEL ER retention sequence (Oh-hashi et al., 2011). Instead, CRELD2 contains a C-terminal REDL motif also described as an “imperfect KDEL” (Hartley et al., 2013). Previous studies have postulated that this motif may be a targeting motif for ER retrieval as REDL motif is implicated in toxin endocytosis (Hessler and Kreitman, 1997). The subcellular localisation data presented in this thesis identified CRELD2 within exosomes indicating that it is secreted. The C-terminal REDL motif found in CRELD2 could therefore act as an ER targeting motif, retrieving extracellular CRELD2 back to the ER. A search of the UniProt database for proteins containing a C-terminal REDL sequence identified 4 other proteins with this motif (Table 6). Interestingly, two of these proteins are chaperones that play a role in folding, maturation and cell surface expression of receptor proteins. For example, canopy 4 (CPNY4) is an ER chaperone found to promote the cell surface expression of toll-like receptor 4 (TLR4) (Konno et al., 2006). Interestingly, the online

InterPro database of protein famililes and domains reveal that the canopy proteins are the only proteins to contain the domain of unknown function (DUF3456) also present in CRELD2 (Finn et al., 2017). A second protein with an REDL motif and involved in trafficking of a cell surface receptor is mesoderm development candidate 2 (MESDC2), shown to play an important role in folding, trafficking and maturation of LRP4, LRP5 and LRP6 (Hsieh et al., 2003, Koduri and Blacklow, 2007, Hoshi et al., 2013). An ablation of *Mesdc2 in vivo* resuls in embryonic lethality with mice resembling the phenotype of *Wnt3*-null mice. This suggested a role of MESDC2 in modulating WNT signalling in development by promoting the maturation of WNT co-receptors (Hsieh et al., 2003).

Table 8. **Proteins containing a C-terminal REDL sequence.**

Protein Symbol	Protein name	Subcellular localisation	Function	Reference
CRELD2	Cysteine-rich with EGF-like repeats2	Endoplasmic reticulum, Extracellular, Golgi apparatus	An ER-stress inducible protein and putative PDI.	(Hartley et al., 2013)
GTDC1	Glycosyltransferase-like domain containing 1	Cytosol	Unknown. Potentially plays a role in the transfer of a sugar moiety from active donors to acceptors.	(Zhao et al., 2004)
GPX7	Glutathione Peroxidase 7	Endoplasmic reticulum, Extracellular	Oxidative stress sensor that shuttles disulphide bonds in various stresses activating target proteins such as BIP.	(Wei et al., 2012)
CNPY4	Canopy 4	Extracellular	Chaperone that controls the cell surface expression of TLR4.	(Konno et al., 2006)
MESDC2	Mesoderm development candidate 2	Endoplasmic reticulum, Extracellular	Chaperone that promotes the folding, maturation and cell surface expression of LRP4, LRP5 and LRP6.	(Hsieh et al., 2003, Koduri and Blacklow, 2007, Hoshi et al., 2013)

The analysis of putative CRELD2 binding partners showed that CRELD2 co-precipitated with several extracellular and transmembrane proteins such as TSP1,

CYR61 and LRP1. It has previously been shown that CRELD2 binds to TSP1 via N-terminal CXXC motifs defining a role for CRELD2 in promoting disulphide bond formation in TSP1 (Hartley et al., 2013). Interestingly, these proteins also interact with each other, suggesting that they were potentially pulled down in a complex (Mikhailenko et al., 1997, Juric et al., 2012). As the other proteins that contain a C-terminal REDL motif are involved in folding and trafficking of receptors, perhaps the most interesting putative binding partner of CRELD2 is the transmembrane receptor LRP1. Based on data from this study, it can be postulated that CRELD2 may be implicated in chaperoning and trafficking LRP1 to the cell surface, with CRELD2 ultimately being recycled back to the ER. If this were the case, the knockout of *Creld2* would result in a reduction in cell surface expression of LRP1 .

LRP1 is a 600 kDa type I membrane receptor and a member of the Low-density lipoprotein (LDL) receptor family that binds many ligands, playing complex roles in various biological processes (Herz and Strickland, 2001). The lack of *Lrp1* results in embryonic lethality in mice confirming that LRP1 plays an important, yet undefined, role in development (Herz et al., 1992). Unfortunately as no *Lrp1* skeletal conditional knockout mouse models have been generated to date, and it is difficult to determine the role of LRP1 in cartilage and bone using solely *in vitro* models.

It was originally postulated that LRP1 functions as a scavenger receptor, but subsequent studies have shown that it also plays roles in extracellular matrix-intracellular signal transduction (Herz and Strickland, 2001). Interestingly, LRP1 has been shown to bind ECM proteins such as THBS1/THBS2 and FBN2, growth factors such as TGFβ and CTGF and associate and modulate the activity of cell surface receptors such as integrins (Lillis et al., 2008). LRP1 can activate PKC signalling, integrin mediated signalling and downstream signalling cascades involving MAPK signalling proteins (Herz and Strickland, 2001) and has also been implicated in downregulating WNT signalling by binding and sequestering the FZD1 WNT co-receptor (Herz and Strickland, 2001, Zilberberg et al., 2004). *In vitro* studies investigating the role of LRP1 in a chondrocyte-like cell line have shown that LRP1, present on proliferating chondrocytes, promotes differentiation and inhibits maturation, depending on the stimulus and signalling initiated (Kawata et al., 2010). Therefore, a disruption to LRP1 cell surface expression could result in a delay in differentiation but the stimulation of maturation. This does not however correlate with the phenotype observed in $Creld2^{Cart\Delta ex3\text{-}5}$ mice, as the level of the hypertrophic marker *Mmp13* is

downregulated in *Creld2* null cartilage. This however could be a secondary effect resulting from a delay in proliferation. Depending on its interaction with the matrix, growth factors and other cell surface receptors, LRP1 transduces different signals to affect the activity of cells. As the differentiation results by Kawata *et al*. were obtained in an *in vitro* monolayer experiment they might not be indicative of an *in vivo* situation in which chondrocytes are interacting with the vast extracellular matrix they secrete (Kawata et al., 2010).

As LRP1 has been implicated in modulating WNT signalling, disruption to this receptor could result in excessive canonical WNT/β-Catenin signalling which would in turn result in a delay in chondrocyte differentiation (Akiyama et al., 2004, Tamamura et al., 2005). LRP1 has been shown to block canonical WNT signalling via interaction with FZD1. However, FZD1 is not activated by any of the canonical WNT proteins expressed in the growth plate (Gazit et al., 1999). This suggests that in the postnatal growth plate, LRP1 may not function primarily to modulate canonical WNT signalling. LRP1 has, however, been shown to stimulate the WNT5A signalling pathway *in vitro* (Woldt et al., 2012). During development, non-canonical WNT5A signalling enhances early chondrogenic differentiation (Hartmann and Tabin, 2000). Concurrent with this, LRP1 positively regulates a WNT5A signalling pathway that results in the upregulation of chondrogenic genes in vascular cells *in vitro,* whereas the absence of LRP1 inhibited WNT5A signalling (Woldt et al., 2012). Within the growth plate, WNT5A has also been shown to promote the maturation of proliferative chondrocytes (Yang et al., 2003). Therefore, if LRP1 promotes WNT5A signalling in chondrocytes *in vivo,* the disruption to LRP1 cell surface expression could result in a reduction in WNT5A signalling. This in turn could lead to a delay in chondrocyte maturation consistent with the phenotype observed in *Creld2*$^{Cart\Delta ex3\text{-}5}$ mice.

Moreover, LRP1 plays a wide variety of complex roles aside from modulating WNT signalling. For example, LRP1 can bind to the TSP1 domain of CTGF controlling its transport and distribution within the growth plate, therefore suggesting a potential role for this receptor in controlling chondrocyte differentiation and maturation (Kawata et al., 2012). Studies have shown that as well as internalising CTGF for degradation, CTGF also promotes phosphorylation of the cytoplasmic domain of LRP1, thus stimulating downstream ERK1/2 MAPK signalling cascades to modulate myofibroblast differentiation (Segarini et al., 2001, Yang et al., 2004, Kawata et al., 2012). As discussed previously, CTGF has been shown to promote chondrocyte maturation and

hypertrophic differentiation within the growth plate via stimulating PKC, P13K and JNK signalling cascades (Nakanishi et al., 2000, Nishida et al., 2002, Ivkovic et al., 2003, Yosimichi et al., 2006). In addition, WNT5A signalling can upregulate *CTGF* expression (Park et al., 2015a). Interestingly the results presented here show a downregulation in *Ctgf* expression in knockout cartilage. This therefore describes a potential mechanism by which LRP1 promotes chondrocyte maturation via CTGF by promoting WNT5A-mediated *Ctgf* transcription (Figure 61).

Summary

The data presented here suggests a novel and important role for CRELD2 in cartilage development. Phenotypic analysis of *Creld2*$^{Cart\Delta ex3\text{-}5}$ mice showed that knockout mice displayed a distinctive chondrodysplasia phenotype characterised by disproportionate short stature and a bone defect. Mice displayed a disrupted cartilage growth plate with abnormal chondrocyte morphology resulting from impaired primary cilia organisation. This is first study to deep phenotype a cartilage-specific knockout of *Creld2*. The work presented in this thesis suggests that CRELD2 may function as a molecular chaperone for LRP1 and the lack of CRELD2 may impair chondrocyte differentiation and maturation as demonstrated by transcriptome profiling. This study identified a potential novel role for CRELD2 in chondrocytes, however, additional studies are required to delineate the signal pathways that result in promoting chondrocyte proliferation and maturation via LRP1.

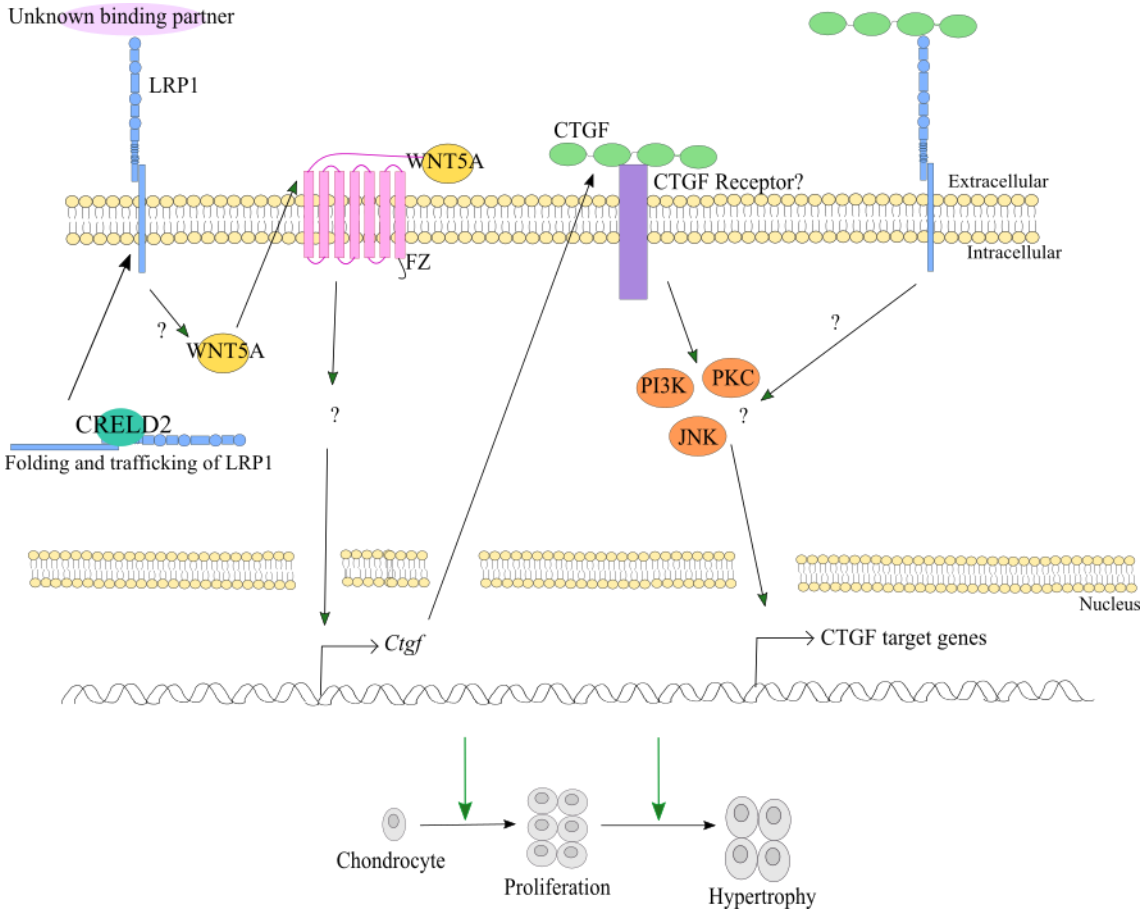

Figure 61. **Potential mechanism for CRELD2 in promoting chondrocyte differentiation and maturation.**

Studies indicate that CRELD2 potentially promotes chondrocyte differentiation and maturation by acting as a molecular chaperone for the cell surface receptor LRP1 and modulating *Ctgf* expression. Studies have shown that LRP1 stimulates WNT5A signalling which upregulates the expression of *Ctgf*. CTGF has been shown to promote chondrocyte maturation and hypertrophic differentiation within the growth plate via stimulating PKC, P13K and JNK signalling cascades though its interaction with an unknown receptor. Furthermore, CTGF has been found to bind LRP1 and stimulate downstream ERK1/2 MAPK signalling cascades to modulate cell differentiation. Therefore, with the ablation of CRELD2, the trafficking of LRP1 would be impaired and chondrocyte differentiation and maturation delayed.

Chapter 6. The role of *Creld2* in bone homeostasis

Chapter 6. The role of *Creld2* in bone homeostasis

6.1 Introduction

As Chapter 4 revealed that *Creld2* bone-specific knockout mice display an osteopenic phenotype with altered bone microarchitecture and impaired bone cell homeostasis, the aim of this chapter was to investigate the role of this novel chaperone in osteoblasts and deduce its function in post-natal bone remodelling and homeostasis.

A variety of histological, molecular biological and OMICS techniques were employed to analyse the mechanism that resulted in the skeletal pathology of *Creld2*$^{Bone\Delta Ex3\text{-}5}$ mice outlined in Chapter 4. This included:

- Trabecular bone apposition was analysed by dynamic histomorphometry to provide a mechanistic link between the lack of CRELD2 in mature osteoblasts and the reduction in bone mineral density with impaired trabecular microstructure observed in *Creld2*$^{Bone\Delta Ex3\text{-}5}$ mice.
- Work presented in Chapter 4 showed that *Creld2*$^{Bone\Delta Ex3\text{-}5}$ mice display a decrease in the number of osteoblasts and an increase on the number of osteoclasts on the trabecular bone. The RANKL/OPG axis was therefore studied at the transcriptomic and proteomic level to analyse homeostasis between osteoblasts and osteoclasts. In addition, the concentrations of extracellular RANKL and OPG were analysed by ELISA.
- To analyse if the impairment to cellular homeostasis had an impact on osteoclastogenesis, which could result in the increased number of osteoclasts present on the trabecular bone of knockout mice, pre-osteoclasts were differentiated *in vitro* in primary osteoblast conditioned media. Osteoclastogenesis was determined by analysing the expression of osteoclast markers including TRAcP (*Acp5),* Cathepsin K (*Ctsk)* and Calcitonin receptor (*Calcr*) by q-PCR.
- The transcriptome of knockout mice was compared to control mice following RNA-sequencing in order to identify dysregulated genes and pathways affected following the ablation of *Creld2* in mature osteoblasts.

6.2 The lack of CRELD2 expression in osteoblasts reduces osteoblast activity *in vivo*

To study the effect of the ablation of *Creld2* on osteoblast activity, dynamic histomorphometry was performed. *In vivo* labelling with alizarin complexone and calcein allowed for investigation of the rate of bone formation. Alizarin complexone and calcein are incorporated into the mineralising surface and can be used to label the newly forming bone (Figure 62A-62D). The mineral appositional rate (MAR) and the bone formation rate (BFR) were assessed from non-decalcified plastic embedded tibial sections of the injected mice.

Dynamic histomorphometry of tibial trabecular bone growth showed that at 9 weeks of age, knockout mice displayed a reduction in the mineral appositional rate with a decrease of 19.4 % ($p<0.05$) compared to control mice (Figure 62E). Subsequently bone formation rate was significantly reduced by 40.6 % ($p<0.05$) in knockout mice relative to control mice, thus suggesting a decrease in trabecular bone formation (Figure 62F). Taken together these data suggest that the ablation of CRELD2 in osteoblasts results in significantly lower levels of bone apposition.

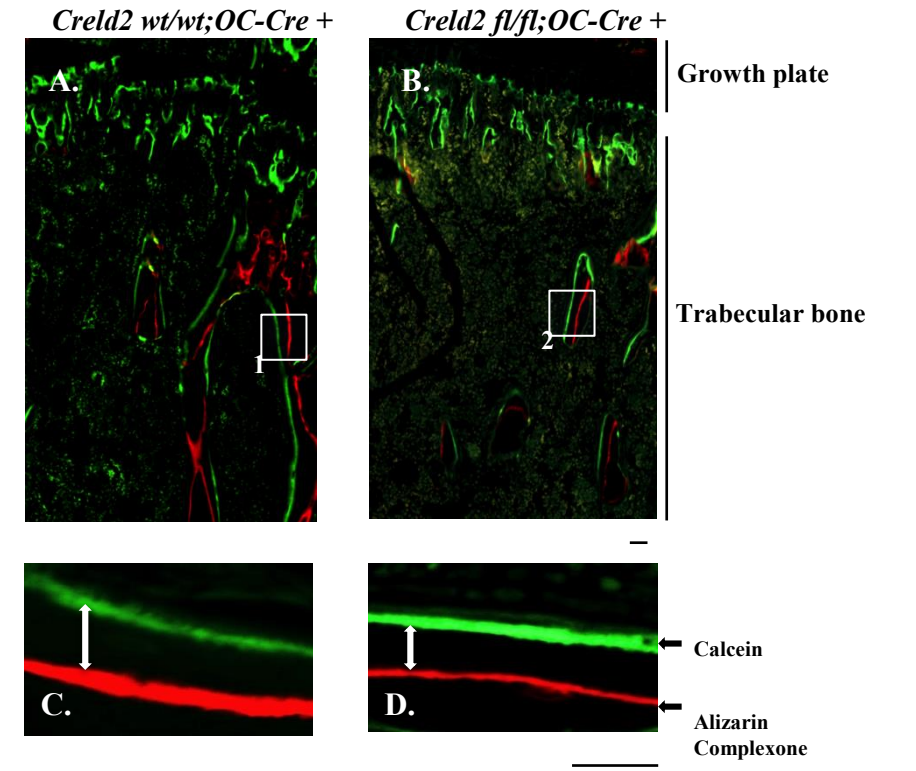

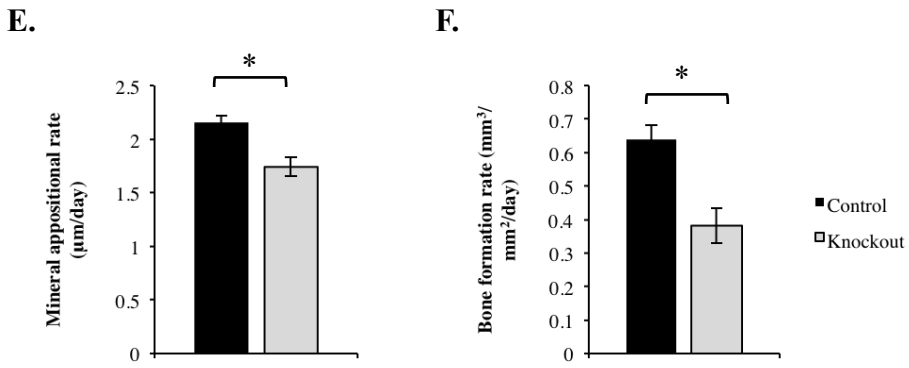

	Mineral appositional rate (µm/day) ± SEM	Bone formation rate (mm^3/mm^2/day) ± SEM
Control	2.16 ± 0.07	0.64 ± 0.04
Knockout	1.74 ± 0.95*	0.38 ± 0.05*

***Figure 62.* Ablation of *Creld2* in osteoblasts results in diminished osteoblast activity indicated by a reduction in the mineral appositional rate and the bone formation rate.**

In vivo double labelling of 9-week tibial bone with alizarin complexone and calcein was used to analyse yhe dynamic properties of bone (**A.** & **B.**). (Box 1 magnified in **C.**, Box 2 magnified in **D.**). *Creld2*$^{Bone\Delta Ex3\text{-}5}$ mice displayed a significantly reduced mineral appositional rate (**E**.) with a reduction of 19.4 % relative to control mice. The bone formation rate was also significantly reduced (**F**.) in knockout mice at 9 weeks by 40.6 %. Numerical data presented in graphs shown in the table. (SEM = standard error of the mean, * $p<0.05$, unpaired t-test, $n>10$ mice per genotype, Scale bar = 25 µm. Male mice showed the same phenotype, data not shown).

6.3 The knockout of CRELD2 results in disruption to the RANKL/OPG axis in osteoblasts

Despite the ablation of *Creld2* in osteoblasts, bone-specific *Creld2* knockout mice display an increase in the number of osteoclasts on the trabecular bone surface. This implies that there is a disruption in the crosstalk between osteoblasts and osteoclasts.

To study the cross talk between bone cells following the knockout of *Creld2* in osteoblasts, RANKL and OPG production was analysed at the transcritptomic and proteomic level. Studies showed that there was a significant 40.0 % ($p<0.05$) upregulation in *Tnfsf11* (encoding RANKL) expression; however, no change was observed in *Tnfrsf11b* (encoding OPG) expression (Figure 63A & 63B). This was also reproduced at the protein level were there was a significant 17.9 % ($p<0.05$) increase in the band intensity of RANKL from knockout osteoblasts (increasing from a relative band intensity of 0.28 in control osteoblast lysates to a relative band intensity of 0.33 in knockout osteoblast lysates Figure 64A). Correlating with the previously defined mRNAs level there was no significant difference in OPG expression since relative band intensities were comparable between the genotypes (Figure 64B).

In summary, RANKL, an osteoclastogenic cytokine, was upregulated in *Creld2*$^{Bone\Delta Ex3\text{-}5}$ mice and this observation may explain the increase in osteoclast number observed in these mice.

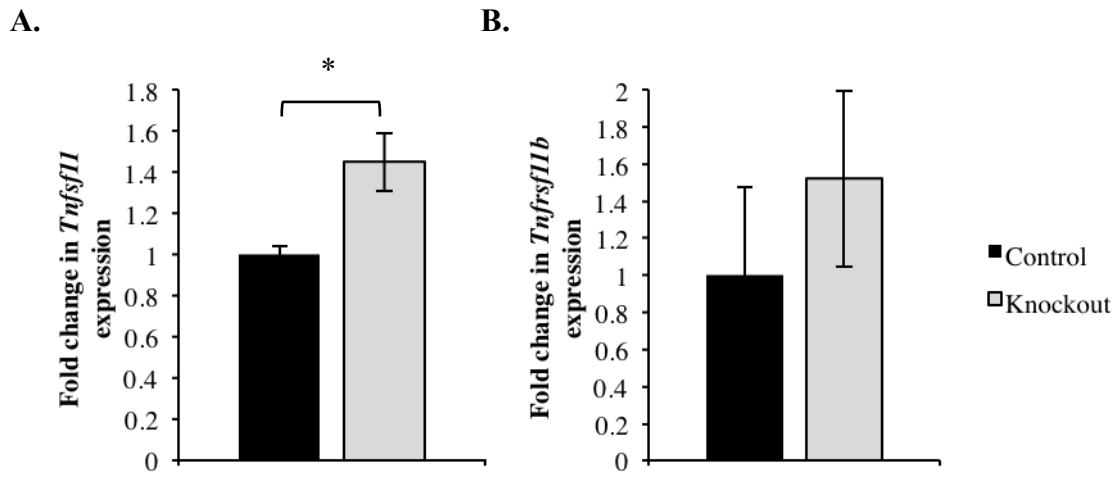

	Fold change in *Tnfsf11* expression ± SEM	Fold change in *Tnfsf11b* expression ± SEM
Control	1.00 ± 0.04	1.00 ± 0.48
Knockout	1.45 ± 0.14*	1.52 ± 0.57

Figure 63. **The knockout of *Creld2* in osteoblasts disrupts the RANKL/OPG axis at the RNA level.**

The levels of *Tnsfs11* (encodes RANKL) and *Tnfrsf11b* (encodes OPG) were examined by q-PCR. Interestingly, the levels of *Tnsfs11* expression from was significantly upregulated by 40 % in primary osteoblasts extracted from *Creld2*$^{Bone\Delta Ex3\text{-}5}$ mice relative to control mice. On the other hand, the levels of *Tnfrsf11b* were unchanged. Numerical data presented in graphs shown in the table. (Expression levels were normalised to the levels of *Actb, Hprt* and *Hmbs,* SEM = standard error of the mean, * $p<0.05$, unpaired t-test, n=3 samples from primary osteoblast extractions from 3 unrelated litters per genotype.).

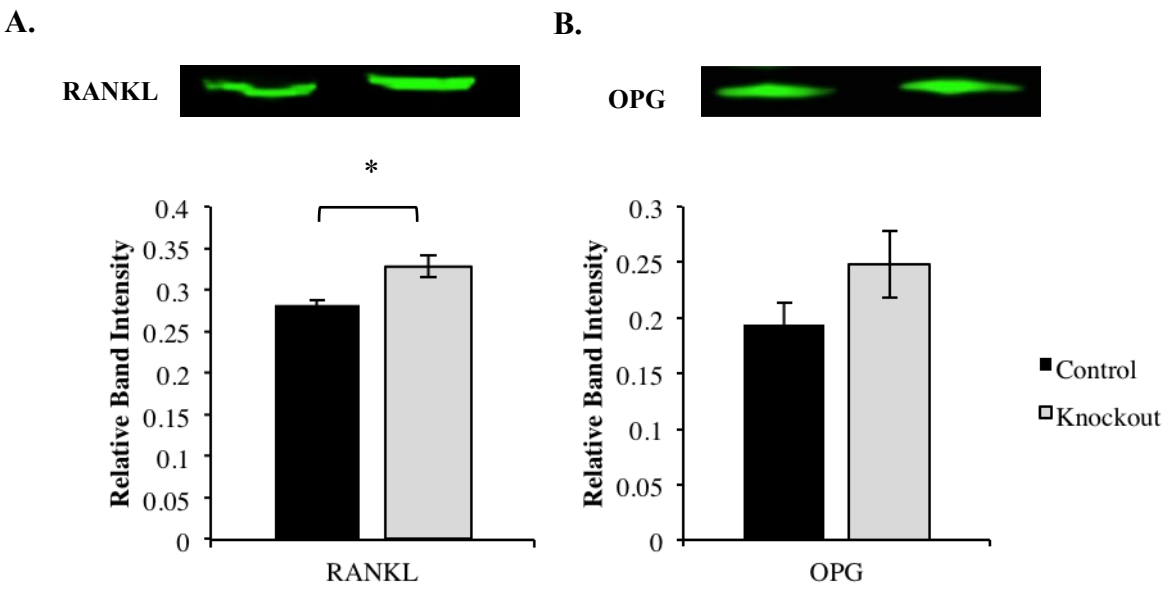

	Relative RANKL band intensity ± SEM	Relative OPG band intensity ± SEM
Control	0.28 ± 0.0057	0.19 ± 0.02
Knockout	0.33 ± 0.012*	0.25 ± 0.03

Figure 64. **The knockout of *Creld2* in osteoblasts the RANKL/OPG axis at the protein level.**

As *Tnfsf11* was upregulated in primary osteoblasts from *Creld2*$^{Bone\Delta Ex3\text{-}5}$ mice, western blotting was performed to confirm this upregulation at the protein level. Concurrent with the transcriptome level, RANKL was significantly upregulated by 17.9 % relative to control mice. However, there was no significant difference in OPG levels reflecting the quantative PCR results in which the expression of *Tnfrsf11b* was unaffected in primary osteoblasts from *Creld2*$^{Bone\Delta Ex3\text{-}5}$ mice. Numerical data presented in graphs shown in the table. (Samples were normalised to protein loading observed using REVERT™ total protein stain (Appendix D), SEM = standard error of the mean, * $p<0.05$, unpaired t-test, n=3 samples from primary osteoblast extractions from 3 unrelated litters per genotype.).

6.4 The deletion of CRELD2 in osteoblasts promotes the differentiation of osteoclasts

Through the action of proteolytic enzymes, membrane bound RANKL is cleaved from the surface of osteoblasts (Lum et al., 1999, Lynch et al., 2005, Hikita et al., 2006). Since RANKL and OPG are secreted by osteoblasts and play a critical role in controlling osteoclastogenesis the concentrations of RANKL and OPG in primary osteoblast conditioned media were analysed by ELISA.

The results from the ELISA assay showed that the concentration of RANKL in knockout osteoblast conditioned media was significantly higher (5.4-fold increase in concentration) relative to control osteoblast conditioned media (Figure 65A). In contrast, the media concentration of OPG was significantly reduced by 24.7 % in knockout osteoblast conditioned media compared to that found in control osteoblast knockout media (Figure 65B). The RANKL/OPG ratio was calculated using media RANKL levels/media OPG levels, which demonstrated that this ratio was 6.5-fold greater in knockout osteoblast, conditioned media (Figure 65C). As the concentration of RANKL secreted from osteoblasts is higher and the concentration of secreted OPG is lower this could explain the increase in trabecular osteoclast number following the ablation of *Creld2* in osteoblasts.

To analyse if this impaired RANKL/OPG axis in *Creld2*$^{Bone\Delta Ex3\text{-}5}$ mice stimulated osteoclastogenesis, pre-osteoclasts were differentiated *in vitro* in primary osteoblast conditioned media from control and knockout osteoblasts. Osteoclastogenesis was determined by analysing the expression of osteoclast markers *Acp5, Ctsk* and *Calcr* by q-PCR. Interestingly, the levels of *Acp5, Ctsk* and *CalcR* expression were significantly upregulated by 2.15-fold, 1.9-fold and 2.11-fold respectively in primary osteoclasts differentiated in knockout osteoblast conditioned media relative control osteoblast conditioned media (Figure 66). These results suggest that following the ablation of CRELD2 in osteoblasts, the RANKL/OPG was impaired due to an increased production and secretion of RANKL resulting in the stimulation of osteoclast differentiation.

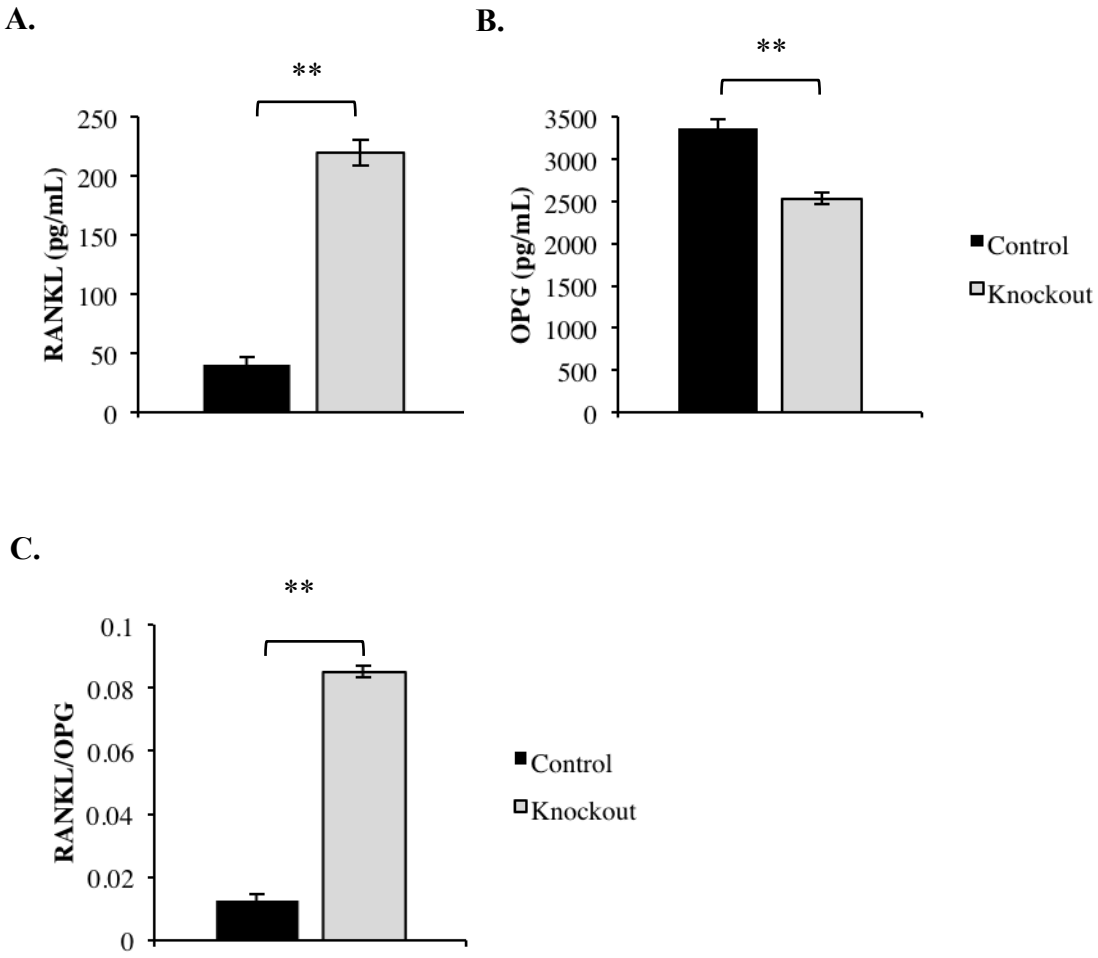

	RANKL (pg/mL) ± SEM	OPG (pg/mL) ± SEM	RANKL/OPG ± SEM
Control	40.86 ± 5.94	3361.18 ± 105.93	0.013 ± 0.0021
Knockout	219.64 ± 11.29 **	2531.74 ± 67.17 **	0.085 ± 0.0017 **

Figure 65. **The knockout of *Creld2* in osteoblasts alters the secretion of RANKL and OPG.**

As RANKL and OPG, both of which are secreted by osteoblasts, play critical roles in physiological bone remodelling the concentrations of secreted RANKL and OPG in osteoblast-conditioned media were examined by ELISA. The concentration of RANKL in knockout osteoblast conditioned media was significantly higher with a 5.4-fold increase in concentration relative to control mice (**A.**). On the other hand, the media concentration of OPG was significantly reduced by 24.7 % in knockout osteoblast conditioned media compared to that in control osteoblast media (**B.**). RANKL/OPG ratio was calculated using media RANKL levels/media OPG levels and showed that this ratio was 6.5-fold greater in knockout osteoblast conditioned media (**C.**). Numerical data presented in graphs shown in the table. (SEM = standard error of the mean, * $p<0.05$, unpaired t-test, n=3 media samples from different primary osteoblast extractions from 3 unrelated litters per genotype.).

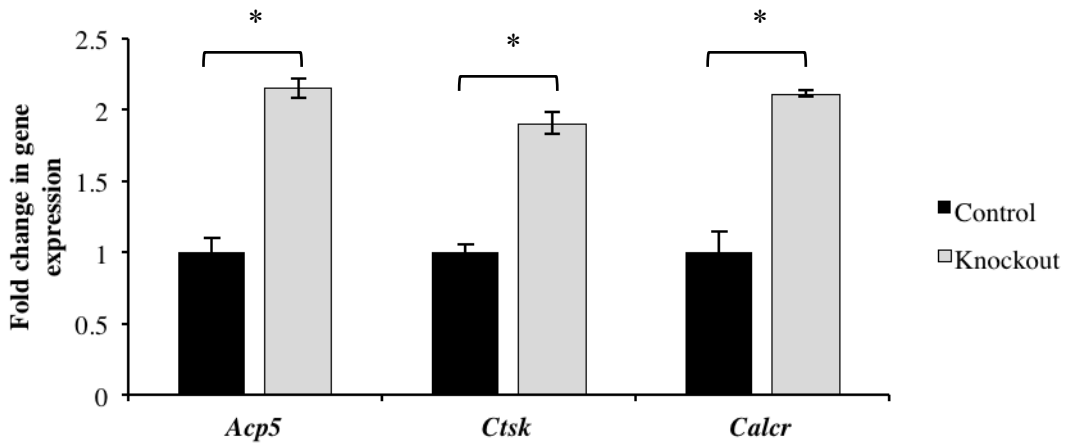

Figure 66. **The ablation of CRELD2 in osteoblasts promotes osteoclastogenesis *in vitro.***

To study if the increased osteoblast RANKL/OPG axis promotes osteoclastogenesis, primary pre-osteoclasts extracted from wild-type mice were differentiated *in vitro* for 1 week in primary osteoblast conditioned media. To study osteoclastogenesis, the levels of osteoclast markers such as *Acp5*, *Ctsk* and *Calcr* were examined by qPCR. Interestingly, the levels of *Acp5, Ctsk and CalcR* expression were significantly upregulated by 2.15-fold, 1.9-fold and 2.11-fold respectively in primary osteoclasts differentiated in knockout osteoblast conditioned media relative to control osteoblast conditioned media. Numerical data presented in graphs shown in the table. (Expression levels were normalised to the levels of *Actb, B2m* and *Hmbs,* SEM = standard error of the mean, * $p<0.05$, unpaired t-test, n = 2 samples from primary osteoclast extractions from 2 unrelated litters.).

6.5 Transcriptome profiling indicates *Creld2* has an anabolic effect on bone, stimulating osteoblastogenesis and repressing osteoclastogenesis.

To obtain a quantitative and unbiased list of differentially expressed genes that contribute to the phenotype resulting from the ablation of *Creld2* in osteoblasts, RNA-sequencing was performed. RNA was extracted from primary calvarial osteoblasts and sent to GATC Biotech for next generation sequencing. The transcriptome of *Creld2*$^{Bone\Delta Ex3\text{-}5}$ mice was compared against that of control mice in order to generate a gene expression profile of genes and genetic pathways that are directly affected by the knockout of *Creld2,* contributing to the phenotype of the mice outlined in Chapter 4.

6.5.1 Quality control check for RNA prior to sequencing

To generate an accurate gene expression prolife the integrity of RNA was analysed using an Agilent 2100 Bioanalyzer a prior to RNA-sequencing. The electropherograms and gel-like images provided by the Bioanalyzer revealed that there are only two large peaks/bands corresponding to the 18S and 28S ribosomal subunit suggesting that the RNA is not degraded (Figure 67). The Bioanalyzer software also assigned a RIN number to the samples based on the gel-like images and electropherograms. The RIN numbers for each of the control and knockout samples were given as 10.0 confirming that the RNA showed no degradation and was therefore used for subsequent RNA sequencing.

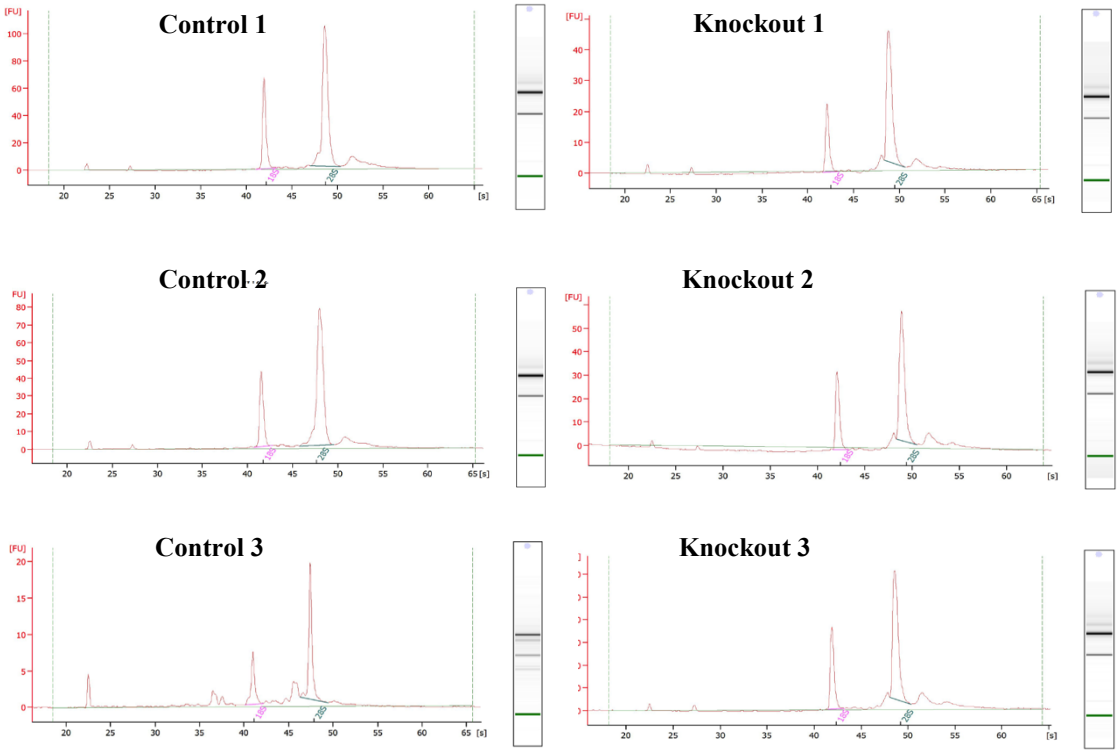

Sample	RIN	Quality control passed (GATC)
Control 1	10.0	Yes
Control 2	10.0	Yes
Control 3	10.0	Yes
Knockout 1	10.0	Yes
Knockout 2	10.0	Yes
Knockout 3	10.0	Yes

Figure 67. **Analysis of RNA integrity from primary osteoblasts.**

The Agilent 2100 Bioanalyzer RNA was used to assess the integrity of the RNA extracted from primary osteoblasts prior to RNA sequencing. The first peak on the electropherogram indicates the marker and the following two peaks denote the 18S and 28S RNA. The gel like images should have two clear bands denoting the 18S and 28S ribosomal subunits. There were no other peaks/bands present and so the RNA was not degraded. All the sample RINs were 10.0 indicating very good quality RNA. These samples (n=3 per genotype) therefore passed the quality control at GATC Biotech and were used for RNA sequencing to generate a transcriptome profile of mice.

6.5.2 Identification of potential candidate pathways affected by the ablation of Creld2 in osteoblasts

Following the ablation of *Creld2* in osteoblasts, 984 genes were differentially expressed (Figure 68). 74.0 % of these genes were found to be upregulated while only 26.0 % of genes were downregulated in *Creld2*$^{Bone\Delta Ex3\text{-}5}$ mice relative to the gene expression profile of control mice.

Correlating to the transcript profile of *Creld2*$^{Cart\Delta Ex3\text{-}5}$ mice in Chapter 5, despite CRELD2 playing a role as an ER-stress inducible gene, no significant fold changes in any genes related to ER stress and/or UPR were differentially expressed following the knockout of *Creld2* in osteoblasts.

The list of significant differentially expressed genes were analysed by the online bioinformatics software DAVID that clusters genes according to GO terms. The online REViGO tool was then used to remove redundant GO terms providing a general overview of the biological changes occurring as a result of the knockout of *Creld2 (Supek et al., 2011)*. GO terms are outlined in Table 9.

When the genes upregulated in *Creld2*$^{Bone\Delta Ex3\text{-}5}$ mice were clustered, the top clusters included genes involved in inflammation and the immune response. For example, genes within the inflammatory response were differentially expressed between the genotypes encoded cytokines such as C-C motif chemokine ligand (CCL) 3 that was upregulated by 23.4-fold and interleukins such as *Il6* that was upregulated by 32.4-fold.

Interestingly, similar to the observations in *Creld2*$^{Cart\Delta Ex3\text{-}5}$ mice outlined in Chapter 5, genes involved in apoptotic processes were differentially expressed in knockout mice. For example, *Fas* was upregulated in knockout osteoblasts but this overexpression was greater than in knockout chondrocytes, with an upregulation of 2.4-fold in comparison to 1.8-fold.

Not only did differentially expressed genes have ubiquitous functions, but they also clustered into genes involved in skeletal system development and bone mineralisation. These genes included *Igf1* that was downregulated by 1.5-fold and plays a role in inducing bone and cartilage formation. *Ctgf* was upregulated by 1.7-fold and functions to inhibit osteoblast maturation and bone mineralisation (Jiang et al., 2006, Govoni et al., 2007, Mundy et al., 2014). Genes were also clustered into genes involved in osteoblast differentiation. For example, *Bmp4* that enhances osteoblast differentiation

was downregulated by 1.4-fold; whereas, *Grem1* encoding a BMP antagonist that inhibits osteoblast differentiation was upregulated by 2.3-fold (Gazzerro et al., 2005, Chang et al., 2009). Despite differentially expressed genes acting to inhibit osteoblast differentiation and maturation, *Wnt11,* which functions to promote osteoblast maturation, was found to be upregulated by 3.2 fold (Friedman et al., 2009).

The crosstalk between osteoblasts and osteoclasts and is controlled partially by a series of cytokines. Differentially expressed genes in *Creld2*$^{BoneΔEx3\text{-}5}$ mice clustered into genes involved in bone resorption. For example, *Ccl2* that stimulates the recruitment and differentiation of osteoclast precursors was upregulated by 28.6-fold (Li et al., 2007). Several genes encoding pro-inflammatory cytokines such as *Il1a* and *Tnf* were also upregulated (by 21-fold and 21.7-fold respectively) and function to promote osteoclastogenesis (Azuma et al., 2000, Kim et al., 2009). Interestingly Tumour necrosis factor (TNF) also reduces bone formation by suppressing osteoblast differentiation (Gilbert et al., 2000). Confirming the work outlined in this chapter, *Tnfsf11* encoding the osteoclastogenic cytokine RANKL was upregulated by 4.2-fold in knockout osteoblasts. Interestingly, *Mmp3* was upregulated by 2.93-fold in *Creld2*$^{BoneΔEx3\text{-}5}$ mice and functions to cleave membrane-bound RANKL (Lynch et al., 2005). Taken together these results indicate that the crosstalk between osteoblasts and osteoclasts is impaired and the resulting genetic changes indicate that osteoclastogenesis is promoted in *Creld2*$^{BoneΔEx3\text{-}5}$ mice.

Several interesting genes that were differentially expressed between knockout and control mice are outlined in Table 10. Taken together these results suggest that the knockout of *Creld2* in mature osteoblasts disrupts bone homeostasis by inhibiting osteoblast differentiation, impairing bone formation and promoting osteoclast differentiation and subsequent bone resorption.

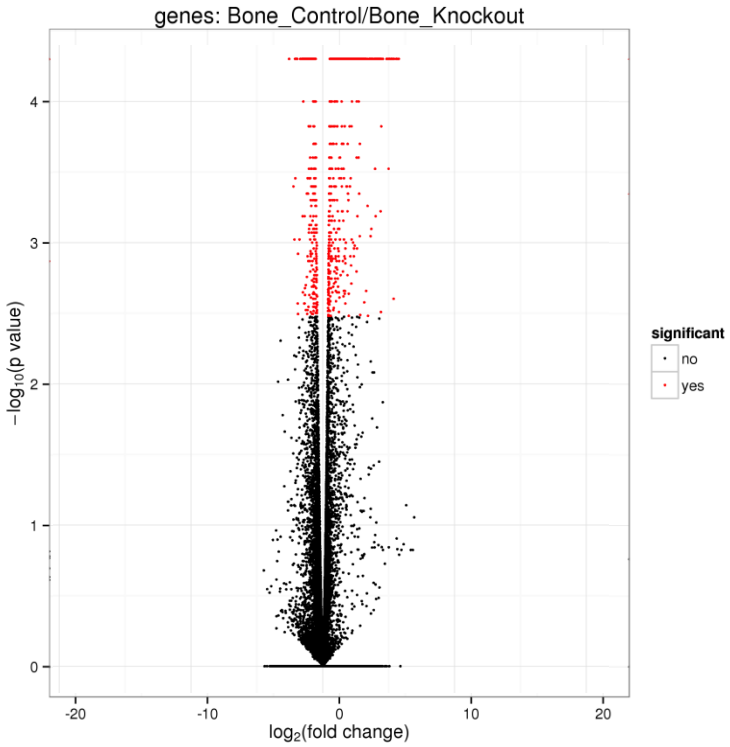

Upregulated genes	Downregulated genes
728	256

Figure 68. **984 genes were found to be differentially expressed in *Creld2* bone4 specific knockout mice relative to control mice.**

A volcano plot of statistical significance against fold-change between *Creld2*$^{Bone\Delta Ex3\text{-}5}$ and control mice, demonstrating significant differentially expressed genes. 984 genes were differentially expressed between the two genotypes. 728 genes (74.0 %) were upregulated and 256 genes (26.0 %) were downregulated in *Creld2*$^{Bone\Delta Ex3\text{-}5}$ mice.

Table 9. **REViGO summary of the GO terms from the 984 significantly differentially expressed genes in *Creld2* bone-specific knockout mice.**

GO:ID	Go term	p value
GO:0002376	Immune system process	9.30E-49
GO:0006954	Inflammatory response	1.50E-27
GO:0010628	Positive regulation of gene expression	1.90E-12
GO:0042346	Positive regulation of NF-kappaB import into nucleus	5.20E-11
GO:0007155	Cell adhesion	4.60E-10
GO:0006915	Apoptotic process	1.10E-08
GO:0006909	Phagocytosis	1.10E-07
GO:0071260	Cellular response to mechanical stimulus	7.90E-06
GO:0055072	Iron ion homeostasis	2.30E-05
GO:0030198	Extracellular matrix organisation	3.30E-05
GO:0051091	Positive regulation of sequence-specific DNA binding transcription factor activity	5.30E-05
GO:0008283	Cell proliferation	1.70E-04
GO:0007179	Transforming growth factor beta receptor signaling pathway	2.30E-04
GO:0006461	Protein complex assembly	2.90E-04
GO:0010629	Negative regulation of gene expression	5.00E-04
GO:0046697	Decidualisation	7.90E-04
GO:1900127	Positive regulation of hyaluronan biosynthetic process	1.00E-03
GO:0070373	Bone mineralisation	1.20E-03
GO:0031100	Animal organ regeneration	1.30E-03
GO:0051216	Cartilage development	1.90E-03
GO:0030154	Cell differentiation	1.90E-03
GO:0042060	Wound healing	1.90E-03
GO:0007613	Memory	2.10E-03
GO:0016477	Cell migration	2.30E-03
GO:0001819	Positive regulation of cytokine production	2.30E-03
GO:0044344	Cellular response to fibroblast growth factor stimulus	2.70E-03
GO:0007165	Signal transduction	3.00E-03
GO:0001934	Positive regulation of protein phosphorylation	3.50E-03
GO:0001775	Cell activation	3.70E-03
GO:0001666	Response to hypoxia	4.00E-03
GO:0007229	Integrin-mediated signaling pathway	5.10E-03
GO:0007167	Enzyme linked receptor protein signaling pathway	5.20E-03
GO:0001501	Skeletal system development	5.50E-03
GO:0045453	Bone resorption	6.20E-03
GO:0032967	Positive regulation of collagen biosynthetic process	7.30E-03
GO:0006874	Cellular calcium ion homeostasis	8.80E-03
GO:0045837	Negative regulation of membrane potential	1.30E-02
GO:0031397	Negative regulation of protein ubiquitination	1.30E-02

GO:0007623	Circadian rhythm	1.50E-02
GO:0043433	Negative regulation of sequence-specific DNA binding transcription factor activity	1.80E-02
GO:0001558	Regulation of cell growth	2.10E-02
GO:0038061	NIK/NF-kappaB signaling	2.10E-02
GO:0007595	Lactation	2.20E-02
GO:0042574	Retinal metabolic process	2.20E-02
GO:0009636	Response to toxic substance	2.30E-02
GO:0050850	Positive regulation of calcium-mediated signaling	2.70E-02
GO:2000377	Regulation of reactive oxygen species metabolic process	3.00E-02
GO:0071499	Cellular response to laminar fluid shear stress	3.10E-02
GO:0006693	Prostaglandin metabolic process	3.30E-02
GO:0050790	Regulation of catalytic activity	3.50E-02
GO:0016311	Dephosphorylation	3.80E-02
GO:0007219	Notch signaling pathway	3.90E-02
GO:0090263	Positive regulation of canonical WNT signaling pathway	4.20E-02
GO:0042541	Haemoglobin biosynthetic process	4.20E-02

Table 10. **Twenty differentially expressed genes in *Creld2* bone-specific knockout mice.**

Gene Symbol	Gene Title	log2(Fold Change)	q value	Subcellular location	Function
Cxcl9	C-X-C Motif Chemokine Ligand 9	**5.42**	1.38E-03	Secreted	Involved in the migration and activation of cells involved in immunity and inflammation.
Cxcl10	C-X-C Motif Chemokine Ligand 10	**5.19**	1.38E-03	Secreted	Monocyte and T-lymphocyte chemoattractant protein.
Il6	Interleukin 6	**5.02**	1.38E-03	Cell membrane, secreted	Roles in immunity, haematopoiesis and bone resorption. Induces the expression of matrix metalloproteinases 2 and 9.
Ccl2	C-C Motif Chemokine Ligand 2	**4.84**	1.38E-03	Secreted	Monocyte and basophil chemoattractant protein.
Tnf	Tumour necrosis factor	**4.44**	1.38E-03	Cell membrane, secreted	Cytokine with a wide variety of functions. Important roles in apoptosis, inflammation and immunity.

Il1a	Interleukin 1 Alpha	**4.39**	1.27E-02	Cytosol, secreted	Cytokine with a wide variety of functions. Important roles in haematopoiesis, inflammation and immunity.
Mmp3	Matrix metallopeptidase 3	**2.93**	1.38E-03	Secreted	Regulates matrix remodelling.
Tnfsf11	Tumour Necrosis Factor Superfamily Member 11(RANKL)	**2.07**	1.38E-03	Cell membrane, secreted	Plays an important role in bone resorption. Cytokine that binds to the RANK receptor, inducing osteoclast differentiation and activation through the oscillation of calcium ions and the activation of NFATc1. The action of RANKL is inhibited by binding a decoy receptor, OPG.
Wnt11	Wnt Family Member 11	**1.7**	1.38E-03	Secreted	Putative developmental signaling protein.
Icam1	Intercellular Adhesion Molecule 1	**1.55**	1.38E-03	Cell membrane, secreted	Promotes endothelial cell adhesion.
Fas	Fas Cell Surface Death Receptor	**1.26**	1.38E-03	Cell membrane, secreted	Mediates apoptosis by caspase-8 proteolytic activation, which initiates the subsequent cascade of caspase enzymes.

Grem1	Gremlin 1, DAN Family BMP Antagonist	**1.19**	1.38E-03	Secreted	Functions as a BMP antagonist during early limb development and downregulates BMP4. Also plays a role in inhibiting monotype chemotaxis.
Twist2	Twist Basic Helix-Loop-Helix Transcription Factor 2	**1.17**	1.38E-03	Nucleus	A transcription factor that may inhibit osteoblast differentiation.
Tnfaip6	Tumour Necrosis Factor Alpha-Inducible Protein 6	**0.75**	1.38E-03	Secreted	Involved in cell-cell and cell-matrix interaction during inflammation.
Vcam1	Vascular Cell Adhesion Molecule 1	**0.73**	1.38E-03	Cell membrane, cytoskeleton, endoplasmic reticulum, golgi apparatus, secreted	Mediates cell-cell recognition and cell adhesion. May play a role in immunity and the recruitment of leukocytes to the sites of inflammation.
Ctgf	Connective Tissue Growth Factor	**0.73**	1.38E-03	Secreted	Mitoattractant secreted by vascular endothelial cells. Promotes differentiation and proliferation of chondrocytes. Mediates cell adhesion.
Bmp4	Bone morphogenic protein 4	**-0.47**	3.21E-02	Secreted	Induces the formation of cartilage and bone.

Igf1	Insulin Growth Factor 1	**-0.62**	1.38E-03	Secreted	Hormone that regulates cell proliferation and apoptosis through the activation of the PI3K-AKT/PKB and the Ras-MAPK pathways.
Fbn2	Fibrillin 2	**-0.67**	1.38E-03	Secreted	Structural component of extracellular calcium-binding microfibrils. Also regulates the maturation of osteoblasts by controlling TGFβ and BMP levels.
Id4	Inhibitor Of DNA Binding 4, Dominant Negative Helix-Loop-Helix Protein	**-0.7**	1.38E-03	Nucleus	Binds to and inhibits the action of basic helix-loop-helix (bHLH) transcription factors. Plays a role in a wide range of processes including cell growth, differentiation and survival. Also plays a role in angiogenesis.

6.6 Discussion

The studies described in this chapter focused on determining the mechanisms following the deletion of *Creld2* in mature osteoblasts that resulted in the skeletal pathology described in Chapter 4.

To maintain skeletal size, shape and integrity bones undergo cycles of remodelling, involving the synchronised action of osteoblasts that synthesise the bone matrix and osteoclasts that resorb the bone (Hadjidakis and Androulakis, 2006). Osteoporosis and osteopenia are two related bone conditions that are characterised by low bone density due to an imbalance in bone formation and bone resorption, ultimately resulting in bone loss (Karsenty, 1999, Jilka, 2003). The diagnostic difference between the two diseases is the measure of bone density as the severity of bone loss is lower in osteopenia compared to that of osteoporosis (Karaguzel and Holick, 2010).

Osteopenia and low bone apposition

The bone pathology outlined in Chapter 4 revealed that *Creld2*$^{Bone\Delta Ex3\text{-}5}$ mice are characterised by growth retardation and an osteopenic phenotype. Morphometric analyses revealed bone abnormalities at the microstructural level. For example, tibial bones from knockout mice displayed a reduced bone volume due to significantly fewer trabeculae and low bone mass that correlated with altered bone microarchitecture with thinner trabeculae.

My studies of a targeted ablation of *Creld2* in mature osteoblasts reveal for the first time a role for CRELD2 in bone formation as bone-related parameters including osteoblast number and osteoid surface were significantly reduced in knockout mice relative to control mice. In this chapter, the osteoblast contribution to the osteopenic phenotype of *Creld2*$^{Bone\Delta Ex3\text{-}5}$ mice was further assessed. The work presented in this chapter showed that knockout mice exhibited significantly lower levels of mineral apposition and bone formation, outlining a novel role for CRELD2 in osteoblast-mediated postnatal bone formation.

Interestingly, physiological ER stress has been shown to play a role in osteoblast differentiation and activity; however, studies are limited to the roles of specific ER-stress inducible proteins. PERK signalling has been implicated in osteoblast differentiation and skeletal development and neonatal *Perk*-null mice displayed severe osteopenia due to impaired osteoblast differentiation and a reduction in the number of mature osteoblasts (Wei et al., 2008). In addition, the mineral appositional rate was reduced in 10-day-old *Perk* knockout mice relative to control mice. Studies have also revealed that the ablation of *Oasis,* a transcription factor that is structurally similar to ATF6 results in growth retardation and severe osteopenia (Murakami et al., 2011a). Bone apposition was impaired in these mice as the bone formation rate was significantly reduced in knockout mice relative to control mice. The phenotypes observed in *Perk-/-* and *Oasis-/-* mice were more severe, albeit similar, to that observed in *Creld2*$^{Bone\Delta Ex3\text{-}5}$ mice. It is important to note that *Perk*-null and *Oasis*-null mice were global knockouts, which could impair osteoblast activity at every stage of development, whereas the knockout mice described in this study results from the targeted ablation of *Creld2* in mature osteoblasts (Zhang et al., 2002b, Wei et al., 2008, Murakami et al., 2011a). This could explain the more severe reduction in the dynamic bone formation related-parameters outlined in the *Perk*-null and *Oasis*-null mice relative to *Creld2*$^{Bone\Delta Ex3\text{-}5}$ mice.

The significantly lower levels of bone apposition observed in *Creld2*$^{Bone\Delta Ex3\text{-}5}$ mice may result in the osteopenic phenotype with impaired bone microstructure described in Chapter 4. It can therefore be hypothesised that CRELD2 is required for the activity of mature osteoblasts and therefore could explain in the low bone mass observed in knockout mice.

A disrupted RANKL/OPG axis

Bone remodelling is a highly controlled process that requires tight coupling between bone resorption and bone formation. Bone turnover requires the synchronised action of osteoclasts and osteoblasts that function to degrade and repair bone thus maintaining skeletal integrity. A disruption to the balance between bone formation and resorption therefore results in bone disorders, such as osteoporosis and osteopenia that are caused by an overall increase in bone loss (Karsenty, 1999, Jilka, 2003).

In addition to the significantly lower levels of bone apposition, bone resorption is a likely contributor to the osteopenic phenotype observed in *Creld2*$^{Bone\Delta Ex3\text{-}5}$ mice. In contrast to *Oasis*-null and *Perk*-null mice, in which osteoclast numbers were unaffected, these data presented in Chapter 4 outlined an important role for CRELD2 in modulating osteoblast/osteoclast crosstalk since the targeted ablation of *Creld2* in mature osteoblasts resulted in an increase in the number of trabecular osteoclasts and a subsequent increase in the erosion surface. This suggests that a pathology resulting from the deletion of PERK and OASIS results solely from impaired bone formation, whereas the osteopenic phenotype observed in *Creld2*$^{Bone\Delta Ex3\text{-}5}$ mice may result from a combination of impaired bone formation and an increase in bone resorption.

The interaction between osteoblasts and osteoclasts is central to maintaining bone homeostasis. Osteoblasts stimulate and inhibit osteoclastogenesis via RANKL and OPG respectively (Boyce and Xing, 2007). The work presented in this thesis shows that the RANKL/OPG axis was disrupted at both the transcriptomic and proteomic level in osteoblasts from *Creld2*$^{Bone\Delta Ex3\text{-}5}$ mice. Following the ablation of *Creld2* in osteoblasts, the levels of *Tnfsf11* and RANKL expression were upregulated by 40.0 % and 17.9 % respectively. On the other hand, the levels of *Tnfsf11b* and OPG expression were unaffected. This therefore is the first study to identify a role for an ER-stress inducible gene in coupling osteoblast and osteoclast activities.

Through the action of ADAM and matrix metalloprotease proteolytic enzymes, membrane bound RANKL is cleaved from the surface of osteoblasts (Lum et al., 1999, Lynch et al., 2005, Hikita et al., 2006). Additionally, OPG is secreted from osteoblasts to inhibit osteoclastogenesis. The results presented here confirm a disruption to the RANKL/OPG axis as secreted RANKL was significantly increased by 5.4-fold. On the other hand, the secretion of OPG was impaired in *Creld2*$^{Bone\Delta Ex3\text{-}5}$ mice as the concentration of extracellular OPG was reduced by 24.7 %. It has been shown that OPG contains four disulphide-rich ligand-binding domains (Schneeweis et al., 2005). As CRELD2 acts as a putative PDI, catalysing the formation of disulphide bonds it can be hypothesised that it functions to promote the folding and stability of the mature OPG protein. Therefore, the ablation of CRELD2 could impair the trafficking of OPG. The work presented here therefore outlines a potential novel bone anabolic effect of CRELD2, promoting OPG folding and potentially inhibiting RANKL cleavage from the membrane.

As histological analyses of cellular parameters in knockout bones revealed an increase in the number of trabecular osteoclasts, an aim of this study was to determine if cellular crosstalk was impaired resulting in the osteopenic phenotype in *Creld2*$^{Bone\Delta Ex3\text{-}5}$ mice. To analyse osteoclast differentiation potential, pre-osteoclasts were differentiated in conditioned media from primary osteoclasts and results revealed that the ablation of *Creld2* in osteoblasts promoted osteoclastogenesis as identified by the upregulation of osteoclast marker genes, *Ctsk* (encoding Cathepsin K), *Acp5* (encoding TRAcP) and *Calcr* (encoding Calcitonin receptor).

This is the first study to implicate a PDI in coupling the actions of osteoblasts and osteoclasts. The work outlined in this chapter suggests a bone anabolic role of CRELD2, promoting bone formation while inhibiting osteoclastogenesis due to promoting OPG secretion and inhibiting RANKL cleavage from the membrane. Taken together the results presented here suggest that CRELD2 is important in osteoblast function and subsequently bone homeostasis.

Cellular response to the deletion of *Creld2* in mature osteoblasts

In order to identify in an unbiased manner novel candidate genes and pathways that are differentially expressed following the ablation of *Creld2* in osteoblasts, RNA sequencing was performed. Due to technical reasons, RNA sequencing was performed on RNA extracted from a mixed population of primary osteoblasts. This makes the analysis of differentially expressed genes difficult, as the osteoblasts are not all at the same stage of differentiation. On the other hand, the uncovered genetic changes are more indicative of the *in vivo* situation.

Consistent with the results described in Chapter 5, following the ablation of *Creld2* in osteoblasts no differences were observed in the levels of UPR and ER stress marker genes, indicating that the skeletal pathologies do not result from initiation of the UPR. It is important to note however that the cellular transcriptomes of the *Creld2*$^{Cart\Delta Ex3\text{-}5}$ and *Creld2*$^{Bone\Delta Ex3\text{-}5}$ mice are not comparable due to the mixed population of osteoblasts. Future work will concentrate on the analysis of the transcriptome from mature, *Bglap* expressing osteoblasts.

The data presented in this thesis suggest an anabolic role for CRELD2 in modulating osteoblast/osteoclast cross talk by impairing osteoclastogenesis as several

upregulated genes in *Creld2* bone-specific knockout mice function to stimulate osteoclast recruitment, differentiation and bone resorption (Table 11).

Table 11. **Dysregulated genes in *Creld2* bone-specific knockout mice that promote osteoclastogenesis.**

Gene	log2(Fold Change)	q value	Contribution to skeletal pathology of *Creld2* cartilage-specific knockout mice	Reference
Cxcl10	**5.19**	1.38E-03	Promotes osteoclastogenesis	(Lee et al., 2012)
Il6	**5.02**	1.38E-03	Promotes osteoclastogenesis	(Jilka et al., 1992, Tamura et al., 1993)
Ccl2	**4.85**	1.38E-03	Recruits osteoclast precursors and stimulates osteoclastogenesis	(Kim et al., 2005, Li et al., 2007)
Tnf	**4.44**	1.38E-03	Promotes osteoclastogenesis and inhibits osteoblast differentiation	(Bertolini et al., 1986, van der Pluijm et al., 1991, Kitazawa et al., 1994)
Il1a	**4.39**	1.27E-02	Promotes osteoclastogenesis	(Wei et al., 2005, Kim et al., 2009)
Tnfsf11	**2.07**	1.38E-03	Promotes osteoclastogenesis	(Li et al., 2000, Kim et al., 2000)
Csf1	**0.76**	1.38E-03	Recruits osteoclast precursors and stimulates osteoclastogenesis	(Lagasse and Weissman, 1997, Graves et al., 1999)

CCL2 also known as MCP1, and CSF1 are two chemokines that have been shown to play a role in bone resorption. Studies show that CCL2 and CSF1 stimulate osteoclast recruitment to initiate bone resorption and promote pre-osteoclast differentiation and fusion into mature multinucleated resorbing osteoclasts (Lagasse and Weissman, 1997, Graves et al., 1999, Kim et al., 2005, Li et al., 2007). CCL2 has also been shown to enhance the effect of RANKL on promoting osteoclastogenesis. Additionally C-X-C Motif chemokine ligand (CXCL) 10 has been shown to recruit immune cells and stimulate RANKL expression promoting osteoclastogenesis (Kwak et al., 2008, Lee et al., 2012). Both CCL2 and CXCL10 were upregulated following the ablation of *Creld2* in osteoblasts and therefore could result in the upregulation of

Tnfsf11. Interestingly, *Mmp3* was upregulated by 2.93-fold in *Creld2*$^{Bone\Delta Ex3\text{-}5}$ mice. MMP3 has been shown to promote the cleavage of membrane-bound RANKL and could result in the increased concentration of secreted RANKL detected by ELISA (Lynch et al., 2005).

TNF has been shown to play multiple roles in bone. The work presented here revealed that TNF was upregulated by 4.44-fold in knockout mice. For example, it has been shown to promote bone resorption *in vivo* and *in vitro* by stimulating osteoclast differentiation and maturation as well as inhibiting osteoblast differentiation and impairing matrix mineralisation (Bertolini et al., 1986, van der Pluijm et al., 1991, Kitazawa et al., 1994, Gilbert et al., 2000). Pro-inflammatory cytokines, such as Interleukin (IL) 1, and IL6 were upregulated following the ablation of *Creld2* in osteoblasts and have been shown to promote osteoclastogenesis (Manolagas, 1995). IL1 has been shown to play a role in bone resorption by stimulating osteoclast differentiation and mediating TNF-induced osteoclastogenesis by enhancing RANKL expression (Wei et al., 2005, Kim et al., 2009). Interestingly, vascular cell adhesion molecule 1 (VCAM1) and intercellular adhesion molecule 1 (ICAM1), two adhesion molecules, have been shown to promote the expression of pro-inflammatory cytokines in osteoblasts (Tanaka et al., 1995). As these genes are upregulated in *Creld2*$^{Bone\Delta Ex3\text{-}5}$ mice this could therefore result in the upregulation of pro-inflammatory cytokines identified by RNA-seq. Taken together, these findings identify a novel anabolic role for CRELD2 in bone, functioning to downregulate osteoclastogenesis and bone resorption.

During endochondral bone formation angiogenesis and osteogenesis are linked as blood vessels supply osteoblast precursors and stimulate bone formation (Zvaifler et al., 2000, Maes et al., 2010). A disruption to angiogenesis therefore results in reduced bone formation (Yang et al., 2012). Interestingly the angiostatic factor CXCL9 released by osteoblasts impairs angiogenesis, which disrupts osteoblast recruitment therefore abrogating osteogenesis (Huang et al., 2016). As *Cxcl9* was upregulated in *Creld2*$^{Bone\Delta Ex3\text{-}5}$ mice this finding indicates that angiogenesis is potentially affected following the ablation of *Creld2* in osteoblasts. This correlates with the data presented in Chapter 5 in which angiogenesis in *Creld2*$^{Cart\Delta Ex3\text{-}5}$ mice was impaired. This impairment in angiogenesis could therefore result in the reduction of the number of osteoblasts observed in *Creld2*$^{Bone\Delta Ex3\text{-}5}$ mice. Interestingly, CRELD1 has been shown to promote VEGF-stimulated calcineurin/NFATc1 signalling, outlining a potential role for CRELD proteins in angiogenesis (Mass et al., 2014).

The results presented here also suggests a potential role for CRELD2 in promoting osteoblast differentiation and maturation as several example dysregulated genes in *Creld2*$^{Bone\Delta Ex3\text{-}5}$ mice function to inhibit osteoblast differentiation, maturation and bone formation (Table 12).

Table 12. **Dysregulated genes in *Creld2* bone-specific knockout mice that lead to the inhibition of osteoblast differentiation and maturation.**

Gene	log2(Fold Change)	q value	Contribution to skeletal pathology of *Creld2* bone-specific knockout mice	Reference
Cxcl9	**5.42**	1.38E-03	Impairs osteoblast recruitment	(Huang et al., 2016)
Wnt11	**1.70**	1.38E-03	Promotes osteoblast maturation	(Friedman et al., 2009)
Fas	**1.26**	1.38E-03	Delays osteoblast differentiation	(Katavic et al., 2003)
Grem1	**1.19**	1.38E-03	Delays osteoblast differentiation	(Gazzerro et al., 2005)
Twist2	**1.17**	1.38E-03	Delays osteoblast differentiation	(Bialek et al., 2004)
Tnfaip6	**0.75**	1.38E-03	Delays osteoblast differentiation	*(Tsukahara et al., 2006)*
Ctgf	**0.73**	1.38E-03	Delays osteoblast maturation	(Smerdel-Ramoya et al., 2008)
Bmp4	**-0.47**	3.21E-02	Delays osteoblast differentiation	(Chang et al., 2009)
Igf1	**-0.62**	1.38E-03	Delays osteoblast differentiation	(Canalis, 1993, Birnbaum et al., 1995)
Fbn2	**-0.67**	1.38E-03	Delays osteoblast maturation and promotes osteoclastogenesis	(Nistala et al., 2010a, Nistala et al., 2010b)
Id4	**-0.70**	1.38E-03	Delays osteoblast differentiation	(Tokuzawa et al., 2010)

Two basic helix-loop-helix (bHLH) transcription factors were differentially expressed following the ablation of Creld2 in osteoblasts. Twist family BHLH transcription factor 2 (TWIST2) was upregulated by 1.17-fold in knockout osteoblasts.

Studies have shown that TWIST2 performs similar functions to TWIST1 in regulating bone formation and inhibits osteoblast differentiation as a deficiency in TWIST2 results in premature osteoblast differentiation (Lee et al., 1999, Bialek et al., 2004, Hayashi et al., 2007, Isenmann et al., 2009). A second BHLH transcription factor, Inhibitor of DNA binding 4 (ID4), was downregulated following the knockout of *Creld2* in osteoblasts. Studies to date have identified a role for ID4 as a pro-osteogenic transcription factor that is enriched during early osteoblast differentiation and promotes osteoblast differentiation *in vitro* (Tokuzawa et al., 2010). Consequently, the knockout of *ID4* results in impaired osteoblast differentiation and promotes adipogenesis (Tokuzawa et al., 2010). The dysregulation of these two bHLH transcription factors indicate that the knockout of CRELD2 impairs osteoblast differentiation *in vivo*.

Tnfaip6 encoding the extracellular matrix protein TNF-stimulated gene 6 protein (TSG6) was upregulated in knockout mice. Under physiological conditions TSG6 is not expressed however its expression is induced by inflammation (Milner and Day, 2003). The work presented in this chapter revealed that the expression of pro-inflammatory cytokines was upregulated following the knockout of *Creld2* in mature osteoblasts and could explain the upregulation of *Tnfaip6.* Interestingly studies have shown that TSG6 inhibits osteoblast differentiation *in vitro,* further indicating that osteoblast differentiation is impaired in *Creld2*$^{Bone\Delta Ex3\text{-}5}$ mice *(Tsukahara et al., 2006).*

The ablation of *Creld2* in mature osteoblasts also resulted in reduced expression of several important signalling proteins that function to promote osteoblast differentiation *in vitro* and *in vivo.* BMP4 has been shown to stimulate osteoblast differentiation *in vitro* by inducing cell cycle arrest at G(0)/G1 transition by upregulating p21$^{(CIP1/WAF1)}$ and p27$^{(KIP1)}$ (Chang et al., 2009). IGF1 has been shown to promote osteoblast differentiation and proliferation therefore stimulating matrix production (Canalis, 1993, Birnbaum et al., 1995). Interestingly, *in vivo* studies have shown that *Igf1* knockout mice are characterised by reduced bone volume with altered trabecular architecture, impaired mineralisation and bone formation, a similar phenotype to that observed in *Creld2* bone-specific knockout mice (Zhang et al., 2002a). Both of these genes are downregulated in *Creld2* knockout osteoblasts and so provide further evidence that CRELD2 plays a role in promoting osteoblast differentiation. Interestingly, IGF1 has also been shown to promote osteoblast survival (Hill et al., 1997). As observed in the *Creld2* knockout chondrocytes, the pro-apoptotic gene *Fas* was upregulated in *Creld2* knockout osteoblasts and *in vitro* studies show that

FAS has the potential to stimulate apoptosis in osteoblasts (Ozeki et al., 2002). Studies have also indicated a novel role for FAS in inhibiting osteoblast differentiation (Kovačić et al., 2007). Moreover, mice lacking a functional FAS ligand display increased bone formation due to an increased number of osteoblasts (Katavic et al., 2003). Taken together these results indicate that osteoblast differentiation is impaired in *Creld2* knockout osteoblasts and could explain the reduction osteoblast number, mineralisation and bone formation in *Creld2*$^{Bone\Delta Ex3\text{-}5}$ mice.

Several genes involved in modulating signalling during osteoblast maturation and bone formation were also differentially expressed between the genotypes. Aside from promoting chondrocyte differentiation and maturation, CTGF has been shown to regulate osteogenesis as *in vivo* knockout studies reveal it is essential for osteoblast maturation (Ivkovic et al., 2003, Kawaki et al., 2008). The roles of CTGF in osteoblast differentiation and maturation are complex as the overexpression of *Ctgf* in osteoblasts also impaired osteoblast maturation by antagonising BMP and WNT signalling resulting in reduced bone formation and an osteopenic phenotype *in vivo* (Smerdel-Ramoya et al., 2008). Interestingly *Ctgf* was upregulated following the ablation of *Creld2* in osteoblasts and therefore was differentially expressed between *Creld2* knockout osteoblasts and *Creld2* knockout chondrocytes. *Grem1* encoding gremlin 1 (GREM1), a second protein found to antagonise BMP2, BMP4, BMP7 and WNT signalling, was upregulated in knockout osteoblasts (Gazzerro et al., 2005). Studies have shown that overexpression of GREM1 results in severe osteopenia as a result of decreased bone formation due to a reduction in the number of osteoblasts (Gazzerro et al., 2005). Additionally *Fbn2* encoding the matrix structural protein fibrilin-2 (FBN2) was downregulated in knockout mice and the loss of FBN2 has been shown to impair osteoblast maturation and stimulate osteoclastogenesis via the upregulation of RANKL by modulating TGFβ and BMP signalling (Nistala et al., 2010a, Nistala et al., 2010b). Based on these findings, the dysregulation of *Ctgf, Grem1* and *Fbn2* outlined in this chapter may disrupt important signalling pathways involved in osteoblast maturation and therefore could result in the osteopenic phenotype of *Creld2*$^{Bone\Delta Ex3\text{-}5}$ mice.

Several genes that potentially contradict the hypothesis that CRELD2 plays a role in promoting osteoblast differentiation and maturation were differentially expressed in *Creld2* knockout osteoblasts. For example WNT11 that has been shown to promote osteoblast maturation was upregulated following the ablation of *Creld2* (Friedman et al., 2009).

This is the first study to outline an important role for CRELD2 in bone homeostasis and the data presented here suggest a novel and important bone anabolic role for CRELD2, promoting osteoblast differentiation and maturation and indirectly inhibiting osteoclast differentiation and activity by downregulating the expression and secretion of pro-osteoclastogenic cytokines.

Implications on osteoblasts from investigating the role of CRELD2 in chondrocytes

To understand how this putative PDI regulates osteoblast differentiation and maturation, the putative binding partners of CRELD2 in osteoblasts need to be identified by mass spectrometry as performed in chondrocyte-like cells. It can be however hypothesised that CRELD2 plays analogous functions in different mesenchymal cell types suggesting that CRELD2 may potentially involved in the trafficking of LRP1 in osteoblasts.

Studies to date have revealed that LRP1 is highly expressed in osteoblasts where it performs anabolic, mitogenic functions (Grey et al., 2004, Niemeier et al., 2005). For example LRP1 has been shown to act as a mitogenic receptor for the multifunctional protein lactoferrin that positively regulates osteoblast activity (Cornish et al., 2004, Grey et al., 2004, Zhang et al., 2014).

The hypothesis presented in Chapter 5 states that following the ablation of CRELD2, LRP1 trafficking is impaired. Furthermore, the expression of *Ctgf* is reduced in chondrocytes, but upregulated in osteoblasts following the ablation of *Creld2*. Interestingly, studies have shown that *Ctgf* is upregulated by WNT signalling stimulated by WNT3A, a WNT that has been shown to interact with FZD1 (Luo et al., 2004). Therefore, if canonical WNT signalling induced by WNT3A was upregulated due to the impaired sequestering of FZD1 receptor by LRP1, the expression of *Ctgf* would be upregulated. Moreover, *Ctgf* is highly expressed in early osteoblast differentiation but is downregulated as differentiation progresses and therefore its expression must be tightly controlled for normal osteoblast differentiation (Luo et al., 2004). Furthermore, the overexpression of *Ctgf* impairs osteoblast differentiation, maturation and activity (Smerdel-Ramoya et al., 2008). This therefore hypothesises that the impaired trafficking of LRP1 could potentially result in increased WNT1/WNT3A signalling leading to the upregulation of *Ctgf* expression and the impairment of osteoblast differentiation and maturation.

The work presented here therefore suggests a novel hypothesis for the role of *Creld2* in osteoblasts involved in the folding and trafficking of the LRP1 receptor. Although this indicates a novel and important role for CRELD2 in promoting osteoblast differentiation and maturation and subsequently bone formation, further studies are required to verify this hypothesis.

Summary

This is the first ever study to deep-phenotype a bone specific knockout of *Creld2* in which *Creld2* was deleted in mature osteoblasts. The data presented here outlines a novel and important role for CRELD2 in bone. Phenotypic analysis of $Creld2^{Bone\Delta Ex3\text{-}5}$ mice revealed that knockout mice are characterised by an osteopenic phenotype. Mice display a reduction in bone apposition due to a decrease in the number of osteoblasts and mineralising surface. Moreover, osteoclastogenesis is promoted following the targeted ablation of *Creld2* in mature osteoblasts as outlined by an increase in the number of osteoclasts correlating with an upregulation and secretion of pro-osteoclastogenic cytokines (Figure 69).

The data presented in this thesis suggest a new role for CRELD2 in regulating bone homeostasis, by linking the activities of osteoblasts and osteoclasts. My data indicates that CRELD2 promotes osteoblast differentiation, maturation and bone formation while inhibiting osteoclastogenesis outlining an anabolic role for CRELD2 in bone. This opens up a series of questions regarding the role of CRELD2 in osteoblasts. This thesis has identified a novel role for CRELD2 in osteoblasts. However, in order to identify the specific role of CRELD2 in stimulating osteoblast differentiation and activity, additional studies are required to determine the binding partners of CRELD2 in osteoblasts as performed in chondrocyte-like cells.

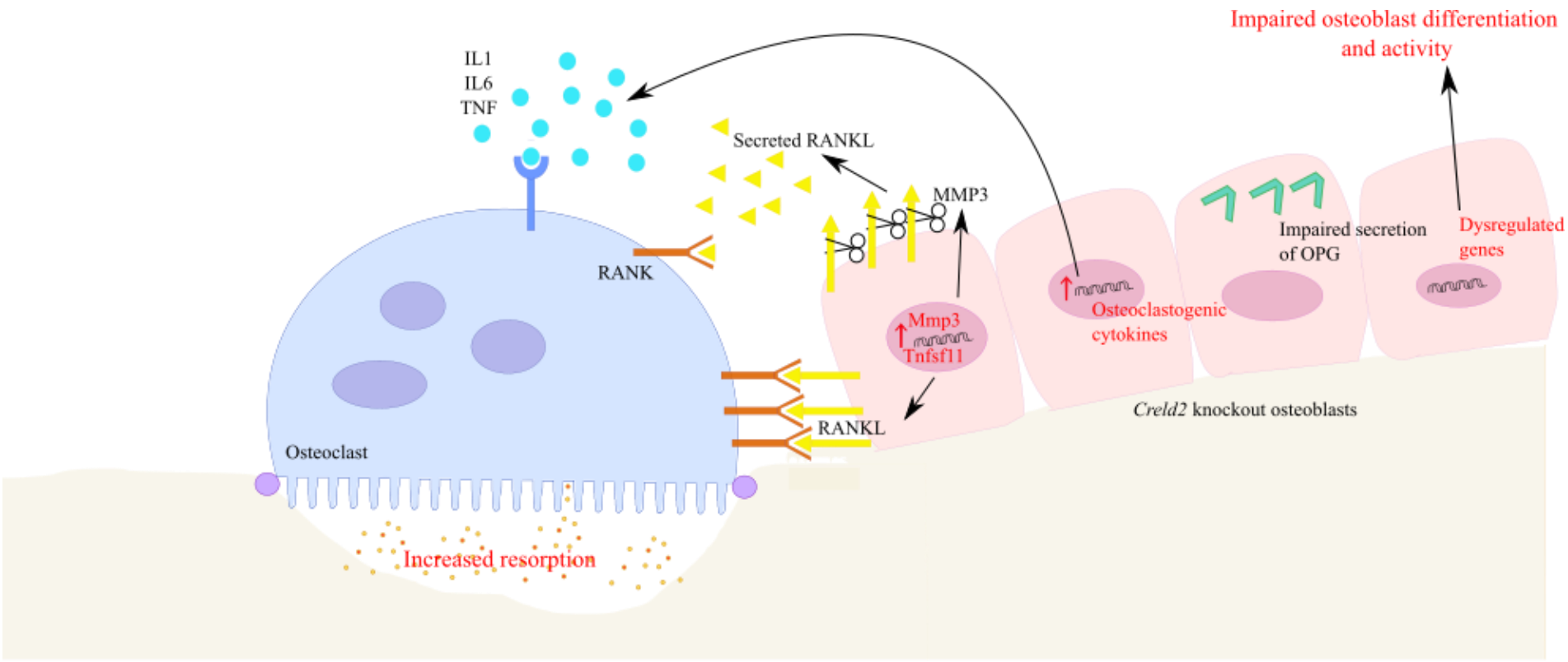

Figure 69. **The effect of the ablation of *Creld2* in osteoblasts on bone homeostasis.**

Studies indicate that CRELD2 plays an anabolic role in bone as the lack of *Creld2* in mature osteoblasts results in impaired osteoblast differentiation and activity. Additionally, the expression of pro-osteoclastogenic cytokines, including IL1, IL6, TNF and RANKL were upregulated following th knockout of *Creld2* in osetoblasts. Interestingly, the expression of *Mmp3* was upregulated, resulting in increased cleavage of RANKL from the membrane. The levels of OPG secretion were reduced in *Creld2* knockout osteoblasts indicating CRELD2 plays a role in folding and trafficking OPG. Together these findings resulted in impaired osteoblast activity and increased osteoclastogenesis and bone resorption.

Chapter 7. Discussion

Chapter 7. Discussion

7.1 A role for CRELD2 in chondrocyte/osteoblast differentiation

Creld2 is a novel ER stress-inducible gene expressed in mouse embryonic skeletal tissues. Studies by Hartley *et al.* have previously identified *Creld2* as an ER stress-inducible protein involved in the pathology of skeletal dysplasia due to its up regulation in a mouse model of MED and MCDS (Hartley et al., 2013). In addition, a novel role has been postulated for CRELD2 in promoting osteogenic differentiation *in vitro* (Zhang et al., 2013b). Despite several roles proposed for CRELD2 in protein folding and trafficking *in vitro*, the precise function of CRELD2 is largely unknown and no transgenic mouse models have been used to study its role *in vivo* (Ortiz et al., 2005, Oh-hashi et al., 2009).

The purpose of this study was therefore to investigate the role of CRELD2 in cartilage and bone using *in vivo* transgenic mouse models. The work presented here describes the first in-depth study of*Creld2* transgenic mouse models and identified a novel role and important for CRELD2 in chondrocytes and osteoblasts *in vivo*.

Analysis of the skeletal phenotype of *Creld2* cartilage-specific knockout mice revealed that knockout mice displayed a chondrodysplasia-like phenotype as a result of an abnormal growth plate with altered chondrocyte morphology. The lengths of the proliferative and hypertrophic zones were reduced in knockout mice and flattened chondrocytes that appeared to have the phenotype of proliferative chondrocytes were found in the hypertrophic zone of knockout growth plates. Additionally chondrocytes were retained within the bone scaffold. The results presented in this thesis suggested a potential role for CRELD2 in chondrocyte differentiation and maturation and the lack of *Creld2* results in a delay of differentiation along the whole axis. This hypothesis was further supported by transcriptomic analysis revealed several dysregulated genes in *Creld2* cartilage-specific knockout mice function to inhibit chondrocyte differentiation, proliferation and maturation. Recent studies have outlined an alternative fate of hypertrophic chondrocytes in which they transdifferentiate into osteoblasts. In fact studies have shown that up to 60 % of osteoblasts are derived from terminal growth plate chondrocytes (Zhou et al., 2014). Osteoblast numbers were reduced in *Creld2* cartilage-specific knockout mice and could therefore be a result of the delayed

chondrocyte differentiation and maturation resulting in delayed terminal transdifferentiation of chondrocytes into osteoblasts.

Analysis of the skeletal phenotype of *Creld2* bone-specific knockout mice revealed that knockout mice displayed an osteopenic phenotype characterised by low bone density and altered trabecular architecture. This study reveals for the first time a potential role for CRELD2 in bone formation since knockout mice displayed a reduction in bone apposition due to a decrease in the number of osteoblasts and mineralising surface and therefore suggested there was an impairment in osteoblast maturation and activity in knockout mice. This hypothesis was further supported by transcriptomic analysis, which revealed several dysregulated genes in *Creld2* bone-specific knockout mice that function to inhibit osteoblast recruitment, differentiation, proliferation and maturation. Additionally, osteoclastogenesis was promoted following the targeted ablation of *Creld2* in mature osteoblasts as outlined by an increase in the number of osteoclast correlating with an up regulation of pro-osteoclastogenic cytokines. The work presented here therefore outlined a potential novel bone anabolic effect of CRELD2, promoting the maturation of osteoblasts and inhibiting osteoclastogenesis by promoting OPG folding and inhibiting RANKL cleavage from the membrane.

As CRELD2 contains a C-terminal REDL motif that has been postulated to function as a targeting motif sequence for ER retrieval, it would be interesting to speculate that it could result in retrieving extracellular CRELD2 back to the ER (Hessler and Kreitman, 1997). Four other proteins have been identified to contain this C-terminal REDL motif. These include CPNY4 and MESDC2 that play roles in the folding, maturation and cell surface expression of the TLR4 and LRP4-6 receptors respectively that are then recycled back to the ER (Hsieh et al., 2003, Konno et al., 2006, Koduri and Blacklow, 2007, Hoshi et al., 2013).

Interestingly, in chondrocyte-like cells CRELD2 was found to bind LRP1, a receptor binds many ligands playing complex roles in various biological processes including modulating WNT signalling by binding FZD1 (Herz and Strickland, 2001, Zilberberg et al., 2004). The data presented in this thesis outlined a possible role for CRELD2 in controlling the differentiation and maturation of chondrocytes and osteoblasts. This was supported by the dysregulation of *Ctgf* expression in knockout chondrocytes and osteoblasts that would result in the inhibition of differentiation and

maturation of both cell types. It is therefore interesting to speculate that CRELD2 is involved in the folding and trafficking of LRP1 and LRP1 modulates differentiation and maturation of osteochondroprogenitor cells of the mesenchymal lineage in a cell-type specific manner potentially by modulating WNT signalling and *Ctgf* expression.

7.2 Future work

The findings from this thesis provide an insight into the role of CRELD2, a novel ER stress-inducible protein in cartilage and bone biology. Following the data presented here it can be hypothesised that CRELD2 plays a novel role in supporting chondrocyte and osteoblast differentiation and promoting skeletal growth and homeostasis.

This thesis has identified that the ablation of *Creld2* has an impact on chondrocyte and osteoblast integrity and activity and enhances the understanding of this novel molecular chaperone. The hypothesised mechanism of action of CRELD2 described here is based on the skeletal pathology of knockout mice, gene expression analysis and the prediction of CRELD2 binding partners. Therefore, further studies are needed to validate this hypothesis.

The work presented here provides a framework for future research and future studies are required to confirm:

1. The role of CRELD2 in chondrocyte/osteoblast differentiation and maturation.
    - In order to confirm the hypothesis that the ablation of *Creld2* in chondrocytes results in a delay in chondrocyte maturation *In situ* hybridisation can be performed to analyse the expression of markers of the proliferative and hypertrophic zones.

    - A different mouse model would be required to study the effects of *Creld2* in osteoblast differentiation and maturation as the mouse used in this study had a targeted deletion of *Creld2* in mature osteoblasts. It would therefore be beneficial to cross mice bearing the conditional *Creld2* allele onto mice either expressing *Osx-Cre* to knock *Creld2* out in immature osteoblasts or *Paired Related Homeobox 1* (*Prx)-Cre* to knock *Creld2* out in the developing limb mesenchyme in order to study both chondrocyte and osteoblast differentiation (Elefteriou and Yang, 2011).

2. The role of CRELD2 in chondrocyte terminal transdifferentiation into osteoblasts.
    - Lineage tracing studies using a reporter mouse strain such as the R26R mouse strain as performed by Park *et al.* are required to study the effects of

the ablation of CRELD2 on chondrocyte transdifferentiation (Park et al., 2015b).

3. The role of CRELD2 in the folding and trafficking of LRP1 in chondrocytes and osteoblasts.
    - The work presented in this thesis outlines that CRELD2 binds to LRP1 in chondrocytes. It can be postulated that CRELD2 plays analogous functions in different cell types and therefore suggests that CRELD2 binds LRP1 in osteoblasts however this must be validated prior to further experiments.

    - Co-expression of LRP1 and CRELD2 *in vitro* can be used to analyse the role of CRELD2 in the folding and trafficking of LRP1.

4. The role of LRP1 in skeletal development and homeostasis.
    - Since the global knockout of *Lrp1* is embryonic lethal, conditional knockout mouse models are required to study the role of *Lrp1* in cartilage and in bone. It would be interesting to knockout *Lrp1* expression in the developing limb mesenchyme using mice expressing the *Prx-Cre* transgene. Additionally *Lrp1* expression could be conditionally deleted in chondrocytes using mice expressing the *Col2a1-Cre* transgene and osteoblasts using mice expressing the *Osx-Cre* transgene to study the role of LRP1 in chondrocyte/osteoblast differentiation and maturation.

5. The extracellular role of CRELD2.
    - Studies have shown that exogenous MESDC2, a molecular chaperone for LRP5 and LRP6, also functions as a WNT inhibitor (Lin et al., 2011). It would therefore be interesting to study the effects of exogenous CRELD2 on differentiation and activity of chondrocytes and osteoblasts *in vitro*.

REFERENCES

ACOSTA-ALVEAR, D., ZHOU, Y., BLAIS, A., TSIKITIS, M., LENTS, N. H., ARIAS, C., LENNON, C. J., KLUGER, Y. & DYNLACHT, B. D. 2007. XBP1 controls diverse cell type- and condition-specific transcriptional regulatory networks. *Molecular Cell Biology,* 27**,** 53-66.

ADACHI, Y., YAMAMOTO, K., OKADA, T., YOSHIDA, H., HARADA, A. & MORI, K. 2008. ATF6 is a transcription factor specializing in the regulation of quality control proteins in the endoplasmic reticulum. *Cell Structure and Function,* 33**,** 75-89.

AEBI, M. 2013. N-linked protein glycosylation in the ER. *Biochimica et Biophysica Acta,* 1833**,** 2430-7.

AGAS, D., SABBIETI, M. G., MARCHETTI, L., XIAO, L. & HURLEY, M. M. 2013. FGF-2 enhances Runx-2/Smads nuclear localization in BMP-2 canonical signaling in osteoblasts. *Journal of Cellular Physiology,* 228**,** 2149-58.

AHMED, Y. A., TATARCZUCH, L., PAGEL, C. N., DAVIES, H. M., MIRAMS, M. & MACKIE, E. J. 2007. Physiological death of hypertrophic chondrocytes. *Osteoarthritis Cartilage,* 15**,** 575-86.

AIKAWA, T., SEGRE, G. V. & LEE, K. 2001. Fibroblast growth factor inhibits chondrocytic growth through induction of p21 and subsequent inactivation of cyclin E-Cdk2. *Journal of Biological Chemistry,* 276**,** 29347-52.

AIZAWA, T., KOKUBUN, S. & TANAKA, Y. 1997. Apoptosis and proliferation of growth plate chondrocytes in rabbits. *Journal of Bone and Joint Surgery British Volume,* 79**,** 483-6.

AKIYAMA, H., CHABOISSIER, M. C., MARTIN, J. F., SCHEDL, A. & DE CROMBRUGGHE, B. 2002. The transcription factor Sox9 has essential roles in successive steps of the chondrocyte differentiation pathway and is required for expression of Sox5 and Sox6. *Genes & Development,* 16**,** 2813-28.

AKIYAMA, H., LYONS, J. P., MORI-AKIYAMA, Y., YANG, X., ZHANG, R., ZHANG, Z., DENG, J. M., TAKETO, M. M., NAKAMURA, T., BEHRINGER, R. R., MCCREA, P. D. & DE CROMBRUGGHE, B. 2004. Interactions between Sox9 and β-catenin control chondrocyte differentiation. *Genes & Development,* 18**,** 1072-87.

ALANEN, H. I., WILLIAMSON, R. A., HOWARD, M. J., HATAHET, F. S., SALO, K. E., KAUPPILA, A., KELLOKUMPU, S. & RUDDOCK, L. W. 2006. ERp27, a new non-catalytic endoplasmic reticulum-located human protein disulfide isomerase family member, interacts with ERp57. *Journal of Biological Chemistry,* 281**,** 33727-38.

ALCANTARA-ORTIGOZA, M. A., DE RUBENS-FIGUEROA, J., REYNA-FABIAN, M. E., ESTANDIA-ORTEGA, B., GONZALEZ-DEL ANGEL, A., MOLINA-ALVAREZ, B., VELAZQUEZ-ARAGON, J. A., VILLAGOMEZ-MARTINEZ, S., PEREIRA-LOPEZ, G. I., MARTINEZ-CRUZ, V., ALVAREZ-GOMEZ, R. M. & DIAZ-GARCIA, L. 2015. Germline mutations in NKX2-5, GATA4, and CRELD1 are rare in a Mexican sample of Down syndrome patients with endocardial cushion and septal heart defects. *Pediatric Cardiology,* 36**,** 802-8.

ALDER, N. N., SHEN, Y., BRODSKY, J. L., HENDERSHOT, L. M. & JOHNSON, A. E. 2005. The molecular mechanisms underlying BiP-mediated gating of the Sec61 translocon of the endoplasmic reticulum. *Journal of Cell Biology,* 168**,** 389-99.

ALLISTON, T., CHOY, L., DUCY, P., KARSENTY, G. & DERYNCK, R. 2001. TGF-beta-induced repression of CBFA1 by Smad3 decreases cbfa1 and osteocalcin expression and inhibits osteoblast differentiation. *EMBO Journal,* 20**,** 2254-72.

AMIZUKA, N., WARSHAWSKY, H., HENDERSON, J. E., GOLTZMAN, D. & KARAPLIS, A. C. 1994. Parathyroid hormone-related peptide-depleted mice show abnormal epiphyseal cartilage development and altered endochondral bone formation. *Journal of Cell Biology,* 126**,** 1611-23.

ANDERSON, H. C. 2003. Matrix vesicles and calcification. *Current Rheumatology Reports,* 5**,** 222-6.

ANDRADE, A. C., NILSSON, O., BARNES, K. M. & BARON, J. 2007. Wnt gene expression in the post-natal growth plate: regulation with chondrocyte differentiation. *Bone,* 40**,** 1361-9.

AOKI, K., SAITO, H., ITZSTEIN, C., ISHIGURO, M., SHIBATA, T., BLANQUE, R., MIAN, A. H., TAKAHASHI, M., SUZUKI, Y., YOSHIMATSU, M., YAMAGUCHI, A., DEPREZ, P., MOLLAT, P., MURALI, R., OHYA, K., HORNE, W. C. & BARON, R. 2006. A TNF receptor loop peptide mimic blocks RANK ligand–induced signaling, bone resorption, and bone loss. *Journal of Clinical Investigation,* 116**,** 1525-34.

ARMSTRONG, L. C., BJÖRKBLOM, B., HANKENSON, K. D., SIADAK, A. W., STILES, C. E. & BORNSTEIN, P. 2002. Thrombospondin 2 Inhibits Microvascular Endothelial Cell Proliferation by a Caspase-independent Mechanism. *Molecular Biology of the Cell,* 13**,** 1893-1905.

ARNOLD, M. A., KIM, Y., CZUBRYT, M. P., PHAN, D., MCANALLY, J., QI, X., SHELTON, J. M., RICHARDSON, J. A., BASSEL-DUBY, R. & OLSON, E. N. 2007. MEF2C transcription factor controls chondrocyte hypertrophy and bone development. *Developmental Cell,* 12**,** 377-89.

ARTAVANIS-TSAKONAS, S., RAND, M. D. & LAKE, R. J. 1999. Notch signaling: cell fate control and signal integration in development. *Science,* 284**,** 770-6.

ASAGIRI, M., SATO, K., USAMI, T., OCHI, S., NISHINA, H., YOSHIDA, H., MORITA, I., WAGNER, E. F., MAK, T. W., SERFLING, E. & TAKAYANAGI, H. 2005. Autoamplification of NFATc1 expression determines its essential role in bone homeostasis. *Journal of Experimental Medicine,* 202**,** 1261-9.

ASZODI, A., HUNZIKER, E. B., BRAKEBUSCH, C. & FASSLER, R. 2003. Beta1 integrins regulate chondrocyte rotation, G1 progression, and cytokinesis. *Genes & Development,* 17**,** 2465-79.

ATTUR, M., BEN-ARTZI, A., YANG, Q., AL-MUSSAWIR, H. E., WORMAN, H. J., PALMER, G. & ABRAMSON, S. B. 2012. Perturbation of nuclear lamin A causes cell death in chondrocytes. *Arthritis & Rheumatism,* 64**,** 1940-1949.

AZUMA, Y., KAJI, K., KATOGI, R., TAKESHITA, S. & KUDO, A. 2000. Tumor necrosis factor-alpha induces differentiation of and bone resorption by osteoclasts. *Journal of Biological Chemistry,* 275**,** 4858-64.

BABIJ, P., ZHAO, W., SMALL, C., KHARODE, Y., YAWORSKY, P. J., BOUXSEIN, M. L., REDDY, P. S., BODINE, P. V., ROBINSON, J. A., BHAT, B., MARZOLF, J., MORAN, R. A. & BEX, F. 2003. High bone mass in mice expressing a mutant LRP5 gene. *Journal of Bone and Mineral Research,* 18**,** 960-74.

BAFFI, M. O., SLATTERY, E., SOHN, P., MOSES, H. L., CHYTIL, A. & SERRA, R. 2004. Conditional deletion of the TGF-beta type II receptor in Col2a expressing cells results in defects in the axial skeleton without alterations in chondrocyte differentiation or embryonic development of long bones. *Developmental Biology,* 276**,** 124-42.

BAI, S., KOPAN, R., ZOU, W., HILTON, M. J., ONG, C. T., LONG, F., ROSS, F. P. & TEITELBAUM, S. L. 2008. NOTCH1 regulates osteoclastogenesis directly in osteoclast precursors and indirectly via osteoblast lineage cells. *Journal of Biological Chemistry,* 283**,** 6509-18.

BAKKER, A. D. & KLEIN-NULEND, J. 2012. Osteoblast Isolation from Murine Calvaria and Long Bones. *In:* HELFRICH, M. H. & RALSTON, S. H. (eds.) *Bone Research Protocols.* Totowa, NJ: Humana Press.

BANDYOPADHYAY, A., TSUJI, K., COX, K., HARFE, B. D., ROSEN, V. & TABIN, C. J. 2006. Genetic Analysis of the Roles of BMP2, BMP4, and BMP7 in Limb Patterning and Skeletogenesis. *PLoS Genetics,* 2.

BATEMAN, J. F., WILSON, R., FREDDI, S., LAMANDE, S. R. & SAVARIRAYAN, R. 2005. Mutations of COL10A1 in Schmid metaphyseal chondrodysplasia. *Human Mutation,* 25**,** 525-34.

BELL, D. M., LEUNG, K. K., WHEATLEY, S. C., NG, L. J., ZHOU, S., LING, K. W., SHAM, M. H., KOOPMAN, P., TAM, P. P. & CHEAH, K. S. 1997. SOX9 directly regulates the type-II collagen gene. *Nature Genetics,* 16**,** 174-8.

BENNETT, C. N., OUYANG, H., MA, Y. L., ZENG, Q., GERIN, I., SOUSA, K. M., LANE, T. F., KRISHNAN, V., HANKENSON, K. D. & MACDOUGALD, O. A. 2007. Wnt10b increases postnatal bone formation by enhancing osteoblast differentiation. *Journal of Bone and Mineral Research,* 22**,** 1924-32.

BERNALES, S., SCHUCK, S. & WALTER, P. 2007. ER-phagy: selective autophagy of the endoplasmic reticulum. *Autophagy,* 3**,** 285-7.

BERTOLINI, D. R., NEDWIN, G. E., BRINGMAN, T. S., SMITH, D. D. & MUNDY, G. R. 1986. Stimulation of bone resorption and inhibition of bone formation in vitro by human tumour necrosis factors. *Nature,* 319**,** 516-8.

BERTOLOTTI, A., WANG, X., NOVOA, I., JUNGREIS, R., SCHLESSINGER, K., CHO, J. H., WEST, A. B. & RON, D. 2001. Increased sensitivity to dextran sodium sulfate colitis in IRE1beta-deficient mice. *Journal of Clinical Investigation,* 107**,** 585-93.

BIALEK, P., KERN, B., YANG, X., SCHROCK, M., SOSIC, D., HONG, N., WU, H., YU, K., ORNITZ, D. M., OLSON, E. N., JUSTICE, M. J. & KARSENTY, G. 2004. A twist code determines the onset of osteoblast differentiation. *Developmental Cell,* 6**,** 423-35.

BIRNBAUM, R. S., BOWSHER, R. R. & WIREN, K. M. 1995. Changes in IGF-I and -II expression and secretion during the proliferation and differentiation of normal rat osteoblasts. *Journal of Endocrinology,* 144**,** 251-9.

BLAIR, H. C., TEITELBAUM, S. L., GHISELLI, R. & GLUCK, S. 1989. Osteoclastic bone resorption by a polarized vacuolar proton pump. *Science,* 245**,** 855-7.

BLUTEAU, G., JULIEN, M., MAGNE, D., MALLEIN-GERIN, F., WEISS, P., DACULSI, G. & GUICHEUX, J. 2007. VEGF and VEGF receptors are differentially expressed in chondrocytes. *Bone,* 40**,** 568-76.

BONEWALD, L. F. 2006. Mechanosensation and Transduction in Osteocytes. *Bonekey Osteovision,* 3**,** 7-15.

BONEWALD, L. F. 2011. The amazing osteocyte. *Journal of Bone and Mineral Research,* 26**,** 229-38.

BOUKER, K. B., SKAAR, T. C., RIGGINS, R. B., HARBURGER, D. S., FERNANDEZ, D. R., ZWART, A., WANG, A. & CLARKE, R. 2005. Interferon regulatory factor-1 (IRF-1) exhibits tumor suppressor activities in breast cancer associated with caspase activation and induction of apoptosis. *Carcinogenesis,* 26**,** 1527-35.

BOULEFTOUR, W., BOUDIFFA, M., WADE-GUEYE, N. M., BOUET, G., CARDELLI, M., LAROCHE, N., VANDEN-BOSSCHE, A., THOMAS, M.,

BONNELYE, E., AUBIN, J. E., VICO, L., LAFAGE-PROUST, M. H. & MALAVAL, L. 2014. Skeletal development of mice lacking bone sialoprotein (BSP)--impairment of long bone growth and progressive establishment of high trabecular bone mass. *PLoS ONE,* 9**,** e95144.

BOYCE, B. F. & XING, L. 2007. Biology of RANK, RANKL, and osteoprotegerin. *Arthritis Research & Therapy,* 9**,** S1.

BOYLE, W. J., SIMONET, W. S. & LACEY, D. L. 2003. Osteoclast differentiation and activation. *Nature,* 423**,** 337-42.

BRAAKMAN, I. & HEBERT, D. N. 2013. Protein folding in the endoplasmic reticulum. *Cold Spring Harbor Perspectives in Biology,* 5**,** a013201.

BRIGGS, M. D., HOFFMAN, S. M., KING, L. M., OLSEN, A. S., MOHRENWEISER, H., LEROY, J. G., MORTIER, G. R., RIMOIN, D. L., LACHMAN, R. S., GAINES, E. S. & ET AL. 1995. Pseudoachondroplasia and multiple epiphyseal dysplasia due to mutations in the cartilage oligomeric matrix protein gene. *Nature Genetics,* 10**,** 330-6.

BRIGHTON, C. T., SUGIOKA, Y. & HUNT, R. M. 1973. Cytoplasmic structures of epiphyseal plate chondrocytes. Quantitative evaluation using electron micrographs of rat costochondral junctions with special reference to the fate of hypertrophic cells. *Journal of Bone and Joint Surgery,* 55**,** 771-84.

BRODSKY, J. L. 2007. The protective and destructive roles played by molecular chaperones during ERAD (endoplasmic-reticulum-associated degradation). *Biochemical Journal,* 404**,** 353-63.

BROWN, R. A. & MCFARLAND, C. D. 1992. Regulation of growth plate cartilage degradation in vitro: effects of calcification and a low molecular weight angiogenic factor (ESAF). *Bone & Mineral Research,* 17**,** 49-57.

BRUNET, L. J., MCMAHON, J. A., MCMAHON, A. P. & HARLAND, R. M. 1998. Noggin, cartilage morphogenesis, and joint formation in the mammalian skeleton. *Science,* 280**,** 1455-7.

BUCAY, N., SAROSI, I., DUNSTAN, C. R., MORONY, S., TARPLEY, J., CAPPARELLI, C., SCULLY, S., TAN, H. L., XU, W., LACEY, D. L., BOYLE, W. J. & SIMONET, W. S. 1998. osteoprotegerin-deficient mice develop early onset osteoporosis and arterial calcification. *Genes & Development,* 12**,** 1260-8.

BUCHTOVA, M., ORALOVA, V., AKLIAN, A., MASEK, J., VESELA, I., OUYANG, Z., OBADALOVA, T., KONECNA, Z., SPOUSTOVA, T., POSPISILOVA, T., MATULA, P., VARECHA, M., BALEK, L., GUDERNOVA, I., JELINKOVA, I., DURAN, I., CERVENKOVA, I., MURAKAMI, S., KOZUBIK, A., DVORAK, P., BRYJA, V. & KREJCI, P. 2015. Fibroblast growth factor and canonical WNT/beta-catenin signaling cooperate in suppression of chondrocyte differentiation in experimental models of FGFR signaling in cartilage. *Biochimica et Biophysica Acta,* 1852**,** 839-50.

BURDAN, F., SZUMILO, J., KOROBOWICZ, A., FAROOQUEE, R., PATEL, S., PATEL, A., DAVE, A., SZUMILO, M., SOLECKI, M., KLEPACZ, R. & DUDKA, J. 2009. Morphology and physiology of the epiphyseal growth plate. *Folia Histochemica Et Cytobiologica,* 47**,** 5-16.

BURSTONE, M. S. 1959. Histochemical demonstration of acid phosphatase activity in osteoclasts. *Journal of Histochemistry & Cytochemistry,* 7**,** 39-41.

BUXTON, P., EDWARDS, C., ARCHER, C. W. & FRANCIS-WEST, P. 2001. Growth/differentiation factor-5 (GDF-5) and skeletal development. *Journal of Bone and Joint Surgery,* 83-A Suppl 1**,** S23-30.

CADIGAN, K. M. & WATERMAN, M. L. 2012. TCF/LEFs and Wnt signaling in the nucleus. *Cold Spring Harbor Perspectives in Biology,* 4.

CAETANO-LOPES, J., CANHAO, H. & FONSECA, J. E. 2007. Osteoblasts and bone formation. *Acta Reumatológica Portuguesa,* 32**,** 103-10.

CAI, H., WANG, C. C. & TSOU, C. L. 1994. Chaperone-like activity of protein disulfide isomerase in the refolding of a protein with no disulfide bonds. *Journal of Biological Chemistry,* 269**,** 24550-2.

CAMERON, T. L., GRESSHOFF, I. L., BELL, K. M., PIROG, K. A., SAMPURNO, L., HARTLEY, C. L., SANFORD, E. M., WILSON, R., ERMANN, J., BOOT-HANDFORD, R. P., GLIMCHER, L. H., BRIGGS, M. D. & BATEMAN, J. F. 2015. Cartilage-specific ablation of XBP1 signaling in mouse results in a chondrodysplasia characterized by reduced chondrocyte proliferation and delayed cartilage maturation and mineralization. *Osteoarthritis Cartilage,* 23**,** 661-70.

CANALIS, E. 1993. Insulin like growth factors and the local regulation of bone formation. *Bone,* 14**,** 273-6.

CANALIS, E. 2008. Notch Signaling in Osteoblasts. *Science Signaling,* 1**,** pe17-pe17.

CANALIS, E., PARKER, K., FENG, J. Q. & ZANOTTI, S. 2013. Osteoblast Lineage-Specific Effects of Notch Activation in the Skeleton. *Endocrinology,* 154**,** 623-34.

CAO, H., YU, S., YAO, Z., GALSON, D. L., JIANG, Y., ZHANG, X., FAN, J., LU, B., GUAN, Y., LUO, M., LAI, Y., ZHU, Y., KURIHARA, N., PATRENE, K., ROODMAN, G. D. & XIAO, G. 2010. Activating transcription factor 4 regulates osteoclast differentiation in mice. *Journal of Clinical Investigation,* 120**,** 2755-66.

CARMELIET, P., FERREIRA, V., BREIER, G., POLLEFEYT, S., KIECKENS, L., GERTSENSTEIN, M., FAHRIG, M., VANDENHOECK, A., HARPAL, K., EBERHARDT, C., DECLERCQ, C., PAWLING, J., MOONS, L., COLLEN, D., RISAU, W. & NAGY, A. 1996. Abnormal blood vessel development and lethality in embryos lacking a single VEGF allele. *Nature,* 380**,** 435-9.

CARO, L. G. & PALADE, G. E. 1964. PROTEIN SYNTHESIS, STORAGE, AND DISCHARGE IN THE PANCREATIC EXOCRINE CELL : An Autoradiographic Study. *The Journal of Cell Biology,* 20**,** 473-495.

CAWTHORN, W. P., BREE, A. J., YAO, Y., DU, B., HEMATI, N., MARTINEZ-SANTIBANEZ, G. & MACDOUGALD, O. A. 2012a. Wnt6, Wnt10a and Wnt10b inhibit adipogenesis and stimulate osteoblastogenesis through a beta-catenin-dependent mechanism. *Bone,* 50**,** 477-89.

CAWTHORN, W. P., BREE, A. J., YAO, Y., DU, B., HEMATI, N., MARTINEZ-SANTIBAÑEZ, G. & MACDOUGALD, O. A. 2012b. Wnt6, Wnt10a and Wnt10b inhibit adipogenesis and stimulate osteoblastogenesis through a β-catenin-dependent mechanism. *Bone,* 50**,** 477-89.

CHAKRABARTI, A., CHEN, A. W. & VARNER, J. D. 2011. A review of the mammalian unfolded protein response. *Biotechnology and Bioengineering,* 108**,** 2777-93.

CHANG, S.-F., CHANG, T.-K., PENG, H.-H., YEH, Y.-T., LEE, D.-Y., YEH, C.-R., ZHOU, J., CHENG, C.-K., CHANG, C. A. & CHIU, J.-J. 2009. BMP-4 Induction of Arrest and Differentiation of Osteoblast-Like Cells via p21(CIP1) and p27(KIP1) Regulation. *Molecular Endocrinology,* 23**,** 1827-1838.

CHAPMAN, K. L., MORTIER, G. R., CHAPMAN, K., LOUGHLIN, J., GRANT, M. E. & BRIGGS, M. D. 2001. Mutations in the region encoding the von Willebrand factor A domain of matrilin-3 are associated with multiple epiphyseal dysplasia. *Nature Genetics,* 28**,** 393-6.

CHEN, C. Y., MALCHUS, N. S., HEHN, B., STELZER, W., AVCI, D., LANGOSCH, D. & LEMBERG, M. K. 2014a. Signal peptide peptidase functions in ERAD to

cleave the unfolded protein response regulator XBP1u. *EMBO Journal,* 33**,** 2492-506.

CHEN, G., DENG, C. & LI, Y. P. 2012. TGF-β and BMP Signaling in Osteoblast Differentiation and Bone Formation. *International Journal of Biological Sciences,* 8**,** 272-88.

CHEN, H., GHORI-JAVED, F. Y., RASHID, H., ADHAMI, M. D., SERRA, R., GUTIERREZ, S. E. & JAVED, A. 2014b. Runx2 Regulates Endochondral Ossification through Control of Chondrocyte Proliferation and Differentiation. *Journal of Bone and Mineral Research,* 29**,** 2653-65.

CHEN, L., LI, C., QIAO, W., XU, X. & DENG, C. 2001. A Ser(365)-->Cys mutation of fibroblast growth factor receptor 3 in mouse downregulates Ihh/PTHrP signals and causes severe achondroplasia. *Human Molecular Genetics,* 10**,** 457-65.

CHEN, M., ZHU, M., AWAD, H., LI, T. F., SHEU, T. J., BOYCE, B. F., CHEN, D. & O'KEEFE, R. J. 2008. Inhibition of β-catenin signaling causes defects in postnatal cartilage development. *Journal of Cell Science,* 121**,** 1455-65.

CHEN, X., ILIOPOULOS, D., ZHANG, Q., TANG, Q., GREENBLATT, M. B., HATZIAPOSTOLOU, M., LIM, E., TAM, W. L., NI, M., CHEN, Y., MAI, J., SHEN, H., HU, D. Z., ADORO, S., HU, B., SONG, M., TAN, C., LANDIS, M. D., FERRARI, M., SHIN, S. J., BROWN, M., CHANG, J. C., LIU, X. S. & GLIMCHER, L. H. 2014c. XBP1 promotes triple-negative breast cancer by controlling the HIF1alpha pathway. *Nature,* 508**,** 103-7.

CHENG, S., XING, W., ZHOU, X. & MOHAN, S. 2013. Haploinsufficiency of osterix in chondrocytes impairs skeletal growth in mice. *Physiological Genomics,* 45**,** 917-23.

CHIBA, S. 2006. Notch signaling in stem cell systems. *Stem Cells,* 24**,** 2437-47.

CHIVERS, P. T., LABOISSIERE, M. C. & RAINES, R. T. 1996. The CXXC motif: imperatives for the formation of native disulfide bonds in the cell. *EMBO Journal,* 15**,** 2659-67.

CHOI, K. Y., KIM, H. J., LEE, M. H., KWON, T. G., NAH, H. D., FURUICHI, T., KOMORI, T., NAM, S. H., KIM, Y. J., KIM, H. J. & RYOO, H. M. 2005. Runx2 regulates FGF2-induced Bmp2 expression during cranial bone development. *Developmenal Dynamics,* 233**,** 115-21.

CHOI, S. C., KIM, S. J., CHOI, J. H., PARK, C. Y., SHIM, W. J. & LIM, D. S. 2008. Fibroblast growth factor-2 and -4 promote the proliferation of bone marrow mesenchymal stem cells by the activation of the PI3K-Akt and ERK1/2 signaling pathways. *Stem Cells and Development,* 17**,** 725-36.

CHUNG, K. T., SHEN, Y. & HENDERSHOT, L. M. 2002. BAP, a mammalian BiP-associated protein, is a nucleotide exchange factor that regulates the ATPase activity of BiP. *Journal of Biological Chemistry,* 277**,** 47557-63.

CHURCH, V., NOHNO, T., LINKER, C., MARCELLE, C. & FRANCIS-WEST, P. 2002. Wnt regulation of chondrocyte differentiation. *Journal of Cell Science,* 115**,** 4809-18.

CLAPHAM, D. E. 2007. Calcium signaling. *Cell,* 131**,** 1047-58.

CLARKE, B. 2008. Normal Bone Anatomy and Physiology. *Clinical Journal of the American Society of Nephrology,* 3**,** S131-9.

COCCIA, E. M., DEL RUSSO, N., STELLACCI, E., ORSATTI, R., BENEDETTI, E., MARZIALI, G., HISCOTT, J. & BATTISTINI, A. 1999. Activation and repression of the 2-5A synthetase and p21 gene promoters by IRF-1 and IRF-2. *Oncogene,* 18**,** 2129-37.

COE, H., JUNG, J., GROENENDYK, J., PRINS, D. & MICHALAK, M. 2010. ERp57 modulates STAT3 signaling from the lumen of the endoplasmic reticulum. *Journal of Biological Chemistry,* 285**,** 6725-38.

COLVIN, J. S., WHITE, A. C., PRATT, S. J. & ORNITZ, D. M. 2001. Lung hypoplasia and neonatal death in Fgf9-null mice identify this gene as an essential regulator of lung mesenchyme. *Development,* 128**,** 2095-106.

CORBIT, K. C., AANSTAD, P., SINGLA, V., NORMAN, A. R., STAINIER, D. Y. & REITER, J. F. 2005. Vertebrate Smoothened functions at the primary cilium. *Nature,* 437**,** 1018-21.

CORNISH, J., CALLON, K. E., NAOT, D., PALMANO, K. P., BANOVIC, T., BAVA, U., WATSON, M., LIN, J. M., TONG, P. C., CHEN, Q., CHAN, V. A., REID, H. E., FAZZALARI, N., BAKER, H. M., BAKER, E. N., HAGGARTY, N. W., GREY, A. B. & REID, I. R. 2004. Lactoferrin is a potent regulator of bone cell activity and increases bone formation in vivo. *Endocrinology,* 145**,** 4366-74.

COTTERILL, S. L., JACKSON, G. C., LEIGHTON, M. P., WAGENER, R., MAKITIE, O., COLE, W. G. & BRIGGS, M. D. 2005. Multiple epiphyseal dysplasia mutations in MATN3 cause misfolding of the A-domain and prevent secretion of mutant matrilin-3. *Human Mutation,* 26**,** 557-65.

DALUISKI, A., ENGSTRAND, T., BAHAMONDE, M. E., GAMER, L. W., AGIUS, E., STEVENSON, S. L., COX, K., ROSEN, V. & LYONS, K. M. 2001. Bone morphogenetic protein-3 is a negative regulator of bone density. *Nature Genetics,* 27**,** 84-8.

DAY, T. F., GUO, X., GARRETT-BEAL, L. & YANG, Y. 2005. Wnt/beta-catenin signaling in mesenchymal progenitors controls osteoblast and chondrocyte differentiation during vertebrate skeletogenesis. *Developmental Cell,* 8**,** 739-50.

DE ANDREA, C. E., WIWEGER, M., PRINS, F., BOVEE, J. V., ROMEO, S. & HOGENDOORN, P. C. 2010. Primary cilia organization reflects polarity in the growth plate and implies loss of polarity and mosaicism in osteochondroma. *Laboratory Investigation,* 90**,** 1091-101.

DE LUCA, F., BARNES, K. M., UYEDA, J. A., DE-LEVI, S., ABAD, V., PALESE, T., MERICQ, V. & BARON, J. 2001. Regulation of growth plate chondrogenesis by bone morphogenetic protein-2. *Endocrinology,* 142**,** 430-6.

DEBIAIS, F., HOTT, M., GRAULET, A. M. & MARIE, P. J. 1998. The effects of fibroblast growth factor-2 on human neonatal calvaria osteoblastic cells are differentiation stage specific. *Journal of Bone and Mineral Research,* 13**,** 645-54.

DELEZOIDE, A. L., BENOIST-LASSELIN, C., LEGEAI-MALLET, L., LE MERRER, M., MUNNICH, A., VEKEMANS, M. & BONAVENTURE, J. 1998. Spatio-temporal expression of FGFR 1, 2 and 3 genes during human embryo-fetal ossification. *Mechanisms of Development,* 77**,** 19-30.

DEREGOWSKI, V., GAZZERRO, E., PRIEST, L., RYDZIEL, S. & CANALIS, E. 2006. Notch 1 overexpression inhibits osteoblastogenesis by suppressing Wnt/beta-catenin but not bone morphogenetic protein signaling. *Journal of Biological Chemistry,* 281**,** 6203-10.

DESCALZI CANCEDDA, F., GENTILI, C., MANDUCA, P. & CANCEDDA, R. 1992. Hypertrophic chondrocytes undergo further differentiation in culture. *Journal of Cell Biology,* 117**,** 427-35.

DEVLIN, R. D., DU, Z., PEREIRA, R. C., KIMBLE, R. B., ECONOMIDES, A. N., JORGETTI, V. & CANALIS, E. 2003. Skeletal overexpression of noggin results in osteopenia and reduced bone formation. *Endocrinology,* 144**,** 1972-8.

DI MAGGIO, N., MEHRKENS, A., PAPADIMITROPOULOS, A., SCHAEREN, S., HEBERER, M., BANFI, A. & MARTIN, I. 2012. Fibroblast growth factor-2 maintains a niche-dependent population of self-renewing highly potent non-adherent mesenchymal progenitors through FGFR2c. *Stem Cells,* 30**,** 1455-64.

DON, M. M., ABLETT, G., BISHOP, C. J., BUNDESEN, P. G., DONALD, K. J., SEARLE, J. & KERR, J. F. 1977. Death of cells by apoptosis following attachment of specifically allergized lymphocytes in vitro. *The Australian Journal of Experimental Biology and Medical Science,* 55**,** 407-17.

DONG, Y. F., SOUNG DO, Y., SCHWARZ, E. M., O'KEEFE, R. J. & DRISSI, H. 2006. Wnt induction of chondrocyte hypertrophy through the Runx2 transcription factor. *Journal of Cellular Physiology,* 208**,** 77-86.

DRISSI, M. H., LI, X., SHEU, T. J., ZUSCIK, M. J., SCHWARZ, E. M., PUZAS, J. E., ROSIER, R. N. & O'KEEFE, R. J. 2003. Runx2/Cbfa1 stimulation by retinoic acid is potentiated by BMP2 signaling through interaction with Smad1 on the collagen X promoter in chondrocytes. *Journal of Cellular Biochemistry,* 90**,** 1287-98.

DUCY, P., ZHANG, R., GEOFFROY, V., RIDALL, A. L. & KARSENTY, G. 1997. Osf2/Cbfa1: a transcriptional activator of osteoblast differentiation. *Cell,* 89**,** 747-54.

DUDLEY, A. T. & ROBERTSON, E. J. 1997. Overlapping expression domains of bone morphogenetic protein family members potentially account for limited tissue defects in BMP7 deficient embryos. *Developmenal Dynamics,* 208**,** 349-62.

DUFOUR, C., GUENOU, H., KAABECHE, K., BOUVARD, D., SANJAY, A. & MARIE, P. J. 2008. FGFR2-Cbl interaction in lipid rafts triggers attenuation of PI3K/Akt signaling and osteoblast survival. *Bone,* 42**,** 1032-9.

DUNWOODIE, S. L., CLEMENTS, M., SPARROW, D. B., SA, X., CONLON, R. A. & BEDDINGTON, R. S. 2002. Axial skeletal defects caused by mutation in the spondylocostal dysplasia/pudgy gene Dll3 are associated with disruption of the segmentation clock within the presomitic mesoderm. *Development,* 129**,** 1795-806.

DUROSE, J. B., TAM, A. B. & NIWA, M. 2006. Intrinsic capacities of molecular sensors of the unfolded protein response to sense alternate forms of endoplasmic reticulum stress. *Molecular Biology of the Cell,* 17**,** 3095-107.

DVORAK, H. F., BROWN, L. F., DETMAR, M. & DVORAK, A. M. 1995. Vascular permeability factor/vascular endothelial growth factor, microvascular hyperpermeability, and angiogenesis. *American Journal of Pathology,* 146**,** 1029-39.

DWEK, J. R. 2010. The periosteum: what is it, where is it, and what mimics it in its absence? *Skeletal Radiology,* 39**,** 319-23.

DY, P., WANG, W., BHATTARAM, P., WANG, Q., WANG, L., BALLOCK, R. T. & LEFEBVRE, V. 2012. Sox9 Directs Hypertrophic Maturation and Blocks Osteoblast Differentiation of Growth Plate Chondrocytes. *Developmental Cell,* 22**,** 597-609.

EISEN, A. & REYNOLDS, G. T. 1985. Source and sinks for the calcium released during fertilization of single sea urchin eggs. *The Journal of Cell Biology,* 100**,** 1522-1527.

ELEFTERIOU, F. & YANG, X. 2011. Genetic mouse models for bone studies—Strengths and limitations. *Bone,* 49**,** 1242-1254.

ELLIS, R. J. & VAN DER VIES, S. M. 1991. Molecular chaperones. *Annual Review of Biochemistry ,* 60**,** 321-47.

ENGIN, F., YAO, Z., YANG, T., ZHOU, G., BERTIN, T., JIANG, M. M., CHEN, Y., WANG, L., ZHENG, H., SUTTON, R. E., BOYCE, B. F. & LEE, B. 2008. DIMORPHIC EFFECTS OF NOTCH SIGNALING IN BONE HOMEOSTASIS. *Nature Medicine,* 14**,** 299-305.

ENGLEMAN, V. W., NICKOLS, G. A., ROSS, F. P., HORTON, M. A., GRIGGS, D. W., SETTLE, S. L., RUMINSKI, P. G. & TEITELBAUM, S. L. 1997. A

peptidomimetic antagonist of the alpha(v)beta3 integrin inhibits bone resorption in vitro and prevents osteoporosis in vivo. *Journal of Clinical Investigation,* 99**,** 2284-92.

ENOMOTO, H., ENOMOTO-IWAMOTO, M., IWAMOTO, M., NOMURA, S., HIMENO, M., KITAMURA, Y., KISHIMOTO, T. & KOMORI, T. 2000. Cbfa1 is a positive regulatory factor in chondrocyte maturation. *Journal of Biological Chemistry,* 275**,** 8695-702.

ERENPREISA, J. & ROACH, H. I. 1998. Aberrant death in dark chondrocytes of the avian growth plate. *Cell Death and Differentiation,* 5**,** 60-6.

ERIKSEN, E. F., ALEXROF, D. W., MELSEN, F. 1994. *Bone Histomorphometry,* New York, Raven Press.

FAGONE, P. & JACKOWSKI, S. 2009. Membrane phospholipid synthesis and endoplasmic reticulum function. *Journal of Lipid Research,* 50 Suppl**,** S311-6.

FAKHRY, A., RATISOONTORN, C., VEDHACHALAM, C., SALHAB, I., KOYAMA, E., LEBOY, P., PACIFICI, M., KIRSCHNER, R. E. & NAH, H. D. 2005. Effects of FGF-2/-9 in calvarial bone cell cultures: differentiation stage-dependent mitogenic effect, inverse regulation of BMP-2 and noggin, and enhancement of osteogenic potential. *Bone,* 36**,** 254-66.

FARNUM, C. E. & WILSMAN, N. J. 1989. Cellular turnover at the chondro-osseous junction of growth plate cartilage: analysis by serial sections at the light microscopical level. *Journal of Orthopaedic Research,* 7**,** 654-66.

FEI, Y., XIAO, L., DOETSCHMAN, T., COFFIN, D. J. & HURLEY, M. M. 2011. Fibroblast growth factor 2 stimulation of osteoblast differentiation and bone formation is mediated by modulation of the Wnt signaling pathway. *Journal of Biological Chemistry,* 286**,** 40575-83.

FELBER, K., ELKS, P. M., LECCA, M. & ROEHL, H. H. 2015. Expression of osterix Is Regulated by FGF and Wnt/beta-Catenin Signalling during Osteoblast Differentiation. *PLoS ONE,* 10**,** e0144982.

FENG, J. Q., WARD, L. M., LIU, S., LU, Y., XIE, Y., YUAN, B., YU, X., RAUCH, F., DAVIS, S. I., ZHANG, S., RIOS, H., DREZNER, M. K., QUARLES, L. D., BONEWALD, L. F. & WHITE, K. E. 2006. Loss of DMP1 causes rickets and osteomalacia and identifies a role for osteocytes in mineral metabolism. *Nature Genetics,* 38**,** 1310-5.

FENG, X. 2005. RANKing intracellular signaling in osteoclasts. *IUBMB Life,* 57**,** 389-95.

FENG, X. & MCDONALD, J. M. 2011. Disorders of Bone Remodeling. *Annual Review of Pathology,* 6**,** 121-45.

FERRARA, N., CARVER-MOORE, K., CHEN, H., DOWD, M., LU, L., O'SHEA, K. S., POWELL-BRAXTON, L., HILLAN, K. J. & MOORE, M. W. 1996. Heterozygous embryonic lethality induced by targeted inactivation of the VEGF gene. *Nature,* 380**,** 439-42.

FINN, R. D., ATTWOOD, T. K., BABBITT, P. C., BATEMAN, A., BORK, P., BRIDGE, A. J., CHANG, H.-Y., DOSZTÁNYI, Z., EL-GEBALI, S., FRASER, M., GOUGH, J., HAFT, D., HOLLIDAY, G. L., HUANG, H., HUANG, X., LETUNIC, I., LOPEZ, R., LU, S., MARCHLER-BAUER, A., MI, H., MISTRY, J., NATALE, D. A., NECCI, M., NUKA, G., ORENGO, C. A., PARK, Y., PESSEAT, S., PIOVESAN, D., POTTER, S. C., RAWLINGS, N. D., REDASCHI, N., RICHARDSON, L., RIVOIRE, C., SANGRADOR-VEGAS, A., SIGRIST, C., SILLITOE, I., SMITHERS, B., SQUIZZATO, S., SUTTON, G., THANKI, N., THOMAS, P. D., TOSATTO, SILVIO C E., WU, C. H., XENARIOS, I., YEH, L.-S., YOUNG, S.-Y. & MITCHELL, A. L. 2017.

InterPro in 2017—beyond protein family and domain annotations. *Nucleic Acids Research,* 45**,** D190-D199.

FLORENCIO-SILVA, R., SASSO, G. R. S., SASSO-CERRI, E., SIMÕES, M. J. & CERRI, P. S. 2015. Biology of Bone Tissue: Structure, Function, and Factors That Influence Bone Cells. *BioMed Research International,* 2015.

FLYNN, G. C., CHAPPELL, T. G. & ROTHMAN, J. E. 1989. Peptide binding and release by proteins implicated as catalysts of protein assembly. *Science,* 245**,** 385-90.

FLYNN, G. C., POHL, J., FLOCCO, M. T. & ROTHMAN, J. E. 1991. Peptide-binding specificity of the molecular chaperone BiP. *Nature,* 353**,** 726-30.

FOLDYNOVA-TRANTIRKOVA, S., WILCOX, W. R. & KREJCI, P. 2012. Sixteen years and counting: the current understanding of fibroblast growth factor receptor 3 (FGFR3) signaling in skeletal dysplasias. *Human Mutation,* 33**,** 29-41.

FOSTER, J. W., DOMINGUEZ-STEGLICH, M. A., GUIOLI, S., KWOK, C., WELLER, P. A., STEVANOVIC, M., WEISSENBACH, J., MANSOUR, S., YOUNG, I. D., GOODFELLOW, P. N. & ET AL. 1994. Campomelic dysplasia and autosomal sex reversal caused by mutations in an SRY-related gene. *Nature,* 372**,** 525-30.

FRANZ-ODENDAAL, T. A., HALL, B. K. & WITTEN, P. E. 2006. Buried alive: how osteoblasts become osteocytes. *Developmenal Dynamics,* 235**,** 176-90.

FRIEDENSTEIN, A. J. 1976. Precursor cells of mechanocytes. *International Review of Cytology,* 47**,** 327-59.

FRIEDMAN, M. S., OYSERMAN, S. M. & HANKENSON, K. D. 2009. Wnt11 promotes osteoblast maturation and mineralization through R-spondin 2. *Journal of Biological Chemistry,* 284**,** 14117-25.

FURDUI, C. M., LEW, E. D., SCHLESSINGER, J. & ANDERSON, K. S. 2006. Autophosphorylation of FGFR1 kinase is mediated by a sequential and precisely ordered reaction. *Molecular Cell,* 21**,** 711-7.

FURUYA, Y., INAGAKI, A., KHAN, M., MORI, K., PENNINGER, J. M., NAKAMURA, M., UDAGAWA, N., AOKI, K., OHYA, K., UCHIDA, K. & YASUDA, H. 2013. Stimulation of bone formation in cortical bone of mice treated with a receptor activator of nuclear factor-kappaB ligand (RANKL)-binding peptide that possesses osteoclastogenesis inhibitory activity. *Journal of Biological Chemistry,* 288**,** 5562-71.

GALLI, C., ZELLA, L. A., FRETZ, J. A., FU, Q., PIKE, J. W., WEINSTEIN, R. S., MANOLAGAS, S. C. & O'BRIEN, C. A. 2008. Targeted deletion of a distant transcriptional enhancer of the receptor activator of nuclear factor-kappaB ligand gene reduces bone remodeling and increases bone mass. *Endocrinology,* 149**,** 146-53.

GAMER, L. W., COX, K., CARLO, J. M. & ROSEN, V. 2009. Overexpression of BMP3 in the developing skeleton alters endochondral bone formation resulting in spontaneous rib fractures. *Developmenal Dynamics,* 238**,** 2374-81.

GARCIADIEGO-CAZARES, D., ROSALES, C., KATOH, M. & CHIMAL-MONROY, J. 2004. Coordination of chondrocyte differentiation and joint formation by alpha5beta1 integrin in the developing appendicular skeleton. *Development,* 131**,** 4735-42.

GAROFALO, S., KLIGER-SPATZ, M., COOKE, J. L., WOLSTIN, O., LUNSTRUM, G. P., MOSHKOVITZ, S. M., HORTON, W. A. & YAYON, A. 1999. Skeletal dysplasia and defective chondrocyte differentiation by targeted overexpression of fibroblast growth factor 9 in transgenic mice. *Journal of Bone and Mineral Research,* 14**,** 1909-15.

GARRISON, P., YUE, S., HANSON, J., BARON, J. & LUI, J. C. 2017. Spatial regulation of bone morphogenetic proteins (BMPs) in postnatal articular and growth plate cartilage. *PLoS ONE,* 12**,** e0176752.

GAUR, T., LENGNER, C. J., HOVHANNISYAN, H., BHAT, R. A., BODINE, P. V., KOMM, B. S., JAVED, A., VAN WIJNEN, A. J., STEIN, J. L., STEIN, G. S. & LIAN, J. B. 2005. Canonical WNT signaling promotes osteogenesis by directly stimulating Runx2 gene expression. *Journal of Biological Chemistry,* 280**,** 33132-40.

GAZIT, A., YANIV, A., BAFICO, A., PRAMILA, T., IGARASHI, M., KITAJEWSKI, J. & AARONSON, S. A. 1999. Human frizzled 1 interacts with transforming Wnts to transduce a TCF dependent transcriptional response. *Oncogene,* 18**,** 5959-66.

GAZZERRO, E., PEREIRA, R. C., JORGETTI, V., OLSON, S., ECONOMIDES, A. N. & CANALIS, E. 2005. Skeletal overexpression of gremlin impairs bone formation and causes osteopenia. *Endocrinology,* 146**,** 655-65.

GE, C., YANG, Q., ZHAO, G., YU, H., KIRKWOOD, K. L. & FRANCESCHI, R. T. 2012. Interactions between extracellular signal-regulated kinase 1/2 and p38 MAP kinase pathways in the control of RUNX2 phosphorylation and transcriptional activity. *Journal of Bone and Mineral Research,* 27**,** 538-51.

GEETHA-LOGANATHAN, P., NIMMAGADDA, S. & SCAAL, M. 2008. Wnt signaling in limb organogenesis. *Organogenesis,* 4**,** 109-15.

GENTILI, C., BIANCO, P., NERI, M., MALPELI, M., CAMPANILE, G., CASTAGNOLA, P., CANCEDDA, R. & CANCEDDA, F. D. 1993. Cell proliferation, extracellular matrix mineralization, and ovotransferrin transient expression during in vitro differentiation of chick hypertrophic chondrocytes into osteoblast-like cells. *Journal of Cell Biology,* 122**,** 703-12.

GENTILI, C. & CANCEDDA, R. 2009. Cartilage and bone extracellular matrix. *Current Pharmaceutical Design,* 15**,** 1334-48.

GERBER, H. P., VU, T. H., RYAN, A. M., KOWALSKI, J., WERB, Z. & FERRARA, N. 1999. VEGF couples hypertrophic cartilage remodeling, ossification and angiogenesis during endochondral bone formation. *Nature Medicine,* 5**,** 623-8.

GILBERT, L., HE, X., FARMER, P., BODEN, S., KOZLOWSKI, M., RUBIN, J. & NANES, M. S. 2000. Inhibition of osteoblast differentiation by tumor necrosis factor-alpha. *Endocrinology,* 141**,** 3956-64.

GILBERT, S. F. 2000. *Developmental Biology, 6th Edition,* Sunderland (MA), Sinauer Associates.

GLASS, D. A., 2ND, BIALEK, P., AHN, J. D., STARBUCK, M., PATEL, M. S., CLEVERS, H., TAKETO, M. M., LONG, F., MCMAHON, A. P., LANG, R. A. & KARSENTY, G. 2005. Canonical Wnt signaling in differentiated osteoblasts controls osteoclast differentiation. *Developmental Cell,* 8**,** 751-64.

GOHDA, J., AKIYAMA, T., KOGA, T., TAKAYANAGI, H., TANAKA, S. & INOUE, J. 2005. RANK-mediated amplification of TRAF6 signaling leads to NFATc1 induction during osteoclastogenesis. *EMBO Journal,* 24**,** 790-9.

GOVONI, K. E., WERGEDAL, J. E., FLORIN, L., ANGEL, P., BAYLINK, D. J. & MOHAN, S. 2007. Conditional deletion of insulin-like growth factor-I in collagen type 1alpha2-expressing cells results in postnatal lethality and a dramatic reduction in bone accretion. *Endocrinology,* 148**,** 5706-15.

GOWEN, M., LAZNER, F., DODDS, R., KAPADIA, R., FEILD, J., TAVARIA, M., BERTONCELLO, I., DRAKE, F., ZAVARSELK, S., TELLIS, I., HERTZOG, P., DEBOUCK, C. & KOLA, I. 1999. Cathepsin K knockout mice develop osteopetrosis due to a deficit in matrix degradation but not demineralization. *Journal of Bone and Mineral Research,* 14**,** 1654-63.

GRAVES, D. T., JIANG, Y. & VALENTE, A. J. 1999. The expression of monocyte chemoattractant protein-1 and other chemokines by osteoblasts. *Frontiers in Bioscience,* 4**,** D571-80.

GREENBLATT, M. B., SHIM, J. H., ZOU, W., SITARA, D., SCHWEITZER, M., HU, D., LOTINUN, S., SANO, Y., BARON, R., PARK, J. M., ARTHUR, S., XIE, M., SCHNEIDER, M. D., ZHAI, B., GYGI, S., DAVIS, R. & GLIMCHER, L. H. 2010. The p38 MAPK pathway is essential for skeletogenesis and bone homeostasis in mice. *Journal of Clinical Investigation,* 120**,** 2457-73.

GREY, A., BANOVIC, T., ZHU, Q., WATSON, M., CALLON, K., PALMANO, K., ROSS, J., NAOT, D., REID, I. R. & CORNISH, J. 2004. The low-density lipoprotein receptor-related protein 1 is a mitogenic receptor for lactoferrin in osteoblastic cells. *Molecular Endocrinology,* 18**,** 2268-78.

GUALENI, B., RAJPAR, M. H., KELLOGG, A., BELL, P. A., ARVAN, P., BOOT-HANDFORD, R. P. & BRIGGS, M. D. 2013. A novel transgenic mouse model of growth plate dysplasia reveals that decreased chondrocyte proliferation due to chronic ER stress is a key factor in reduced bone growth. *Disease Models & Mechaniams,* 6**,** 1414-25.

GUNNELL, L. M., JONASON, J. H., LOISELLE, A. E., KOHN, A., SCHWARZ, E. M., HILTON, M. J. & O'KEEFE, R. J. 2010. TAK1 Regulates Cartilage and Joint Development via the MAPK and BMP Signaling Pathways. *Journal of Bone and Mineral Research,* 25**,** 1784-97.

HADJIDAKIS, D. J. & ANDROULAKIS, II 2006. Bone remodeling. *Annals of the New York Academy of Sciences,* 1092**,** 385-96.

HALL-GLENN, F., DEYOUNG, R. A., SARKISSIAN, E. & LYONS, K. M. 2009. The Roles of CCN1(Cyr61) and CCN2(CTGF) in Chondrogenesis. *55th Annual Meeting of the Orthopaedic Research Society.* Las Vegas, Nevada.

HAMADA, T., SUDA, N. & KURODA, T. 1999. Immunohistochemical localization of fibroblast growth factor receptors in the rat mandibular condylar cartilage and tibial cartilage. *Journal of Bone and Mineral Metabolism,* 17**,** 274-82.

HAMMOND, C., BRAAKMAN, I. & HELENIUS, A. 1994. Role of N-linked oligosaccharide recognition, glucose trimming, and calnexin in glycoprotein folding and quality control. *Proceedings of the National Academy of Sciences of the United States of America,* 91**,** 913-7.

HAN, Y. & LEFEBVRE, V. 2008. L-Sox5 and Sox6 drive expression of the aggrecan gene in cartilage by securing binding of Sox9 to a far-upstream enhancer. *Molecular Cell Biology,* 28**,** 4999-5013.

HARADA, H., TAGASHIRA, S., FUJIWARA, M., OGAWA, S., KATSUMATA, T., YAMAGUCHI, A., KOMORI, T. & NAKATSUKA, M. 1999. Cbfa1 isoforms exert functional differences in osteoblast differentiation. *Journal of Biological Chemistry,* 274**,** 6972-8.

HARDING, H. P., ZHANG, Y. & RON, D. 1999. Protein translation and folding are coupled by an endoplasmic-reticulum-resident kinase. *Nature,* 397**,** 271-4.

HARPER, J. W., ELLEDGE, S. J., KEYOMARSI, K., DYNLACHT, B., TSAI, L. H., ZHANG, P., DOBROWOLSKI, S., BAI, C., CONNELL-CROWLEY, L., SWINDELL, E. & ET AL. 1995. Inhibition of cyclin-dependent kinases by p21. *Molecular Biology of the Cell,* 6**,** 387-400.

HARTLEY, C. L., EDWARDS, S., MULLAN, L., BELL, P. A., FRESQUET, M., BOOT-HANDFORD, R. P. & BRIGGS, M. D. 2013. Armet/Manf and Creld2 are components of a specialized ER stress response provoked by inappropriate formation of disulphide bonds: implications for genetic skeletal diseases. *Human Molecular Genetics,* 22**,** 5262-75.

HARTMANN, C. & TABIN, C. J. 2000. Dual roles of Wnt signaling during chondrogenesis in the chicken limb. *Development,* 127**,** 3141-59.
HATAKEYAMA, Y., TUAN, R. S. & SHUM, L. 2004. Distinct functions of BMP4 and GDF5 in the regulation of chondrogenesis. *Journal of Cellular Biochemistry,* 91**,** 1204-17.
HATORI, M., KLATTE, K. J., TEIXEIRA, C. C. & SHAPIRO, I. M. 1995. End labeling studies of fragmented DNA in the avian growth plate: evidence of apoptosis in terminally differentiated chondrocytes. *Journal of Bone and Mineral Research,* 10**,** 1960-8.
HAYASHI, M., NIMURA, K., KASHIWAGI, K., HARADA, T., TAKAOKA, K., KATO, H., TAMAI, K. & KANEDA, Y. 2007. Comparative roles of Twist-1 and Id1 in transcriptional regulation by BMP signaling. *Journal of Cell Science,* 120**,** 1350-7.
HAYCRAFT, C. J. & SERRA, R. 2008. Cilia involvement in patterning and maintenance of the skeleton. *Current Topics in Developmental Biology,* 85**,** 303-332.
HAYCRAFT, C. J., ZHANG, Q., SONG, B., JACKSON, W. S., DETLOFF, P. J., SERRA, R. & YODER, B. K. 2007. Intraflagellar transport is essential for endochondral bone formation. *Development,* 134**,** 307-16.
HEBERT, D. N., FOELLMER, B. & HELENIUS, A. 1995. Glucose trimming and reglucosylation determine glycoprotein association with calnexin in the endoplasmic reticulum. *Cell,* 81**,** 425-33.
HEBERT, D. N., FOELLMER, B. & HELENIUS, A. 1996. Calnexin and calreticulin promote folding, delay oligomerization and suppress degradation of influenza hemagglutinin in microsomes. *EMBO Journal,* 15**,** 2961-8.
HEBERT, D. N., ZHANG, J. X., CHEN, W., FOELLMER, B. & HELENIUS, A. 1997. The Number and Location of Glycans on Influenza Hemagglutinin Determine Folding and Association with Calnexin and Calreticulin. *Journal of Cell Biology,* 139**,** 613-23.
HERZ, J., CLOUTHIER, D. E. & HAMMER, R. E. 1992. LDL receptor-related protein internalizes and degrades uPA-PAI-1 complexes and is essential for embryo implantation. *Cell,* 71**,** 411-21.
HERZ, J. & STRICKLAND, D. K. 2001. LRP: a multifunctional scavenger and signaling receptor. *Journal of Clinical Investigation,* 108**,** 779-784.
HESSLER, J. L. & KREITMAN, R. J. 1997. An early step in Pseudomonas exotoxin action is removal of the terminal lysine residue, which allows binding to the KDEL receptor. *Biochemistry,* 36**,** 14577-82.
HIKITA, A., YANA, I., WAKEYAMA, H., NAKAMURA, M., KADONO, Y., OSHIMA, Y., NAKAMURA, K., SEIKI, M. & TANAKA, S. 2006. Negative regulation of osteoclastogenesis by ectodomain shedding of receptor activator of NF-kappaB ligand. *Journal of Biological Chemistry,* 281**,** 36846-55.
HILL, P. A., TUMBER, A. & MEIKLE, M. C. 1997. Multiple extracellular signals promote osteoblast survival and apoptosis. *Endocrinology,* 138**,** 3849-58.
HILL, T. P., SPATER, D., TAKETO, M. M., BIRCHMEIER, W. & HARTMANN, C. 2005. Canonical Wnt/beta-catenin signaling prevents osteoblasts from differentiating into chondrocytes. *Developmental Cell,* 8**,** 727-38.
HILTON, M. J., TU, X., WU, X., BAI, S., ZHAO, H., KOBAYASHI, T., KRONENBERG, H. M., TEITELBAUM, S. L., ROSS, F. P., KOPAN, R. & LONG, F. 2008. Notch signaling maintains bone marrow mesenchymal progenitors by suppressing osteoblast differentiation. *Nature Medicine,* 14**,** 306-14.

HINO, K., SAITO, A., KIDO, M., KANEMOTO, S., ASADA, R., TAKAI, T., CUI, M., CUI, X. & IMAIZUMI, K. 2014. Master regulator for chondrogenesis, Sox9, regulates transcriptional activation of the endoplasmic reticulum stress transducer BBF2H7/CREB3L2 in chondrocytes. *Journal of Biological Chemistry,* 289**,** 13810-20.

HINO, S.-I., KONDO, S., YOSHINAGA, K., SAITO, A., MURAKAMI, T., KANEMOTO, S., SEKIYA, H., CHIHARA, K., AIKAWA, Y., HARA, H., KUDO, T., SEKIMOTO, T., FUNAMOTO, T., CHOSA, E. & IMAIZUMI, K. 2010. Regulation of ER molecular chaperone prevents bone loss in a murine model for osteoporosis. *Journal of Bone and Mineral Metabolism,* 28**,** 131-138.

HIRAMATSU, K., IWAI, T., YOSHIKAWA, H. & TSUMAKI, N. 2011. Expression of dominant negative TGF-beta receptors inhibits cartilage formation in conditional transgenic mice. *Journal of Bone and Mineral Metabolism,* 29**,** 493-500.

HOLBOURN, K. P., ACHARYA, K. R. & PERBAL, B. 2008. The CCN family of proteins: structure–function relationships. *Trends in Biochemical Sciences,* 33**,** 461-473.

HOLMEN, S. L., ZYLSTRA, C. R., MUKHERJEE, A., SIGLER, R. E., FAUGERE, M. C., BOUXSEIN, M. L., DENG, L., CLEMENS, T. L. & WILLIAMS, B. O. 2005. Essential role of beta-catenin in postnatal bone acquisition. *Journal of Biological Chemistry,* 280**,** 21162-8.

HONG, M., LUO, S., BAUMEISTER, P., HUANG, J. M., GOGIA, R. K., LI, M. & LEE, A. S. 2004. Underglycosylation of ATF6 as a novel sensing mechanism for activation of the unfolded protein response. *Journal of Biological Chemistry,* 279**,** 11354-63.

HORNER, A., BISHOP, N. J., BORD, S., BEETON, C., KELSALL, A. W., COLEMAN, N. & COMPSTON, J. E. 1999. Immunolocalisation of vascular endothelial growth factor (VEGF) in human neonatal growth plate cartilage. *Journal of Anatomy,* 194**,** 519-24.

HORVAT, R., HOVORKA, A., DEKAN, G., POCZEWSKI, H. & KERJASCHKI, D. 1986. Endothelial cell membranes contain podocalyxin--the major sialoprotein of visceral glomerular epithelial cells. *Journal of Cell Biology,* 102**,** 484-91.

HOSHI, T., TEZUKA, T., YOKOYAMA, K., IEMURA, S., NATSUME, T. & YAMANASHI, Y. 2013. Mesdc2 plays a key role in cell-surface expression of Lrp4 and postsynaptic specialization in myotubes. *FEBS Letters,* 587**,** 3749-54.

HSIEH, J. C., LEE, L., ZHANG, L., WEFER, S., BROWN, K., DEROSSI, C., WINES, M. E., ROSENQUIST, T. & HOLDENER, B. C. 2003. Mesd encodes an LRP5/6 chaperone essential for specification of mouse embryonic polarity. *Cell,* 112**,** 355-67.

HU, H., HILTON, M. J., TU, X., YU, K., ORNITZ, D. M. & LONG, F. 2005. Sequential roles of Hedgehog and Wnt signaling in osteoblast development. *Development,* 132**,** 49-60.

HUANG, B., WANG, W., LI, Q., WANG, Z., YAN, B., ZHANG, Z., WANG, L., HUANG, M., JIA, C., LU, J., LIU, S., CHEN, H., LI, M., CAI, D., JIANG, Y., JIN, D. & BAI, X. 2016. Osteoblasts secrete Cxcl9 to regulate angiogenesis in bone. *Nature Communications,* 7**,** 13885.

HUANG, H., CHANG, E. J., RYU, J., LEE, Z. H., LEE, Y. & KIM, H. H. 2006. Induction of c-Fos and NFATc1 during RANKL-stimulated osteoclast differentiation is mediated by the p38 signaling pathway. *Biochemical and Biophysical Research Communications,* 351**,** 99-105.

HUANG, W., YANG, S., SHAO, J. & LI, Y. P. 2007. Signaling and transcriptional regulation in osteoblast commitment and differentiation. *Frontiers in Bioscience,* 12**,** 3068-92.

HUANG, Z., REN, P. G., MA, T., SMITH, R. L. & GOODMAN, S. B. 2010. Modulating osteogenesis of mesenchymal stem cells by modifying growth factor availability. *Cytokine,* 51**,** 305-10.

HUGHES, A., KLEINE-ALBERS, J., HELFRICH, M. H., RALSTON, S. H. & ROGERS, M. J. 2012. A Class III Semaphorin (Sema3e) Inhibits Mouse Osteoblast Migration and Decreases Osteoclast Formation In Vitro. *Calcified Tissue International,* 90**,** 151-162.

HUGHES, A. E., RALSTON, S. H., MARKEN, J., BELL, C., MACPHERSON, H., WALLACE, R. G., VAN HUL, W., WHYTE, M. P., NAKATSUKA, K., HOVY, L. & ANDERSON, D. M. 2000. Mutations in TNFRSF11A, affecting the signal peptide of RANK, cause familial expansile osteolysis. *Nature Genetics,* 24**,** 45-8.

HUGHES-FULFORD, M. & LI, C. F. 2011. The role of FGF-2 and BMP-2 in regulation of gene induction, cell proliferation and mineralization. *Journal of Orthopaedic Surgery and Research,* 6**,** 8.

HUNZIKER, E. B., SCHENK, R. K. & CRUZ-ORIVE, L. M. 1987. Quantitation of chondrocyte performance in growth-plate cartilage during longitudinal bone growth. *Journal of Bone and Joint Surgery,* 69**,** 162-73.

IJIRI, K., ZERBINI, L. F., PENG, H., CORREA, R. G., LU, B., WALSH, N., ZHAO, Y., TANIGUCHI, N., HUANG, X. L., OTU, H., WANG, H., WANG, J. F., KOMIYA, S., DUCY, P., RAHMAN, M. U., FLAVELL, R. A., GRAVALLESE, E. M., OETTGEN, P., LIBERMANN, T. A. & GOLDRING, M. B. 2005. A novel role for GADD45beta as a mediator of MMP-13 gene expression during chondrocyte terminal differentiation. *Journal of Biological Chemistry,* 280**,** 38544-55.

IKEGAMI, D., AKIYAMA, H., SUZUKI, A., NAKAMURA, T., NAKANO, T., YOSHIKAWA, H. & TSUMAKI, N. 2011. Sox9 sustains chondrocyte survival and hypertrophy in part through Pik3ca-Akt pathways. *Development,* 138**,** 1507-19.

INADA, M., YASUI, T., NOMURA, S., MIYAKE, S., DEGUCHI, K., HIMENO, M., SATO, M., YAMAGIWA, H., KIMURA, T., YASUI, N., OCHI, T., ENDO, N., KITAMURA, Y., KISHIMOTO, T. & KOMORI, T. 1999. Maturational disturbance of chondrocytes in Cbfa1-deficient mice. *Developmenal Dynamics,* 214**,** 279-90.

IONESCU, A., KOZHEMYAKINA, E., NICOLAE, C., KAESTNER, K. H., OLSEN, B. R. & LASSAR, A. B. 2012. FoxA family members are crucial regulators of the hypertrophic chondrocyte differentiation program. *Developmental Cell,* 22**,** 927-39.

ISENMANN, S., ARTHUR, A., ZANNETTINO, A. C., TURNER, J. L., SHI, S., GLACKIN, C. A. & GRONTHOS, S. 2009. TWIST family of basic helix-loop-helix transcription factors mediate human mesenchymal stem cell growth and commitment. *Stem Cells,* 27**,** 2457-68.

ISHIDA, Y., YAMAMOTO, A., KITAMURA, A., LAMANDE, S. R., YOSHIMORI, T., BATEMAN, J. F., KUBOTA, H. & NAGATA, K. 2009. Autophagic elimination of misfolded procollagen aggregates in the endoplasmic reticulum as a means of cell protection. *Molecular Biology of the Cell,* 20**,** 2744-54.

ISO, T., KEDES, L. & HAMAMORI, Y. 2003. HES and HERP families: multiple effectors of the Notch signaling pathway. *Journal of Cellular Physiology,* 194**,** 237-55.

IVKOVIC, S., YOON, B. S., POPOFF, S. N., SAFADI, F. F., LIBUDA, D. E., STEPHENSON, R. C., DALUISKI, A. & LYONS, K. M. 2003. Connective

tissue growth factor coordinates chondrogenesis and angiogenesis during skeletal development. *Development,* 130**,** 2779-91.

IWATA, J., HOSOKAWA, R., SANCHEZ-LARA, P. A., URATA, M., SLAVKIN, H. & CHAI, Y. 2010. Transforming Growth Factor-β Regulates Basal Transcriptional Regulatory Machinery to Control Cell Proliferation and Differentiation in Cranial Neural Crest-derived Osteoprogenitor Cells. *Journal of Biological Chemistry,* 285**,** 4975-82.

IWATA, T., CHEN, L., LI, C., OVCHINNIKOV, D. A., BEHRINGER, R. R., FRANCOMANO, C. A. & DENG, C. X. 2000. A neonatal lethal mutation in FGFR3 uncouples proliferation and differentiation of growth plate chondrocytes in embryos. *Human Molecular Genetics,* 9**,** 1603-13.

JACOB, A. L., SMITH, C., PARTANEN, J. & ORNITZ, D. M. 2006. Fibroblast growth factor receptor 1 signaling in the osteo-chondrogenic cell lineage regulates sequential steps of osteoblast maturation. *Developmental Biology,* 296**,** 315-28.

JANG, W. G., KIM, E. J., KIM, D. K., RYOO, H. M., LEE, K. B., KIM, S. H., CHOI, H. S. & KOH, J. T. 2012. BMP2 protein regulates osteocalcin expression via Runx2-mediated Atf6 gene transcription. *Journal of Biological Chemistry,* 287**,** 905-15.

JAVED, A., BARNES, G. L., JASANYA, B. O., STEIN, J. L., GERSTENFELD, L., LIAN, J. B. & STEIN, G. S. 2001. runt homology domain transcription factors (Runx, Cbfa, and AML) mediate repression of the bone sialoprotein promoter: evidence for promoter context-dependent activity of Cbfa proteins. *Molecular Cell Biology,* 21**,** 2891-905.

JESSOP, C. E., CHAKRAVARTHI, S., GARBI, N., HAMMERLING, G. J., LOVELL, S. & BULLEID, N. J. 2007. ERp57 is essential for efficient folding of glycoproteins sharing common structural domains. *EMBO Journal,* 26**,** 28-40.

JESSOP, C. E., TAVENDER, T. J., WATKINS, R. H., CHAMBERS, J. E. & BULLEID, N. J. 2009. Substrate Specificity of the Oxidoreductase ERp57 Is Determined Primarily. *Journal of Biological Chemistry,* 284**,** 2194-202.

JIAN, H., SHEN, X., LIU, I., SEMENOV, M., HE, X. & WANG, X. F. 2006. Smad3-dependent nuclear translocation of β-catenin is required for TGF-β1-induced proliferation of bone marrow-derived adult human mesenchymal stem cells. *Genes & Development,* 20**,** 666-74.

JIANG, J., LICHTLER, A. C., GRONOWICZ, G. A., ADAMS, D. J., CLARK, S. H., ROSEN, C. J. & KREAM, B. E. 2006. Transgenic mice with osteoblast-targeted insulin-like growth factor-I show increased bone remodeling. *Bone,* 39**,** 494-504.

JIANG, T. X., YI, J. R., YING, S. Y. & CHUONG, C. M. 1993. Activin enhances chondrogenesis of limb bud cells: stimulation of precartilaginous mesenchymal condensations and expression of NCAM. *Developmental Biology,* 155**,** 545-57.

JIANG, X., ISEKI, S., MAXSON, R. E., SUCOV, H. M. & MORRISS-KAY, G. M. 2002. Tissue origins and interactions in the mammalian skull vault. *Developmental Biology,* 241**,** 106-16.

JILKA, R. L. 2003. Biology of the basic multicellular unit and the pathophysiology of osteoporosis. *Medical and Pediatric Oncology,* 41**,** 182-5.

JILKA, R. L., HANGOC, G., GIRASOLE, G., PASSERI, G., WILLIAMS, D. C., ABRAMS, J. S., BOYCE, B., BROXMEYER, H. & MANOLAGAS, S. C. 1992. Increased osteoclast development after estrogen loss: mediation by interleukin-6. *Science,* 257**,** 88-91.

JOENG, K. S., SCHUMACHER, C. A., ZYLSTRA-DIEGEL, C. R., LONG, F. & WILLIAMS, B. O. 2011. Lrp5 and Lrp6 redundantly control skeletal development in the mouse embryo. *Developmental Biology,* 359**,** 222-9.

JOPLING, C., BOUE, S. & IZPISUA BELMONTE, J. C. 2011. Dedifferentiation, transdifferentiation and reprogramming: three routes to regeneration. *Nature Reviews Molecular Cell Biology Cell Biology,* 12**,** 79-89.

JURIC, V., CHEN, C.-C. & LAU, L. F. 2012. TNF α -Induced Apoptosis Enabled by CCN1/CYR61: Pathways of Reactive Oxygen Species Generation and Cytochrome c Release. *PLoS ONE,* 7**,** e31303.

KAHLER, R. A., GALINDO, M., LIAN, J., STEIN, G. S., VAN WIJNEN, A. J. & WESTENDORF, J. J. 2006. Lymphocyte enhancer-binding factor 1 (Lef1) inhibits terminal differentiation of osteoblasts. *Journal of Cellular Biochemistry,* 97**,** 969-83.

KAHLER, R. A. & WESTENDORF, J. J. 2003. Lymphoid enhancer factor-1 and beta-catenin inhibit Runx2-dependent transcriptional activation of the osteocalcin promoter. *Journal of Biological Chemistry,* 278**,** 11937-44.

KAHLER, R. A., YINGST, S. M., HOEPPNER, L. H., JENSEN, E. D., KRAWCZAK, D., OXFORD, J. T. & WESTENDORF, J. J. 2008. Collagen 11a1 is indirectly activated by lymphocyte enhancer-binding factor 1 (Lef1) and negatively regulates osteoblast maturation. *Matrix Biology,* 27**,** 330-8.

KAMIYA, N., KOBAYASHI, T., MOCHIDA, Y., YU, P. B., YAMAUCHI, M., KRONENBERG, H. M. & MISHINA, Y. 2010. Wnt inhibitors Dkk1 and Sost are downstream targets of BMP signaling through the type IA receptor (BMPRIA) in osteoblasts. *Journal of Bone and Mineral Research,* 25**,** 200-10.

KARAGUZEL, G. & HOLICK, M. F. 2010. Diagnosis and treatment of osteopenia. *Reviews in Endocrine and Metabolic Disorders,* 11**,** 237-51.

KARAPLIS, A. C., LUZ, A., GLOWACKI, J., BRONSON, R. T., TYBULEWICZ, V. L., KRONENBERG, H. M. & MULLIGAN, R. C. 1994. Lethal skeletal dysplasia from targeted disruption of the parathyroid hormone-related peptide gene. *Genes & Development,* 8**,** 277-89.

KAROLAK, M. R., YANG, X. & ELEFTERIOU, F. 2015. FGFR1 signaling in hypertrophic chondrocytes is attenuated by the Ras-GAP neurofibromin during endochondral bone formation. *Human Molecular Genetics,* 24**,** 2552-64.

KARSENTY, G. 1999. The genetic transformation of bone biology. *Genes & Development,* 13**,** 3037-51.

KATAVIC, V., LUKIC, I. K., KOVACIC, N., GRCEVIC, D., LORENZO, J. A. & MARUSIC, A. 2003. Increased bone mass is a part of the generalized lymphoproliferative disorder phenotype in the mouse. *Journal of Immunology,* 170**,** 1540-7.

KATO, M., PATEL, M. S., LEVASSEUR, R., LOBOV, I., CHANG, B. H., GLASS, D. A., 2ND, HARTMANN, C., LI, L., HWANG, T. H., BRAYTON, C. F., LANG, R. A., KARSENTY, G. & CHAN, L. 2002. Cbfa1-independent decrease in osteoblast proliferation, osteopenia, and persistent embryonic eye vascularization in mice deficient in Lrp5, a Wnt coreceptor. *Journal of Cell Biology,* 157**,** 303-14.

KATSUBE, K., SAKAMOTO, K., TAMAMURA, Y. & YAMAGUCHI, A. 2009. Role of CCN, a vertebrate specific gene family, in development. *Development, Growth & Differentiationer,* 51**,** 55-67.

KAWAKI, H., KUBOTA, S., SUZUKI, A., YAMADA, T., MATSUMURA, T., MANDAI, T., YAO, M., MAEDA, T., LYONS, K. M. & TAKIGAWA, M. 2008. Functional requirement of CCN2 for intramembranous bone formation in embryonic mice. *Biochemical and Biophysical Research Communications,* 366**,** 450-6.

KAWATA, K., KUBOTA, S., EGUCHI, T., AOYAMA, E., MORITANI, N. H., KONDO, S., NISHIDA, T. & TAKIGAWA, M. 2012. Role of LRP1 in

transport of CCN2 protein in chondrocytes. *Journal of Cell Science,* 125**,** 2965-72.

KAWATA, K., KUBOTA, S., EGUCHI, T., MORITANI, N. H., SHIMO, T., KONDO, S., NISHIDA, T., MINAGI, S. & TAKIGAWA, M. 2010. Role of the low-density lipoprotein receptor-related protein-1 in regulation of chondrocyte differentiation. *Journal of Cellular Physiology,* 222**,** 138-48.

KELAINI, S., COCHRANE, A. & MARGARITI, A. 2014. Direct reprogramming of adult cells: avoiding the pluripotent state. *Stem Cells Cloning,* 7**,** 19-29.

KERN, B., SHEN, J., STARBUCK, M. & KARSENTY, G. 2001. Cbfa1 contributes to the osteoblast-specific expression of type I collagen genes. *Journal of Biological Chemistry,* 276**,** 7101-7.

KIELTY, C. M., KWAN, A. P., HOLMES, D. F., SCHOR, S. L. & GRANT, M. E. 1985. Type X collagen, a product of hypertrophic chondrocytes. *Biochemical Journal,* 227**,** 545-54.

KIESLINGER, M., FOLBERTH, S., DOBREVA, G., DORN, T., CROCI, L., ERBEN, R., CONSALEZ, G. G. & GROSSCHEDL, R. 2005. EBF2 regulates osteoblast-dependent differentiation of osteoclasts. *Developmental Cell,* 9**,** 757-67.

KIM, H. J., KIM, J. H., BAE, S. C., CHOI, J. Y., KIM, H. J. & RYOO, H. M. 2003. The protein kinase C pathway plays a central role in the fibroblast growth factor-stimulated expression and transactivation activity of Runx2. *Journal of Biological Chemistry,* 278**,** 319-26.

KIM, I. S., OTTO, F., ZABEL, B. & MUNDLOS, S. 1999. Regulation of chondrocyte differentiation by Cbfa1. *Mechanisms of Development,* 80**,** 159-70.

KIM, J. H., JIN, H. M., KIM, K., SONG, I., YOUN, B. U., MATSUO, K. & KIM, N. 2009. The mechanism of osteoclast differentiation induced by IL-1. *Journal of Immunology,* 183**,** 1862-70.

KIM, M. S., DAY, C. J. & MORRISON, N. A. 2005. MCP-1 is induced by receptor activator of nuclear factor-{kappa}B ligand, promotes human osteoclast fusion, and rescues granulocyte macrophage colony-stimulating factor suppression of osteoclast formation. *Journal of Biological Chemistry,* 280**,** 16163-9.

KIM, N., ODGREN, P. R., KIM, D. K., MARKS, S. C., JR. & CHOI, Y. 2000. Diverse roles of the tumor necrosis factor family member TRANCE in skeletal physiology revealed by TRANCE deficiency and partial rescue by a lymphocyte-expressed TRANCE transgene. *Proceedings of the National Academy of Sciences of the United States of America,* 97**,** 10905-10.

KIRCHHOFF, S., SCHAPER, F. & HAUSER, H. 1993. Interferon regulatory factor 1 (IRF-1) mediates cell growth inhibition by transactivation of downstream target genes. *Nucleic Acids Research,* 21**,** 2881-2889.

KITAZAWA, R., KIMBLE, R. B., VANNICE, J. L., KUNG, V. T. & PACIFICI, R. 1994. Interleukin-1 receptor antagonist and tumor necrosis factor binding protein decrease osteoclast formation and bone resorption in ovariectomized mice. *Journal of Clinical Investigation,* 94**,** 2397-406.

KOBAYASHI, H., GAO, Y., UETA, C., YAMAGUCHI, A. & KOMORI, T. 2000. Multilineage differentiation of Cbfa1-deficient calvarial cells in vitro. *Biochemical and Biophysical Research Communications,* 273**,** 630-6.

KOBAYASHI, T., LYONS, K. M., MCMAHON, A. P. & KRONENBERG, H. M. 2005. BMP signaling stimulates cellular differentiation at multiple steps during cartilage development. *Proceedings of the National Academy of Sciences of the United States of America,* 102**,** 18023-7.

KOCH, S. & CLAESSON-WELSH, L. 2012. Signal Transduction by Vascular Endothelial Growth Factor Receptors. *Cold Spring Harbor Perspectives in Medicine,* 2.

KODURI, V. & BLACKLOW, S. C. 2007. Requirement for natively unstructured regions of mesoderm development candidate 2 in promoting low-density lipoprotein receptor-related protein 6 maturation. *Biochemistry,* 46**,** 6570-7.

KOHN, A. D. & MOON, R. T. 2005. Wnt and calcium signaling: beta-catenin-independent pathways. *Cell Calcium,* 38**,** 439-46.

KOKABU, S., GAMER, L., COX, K., LOWERY, J., TSUJI, K., RAZ, R., ECONOMIDES, A., KATAGIRI, T. & ROSEN, V. 2012. BMP3 Suppresses Osteoblast Differentiation of Bone Marrow Stromal Cells via Interaction with Acvr2b. *Molecular Endocrinology,* 26**,** 87-94.

KOKUBU, C., HEINZMANN, U., KOKUBU, T., SAKAI, N., KUBOTA, T., KAWAI, M., WAHL, M. B., GALCERAN, J., GROSSCHEDL, R., OZONO, K. & IMAI, K. 2004. Skeletal defects in ringelschwanz mutant mice reveal that Lrp6 is required for proper somitogenesis and osteogenesis. *Development,* 131**,** 5469-80.

KOLUPAEVA, V., DAEMPFLING, L. & BASILICO, C. 2013. The B55 α Regulatory Subunit of Protein Phosphatase 2A Mediates Fibroblast Growth Factor-Induced p107 Dephosphorylation and Growth Arrest in Chondrocytes. *Molecular and Cellular Biology,* 33**,** 2865-2878.

KOMIYA, Y. & HABAS, R. 2008. Wnt signal transduction pathways. *Organogenesis,* 4**,** 68-75.

KOMORI, T. 2002. Runx2, a multifunctional transcription factor in skeletal development. *Journal of Cellular Biochemistry,* 87**,** 1-8.

KOMORI, T. 2006. Regulation of osteoblast differentiation by transcription factors. *Journal of Cellular Biochemistry,* 99**,** 1233-9.

KOMORI, T. 2010. Regulation of Osteoblast Differentiation by Runx2. *In:* CHOI, Y. (ed.) *Osteoimmunology: Interactions of the Immune and skeletal systems II.* Boston, MA: Springer US.

KOMORI, T. 2015. The functions of Runx family transcription factors and Cbfb in skeletal development. *Oral Science International,* 12**,** 1-4.

KOMORI, T., YAGI, H., NOMURA, S., YAMAGUCHI, A., SASAKI, K., DEGUCHI, K., SHIMIZU, Y., BRONSON, R. T., GAO, Y. H., INADA, M., SATO, M., OKAMOTO, R., KITAMURA, Y., YOSHIKI, S. & KISHIMOTO, T. 1997. Targeted disruption of Cbfa1 results in a complete lack of bone formation owing to maturational arrest of osteoblasts. *Cell,* 89**,** 755-64.

KONDO, S., SAITO, A., HINO, S., MURAKAMI, T., OGATA, M., KANEMOTO, S., NARA, S., YAMASHITA, A., YOSHINAGA, K., HARA, H. & IMAIZUMI, K. 2007. BBF2H7, a novel transmembrane bZIP transcription factor, is a new type of endoplasmic reticulum stress transducer. *Molecular Cell Biology,* 27**,** 1716-29.

KONNO, K., WAKABAYASHI, Y., AKASHI-TAKAMURA, S., ISHII, T., KOBAYASHI, M., TAKAHASHI, K., KUSUMOTO, Y., SAITOH, S., YOSHIZAWA, Y. & MIYAKE, K. 2006. A molecule that is associated with Toll-like receptor 4 and regulates its cell surface expression. *Biochemical and Biophysical Research Communications,* 339**,** 1076-82.

KOPAN, R. & ILAGAN, M. X. G. 2009. The Canonical Notch Signaling Pathway: Unfolding the Activation Mechanism. *Cell,* 137**,** 216-33.

KOURI-FLORES, J. B., ABBUD-LOZOYA, K. A. & ROJA-MORALES, L. 2002. Kinetics of the ultrastructural changes in apoptotic chondrocytes from an osteoarthrosis rat model: a window of comparison to the cellular mechanism of apoptosis in human chondrocytes. *Ultrastructural Pathology,* 26**,** 33-40.

KOVAČIĆ, N., LUKIĆ, I. K., GRČEVIĆ, D., KATAVIĆ, V., CROUCHER, P. & MARUŠIĆ, A. 2007. Fas/Fas ligand system inhibits differentiation of murine

osteoblasts but has a limited role in osteoblast and osteoclast apoptosis. *Journal of Immunology,* 178**,** 3379-3389.

KOYAMA, E., YOUNG, B., NAGAYAMA, M., SHIBUKAWA, Y., ENOMOTO-IWAMOTO, M., IWAMOTO, M., MAEDA, Y., LANSKE, B., SONG, B., SERRA, R. & PACIFICI, M. 2007. Conditional Kif3a ablation causes abnormal hedgehog signaling topography, growth plate dysfunction, and excessive bone and cartilage formation during mouse skeletogenesis. *Development,* 134**,** 2159-69.

KOZHEMYAKINA, E., LASSAR, A. B. & ZELZER, E. 2015. A pathway to bone: signaling molecules and transcription factors involved in chondrocyte development and maturation. *Development,* 142**,** 817-31.

KREJCI, P., AKLIAN, A., KAUCKA, M., SEVCIKOVA, E., PROCHAZKOVA, J., MASEK, J. K., MIKOLKA, P., POSPISILOVA, T., SPOUSTOVA, T., WEIS, M., PAZNEKAS, W. A., WOLF, J. H., GUTKIND, J. S., WILCOX, W. R., KOZUBIK, A., JABS, E. W., BRYJA, V., SALAZAR, L., VESELA, I. & BALEK, L. 2012. Receptor tyrosine kinases activate canonical WNT/beta-catenin signaling via MAP kinase/LRP6 pathway and direct beta-catenin phosphorylation. *PLoS ONE,* 7**,** e35826.

KRONENBERG, H. M. 2003. Developmental regulation of the growth plate. *Nature,* 423**,** 332-6.

KUMAR, D. & LASSAR, A. B. 2014. FGF maintains chondrogenic potential of limb bud mesenchymal cells by modulating DNMT3A recruitment. *Cell reports,* 8**,** 1419-1431.

KURIMCHAK, A., HAINES, D. S., GARRIGA, J., WU, S., DE LUCA, F., SWEREDOSKI, M. J., DESHAIES, R. J., HESS, S. & GRAÑA, X. 2013. Activation of p107 by Fibroblast Growth Factor, Which Is Essential for Chondrocyte Cell Cycle Exit, Is Mediated by the Protein Phosphatase 2A/B55 α Holoenzyme. *Molecular and Cellular Biology,* 33**,** 3330-3342.

KWAK, H. B., HA, H., KIM, H. N., LEE, J. H., KIM, H. S., LEE, S., KIM, H. M., KIM, J. Y., KIM, H. H., SONG, Y. W. & LEE, Z. H. 2008. Reciprocal cross-talk between RANKL and interferon-gamma-inducible protein 10 is responsible for bone-erosive experimental arthritis. *Arthritis & Rheumatism,* 58**,** 1332-42.

LAGASSE, E. & WEISSMAN, I. L. 1997. Enforced expression of Bcl-2 in monocytes rescues macrophages and partially reverses osteopetrosis in op/op mice. *Cell,* 89**,** 1021-31.

LAKKAKORPI, P., TUUKKANEN, J., HENTUNEN, T., JARVELIN, K. & VAANANEN, K. 1989. Organization of osteoclast microfilaments during the attachment to bone surface in vitro. *Journal of Bone and Mineral Research,* 4**,** 817-25.

LAMOTHE, B., WEBSTER, W. K., GOPINATHAN, A., BESSE, A., CAMPOS, A. D. & DARNAY, B. G. 2007. TRAF6 Ubiquitin Ligase is Essential for RANKL Signaling and Osteoclast Differentiation. *Biochemical and Biophysical Research Communications,* 359**,** 1044-9.

LANSKE, B., KARAPLIS, A. C., LEE, K., LUZ, A., VORTKAMP, A., PIRRO, A., KARPERIEN, M., DEFIZE, L. H., HO, C., MULLIGAN, R. C., ABOU-SAMRA, A. B., JUPPNER, H., SEGRE, G. V. & KRONENBERG, H. M. 1996. PTH/PTHrP receptor in early development and Indian hedgehog-regulated bone growth. *Science,* 273**,** 663-6.

LEBOY, P., GRASSO-KNIGHT, G., D'ANGELO, M., VOLK, S. W., LIAN, J. V., DRISSI, H., STEIN, G. S. & ADAMS, S. L. 2001. Smad-Runx interactions during chondrocyte maturation. *Journal of Bone and Joint Surgery,* 83-A Suppl 1**,** S15-22.

LEE, A. H., IWAKOSHI, N. N. & GLIMCHER, L. H. 2003. XBP-1 regulates a subset of endoplasmic reticulum resident chaperone genes in the unfolded protein response. *Molecular Cell Biology,* 23**,** 7448-59.

LEE, H.-H. & BEHRINGER, R. R. 2007. Conditional Expression of Wnt4 during Chondrogenesis Leads to Dwarfism in Mice. *PLoS ONE,* 2**,** e450.

LEE, J. H., KIM, H. N., KIM, K. O., JIN, W. J., LEE, S., KIM, H. H., HA, H. & LEE, Z. H. 2012. CXCL10 promotes osteolytic bone metastasis by enhancing cancer outgrowth and osteoclastogenesis. *Cancer Research,* 72**,** 3175-86.

LEE, K. S., HONG, S. H. & BAE, S. C. 2002. Both the Smad and p38 MAPK pathways play a crucial role in Runx2 expression following induction by transforming growth factor-beta and bone morphogenetic protein. *Oncogene,* 21**,** 7156-63.

LEE, M. S., LOWE, G. N., STRONG, D. D., WERGEDAL, J. E. & GLACKIN, C. A. 1999. TWIST, a basic helix-loop-helix transcription factor, can regulate the human osteogenic lineage. *Journal of Cellular Biochemistry,* 75**,** 566-77.

LEFEBVRE, V., BEHRINGER, R. R. & DE CROMBRUGGHE, B. 2001. L-Sox5, Sox6 and Sox9 control essential steps of the chondrocyte differentiation pathway. *Osteoarthritis Cartilage,* 9 Suppl A**,** S69-75.

LEFEBVRE, V., HUANG, W., HARLEY, V. R., GOODFELLOW, P. N. & DE CROMBRUGGHE, B. 1997. SOX9 is a potent activator of the chondrocyte-specific enhancer of the pro alpha1(II) collagen gene. *Molecular Cell Biology,* 17**,** 2336-46.

LEFEBVRE, V., LI, P. & DE CROMBRUGGHE, B. 1998. A new long form of Sox5 (L-Sox5), Sox6 and Sox9 are coexpressed in chondrogenesis and cooperatively activate the type II collagen gene. *EMBO Journal,* 17**,** 5718-33.

LEGEAI-MALLET, L., BENOIST-LASSELIN, C., MUNNICH, A. & BONAVENTURE, J. 2004. Overexpression of FGFR3, Stat1, Stat5 and p21Cip1 correlates with phenotypic severity and defective chondrocyte differentiation in FGFR3-related chondrodysplasias. *Bone,* 34**,** 26-36.

LEIGHTON, M. P., NUNDLALL, S., STARBORG, T., MEADOWS, R. S., SULEMAN, F., KNOWLES, L., WAGENER, R., THORNTON, D. J., KADLER, K. E., BOOT-HANDFORD, R. P. & BRIGGS, M. D. 2007. Decreased chondrocyte proliferation and dysregulated apoptosis in the cartilage growth plate are key features of a murine model of epiphyseal dysplasia caused by a matn3 mutation. *Human Molecular Genetics,* 16**,** 1728-41.

LEMMON, M. A. & SCHLESSINGER, J. 2010. Cell signaling by receptor tyrosine kinases. *Cell,* 141**,** 1117-34.

LI, J., SAROSI, I., CATTLEY, R. C., PRETORIUS, J., ASUNCION, F., GRISANTI, M., MORONY, S., ADAMU, S., GENG, Z., QIU, W., KOSTENUIK, P., LACEY, D. L., SIMONET, W. S., BOLON, B., QIAN, X., SHALHOUB, V., OMINSKY, M. S., ZHU KE, H., LI, X. & RICHARDS, W. G. 2006. Dkk1-mediated inhibition of Wnt signaling in bone results in osteopenia. *Bone,* 39**,** 754-66.

LI, J., SAROSI, I., YAN, X. Q., MORONY, S., CAPPARELLI, C., TAN, H. L., MCCABE, S., ELLIOTT, R., SCULLY, S., VAN, G., KAUFMAN, S., JUAN, S. C., SUN, Y., TARPLEY, J., MARTIN, L., CHRISTENSEN, K., MCCABE, J., KOSTENUIK, P., HSU, H., FLETCHER, F., DUNSTAN, C. R., LACEY, D. L. & BOYLE, W. J. 2000. RANK is the intrinsic hematopoietic cell surface receptor that controls osteoclastogenesis and regulation of bone mass and calcium metabolism. *Proceedings of the National Academy of Sciences of the United States of America,* 97**,** 1566-71.

LI, X., OMINSKY, M. S., NIU, Q. T., SUN, N., DAUGHERTY, B., D'AGOSTIN, D., KURAHARA, C., GAO, Y., CAO, J., GONG, J., ASUNCION, F., BARRERO,

M., WARMINGTON, K., DWYER, D., STOLINA, M., MORONY, S., SAROSI, I., KOSTENUIK, P. J., LACEY, D. L., SIMONET, W. S., KE, H. Z. & PASZTY, C. 2008. Targeted deletion of the sclerostin gene in mice results in increased bone formation and bone strength. *Journal of Bone and Mineral Research,* 23**,** 860-9.

LI, X., QIN, L., BERGENSTOCK, M., BEVELOCK, L. M., NOVACK, D. V. & PARTRIDGE, N. C. 2007. Parathyroid hormone stimulates osteoblastic expression of MCP-1 to recruit and increase the fusion of pre/osteoclasts. *Journal of Biological Chemistry,* 282**,** 33098-106.

LI, X., ZHANG, Y., KANG, H., LIU, W., LIU, P., ZHANG, J., HARRIS, S. E. & WU, D. 2005. Sclerostin binds to LRP5/6 and antagonizes canonical Wnt signaling. *Journal of Biological Chemistry,* 280**,** 19883-7.

LIAN, J. B., MCKEE, M. D., TODD, A. M. & GERSTENFELD, L. C. 1993. Induction of bone-related proteins, osteocalcin and osteopontin, and their matrix ultrastructural localization with development of chondrocyte hypertrophy in vitro. *Journal of Cellular Biochemistry,* 52**,** 206-19.

LILLIS, A. P., VAN DUYN, L. B., MURPHY-ULLRICH, J. E. & STRICKLAND, D. K. 2008. The low density lipoprotein receptor-related protein 1: Unique tissue-specific functions revealed by selective gene knockout studies. *Physiological reviews,* 88**,** 887-918.

LIN, C., LU, W., ZHAI, L., BETHEA, T., BERRY, K., QU, Z., WAUD, W. R. & LI, Y. 2011. Mesd Is A General Inhibitor of Different Wnt Ligands In Wnt/LRP Signaling and Inhibits PC-3 Tumor Growth In Vivo. *FEBS Letters,* 585**,** 3120-3125.

LIN, C., MCGOUGH, R., ASWAD, B., BLOCK, J. A. & TEREK, R. 2004. Hypoxia induces HIF-1alpha and VEGF expression in chondrosarcoma cells and chondrocytes. *Journal of Orthopaedic Research,* 22**,** 1175-81.

LIN, J. H., WALTER, P. & YEN, T. S. 2008. Endoplasmic reticulum stress in disease pathogenesis. *Annual Review of Pathology,* 3**,** 399-425.

LIN, S. E., OYAMA, T., NAGASE, T., HARIGAYA, K. & KITAGAWA, M. 2002. Identification of new human mastermind proteins defines a family that consists of positive regulators for notch signaling. *Journal of Biological Chemistry,* 277**,** 50612-20.

LINZ, A., KNIEPER, Y., GRONAU, T., HANSEN, U., ASZODI, A., GARBI, N., HAMMERLING, G. J., PAP, T., BRUCKNER, P. & DREIER, R. 2015. ER Stress During the Pubertal Growth Spurt Results in Impaired Long-Bone Growth in Chondrocyte-Specific ERp57 Knockout Mice. *Journal of Bone and Mineral Research,* 30**,** 1481-93.

LITTLE, R. D., CARULLI, J. P., DEL MASTRO, R. G., DUPUIS, J., OSBORNE, M., FOLZ, C., MANNING, S. P., SWAIN, P. M., ZHAO, S. C., EUSTACE, B., LAPPE, M. M., SPITZER, L., ZWEIER, S., BRAUNSCHWEIGER, K., BENCHEKROUN, Y., HU, X., ADAIR, R., CHEE, L., FITZGERALD, M. G., TULIG, C., CARUSO, A., TZELLAS, N., BAWA, A., FRANKLIN, B., MCGUIRE, S., NOGUES, X., GONG, G., ALLEN, K. M., ANISOWICZ, A., MORALES, A. J., LOMEDICO, P. T., RECKER, S. M., VAN EERDEWEGH, P., RECKER, R. R. & JOHNSON, M. L. 2002. A mutation in the LDL receptor-related protein 5 gene results in the autosomal dominant high-bone-mass trait. *American Journal of Human Genetics,* 70**,** 11-9.

LIU, S., ZHOU, J., TANG, W., JIANG, X., ROWE, D. W. & QUARLES, L. D. 2006. Pathogenic role of Fgf23 in Hyp mice. *American Journal of Physiology-Endocrinology and Metabolism,* 291**,** E38-49.

LIU, W., TOYOSAWA, S., FURUICHI, T., KANATANI, N., YOSHIDA, C., LIU, Y., HIMENO, M., NARAI, S., YAMAGUCHI, A. & KOMORI, T. 2001. Overexpression of Cbfa1 in osteoblasts inhibits osteoblast maturation and causes osteopenia with multiple fractures. *Journal of Cell Biology,* 155**,** 157-66.

LIU, Z., XU, J., COLVIN, J. S. & ORNITZ, D. M. 2002. Coordination of chondrogenesis and osteogenesis by fibroblast growth factor 18. *Genes & Development,* 16**,** 859-69.

LU, P. D., HARDING, H. P. & RON, D. 2004. Translation reinitiation at alternative open reading frames regulates gene expression in an integrated stress response. *Journal of Cell Biology,* 167**,** 27-33.

LUM, L., WONG, B. R., JOSIEN, R., BECHERER, J. D., ERDJUMENT-BROMAGE, H., SCHLONDORFF, J., TEMPST, P., CHOI, Y. & BLOBEL, C. P. 1999. Evidence for a role of a tumor necrosis factor-alpha (TNF-alpha)-converting enzyme-like protease in shedding of TRANCE, a TNF family member involved in osteoclastogenesis and dendritic cell survival. *Journal of Biological Chemistry,* 274**,** 13613-8.

LUO, Q., KANG, Q., SI, W., JIANG, W., PARK, J. K., PENG, Y., LI, X., LUU, H. H., LUO, J., MONTAG, A. G., HAYDON, R. C. & HE, T. C. 2004. Connective tissue growth factor (CTGF) is regulated by Wnt and bone morphogenetic proteins signaling in osteoblast differentiation of mesenchymal stem cells. *Journal of Biological Chemistry,* 279**,** 55958-68.

LYNCH, C. C., HIKOSAKA, A., ACUFF, H. B., MARTIN, M. D., KAWAI, N., SINGH, R. K., VARGO-GOGOLA, T. C., BEGTRUP, J. L., PETERSON, T. E., FINGLETON, B., SHIRAI, T., MATRISIAN, L. M. & FUTAKUCHI, M. 2005. MMP-7 promotes prostate cancer-induced osteolysis via the solubilization of RANKL. *Cancer Cell,* 7**,** 485-96.

LYONS, K. M., HOGAN, B. L. & ROBERTSON, E. J. 1995. Colocalization of BMP 7 and BMP 2 RNAs suggests that these factors cooperatively mediate tissue interactions during murine development. *Mechanisms of Development,* 50**,** 71-83.

MA, Y., BREWER, J. W., DIEHL, J. A. & HENDERSHOT, L. M. 2002. Two distinct stress signaling pathways converge upon the CHOP promoter during the mammalian unfolded protein response. *Journal of Molecular Biology,* 318**,** 1351-65.

MACKIE, E. J., AHMED, Y. A., TATARCZUCH, L., CHEN, K. S. & MIRAMS, M. 2008. Endochondral ossification: how cartilage is converted into bone in the developing skeleton. *International Journal of Biochemical Cell Biology,* 40**,** 46-62.

MACSAI, C. E., FOSTER, B. K. & XIAN, C. J. 2008. Roles of Wnt signalling in bone growth, remodelling, skeletal disorders and fracture repair. *Journal of Cellular Physiology,* 215**,** 578-87.

MAEDA, Y., NAKAMURA, E., NGUYEN, M. T., SUVA, L. J., SWAIN, F. L., RAZZAQUE, M. S., MACKEM, S. & LANSKE, B. 2007. Indian Hedgehog produced by postnatal chondrocytes is essential for maintaining a growth plate and trabecular bone. *Proceedings of the National Academy of Sciences of the United States of America,* 104**,** 6382-7.

MAES, C., KOBAYASHI, T., SELIG, M. K., TORREKENS, S., ROTH, S. I., MACKEM, S., CARMELIET, G. & KRONENBERG, H. M. 2010. Osteoblast precursors, but not mature osteoblasts, move into developing and fractured bones along with invading blood vessels. *Developmental Cell,* 19**,** 329-44.

MAIUOLO, J., BULOTTA, S., VERDERIO, C., BENFANTE, R. & BORGESE, N. 2011. Selective activation of the transcription factor ATF6 mediates

endoplasmic reticulum proliferation triggered by a membrane protein. *Proceedings of the National Academy of Sciences of the United States of America,* 108**,** 7832-7.
MANOLAGAS, S. C. 1995. Role of cytokines in bone resorption. *Bone,* 17**,** 63S-67S.
MANSUKHANI, A., BELLOSTA, P., SAHNI, M. & BASILICO, C. 2000. Signaling by fibroblast growth factors (FGF) and fibroblast growth factor receptor 2 (FGFR2)-activating mutations blocks mineralization and induces apoptosis in osteoblasts. *Journal of Cell Biology,* 149**,** 1297-308.
MAO, Y., KUTA, A., CRESPO-ENRIQUEZ, I., WHITING, D., MARTIN, T., MULVANEY, J., IRVINE, K. D. & FRANCIS-WEST, P. 2016. Dchs1-Fat4 regulation of polarized cell behaviours during skeletal morphogenesis. *Nature Communications,* 7**,** 11469.
MARCHISIO, P. C., CIRILLO, D., NALDINI, L., PRIMAVERA, M. V., TETI, A. & ZAMBONIN-ZALLONE, A. 1984. Cell-substratum interaction of cultured avian osteoclasts is mediated by specific adhesion structures. *Journal of Cell Biology,* 99**,** 1696-705.
MARCINIAK, S. J., YUN, C. Y., OYADOMARI, S., NOVOA, I., ZHANG, Y., JUNGREIS, R., NAGATA, K., HARDING, H. P. & RON, D. 2004. CHOP induces death by promoting protein synthesis and oxidation in the stressed endoplasmic reticulum. *Genes & Development,* 18**,** 3066-77.
MARIE, P. J. 2003. Fibroblast growth factor signaling controlling osteoblast differentiation. *Gene,* 316**,** 23-32.
MARIGO, V., DAVEY, R. A., ZUO, Y., CUNNINGHAM, J. M. & TABIN, C. J. 1996. Biochemical evidence that patched is the Hedgehog receptor. *Nature,* 384**,** 176-9.
MARINO, S., LOGAN, J. G., MELLIS, D. & CAPULLI, M. 2014. Generation and culture of osteoclasts. *Bonekey Reports,* 3.
MARTIN, A., LIU, S., DAVID, V., LI, H., KARYDIS, A., FENG, J. Q. & QUARLES, L. D. 2011. Bone proteins PHEX and DMP1 regulate fibroblastic growth factor Fgf23 expression in osteocytes through a common pathway involving FGF receptor (FGFR) signaling. *FASEB JOURNALOURNAL,* 25**,** 2551-62.
MARTIN, G. R. 1998. The roles of FGFs in the early development of vertebrate limbs. *Genes & Development,* 12**,** 1571-86.
MARUYAMA, Z., YOSHIDA, C. A., FURUICHI, T., AMIZUKA, N., ITO, M., FUKUYAMA, R., MIYAZAKI, T., KITAURA, H., NAKAMURA, K., FUJITA, T., KANATANI, N., MORIISHI, T., YAMANA, K., LIU, W., KAWAGUCHI, H., NAKAMURA, K. & KOMORI, T. 2007. Runx2 determines bone maturity and turnover rate in postnatal bone development and is involved in bone loss in estrogen deficiency. *Developmenal Dynamics,* 236**,** 1876-90.
MASLEN, C. L., BABCOCK, D., REDIG, J. K., KAPELI, K., AKKARI, Y. M. & OLSON, S. B. 2006. CRELD2: gene mapping, alternate splicing, and comparative genomic identification of the promoter region. *Gene,* 382**,** 111-20.
MASS, E., WACHTEN, D., ASCHENBRENNER, A. C., VOELZMANN, A. & HOCH, M. 2014. Murine Creld1 controls cardiac development through activation of calcineurin/NFATc1 signaling. *Developmental Cell,* 28**,** 711-26.
MATEOS, J., DE LA FUENTE, A., LESENDE-RODRIGUEZ, I., FERNANDEZ-PERNAS, P., ARUFE, M. C. & BLANCO, F. J. 2013. Lamin A deregulation in human mesenchymal stem cells promotes an impairment in their chondrogenic potential and imbalance in their response to oxidative stress. *Stem Cell Research,* 11**,** 1137-48.
MATSUBARA, T., KIDA, K., YAMAGUCHI, A., HATA, K., ICHIDA, F., MEGURO, H., ABURATANI, H., NISHIMURA, R. & YONEDA, T. 2008.

BMP2 regulates Osterix through Msx2 and Runx2 during osteoblast differentiation. *Journal of Biological Chemistry,* 283**,** 29119-25.

MATSUNOBU, T., TORIGOE, K., ISHIKAWA, M., DE VEGA, S., KULKARNI, A. B., IWAMOTO, Y. & YAMADA, Y. 2009. Critical roles of the TGF-β type I receptor ALK5 in perichondrial formation and function, cartilage integrity, and osteoblast differentiation during growth plate development. *Developmental Biology,* 332**,** 325-38.

MATSUO, K., IRIE, N. 2008. Osteoclast–osteoblast communication. *Archives of Biochemistry and Biophysics,* 473**,** 201-209.

MATTSSON, J. P., SCHLESINGER, P. H., KEELING, D. J., TEITELBAUM, S. L., STONE, D. K. & XIE, X. S. 1994. Isolation and reconstitution of a vacuolar-type proton pump of osteoclast membranes. *Journal of Biological Chemistry,* 269**,** 24979-82.

MCGLASHAN, S. R., HAYCRAFT, C. J., JENSEN, C. G., YODER, B. K. & POOLE, C. A. 2007. Articular cartilage and growth plate defects are associated with chondrocyte cytoskeletal abnormalities in Tg737orpk mice lacking the primary cilia protein polaris. *Matrix Biology,* 26**,** 234-46.

MELNICK, J., DUL, J. L. & ARGON, Y. 1994. Sequential interaction of the chaperones BiP and GRP94 with immunoglobulin chains in the endoplasmic reticulum. *Nature,* 370**,** 373-5.

MIAO, D. & SCUTT, A. 2002. Histochemical localization of alkaline phosphatase activity in decalcified bone and cartilage. *Journal of Histochemistry & Cytochemistry,* 50**,** 333-40.

MIKHAILENKO, I., KRYLOV, D., ARGRAVES, K. M., ROBERTS, D. D., LIAU, G. & STRICKLAND, D. K. 1997. Cellular internalization and degradation of thrombospondin-1 is mediated by the amino-terminal heparin binding domain (HBD). High affinity interaction of dimeric HBD with the low density lipoprotein receptor-related protein. *Journal of Biological Chemistry,* 272**,** 6784-91.

MIKUNI-TAKAGAKI, Y., KAKAI, Y., SATOYOSHI, M., KAWANO, E., SUZUKI, Y., KAWASE, T. & SAITO, S. 1995. Matrix mineralization and the differentiation of osteocyte-like cells in culture. *Journal of Bone and Mineral Research,* 10**,** 231-42.

MILNER, C. M. & DAY, A. J. 2003. TSG-6: a multifunctional protein associated with inflammation. *Journal of Cell Science,* 116**,** 1863-73.

MININA, E., WENZEL, H. M., KRESCHEL, C., KARP, S., GAFFIELD, W., MCMAHON, A. P. & VORTKAMP, A. 2001. BMP and Ihh/PTHrP signaling interact to coordinate chondrocyte proliferation and differentiation. *Development,* 128**,** 4523-34.

MIRAOUI, H., OUDINA, K., PETITE, H., TANIMOTO, Y., MORIYAMA, K. & MARIE, P. J. 2009. Fibroblast growth factor receptor 2 promotes osteogenic differentiation in mesenchymal cells via ERK1/2 and protein kinase C signaling. *Journal of Biological Chemistry,* 284**,** 4897-904.

MISHINA, Y., STARBUCK, M. W., GENTILE, M. A., FUKUDA, T., KASPARCOVA, V., SEEDOR, J. G., HANKS, M. C., AMLING, M., PINERO, G. J., HARADA, S. & BEHRINGER, R. R. 2004. Bone morphogenetic protein type IA receptor signaling regulates postnatal osteoblast function and bone remodeling. *Journal of Biological Chemistry,* 279**,** 27560-6.

MIZUKAMI, J., TAKAESU, G., AKATSUKA, H., SAKURAI, H., NINOMIYA-TSUJI, J., MATSUMOTO, K. & SAKURAI, N. 2002. Receptor Activator of NF-κB Ligand (RANKL) Activates TAK1 Mitogen-Activated Protein Kinase

Kinase Kinase through a Signaling Complex Containing RANK, TAB2, and TRAF6. *Molecular Cell Biology,* 22**,** 992-1000.

MKRTCHIAN, S. & SANDALOVA, T. 2006. ERp29, an unusual redox-inactive member of the thioredoxin family. *Antioxidants & Redox Signalling,* 8**,** 325-37.

MO, F.-E., MUNTEAN, A. G., CHEN, C.-C., STOLZ, D. B., WATKINS, S. C. & LAU, L. F. 2002. CYR61 (CCN1) Is Essential for Placental Development and Vascular Integrity. *Molecular and Cellular Biology,* 22**,** 8709-8720.

MONTERO, A., OKADA, Y., TOMITA, M., ITO, M., TSURUKAMI, H., NAKAMURA, T., DOETSCHMAN, T., COFFIN, J. D. & HURLEY, M. M. 2000. Disruption of the fibroblast growth factor-2 gene results in decreased bone mass and bone formation. *Journal of Clinical Investigation,* 105**,** 1085-93.

MORVAN, F., BOULUKOS, K., CLEMENT-LACROIX, P., ROMAN ROMAN, S., SUC-ROYER, I., VAYSSIERE, B., AMMANN, P., MARTIN, P., PINHO, S., POGNONEC, P., MOLLAT, P., NIEHRS, C., BARON, R. & RAWADI, G. 2006. Deletion of a single allele of the Dkk1 gene leads to an increase in bone formation and bone mass. *Journal of Bone and Mineral Research,* 21**,** 934-45.

MOSES, M. A., SUDHALTER, J. & LANGER, R. 1990. Identification of an inhibitor of neovascularization from cartilage. *Science,* 248**,** 1408-10.

MOSES, M. A., SUDHALTER, J. & LANGER, R. 1992. Isolation and characterization of an inhibitor of neovascularization from scapular chondrocytes. *Journal of Cell Biology,* 119**,** 475-82.

MOSKALEWSKI, S. & MALEJCZYK, J. 1989. Bone formation following intrarenal transplantation of isolated murine chondrocytes: chondrocyte-bone cell transdifferentiation? *Development,* 107**,** 473-80.

MUNDY, C., GANNON, M. & POPOFF, S. N. 2014. Connective Tissue Growth Factor (CTGF/CCN2) Negatively Regulates BMP-2 Induced Osteoblast Differentiation and Signaling. *Journal of Cellular Physiology,* 229**,** 672-681.

MURAGAKI, Y., MARIMAN, E. C., VAN BEERSUM, S. E., PERALA, M., VAN MOURIK, J. B., WARMAN, M. L., OLSEN, B. R. & HAMEL, B. C. 1996. A mutation in the gene encoding the alpha 2 chain of the fibril-associated collagen IX, COL9A2, causes multiple epiphyseal dysplasia (EDM2). *Nature Genetics,* 12**,** 103-5.

MURAKAMI, S., KAN, M., MCKEEHAN, W. L. & DE CROMBRUGGHE, B. 2000. Up-regulation of the chondrogenic Sox9 gene by fibroblast growth factors is mediated by the mitogen-activated protein kinase pathway. *Proceedings of the National Academy of Sciences of the United States of America,* 97**,** 1113-1118.

MURAKAMI, T., HINO, S., NISHIMURA, R., YONEDA, T., WANAKA, A. & IMAIZUMI, K. 2011a. Distinct mechanisms are responsible for osteopenia and growth retardation in OASIS-deficient mice. *Bone,* 48**,** 514-23.

MURAKAMI, T., HINO, S.-I., NISHIMURA, R., YONEDA, T., WANAKA, A. & IMAIZUMI, K. 2011b. Distinct mechanisms are responsible for osteopenia and growth retardation in OASIS-deficient mice. *Bone,* 48**,** 514-523.

MURAKAMI, T., SAITO, A., HINO, S., KONDO, S., KANEMOTO, S., CHIHARA, K., SEKIYA, H., TSUMAGARI, K., OCHIAI, K., YOSHINAGA, K., SAITOH, M., NISHIMURA, R., YONEDA, T., KOU, I., FURUICHI, T., IKEGAWA, S., IKAWA, M., OKABE, M., WANAKA, A. & IMAIZUMI, K. 2009. Signalling mediated by the endoplasmic reticulum stress transducer OASIS is involved in bone formation. *Nature Cell Biology,* 11**,** 1205-11.

NAGAI, H. & AOKI, M. 2002. Inhibition of growth plate angiogenesis and endochondral ossification with diminished expression of MMP-13 in hypertrophic chondrocytes in FGF-2-treated rats. *Journal of Bone and Mineral Metabolism,* 20**,** 142-7.

NAGANAWA, T., XIAO, L., COFFIN, J. D., DOETSCHMAN, T., SABBIETI, M. G., AGAS, D. & HURLEY, M. M. 2008. Reduced expression and function of bone morphogenetic protein-2 in bones of Fgf2 null mice. *Journal of Cellular Biochemistry,* 103**,** 1975-88.

NAKANISHI, T., NISHIDA, T., SHIMO, T., KOBAYASHI, K., KUBO, T., TAMATANI, T., TEZUKA, K. & TAKIGAWA, M. 2000. Effects of CTGF/Hcs24, a product of a hypertrophic chondrocyte-specific gene, on the proliferation and differentiation of chondrocytes in culture. *Endocrinology,* 141**,** 264-73.

NAKASHIMA, K., ZHOU, X., KUNKEL, G., ZHANG, Z., DENG, J. M., BEHRINGER, R. R. & DE CROMBRUGGHE, B. 2002. The novel zinc finger-containing transcription factor osterix is required for osteoblast differentiation and bone formation. *Cell,* 108**,** 17-29.

NAMPEI, A., HASHIMOTO, J., HAYASHIDA, K., TSUBOI, H., SHI, K., TSUJI, I., MIYASHITA, H., YAMADA, T., MATSUKAWA, N., MATSUMOTO, M., MORIMOTO, S., OGIHARA, T., OCHI, T. & YOSHIKAWA, H. 2004. Matrix extracellular phosphoglycoprotein (MEPE) is highly expressed in osteocytes in human bone. *Journal of Bone and Mineral Metabolism,* 22**,** 176-84.

NASKI, M. C., COLVIN, J. S., COFFIN, J. D. & ORNITZ, D. M. 1998. Repression of hedgehog signaling and BMP4 expression in growth plate cartilage by fibroblast growth factor receptor 3. *Development,* 125**,** 4977-88.

NIEMEIER, A., KASSEM, M., TOEDTER, K., WENDT, D., RUETHER, W., BEISIEGEL, U. & HEEREN, J. 2005. Expression of LRP1 by human osteoblasts: a mechanism for the delivery of lipoproteins and vitamin K1 to bone. *Journal of Bone and Mineral Research,* 20**,** 283-93.

NIGER, C., LUCIOTTI, M. A., BUO, A. M., HEBERT, C., MA, V. & STAINS, J. P. 2013. The Regulation of Runx2 by FGF2 and Connexin43 Requires the Inositol Polyphosphate/Protein Kinase C δ Cascade. *Journal of Bone and Mineral Research,* 28**,** 1468-77.

NIKAIDO, T., YOKOYA, S., MORI, T., HAGINO, S., ISEKI, K., ZHANG, Y., TAKEUCHI, M., TAKAKI, H., KIKUCHI, S. & WANAKA, A. 2001. Expression of the novel transcription factor OASIS, which belongs to the CREB/ATF family, in mouse embryo with special reference to bone development. *Histochemistry and Cell Biology,* 116**,** 141-8.

NILSSON, O., PARKER, E. A., HEGDE, A., CHAU, M., BARNES, K. M. & BARON, J. 2007. Gradients in bone morphogenetic protein-related gene expression across the growth plate. *Journal of Endocrinology,* 193**,** 75-84.

NISHIDA, T., KUBOTA, S., NAKANISHI, T., KUBOKI, T., YOSIMICHI, G., KONDO, S. & TAKIGAWA, M. 2002. CTGF/Hcs24, a hypertrophic chondrocyte-specific gene product, stimulates proliferation and differentiation, but not hypertrophy of cultured articular chondrocytes. *Journal of Cellular Physiology,* 192**,** 55-63.

NISTALA, H., LEE-ARTEAGA, S., SMALDONE, S., SICILIANO, G., CARTA, L., ONO, R. N., SENGLE, G., ARTEAGA-SOLIS, E., LEVASSEUR, R., DUCY, P., SAKAI, L. Y., KARSENTY, G. & RAMIREZ, F. 2010a. Fibrillin-1 and -2 differentially modulate endogenous TGF-β and BMP bioavailability during bone formation. *The Journal of Cell Biology,* 190**,** 1107-1121.

NISTALA, H., LEE-ARTEAGA, S., SMALDONE, S., SICILIANO, G. & RAMIREZ, F. 2010b. Extracellular Microfibrils Control Osteoblast-supported Osteoclastogenesis by Restricting TGFβ Stimulation of RANKL Production. *The Journal of Biological Chemistry,* 285**,** 34126-34133.

NOEL, D., GAZIT, D., BOUQUET, C., APPARAILLY, F., BONY, C., PLENCE, P., MILLET, V., TURGEMAN, G., PERRICAUDET, M., SANY, J. & JORGENSEN, C. 2004. Short-term BMP-2 expression is sufficient for in vivo osteochondral differentiation of mesenchymal stem cells. *Stem Cells,* 22**,** 74-85.

NUNDLALL, S., RAJPAR, M. H., BELL, P. A., CLOWES, C., ZEEFF, L. A., GARDNER, B., THORNTON, D. J., BOOT-HANDFORD, R. P. & BRIGGS, M. D. 2010. An unfolded protein response is the initial cellular response to the expression of mutant matrilin-3 in a mouse model of multiple epiphyseal dysplasia. *Cell Stress Chaperones,* 15**,** 835-49.

OBERLENDER, S. A. & TUAN, R. S. 1994. Expression and functional involvement of N-cadherin in embryonic limb chondrogenesis. *Development,* 120**,** 177-87.

OH, S. K., SHIN, J. O., BAEK, J. I., LEE, J., BAE, J. W., ANKAMERDDY, H., KIM, M. J., HUH, T. L., RYOO, Z. Y., KIM, U. K., BOK, J. & LEE, K. Y. 2015. Pannexin 3 is required for normal progression of skeletal development in vertebrates. *FASEB Journal,* 29**,** 4473-84.

OH-HASHI, K., KOGA, H., IKEDA, S., SHIMADA, K., HIRATA, Y. & KIUCHI, K. 2009. CRELD2 is a novel endoplasmic reticulum stress-inducible gene. *Biochemical and Biophysical Research Communications,* 387**,** 504-10.

OH-HASHI, K., KUNIEDA, R., HIRATA, Y. & KIUCHI, K. 2011. Biosynthesis and secretion of mouse cysteine-rich with EGF-like domains 2. *FEBS Letters,* 585**,** 2481-7.

OHBAYASHI, N., SHIBAYAMA, M., KUROTAKI, Y., IMANISHI, M., FUJIMORI, T., ITOH, N. & TAKADA, S. 2002. FGF18 is required for normal cell proliferation and differentiation during osteogenesis and chondrogenesis. *Genes & Development,* 16**,** 870-9.

OKA, K., OKA, S., SASAKI, T., ITO, Y., BRINGAS, P., NONAKA, K. & CHAI, Y. 2007. The role of TGF-β signaling in regulating chondrogenesis and osteogenesis during mandibular development. *Developmental Biology,* 303**,** 391-404.

ORCI, L., STAMNES, M., RAVAZZOLA, M., AMHERDT, M., PERRELET, A., SOLLNER, T. H. & ROTHMAN, J. E. 1997. Bidirectional transport by distinct populations of COPI-coated vesicles. *Cell,* 90**,** 335-49.

ORIMO, H. 2010. The mechanism of mineralization and the role of alkaline phosphatase in health and disease. *Journal of Nippen Medical School,* 77**,** 4-12.

ORNITZ, D. M. 2000. FGFs, heparan sulfate and FGFRs: complex interactions essential for development. *Bioessays,* 22**,** 108-12.

ORNITZ, D. M. & ITOH, N. 2001. Fibroblast growth factors. *Genome Biology,* 2**,** reviews3005.1-reviews3005.12.

ORNITZ, D. M. & MARIE, P. J. 2015. Fibroblast growth factor signaling in skeletal development and disease. *Genes & Development,* 29**,** 1463-86.

ORR-URTREGER, A., GIVOL, D., YAYON, A., YARDEN, Y. & LONAI, P. 1991. Developmental expression of two murine fibroblast growth factor receptors, flg and bek. *Development,* 113**,** 1419-34.

ORTIZ, J. A., CASTILLO, M., DEL TORO, E. D., MULET, J., GERBER, S., VALOR, L. M., SALA, S., SALA, F., GUTIERREZ, L. M. & CRIADO, M. 2005. The cysteine-rich with EGF-like domains 2 (CRELD2) protein interacts with the large cytoplasmic domain of human neuronal nicotinic acetylcholine receptor alpha4 and beta2 subunits. *Journal of Neurochemistry,* 95**,** 1585-96.

ORTUNO, M. J., RUIZ-GASPA, S., RODRIGUEZ-CARBALLO, E., SUSPERREGUI, A. R., BARTRONS, R., ROSA, J. L. & VENTURA, F. 2010. p38 regulates expression of osteoblast-specific genes by phosphorylation of osterix. *Journal of Biological Chemistry,* 285**,** 31985-94.

OTTEN, C., HANSEN, U., TALKE, A., WAGENER, R., PAULSSON, M. & ZAUCKE, F. 2010. A matrilin-3 mutation associated with osteoarthritis does not affect collagen affinity but promotes the formation of wider cartilage collagen fibrils. *Human Mutation,* 31**,** 254-63.

OTTO, F., THORNELL, A. P., CROMPTON, T., DENZEL, A., GILMOUR, K. C., ROSEWELL, I. R., STAMP, G. W., BEDDINGTON, R. S., MUNDLOS, S., OLSEN, B. R., SELBY, P. B. & OWEN, M. J. 1997. Cbfa1, a candidate gene for cleidocranial dysplasia syndrome, is essential for osteoblast differentiation and bone development. *Cell,* 89**,** 765-71.

OZCAN, U., YILMAZ, E., OZCAN, L., FURUHASHI, M., VAILLANCOURT, E., SMITH, R. O., GORGUN, C. Z. & HOTAMISLIGIL, G. S. 2006. Chemical chaperones reduce ER stress and restore glucose homeostasis in a mouse model of type 2 diabetes. *Science,* 313**,** 1137-40.

OZEKI, N., MOGI, M., NAKAMURA, H. & TOGARI, A. 2002. Differential expression of the Fas-Fas ligand system on cytokine-induced apoptotic cell death in mouse osteoblastic cells. *Archives of Oral Biology,* 47**,** 511-7.

PAASSILTA, P., LOHINIVA, J., ANNUNEN, S., BONAVENTURE, J., LE MERRER, M., PAI, L. & ALA-KOKKO, L. 1999. COL9A3: A third locus for multiple epiphyseal dysplasia. *American Journal of Human Genetics,* 64**,** 1036-44.

PALUMBO, C., PALAZZINI, S., ZAFFE, D. & MAROTTI, G. 1990. Osteocyte differentiation in the tibia of newborn rabbit: an ultrastructural study of the formation of cytoplasmic processes. *Acta Anatomica (Basel),* 137**,** 350-8.

PARK, H. W., KIM, Y. C., YU, B., MOROISHI, T., MO, J. S., PLOUFFE, S. W., MENG, Z., LIN, K. C., YU, F. X., ALEXANDER, C. M., WANG, C. Y. & GUAN, K. L. 2015a. Alternative Wnt Signaling Activates YAP/TAZ. *Cell,* 162**,** 780-94.

PARK, J., GEBHARDT, M., GOLOVCHENKO, S., PEREZ-BRANGULI, F., HATTORI, T., HARTMANN, C., ZHOU, X., DECROMBRUGGHE, B., STOCK, M., SCHNEIDER, H. & VON DER MARK, K. 2015b. Dual pathways to endochondral osteoblasts: a novel chondrocyte-derived osteoprogenitor cell identified in hypertrophic cartilage. *Biology Open,* 4**,** 608-21.

PARK, O. J., KIM, H. J., WOO, K. M., BAEK, J. H. & RYOO, H. M. 2010. FGF2-activated ERK mitogen-activated protein kinase enhances Runx2 acetylation and stabilization. *Journal of Biological Chemistry,* 285**,** 3568-74.

PATHI, S., RUTENBERG, J. B., JOHNSON, R. L. & VORTKAMP, A. 1999. Interaction of Ihh and BMP/Noggin Signaling during Cartilage Differentiation. *Developmental Biology,* 209**,** 239-253.

PEARSE, B. R., GABRIEL, L., WANG, N. & HEBERT, D. N. 2008. A cell-based reglucosylation assay demonstrates the role of GT1 in the quality control of a maturing glycoprotein. *Journal of Cell Biology,* 181**,** 309-20.

PEDERSON, L., RUAN, M., WESTENDORF, J. J., KHOSLA, S. & OURSLER, M. J. 2008. Regulation of bone formation by osteoclasts involves Wnt/BMP signaling and the chemokine sphingosine-1-phosphate. *Proceedings of the National Academy of Sciences of the United States of America,* 105**,** 20764-9.

PEPPER, M. S., MONTESANO, R., VASSALLI, J. D. & ORCI, L. 1991. Chondrocytes inhibit endothelial sprout formation in vitro: evidence for involvement of a transforming growth factor-beta. *Journal of Cellular Physiology,* 146**,** 170-9.

PETERS, K., ORNITZ, D., WERNER, S. & WILLIAMS, L. 1993. Unique expression pattern of the FGF receptor 3 gene during mouse organogenesis. *Developmental Biology,* 155**,** 423-30.

PETERS, K. G., WERNER, S., CHEN, G. & WILLIAMS, L. T. 1992. Two FGF receptor genes are differentially expressed in epithelial and mesenchymal tissues during limb formation and organogenesis in the mouse. *Development,* 114**,** 233-43.

PETERSON, J. R., ORA, A., VAN, P. N. & HELENIUS, A. 1995. Transient, lectin-like association of calreticulin with folding intermediates of cellular and viral glycoproteins. *Molecular Biology of the Cell,* 6**,** 1173-84.

PFEILSCHIFTER, J. & MUNDY, G. R. 1987. Modulation of type beta transforming growth factor activity in bone cultures by osteotropic hormones. *Proceedings of the National Academy of Sciences of the United States of America,* 84**,** 2024-8.

PIRÓG-GARCIA, K. A., MEADOWS, R. S., KNOWLES, L., HEINEGÅRD, D., THORNTON, D. J., KADLER, K. E., BOOT-HANDFORD, R. P. & BRIGGS, M. D. 2007. Reduced cell proliferation and increased apoptosis are significant pathological mechanisms in a murine model of mild pseudoachondroplasia resulting from a mutation in the C-terminal domain of COMP. *Human Molecular Genetics,* 16**,** 2072-88.

PITERS, E., CULHA, C., MOESTER, M., VAN BEZOOIJEN, R., ADRIAENSEN, D., MUELLER, T., WEIDAUER, S., JENNES, K., DE FREITAS, F., LOWIK, C., TIMMERMANS, J. P., VAN HUL, W. & PAPAPOULOS, S. 2010. First missense mutation in the SOST gene causing sclerosteosis by loss of sclerostin function. *Human Mutation,* 31**,** E1526-43.

PITTENGER, M. F., MACKAY, A. M., BECK, S. C., JAISWAL, R. K., DOUGLAS, R., MOSCA, J. D., MOORMAN, M. A., SIMONETTI, D. W., CRAIG, S. & MARSHAK, D. R. 1999. Multilineage potential of adult human mesenchymal stem cells. *Science,* 284**,** 143-7.

POGUE, R. & LYONS, K. 2006. BMP signaling in the cartilage growth plate. *Current Topics in Developmental Biology,* 76**,** 1-48.

POOLE, K. E., VAN BEZOOIJEN, R. L., LOVERIDGE, N., HAMERSMA, H., PAPAPOULOS, S. E., LOWIK, C. W. & REEVE, J. 2005. Sclerostin is a delayed secreted product of osteocytes that inhibits bone formation. *FASEB Journal,* 19**,** 1842-4.

PROCKOP, D. J. 1997. Marrow stromal cells as stem cells for nonhematopoietic tissues. *Science,* 276**,** 71-4.

PURCELL, P., JOO, B. W., HU, J. K., TRAN, P. V., CALICCHIO, M. L., O'CONNELL, D. J., MAAS, R. L. & TABIN, C. J. 2009. Temporomandibular joint formation requires two distinct hedgehog-dependent steps. *Proceedings of the National Academy of Sciences of the United States of America,* 106**,** 18297-302.

QING, H., ARDESHIRPOUR, L., PAJEVIC, P. D., DUSEVICH, V., JAHN, K., KATO, S., WYSOLMERSKI, J. & BONEWALD, L. F. 2012. Demonstration of osteocytic perilacunar/canalicular remodeling in mice during lactation. *Journal of Bone and Mineral Research,* 27**,** 1018-29.

RAJPAR, M. H., MCDERMOTT, B., KUNG, L., EARDLEY, R., KNOWLES, L., HEERAN, M., THORNTON, D. J., WILSON, R., BATEMAN, J. F., POULSOM, R., ARVAN, P., KADLER, K. E., BRIGGS, M. D. & BOOT-HANDFORD, R. P. 2009. Targeted induction of endoplasmic reticulum stress induces cartilage pathology. *PLoS Genetics,* 5**,** e1000691.

RAPOPORT, T. A. 2007. Protein translocation across the eukaryotic endoplasmic reticulum and bacterial plasma membranes. *Nature,* 450**,** 663-9.

RAWADI, G., VAYSSIERE, B., DUNN, F., BARON, R. & ROMAN-ROMAN, S. 2003. BMP-2 controls alkaline phosphatase expression and osteoblast

mineralization by a Wnt autocrine loop. *Journal of Bone and Mineral Research,* 18**,** 1842-53.

REDIG, J. K., FOUAD, G. T., BABCOCK, D., RESHEY, B., FEINGOLD, E., REEVES, R. H. & MASLEN, C. L. 2014. Allelic Interaction between CRELD1 and VEGFA in the Pathogenesis of Cardiac Atrioventricular Septal Defects. *AIMS Genetics,* 1**,** 1-19.

REID, D. W. & NICCHITTA, C. V. 2015. Diversity and selectivity in mRNA translation on the endoplasmic reticulum. *Nature Reviews Molecular Cell Biology Cell Biology,* 16**,** 221-231.

REINHOLD, M. I., ABE, M., KAPADIA, R. M., LIAO, Z. & NASKI, M. C. 2004. FGF18 represses noggin expression and is induced by calcineurin. *Journal of Biological Chemistry,* 279**,** 38209-19.

RETTING, K. N., SONG, B., YOON, B. S. & LYONS, K. M. 2009. BMP canonical Smad signaling through Smad1 and Smad5 is. *Development,* 136**,** 1093-104.

RIGUEUR, D., BRUGGER, S., ANBARCHIAN, T., KIM, J. K., LEE, Y. J. & LYONS, K. 2015. The type I BMP receptor ACVR1/ALK2 is required for chondrogenesis during development. *Journal of Bone and Mineral Research,* 30**,** 733-41.

ROACH, H. I. 1994. Why does bone matrix contain non-collagenous proteins? The possible roles of osteocalcin, osteonectin, osteopontin and bone sialoprotein in bone mineralisation and resorption. *Cell Biology International,* 18**,** 617-28.

ROACH, H. I., AIGNER, T. & KOURI, J. B. 2004. Chondroptosis: a variant of apoptotic cell death in chondrocytes? *Apoptosis,* 9**,** 265-77.

ROACH, H. I. & CLARKE, N. M. 1999. "Cell paralysis" as an intermediate stage in the programmed cell death of epiphyseal chondrocytes during development. *Journal of Bone and Mineral Research,* 14**,** 1367-78.

ROACH, H. I. & CLARKE, N. M. 2000. Physiological cell death of chondrocytes in vivo is not confined to apoptosis. New observations on the mammalian growth plate. *Journal of Bone and Joint Surgery British Volume,* 82**,** 601-13.

ROBINSON, S. W., MORRIS, C. D., GOLDMUNTZ, E., RELLER, M. D., JONES, M. A., STEINER, R. D. & MASLEN, C. L. 2003. Missense mutations in CRELD1 are associated with cardiac atrioventricular septal defects. *American Journal of Human Genetics,* 72**,** 1047-52.

RODRIGUEZ-CARBALLO, E., ULSAMER, A., SUSPERREGUI, A. R., MANZANARES-CESPEDES, C., SANCHEZ-GARCIA, E., BARTRONS, R., ROSA, J. L. & VENTURA, F. 2011. Conserved regulatory motifs in osteogenic gene promoters integrate cooperative effects of canonical Wnt and BMP pathways. *Journal of Bone and Mineral Research,* 26**,** 718-29.

ROHATGI, R., MILENKOVIC, L. & SCOTT, M. P. 2007. Patched1 regulates hedgehog signaling at the primary cilium. *Science,* 317**,** 372-6.

ROUSSEAU, F., BONAVENTURE, J., LEGEAI-MALLET, L., PELET, A., ROZET, J. M., MAROTEAUX, P., LE MERRER, M. & MUNNICH, A. 1994. Mutations in the gene encoding fibroblast growth factor receptor-3 in achondroplasia. *Nature,* 371**,** 252-4.

RUDNICKI, J. A. & BROWN, A. M. 1997. Inhibition of chondrogenesis by Wnt gene expression in vivo and in vitro. *Developmental Biology,* 185**,** 104-18.

RUHLEN, R. & MARBERRY, K. 2014. The chondrocyte primary cilium. *Osteoarthritis Cartilage,* 22**,** 1071-6.

RUPP, P. A., FOUAD, G. T., EGELSTON, C. A., REIFSTECK, C. A., OLSON, S. B., KNOSP, W. M., GLANVILLE, R. W., THORNBURG, K. L., ROBINSON, S. W. & MASLEN, C. L. 2002. Identification, genomic organization and mRNA

expression of CRELD1, the founding member of a unique family of matricellular proteins. *Gene,* 293**,** 47-57.

RUTKOVSKIY, A., STENSLØKKEN, K. O. & VAAGE, I. J. 2016. Osteoblast Differentiation at a Glance. *Med Sci Monit Basic Res,* 22**,** 95-106.

SABURI, S., HESTER, I., FISCHER, E., PONTOGLIO, M., EREMINA, V., GESSLER, M., QUAGGIN, S. E., HARRISON, R., MOUNT, R. & MCNEILL, H. 2008. Loss of Fat4 disrupts PCP signaling and oriented cell division and leads to cystic kidney disease. *Nature Genetics,* 40**,** 1010-5.

SAITO, A., HINO, S., MURAKAMI, T., KANEMOTO, S., KONDO, S., SAITOH, M., NISHIMURA, R., YONEDA, T., FURUICHI, T., IKEGAWA, S., IKAWA, M., OKABE, M. & IMAIZUMI, K. 2009. Regulation of endoplasmic reticulum stress response by a BBF2H7-mediated Sec23a pathway is essential for chondrogenesis. *Nature Cell Biology,* 11**,** 1197-204.

SAITO, A., KANEMOTO, S., ZHANG, Y., ASADA, R., HINO, K. & IMAIZUMI, K. 2014. Chondrocyte proliferation regulated by secreted luminal domain of ER stress transducer BBF2H7/CREB3L2. *Molecular Cell,* 53**,** 127-39.

SALAZAR, V. S., ZARKADIS, N., HUANG, L., WATKINS, M., KADING, J., BONAR, S., NORRIS, J., MBALAVIELE, G. & CIVITELLI, R. 2013. Postnatal ablation of osteoblast Smad4 enhances proliferative responses to canonical Wnt signaling through interactions with beta-catenin. *Journal of Cell Science,* 126**,** 5598-609.

SCAFFIDI, C., FULDA, S., SRINIVASAN, A., FRIESEN, C., LI, F., TOMASELLI, K. J., DEBATIN, K. M., KRAMMER, P. H. & PETER, M. E. 1998. Two CD95 (APO-1/Fas) signaling pathways. *The EMBO JOURNALournal,* 17**,** 1675-1687.

SCHINDLER, A. J. & SCHEKMAN, R. 2009. In vitro reconstitution of ER-stress induced ATF6 transport in COPII vesicles. *Proceedings of the National Academy of Sciences of the United States of America,* 106**,** 17775-80.

SCHIPANI, E., LANSKE, B., HUNZELMAN, J., LUZ, A., KOVACS, C. S., LEE, K., PIRRO, A., KRONENBERG, H. M. & JUPPNER, H. 1997. Targeted expression of constitutively active receptors for parathyroid hormone and parathyroid hormone-related peptide delays endochondral bone formation and rescues mice that lack parathyroid hormone-related peptide. *Proceedings of the National Academy of Sciences of the United States of America,* 94**,** 13689-94.

SCHLESINGER, P. H., BLAIR, H. C., TEITELBAUM, S. L. & EDWARDS, J. C. 1997. Characterization of the osteoclast ruffled border chloride channel and its role in bone resorption. *Journal of Biological Chemistry,* 272**,** 18636-43.

SCHLESSINGER, J., PLOTNIKOV, A. N., IBRAHIMI, O. A., ELISEENKOVA, A. V., YEH, B. K., YAYON, A., LINHARDT, R. J. & MOHAMMADI, M. 2000. Crystal structure of a ternary FGF-FGFR-heparin complex reveals a dual role for heparin in FGFR binding and dimerization. *Molecular Cell,* 6**,** 743-50.

SCHNEEWEIS, L. A., WILLARD, D. & MILLA, M. E. 2005. Functional dissection of osteoprotegerin and its interaction with receptor activator of NF-kappaB ligand. *Journal of Biological Chemistry,* 280**,** 41155-64.

SCHROETER, E. H., KISSLINGER, J. A. & KOPAN, R. 1998. Notch-1 signalling requires ligand-induced proteolytic release of intracellular domain. *Nature,* 393**,** 382-6.

SCHUMACHER, C. A., JOINER, D. M., LESS, K. D., DREWRY, M. O. & WILLIAMS, B. O. 2016. Characterization of genetically engineered mouse models carrying Col2a1-cre-induced deletions of Lrp5 and/or Lrp6. *Bone Research,* 4**,** 15042.

SCHWARZ, D. S. & BLOWER, M. D. 2016. The endoplasmic reticulum: structure, function and response to cellular signaling. *Cellular and Molecular Life Sciences,* 73**,** 79-94.

SEGARINI, P. R., NESBITT, J. E., LI, D., HAYS, L. G., YATES, J. R., 3RD & CARMICHAEL, D. F. 2001. The low density lipoprotein receptor-related protein/alpha2-macroglobulin receptor is a receptor for connective tissue growth factor. *Journal of Biological Chemistry,* 276**,** 40659-67.

SEKI, K. & HATA, A. 2004. Indian hedgehog gene is a target of the bone morphogenetic protein signaling pathway. *Journal of Biological Chemistry,* 279**,** 18544-9.

SELVAMURUGAN, N., PULUMATI, M. R., TYSON, D. R. & PARTRIDGE, N. C. 2000. Parathyroid hormone regulation of the rat collagenase-3 promoter by protein kinase A-dependent transactivation of core binding factor alpha1. *Journal of Biological Chemistry,* 275**,** 5037-42.

SEVERE, N., DIEUDONNE, F. X. & MARIE, P. J. 2013. E3 ubiquitin ligase-mediated regulation of bone formation and tumorigenesis. *Cell Death & Disease,* 4**,** e463.

SHEEBA, C. J., ANDRADE, R. P., DUPREZ, D. & PALMEIRIM, I. 2010. Comprehensive analysis of fibroblast growth factor receptor expression patterns during chick forelimb development. *International Journal of Developmental Biology,* 54**,** 1517-26.

SHELDAHL, L. C., SLUSARSKI, D. C., PANDUR, P., MILLER, J. R., KUHL, M. & MOON, R. T. 2003. Dishevelled activates Ca2+ flux, PKC, and CamKII in vertebrate embryos. *Journal of Cell Biology,* 161**,** 769-77.

SHEN, B., WEI, A., WHITTAKER, S., WILLIAMS, L. A., TAO, H., MA, D. D. & DIWAN, A. D. 2010. The role of BMP-7 in chondrogenic and osteogenic differentiation of human bone marrow multipotent mesenchymal stromal cells in vitro. *Journal of Cellular Biochemistry,* 109**,** 406-16.

SHEN, J., CHEN, X., HENDERSHOT, L. & PRYWES, R. 2002. ER stress regulation of ATF6 localization by dissociation of BiP/GRP78 binding and unmasking of Golgi localization signals. *Developmental Cell,* 3**,** 99-111.

SHIANG, R., THOMPSON, L. M., ZHU, Y. Z., CHURCH, D. M., FIELDER, T. J., BOCIAN, M., WINOKUR, S. T. & WASMUTH, J. J. 1994. Mutations in the transmembrane domain of FGFR3 cause the most common genetic form of dwarfism, achondroplasia. *Cell,* 78**,** 335-42.

SHIM, K. S. 2015. Pubertal growth and epiphyseal fusion. *Annals of Pediatric Endocrinology & Metabolism,* 20**,** 8-12.

SHORE, E. M., XU, M., FELDMAN, G. J., FENSTERMACHER, D. A., CHO, T. J., CHOI, I. H., CONNOR, J. M., DELAI, P., GLASER, D. L., LEMERRER, M., MORHART, R., ROGERS, J. G., SMITH, R., TRIFFITT, J. T., URTIZBEREA, J. A., ZASLOFF, M., BROWN, M. A. & KAPLAN, F. S. 2006. A recurrent mutation in the BMP type I receptor ACVR1 causes inherited and sporadic fibrodysplasia ossificans progressiva. *Nature Genetics,* 38**,** 525-7.

SHU, B., ZHANG, M., XIE, R., WANG, M., JIN, H., HOU, W., TANG, D., HARRIS, S. E., MISHINA, Y., O'KEEFE, R. J., HILTON, M. J., WANG, Y. & CHEN, D. 2011. BMP2, but not BMP4, is crucial for chondrocyte proliferation and maturation during endochondral bone development. *Journal of Cell Science,* 124**,** 3428-40.

SHUM, L., RABIE, A. B. & HAGG, U. 2004. Vascular endothelial growth factor expression and bone formation in posterior glenoid fossa during stepwise mandibular advancement. *American Journal of Orthodontics and Dentofacial Orthopedics,* 125**,** 185-90.

SHUNG, C. Y., OTA, S., ZHOU, Z. Q., KEENE, D. R. & HURLIN, P. J. 2012. Disruption of a Sox9-beta-catenin circuit by mutant Fgfr3 in thanatophoric dysplasia type II. *Human Molecular Genetics,* 21**,** 4628-44.

SI, W., KANG, Q., LUU, H. H., PARK, J. K., LUO, Q., SONG, W. X., JIANG, W., LUO, X., LI, X., YIN, H., MONTAG, A. G., HAYDON, R. C. & HE, T. C. 2006. CCN1/Cyr61 is regulated by the canonical Wnt signal and plays an important role in Wnt3A-induced osteoblast differentiation of mesenchymal stem cells. *Molecular Cell Biology,* 26**,** 2955-64.

SILBERMANN, M., LEWINSON, D., GONEN, H., LIZARBE, M. A. & VON DER MARK, K. 1983. In vitro transformation of chondroprogenitor cells into osteoblasts and the formation of new membrane bone. *The Anatomical Record,* 206**,** 373-83.

SILVA, M. T. 2010. Secondary necrosis: the natural outcome of the complete apoptotic program. *FEBS Letters,* 584**,** 4491-9.

SILVER, I. A., MURRILLS, R. J. & ETHERINGTON, D. J. 1988. Microelectrode studies on the acid microenvironment beneath adherent macrophages and osteoclasts. *Experimental Cell Research,* 175**,** 266-76.

SIMANTOV, R., FEBBRAIO, M. & SILVERSTEIN, R. L. 2005. The antiangiogenic effect of thrombospondin-2 is mediated by CD36 and modulated by histidine-rich glycoprotein. *Matrix Biology,* 24**,** 27-34.

SIMONET, W. S., LACEY, D. L., DUNSTAN, C. R., KELLEY, M., CHANG, M. S., LUTHY, R., NGUYEN, H. Q., WOODEN, S., BENNETT, L., BOONE, T., SHIMAMOTO, G., DEROSE, M., ELLIOTT, R., COLOMBERO, A., TAN, H. L., TRAIL, G., SULLIVAN, J., DAVY, E., BUCAY, N., RENSHAW-GEGG, L., HUGHES, T. M., HILL, D., PATTISON, W., CAMPBELL, P., SANDER, S., VAN, G., TARPLEY, J., DERBY, P., LEE, R. & BOYLE, W. J. 1997. Osteoprotegerin: a novel secreted protein involved in the regulation of bone density. *Cell,* 89**,** 309-19.

SIMS, N. A. & MARTIN, T. J. 2015. Coupling Signals between the Osteoclast and Osteoblast: How are Messages Transmitted between These Temporary Visitors to the Bone Surface? *Frontiers in Endocrinology (Lausanne),* 6.

SMERDEL-RAMOYA, A., ZANOTTI, S., STADMEYER, L., DURANT, D. & CANALIS, E. 2008. Skeletal Overexpression of Connective Tissue Growth Factor Impairs Bone Formation and Causes Osteopenia. *Endocrinology,* 149**,** 4374-4381.

SOLLOWAY, M. J. & ROBERTSON, E. J. 1999. Early embryonic lethality in Bmp5;Bmp7 double mutant mice suggests functional redundancy within the 60A subgroup. *Development,* 126**,** 1753-68.

SONG, B., HAYCRAFT, C. J., SEO, H., YODER, B. K. & SERRA, R. 2007. Development of the post-natal growth plate requires intraflagellar transport proteins. *Developmental Biology,* 305**,** 202-16.

SONG, J. L. & WANG, C. C. 1995. Chaperone-like activity of protein disulfide-isomerase in the refolding of rhodanese. *European Journal of Biochemistry,* 231**,** 312-6.

SOUSA, M. & PARODI, A. J. 1995. The molecular basis for the recognition of misfolded glycoproteins by the UDP-Glc:glycoprotein glucosyltransferase. *EMBO Journal,* 14**,** 4196-203.

ST-JACQUES, B., HAMMERSCHMIDT, M. & MCMAHON, A. P. 1999. Indian hedgehog signaling regulates proliferation and differentiation of chondrocytes and is essential for bone formation. *Genes & Development,* 13**,** 2072-2086.

STÄHELIN, B. J., MARTI, U., SOLIOZ, M., ZIMMERMANN, H. & REICHEN, J. 1998. False positive staining in the TUNEL assay to detect apoptosis in liver and

intestine is caused by endogenous nucleases and inhibited by diethyl pyrocarbonate. *Molecular Pathology,* 51**,** 204-208.

STANLEY, P. 2016. N-Linked Glycans (N-Glycans). *Encyclopedia of Cell Biology.* Waltham: Academic Press.

STEPHENS, A. S., STEPHENS, S. R. & MORRISON, N. A. 2011. Internal control genes for quantitative RT-PCR expression analysis in mouse osteoblasts, osteoclasts and macrophages. *BMC Research Notes,* 4**,** 410.

STICKENS, D., BEHONICK, D. J., ORTEGA, N., HEYER, B., HARTENSTEIN, B., YU, Y., FOSANG, A. J., SCHORPP-KISTNER, M., ANGEL, P. & WERB, Z. 2004. Altered endochondral bone development in matrix metalloproteinase 13-deficient mice. *Development,* 131**,** 5883-95.

STREB, H., IRVINE, R. F., BERRIDGE, M. J. & SCHULZ, I. 1983. Release of Ca2+ from a nonmitochondrial intracellular store in pancreatic acinar cells by inositol-1,4,5-trisphosphate. *Nature,* 306**,** 67-9.

SU, J. L., CHIOU, J., TANG, C. H., ZHAO, M., TSAI, C. H., CHEN, P. S., CHANG, Y. W., CHIEN, M. H., PENG, C. Y., HSIAO, M., KUO, M. L. & YEN, M. L. 2010. CYR61 regulates BMP-2-dependent osteoblast differentiation through the {alpha}v{beta}3 integrin/integrin-linked kinase/ERK pathway. *Journal of Biological Chemistry,* 285**,** 31325-36.

SU, N., JIN, M. & CHEN, L. 2014. Role of FGF/FGFR signaling in skeletal development and homeostasis: learning from mouse models. *Bone Research,* 2**,** 14003.

SUK, K., CHANG, I., KIM, Y. H., KIM, S., KIM, J. Y., KIM, H. & LEE, M. S. 2001. Interferon gamma (IFNgamma) and tumor necrosis factor alpha synergism in ME-180 cervical cancer cell apoptosis and necrosis. IFNgamma inhibits cytoprotective NF-kappa B through STAT1/IRF-1 pathways. *Journal of Biological Chemistry,* 276**,** 13153-9.

SULEMAN, F., GUALENI, B., GREGSON, H. J., LEIGHTON, M. P., PIROG, K. A., EDWARDS, S., HOLDEN, P., BOOT-HANDFORD, R. P. & BRIGGS, M. D. 2012. A novel form of chondrocyte stress is triggered by a COMP mutation causing pseudoachondroplasia. *Human Mutation,* 33**,** 218-31.

SUPEK, F., BOŠNJAK, M., ŠKUNCA, N. & ŠMUC, T. 2011. REVIGO Summarizes and Visualizes Long Lists of Gene Ontology Terms. *PLoS ONE,* 6**,** e21800.

SUTHERLAND, M. K., GEOGHEGAN, J. C., YU, C., TURCOTT, E., SKONIER, J. E., WINKLER, D. G. & LATHAM, J. A. 2004. Sclerostin promotes the apoptosis of human osteoblastic cells: a novel regulation of bone formation. *Bone,* 35**,** 828-35.

SZEGEZDI, E., LOGUE, S. E., GORMAN, A. M. & SAMALI, A. 2006. Mediators of endoplasmic reticulum stress-induced apoptosis. *EMBO Reports,* 7**,** 880-5.

SZKLARCZYK, D., MORRIS, J. H., COOK, H., KUHN, M., WYDER, S., SIMONOVIC, M., SANTOS, A., DONCHEVA, N. T., ROTH, A., BORK, P., JENSEN, L. J. & VON MERING, C. 2017. The STRING database in 2017: quality-controlled protein-protein association networks, made broadly accessible. *Nucleic Acids Research,* 45**,** D362-D368.

TACHI, K., TAKAMI, M., SATO, H., MOCHIZUKI, A., ZHAO, B., MIYAMOTO, Y., TSUKASAKI, H., INOUE, T., SHINTANI, S., KOIKE, T., HONDA, Y., SUZUKI, O., BABA, K. & KAMIJO, R. 2011. Enhancement of bone morphogenetic protein-2-induced ectopic bone formation by transforming growth factor-beta1. *Tissue Engineering Part A,* 17**,** 597-606.

TAIPALE, J., COOPER, M. K., MAITI, T. & BEACHY, P. A. 2002. Patched acts catalytically to suppress the activity of Smoothened. *Nature,* 418**,** 892-7.

TAKAI, Y., KISHIMOTO, A., KIKKAWA, U., MORI, T. & NISHIZUKA, Y. 1979. Unsaturated diacylglycerol as a possible messenger for the activation of calcium-activated, phospholipid-dependent protein kinase system. *Biochemical and Biophysical Research Communications,* 91**,** 1218-24.

TAKEDA, S., BONNAMY, J. P., OWEN, M. J., DUCY, P. & KARSENTY, G. 2001. Continuous expression of Cbfa1 in nonhypertrophic chondrocytes uncovers its ability to induce hypertrophic chondrocyte differentiation and partially rescues Cbfa1-deficient mice. *Genes & Development,* 15**,** 467-81.

TAMAMURA, Y., OTANI, T., KANATANI, N., KOYAMA, E., KITAGAKI, J., KOMORI, T., YAMADA, Y., COSTANTINI, F., WAKISAKA, S., PACIFICI, M., IWAMOTO, M. & ENOMOTO-IWAMOTO, M. 2005. Developmental regulation of Wnt/beta-catenin signals is required for growth plate assembly, cartilage integrity, and endochondral ossification. *Journal of Biological Chemistry,* 280**,** 19185-95.

TAMURA, T., ISHIHARA, M., LAMPHIER, M. S., TANAKA, N., OISHI, I., AIZAWA, S., MATSUYAMA, T., MAK, T. W., TAKI, S. & TANIGUCHI, T. 1995. An IRF-1-dependent pathway of DNA damage-induced apoptosis in mitogen-activated T lymphocytes. *Nature,* 376**,** 596-9.

TAMURA, T., UDAGAWA, N., TAKAHASHI, N., MIYAURA, C., TANAKA, S., YAMADA, Y., KOISHIHARA, Y., OHSUGI, Y., KUMAKI, K. & TAGA, T. 1993. Soluble interleukin-6 receptor triggers osteoclast formation by interleukin 6. *Proceedings of the National Academy of Sciences of the United States of America,* 90**,** 11924-11928.

TANAKA, Y., MORIMOTO, I., NAKANO, Y., OKADA, Y., HIROTA, S., NOMURA, S., NAKAMURA, T. & ETO, S. 1995. Osteoblasts are regulated by the cellular adhesion through ICAM-1 and VCAM-1. *Journal of Bone and Mineral Research,* 10**,** 1462-9.

TANG, N., SONG, W. X., LUO, J., LUO, X., CHEN, J., SHARFF, K. A., BI, Y., HE, B. C., HUANG, J. Y., ZHU, G. H., SU, Y. X., JIANG, W., TANG, M., HE, Y., WANG, Y., CHEN, L., ZUO, G. W., SHEN, J., PAN, X., REID, R. R., LUU, H. H., HAYDON, R. C. & HE, T. C. 2009a. BMP-9-induced osteogenic differentiation of mesenchymal progenitors requires functional canonical Wnt/beta-catenin signalling. *Journal of Cellular and Molecular Medicine,* 13**,** 2448-64.

TANG, Y., WU, X., LEI, W., PANG, L., WAN, C., SHI, Z., ZHAO, L., NAGY, T. R., PENG, X., HU, J., FENG, X., VAN HUL, W., WAN, M. & CAO, X. 2009b. TGF-β 1-induced Migration of Bone Mesenchymal Stem Cells Couples Bone Resorption and Formation. *Nature Medicine,* 15**,** 757-65.

TEITELBAUM, S. L. 2000. Bone resorption by osteoclasts. *Science,* 289**,** 1504-8.

THESINGH, C. W., GROOT, C. G. & WASSENAAR, A. M. 1991. Transdifferentiation of hypertrophic chondrocytes into osteoblasts in murine fetal metatarsal bones, induced by co-cultured cerebrum. *Journal of Bone and Mineral Research,* 12**,** 25-40.

TIAN, Y., XU, Y., FU, Q. & HE, M. 2011. Parathyroid hormone regulates osteoblast differentiation in a Wnt/beta-catenin-dependent manner. *Molecular Cell Biochemistry,* 355**,** 211-6.

TOHMONDA, T., MIYAUCHI, Y., GHOSH, R., YODA, M., UCHIKAWA, S., TAKITO, J., MORIOKA, H., NAKAMURA, M., IWAWAKI, T., CHIBA, K., TOYAMA, Y., URANO, F. & HORIUCHI, K. 2011. The IRE1α–XBP1 pathway is essential for osteoblast differentiation through promoting transcription of Osterix. *EMBO Reports,* 12**,** 451-7.

TOHMONDA, T., YODA, M., IWAWAKI, T., MATSUMOTO, M., NAKAMURA, M., MIKOSHIBA, K., TOYAMA, Y. & HORIUCHI, K. 2015. IRE1alpha/XBP1-mediated branch of the unfolded protein response regulates osteoclastogenesis. *Journal of Clinical Investigation,* 125**,** 3269-79.

TOKUZAWA, Y., YAGI, K., YAMASHITA, Y., NAKACHI, Y., NIKAIDO, I., BONO, H., NINOMIYA, Y., KANESAKI-YATSUKA, Y., AKITA, M., MOTEGI, H., WAKANA, S., NODA, T., SABLITZKY, F., ARAI, S., KUROKAWA, R., FUKUDA, T., KATAGIRI, T., SCHONBACH, C., SUDA, T., MIZUNO, Y. & OKAZAKI, Y. 2010. Id4, a new candidate gene for senile osteoporosis, acts as a molecular switch promoting osteoblast differentiation. *PLoS Genetics,* 6**,** e1001019.

TORRES, M., MEDINAS, D. B., MATAMALA, J. M., WOEHLBIER, U., CORNEJO, V. H., SOLDA, T., ANDREU, C., ROZAS, P., MATUS, S., MUNOZ, N., VERGARA, C., CARTIER, L., SOTO, C., MOLINARI, M. & HETZ, C. 2015. The Protein-disulfide Isomerase ERp57 Regulates the Steady-state Levels of the Prion Protein. *Journal of Biological Chemistry,* 290**,** 23631-45.

TSANG, K. Y., CHAN, D., CHESLETT, D., CHAN, W. C., SO, C. L., MELHADO, I. G., CHAN, T. W., KWAN, K. M., HUNZIKER, E. B., YAMADA, Y., BATEMAN, J. F., CHEUNG, K. M. & CHEAH, K. S. 2007. Surviving endoplasmic reticulum stress is coupled to altered chondrocyte differentiation and function. *PLoS Biology,* 5**,** e44.

TSUKAHARA, S., IKEDA, R., GOTO, S., YOSHIDA, K., MITSUMORI, R., SAKAMOTO, Y., TAJIMA, A., YOKOYAMA, T., TOH, S., FURUKAWA, K. & INOUE, I. 2006. Tumour necrosis factor alpha-stimulated gene-6 inhibits osteoblastic differentiation of human mesenchymal stem cells induced by osteogenic differentiation medium and BMP-2. *Biochemical Journal,* 398**,** 595-603.

TSUMAKI, N., NAKASE, T., MIYAJI, T., KAKIUCHI, M., KIMURA, T., OCHI, T. & YOSHIKAWA, H. 2002. Bone morphogenetic protein signals are required for cartilage formation and differently regulate joint development during skeletogenesis. *Journal of Bone and Mineral Research,* 17**,** 898-906.

TU, X., CHEN, J., LIM, J., KARNER, C. M., LEE, S. Y., HEISIG, J., WIESE, C., SURENDRAN, K., KOPAN, R., GESSLER, M. & LONG, F. 2012. Physiological notch signaling maintains bone homeostasis via RBPjk and Hey upstream of NFATc1. *PLoS Genetics,* 8**,** e1002577.

TU, X., JOENG, K. S., NAKAYAMA, K. I., NAKAYAMA, K., RAJAGOPAL, J., CARROLL, T. J., MCMAHON, A. P. & LONG, F. 2007. Noncanonical Wnt Signaling through G Protein-Linked PKC δ Activation Promotes Bone Formation. *Developmental Cell,* 12**,** 113-27.

TUCKERMANN, J. P., PITTOIS, K., PARTRIDGE, N. C., MERREGAERT, J. & ANGEL, P. 2000. Collagenase-3 (MMP-13) and integral membrane protein 2a (Itm2a) are marker genes of chondrogenic/osteoblastic cells in bone formation: sequential temporal, and spatial expression of Itm2a, alkaline phosphatase, MMP-13, and osteocalcin in the mouse. *Journal of Bone and Mineral Research,* 15**,** 1257-65.

UETA, C., IWAMOTO, M., KANATANI, N., YOSHIDA, C., LIU, Y., ENOMOTO-IWAMOTO, M., OHMORI, T., ENOMOTO, H., NAKATA, K., TAKADA, K., KURISU, K. & KOMORI, T. 2001. Skeletal malformations caused by overexpression of Cbfa1 or its dominant negative form in chondrocytes. *Journal of Cell Biology,* 153**,** 87-100.

URANO, F., WANG, X., BERTOLOTTI, A., ZHANG, Y., CHUNG, P., HARDING, H. P. & RON, D. 2000. Coupling of stress in the ER to activation of JNK protein kinases by transmembrane protein kinase IRE1. *Science,* 287**,** 664-6.

USAMI, Y., GUNAWARDENA, A. T., IWAMOTO, M. & ENOMOTO-IWAMOTO, M. 2016. Wnt Signaling in Cartilage Development and Diseases: Lessons from Animal Studies. *Laboratory Investigation,* 96**,** 186-96.

VAANANEN, H. K. & HORTON, M. 1995. The osteoclast clear zone is a specialized cell-extracellular matrix adhesion structure. *Journal of Cell Science,* 108 (Pt 8)**,** 2729-32.

VALCOURT, U., GOUTTENOIRE, J., MOUSTAKAS, A., HERBAGE, D. & MALLEIN-GERIN, F. 2002. Functions of transforming growth factor-beta family type I receptors and Smad proteins in the hypertrophic maturation and osteoblastic differentiation of chondrocytes. *Journal of Biological Chemistry,* 277**,** 33545-58.

VAN DEN HEUVEL, M. & INGHAM, P. W. 1996. smoothened encodes a receptor-like serpentine protein required for hedgehog signalling. *Nature,* 382**,** 547-51.

VAN DER PLUIJM, G., MOST, W., VAN DER WEE-PALS, L., DE GROOT, H., PAPAPOULOS, S. & LOWIK, C. 1991. Two distinct effects of recombinant human tumor necrosis factor-alpha on osteoclast development and subsequent resorption of mineralized matrix. *Endocrinology,* 129**,** 1596-604.

VAN DINTHER, M., VISSER, N., DE GORTER, D. J., DOORN, J., GOUMANS, M. J., DE BOER, J. & TEN DIJKE, P. 2010. ALK2 R206H mutation linked to fibrodysplasia ossificans progressiva confers constitutive activity to the BMP type I receptor and sensitizes mesenchymal cells to BMP-induced osteoblast differentiation and bone formation. *Journal of Bone and Mineral Research,* 25**,** 1208-15.

VAN LEEUWEN, J. E. & KEARSE, K. P. 1997. Reglucosylation of N-linked glycans is critical for calnexin assembly with T cell receptor (TCR) alpha proteins but not TCRbeta proteins. *Journal of Biological Chemistry,* 272**,** 4179-86.

VASSILAKOS, A., COHEN-DOYLE, M. F., PETERSON, P. A., JACKSON, M. R. & WILLIAMS, D. B. 1996. The molecular chaperone calnexin facilitates folding and assembly of class I histocompatibility molecules. *EMBO Journal,* 15**,** 1495-506.

VIDAL, R. L. & HETZ, C. 2013. Unspliced XBP1 controls autophagy through FoxO1. *Cell Research,* 23**,** 463-464.

VOLBRACHT, C., LEIST, M., KOLB, S. A. & NICOTERA, P. 2001. Apoptosis in caspase-inhibited neurons. *Molecular Medicine,* 7**,** 36-48.

VORTKAMP, A., LEE, K., LANSKE, B., SEGRE, G. V., KRONENBERG, H. M. & TABIN, C. J. 1996. Regulation of rate of cartilage differentiation by Indian hedgehog and PTH-related protein. *Science,* 273**,** 613-22.

VU, T. H., SHIPLEY, J. M., BERGERS, G., BERGER, J. E., HELMS, J. A., HANAHAN, D., SHAPIRO, S. D., SENIOR, R. M. & WERB, Z. 1998. MMP-9/Gelatinase B Is a Key Regulator of Growth Plate Angiogenesis and Apoptosis of Hypertrophic Chondrocytes. *Cell,* 93**,** 411-422.

WAGNER, T., WIRTH, J., MEYER, J., ZABEL, B., HELD, M., ZIMMER, J., PASANTES, J., BRICARELLI, F. D., KEUTEL, J., HUSTERT, E., WOLF, U., TOMMERUP, N., SCHEMPP, W. & SCHERER, G. 1994. Autosomal sex reversal and campomelic dysplasia are caused by mutations in and around the SRY-related gene SOX9. *Cell,* 79**,** 1111-20.

WANG, J., WANG, X., HOLZ, J. D., RUTKOWSKI, T., WANG, Y., ZHU, Z. & DONG, Y. 2013. Runx1 Is Critical for PTH-induced Onset of Mesenchymal Progenitor Cell Chondrogenic Differentiation. *PLoS ONE,* 8.

WANG, J., ZHOU, J. & BONDY, C. A. 1999. Igf1 promotes longitudinal bone growth by insulin-like actions augmenting chondrocyte hypertrophy. *FASEB Journal,* 13**,** 1985-90.

WANG, M., JIN, H., TANG, D., HUANG, S., ZUSCIK, M. J. & CHEN, D. 2011. Smad1 plays an essential role in bone development and postnatal bone formation. *Osteoarthritis Cartilage,* 19**,** 751-62.

WANG, M., YE, R., BARRON, E., BAUMEISTER, P., MAO, C., LUO, S., FU, Y., LUO, B., DUBEAU, L., HINTON, D. R. & LEE, A. S. 2010. Essential role of the unfolded protein response regulator GRP78/BiP in protection from neuronal apoptosis. *Cell death & Differentiation,* 17**,** 488-498.

WANG, W., LIAN, N., LI, L., MOSS, H. E., WANG, W., PERRIEN, D. S., ELEFTERIOU, F. & YANG, X. 2009. Atf4 regulates chondrocyte proliferation and differentiation during endochondral ossification by activating Ihh transcription. *Development,* 136**,** 4143-53.

WEALTHALL, R. J. & HERRING, S. W. 2006. Endochondral ossification of the mouse nasal septum. *The Anatomical Record. Part A, Discoveries in Molecular, Cellular, and Evolutionary Biologyvol Biol,* 288**,** 1163-72.

WEI, J., SHENG, X., FENG, D., MCGRATH, B. & CAVENER, D. R. 2008. PERK is essential for neonatal skeletal development to regulate osteoblast proliferation and differentiation. *Journal of Cellular Physiology,* 217**,** 693-707.

WEI, P. C., HSIEH, Y. H., SU, M. I., JIANG, X., HSU, P. H., LO, W. T., WENG, J. Y., JENG, Y. M., WANG, J. M., CHEN, P. L., CHANG, Y. C., LEE, K. F., TSAI, M. D., SHEW, J. Y. & LEE, W. H. 2012. Loss of the oxidative stress sensor NPGPx compromises GRP78 chaperone activity and induces systemic disease. *Molecular Cell,* 48**,** 747-59.

WEI, S., KITAURA, H., ZHOU, P., ROSS, F. P. & TEITELBAUM, S. L. 2005. IL-1 mediates TNF-induced osteoclastogenesis. *Journal of Clinical Investigation,* 115**,** 282-90.

WEIR, E. C., PHILBRICK, W. M., AMLING, M., NEFF, L. A., BARON, R. & BROADUS, A. E. 1996. Targeted overexpression of parathyroid hormone-related peptide in chondrocytes causes chondrodysplasia and delayed endochondral bone formation. *Proceedings of the National Academy of Sciences of the United States of America,* 93**,** 10240-5.

WILSMAN, N. J., FARNUM, C. E., HILLEY, H. D. & CARLSON, C. S. 1981. Ultrastructural evidence of a functional heterogeneity among physeal chondrocytes in growing swine. *American Journal of Veterinary Research,* 42**,** 1547-53.

WILSON, C. W., CHEN, M.-H. & CHUANG, P.-T. 2009. Smoothened Adopts Multiple Active and Inactive Conformations Capable of Trafficking to the Primary Cilium. *PLoS ONE,* 4**,** e5182.

WILSON, R., LEES, J. F. & BULLEID, N. J. 1998. Protein disulfide isomerase acts as a molecular chaperone during the assembly of procollagen. *Journal of Biological Chemistry,* 273**,** 9637-43.

WINNIER, G., BLESSING, M., LABOSKY, P. A. & HOGAN, B. L. 1995. Bone morphogenetic protein-4 is required for mesoderm formation and patterning in the mouse. *Genes & Development,* 9**,** 2105-16.

WOLDT, E., TERRAND, J., MLIH, M., MATZ, R. L., BRUBAN, V., COUDANE, F., FOPPOLO, S., EL ASMAR, Z., CHOLLET, M. E., NINIO, E., BEDNARCZYK, A., THIERSÉ, D., SCHAEFFER, C., VAN DORSSELAER, A., BOUDIER, C., WAHLI, W., CHAMBON, P., METZGER, D., HERZ, J. & BOUCHER, P. 2012. PPAR γ COUNTERACTS LRP1-INDUCED

VASCULAR CALCIFICATION BY INHIBITING A WNT5A SIGNALING PATHWAY. *Nature Communications,* 3**,** 1077-1077.

WONG, B. R., BESSER, D., KIM, N., ARRON, J. R., VOLOGODSKAIA, M., HANAFUSA, H. & CHOI, Y. 1999. TRANCE, a TNF family member, activates Akt/PKB through a signaling complex involving TRAF6 and c-Src. *Molecular Cell,* 4**,** 1041-9.

WONG, M., KIREEVA, M. L., KOLESNIKOVA, T. V. & LAU, L. F. 1997a. Cyr61, product of a growth factor-inducible immediate-early gene, regulates chondrogenesis in mouse limb bud mesenchymal cells. *Developmental Biology,* 192**,** 492-508.

WONG, P. C., ZHENG, H., CHEN, H., BECHER, M. W., SIRINATHSINGHJI, D. J., TRUMBAUER, M. E., CHEN, H. Y., PRICE, D. L., VAN DER PLOEG, L. H. & SISODIA, S. S. 1997b. Presenilin 1 is required for Notch1 and DII1 expression in the paraxial mesoderm. *Nature,* 387**,** 288-92.

WOZNEY, J. M., ROSEN, V., CELESTE, A. J., MITSOCK, L. M., WHITTERS, M. J., KRIZ, R. W., HEWICK, R. M. & WANG, E. A. 1988. Novel regulators of bone formation: molecular clones and activities. *Science,* 242**,** 1528-34.

WU, H., NG B , S. H. & THIBAULT, G. 2014. Endoplasmic reticulum stress response in yeast and humans. *Bioscience Reports,* 34.

WU, J., RUTKOWSKI, D. T., DUBOIS, M., SWATHIRAJAN, J., SAUNDERS, T., WANG, J., SONG, B., YAU, G. D. & KAUFMAN, R. J. 2007. ATF6alpha optimizes long-term endoplasmic reticulum function to protect cells from chronic stress. *Developmental Cell,* 13**,** 351-64.

WU, L., SUN, T., KOBAYASHI, K., GAO, P. & GRIFFIN, J. D. 2002. Identification of a Family of Mastermind-Like Transcriptional Coactivators for Mammalian Notch Receptors. *Molecular Cell Biology,* 22**,** 7688-700.

WU, M., CHEN, G. & LI, Y. P. 2016. TGF-beta and BMP signaling in osteoblast, skeletal development, and bone formation, homeostasis and disease. *Bone Research,* 4**,** 16009.

XIANG, R. & ZHAO, S. 2009. RTN3 inducing apoptosis is modulated by an adhesion protein CRELD1. *Molecular Cell Biochemistry,* 331**,** 225-30.

XIAO, G., JIANG, D., GOPALAKRISHNAN, R. & FRANCESCHI, R. T. 2002. Fibroblast growth factor 2 induction of the osteocalcin gene requires MAPK activity and phosphorylation of the osteoblast transcription factor, Cbfa1/Runx2. *Journal of Biological Chemistry,* 277**,** 36181-7.

XIAO, L., SOBUE, T., ESLIGER, A., KRONENBERG, M. S., COFFIN, J. D., DOETSCHMAN, T. & HURLEY, M. M. 2010. Disruption of the Fgf2 gene activates the adipogenic and suppresses the osteogenic program in mesenchymal marrow stromal stem cells. *Bone,* 47**,** 360-70.

YAMADA, T., YAMAZAKI, H., YAMANE, T., YOSHINO, M., OKUYAMA, H., TSUNETO, M., KURINO, T., HAYASHI, S. & SAKANO, S. 2003. Regulation of osteoclast development by Notch signaling directed to osteoclast precursors and through stromal cells. *Blood,* 101**,** 2227-34.

YANG, C., YANG, L., WAN, M. & CAO, X. 2010. Generation of a mouse model with expression of bone morphogenetic protein type II receptor lacking the cytoplasmic domain in osteoblasts. *Annals of the New York Academy of Sciences,* 1192**,** 286-91.

YANG, G., ZHU, L., HOU, N., LAN, Y., WU, X. M., ZHOU, B., TENG, Y. & YANG, X. 2014a. Osteogenic fate of hypertrophic chondrocytes. *Cell Research* 24**,** 1266-9.

YANG, L., TSANG, K. Y., TANG, H. C., CHAN, D. & CHEAH, K. S. 2014b. Hypertrophic chondrocytes can become osteoblasts and osteocytes in

endochondral bone formation. *Proceedings of the National Academy of Sciences of the United States of America,* 111**,** 12097-102.

YANG, M., HUANG, H., LI, J., LI, D. & WANG, H. 2004. Tyrosine phosphorylation of the LDL receptor-related protein (LRP) and activation of the ERK pathway are required for connective tissue growth factor to potentiate myofibroblast differentiation. *FASEB Journal,* 18**,** 1920-1.

YANG, Y., TOPOL, L., LEE, H. & WU, J. 2003. Wnt5a and Wnt5b exhibit distinct activities in coordinating chondrocyte proliferation and differentiation. *Development,* 130**,** 1003-15.

YANG, Y. Q., TAN, Y. Y., WONG, R., WENDEN, A., ZHANG, L. K. & RABIE, A. B. M. 2012. The role of vascular endothelial growth factor in ossification. *International Journal of Oral Science,* 4**,** 64-8.

YAVROPOULOU, M. P. & YOVOS, J. G. 2007. The role of the Wnt signaling pathway in osteoblast commitment and differentiation. *Hormones (Athens),* 6**,** 279-94.

YE, J., RAWSON, R. B., KOMURO, R., CHEN, X., DAVE, U. P., PRYWES, R., BROWN, M. S. & GOLDSTEIN, J. L. 2000. ER stress induces cleavage of membrane-bound ATF6 by the same proteases that process SREBPs. *Molecular Cell,* 6**,** 1355-64.

YONEDA, T., IMAIZUMI, K., OONO, K., YUI, D., GOMI, F., KATAYAMA, T. & TOHYAMA, M. 2001. Activation of caspase-12, an endoplastic reticulum (ER) resident caspase, through tumor necrosis factor receptor-associated factor 2-dependent mechanism in response to the ER stress. *Journal of Biological Chemistry,* 276**,** 13935-40.

YOSHIDA, C. A., KOMORI, H., MARUYAMA, Z., MIYAZAKI, T., KAWASAKI, K., FURUICHI, T., FUKUYAMA, R., MORI, M., YAMANA, K., NAKAMURA, K., LIU, W., TOYOSAWA, S., MORIISHI, T., KAWAGUCHI, H., TAKADA, K. & KOMORI, T. 2012. SP7 Inhibits Osteoblast Differentiation at a Late Stage in Mice. *PLoS ONE,* 7**,** e32364.

YOSHIDA, C. A., YAMAMOTO, H., FUJITA, T., FURUICHI, T., ITO, K., INOUE, K., YAMANA, K., ZANMA, A., TAKADA, K., ITO, Y. & KOMORI, T. 2004. Runx2 and Runx3 are essential for chondrocyte maturation, and Runx2 regulates limb growth through induction of Indian hedgehog. *Genes & Development,* 18**,** 952-63.

YOSHIDA, H., OKU, M., SUZUKI, M. & MORI, K. 2006. pXBP1(U) encoded in XBP1 pre-mRNA negatively regulates unfolded protein response activator pXBP1(S) in mammalian ER stress response. *Journal of Cell Biology,* 172**,** 565-75.

YOSIMICHI, G., KUBOTA, S., NISHIDA, T., KONDO, S., YANAGITA, T., NAKAO, K., TAKANO-YAMAMOTO, T. & TAKIGAWA, M. 2006. Roles of PKC, PI3K and JNK in multiple transduction of CCN2/CTGF signals in chondrocytes. *Bone,* 38**,** 853-63.

ZAMUROVIC, N., CAPPELLEN, D., ROHNER, D. & SUSA, M. 2004. Coordinated activation of notch, Wnt, and transforming growth factor-beta signaling pathways in bone morphogenic protein 2-induced osteogenesis. Notch target gene Hey1 inhibits mineralization and Runx2 transcriptional activity. *Journal of Biological Chemistry,* 279**,** 37704-15.

ZAPUN, A., DARBY, N. J., TESSIER, D. C., MICHALAK, M., BERGERON, J. J. & THOMAS, D. Y. 1998. Enhanced catalysis of ribonuclease B folding by the interaction of calnexin or calreticulin with ERp57. *Journal of Biological Chemistry,* 273**,** 6009-12.

ZATYKA, M., PRIESTLEY, M., LADUSANS, E. J., FRYER, A. E., MASON, J., LATIF, F. & MAHER, E. R. 2005. Analysis of CRELD1 as a candidate 3p25 atrioventicular septal defect locus (AVSD2). *Clinical Genetics,* 67**,** 526-8.

ZELZER, E., GLOTZER, D. J., HARTMANN, C., THOMAS, D., FUKAI, N., SOKER, S. & OLSEN, B. R. 2001. Tissue specific regulation of VEGF expression during bone development requires Cbfa1/Runx2. *Mechanisms of Development,* 106**,** 97-106.

ZENMYO, M., KOMIYA, S., KAWABATA, R., SASAGURI, Y., INOUE, A. & MORIMATSU, M. 1996. Morphological and biochemical evidence for apoptosis in the terminal hypertrophic chondrocytes of the growth plate. *Journal of Pathology,* 180**,** 430-3.

ZHANG, C. 2010. Transcriptional regulation of bone formation by the osteoblast-specific transcription factor Osx. *Journal of Orthopaedic Surgery and Research,* 5**,** 37.

ZHANG, J., WENG, Y., LIU, X., WANG, J., ZHANG, W., KIM, S. H., ZHANG, H., LI, R., KONG, Y., CHEN, X., SHUI, W., WANG, N., ZHAO, C., WU, N., HE, Y., NAN, G., CHEN, X., WEN, S., ZHANG, H., DENG, F., WAN, L., LUU, H. H., HAYDON, R. C., SHI, L. L., HE, T.-C. & SHI, Q. 2013a. Endoplasmic Reticulum (ER) Stress Inducible Factor Cysteine-Rich with EGF-Like Domains 2 (Creld2) Is an Important Mediator of BMP9-Regulated Osteogenic Differentiation of Mesenchymal Stem Cells. *PLoS ONE,* 8**,** e73086.

ZHANG, J., WENG, Y., LIU, X., WANG, J., ZHANG, W., KIM, S. H., ZHANG, H., LI, R., KONG, Y., CHEN, X., SHUI, W., WANG, N., ZHAO, C., WU, N., HE, Y., NAN, G., CHEN, X., WEN, S., ZHANG, H., DENG, F., WAN, L., LUU, H. H., HAYDON, R. C., SHI, L. L., HE, T. C. & SHI, Q. 2013b. Endoplasmic Reticulum (ER) Stress Inducible Factor Cysteine-Rich with EGF-Like Domains 2 (Creld2) Is an Important Mediator of BMP9-Regulated Osteogenic Differentiation of Mesenchymal Stem Cells. *PLoS ONE,* 8.

ZHANG, M., XUAN, S., BOUXSEIN, M. L., VON STECHOW, D., AKENO, N., FAUGERE, M. C., MALLUCHE, H., ZHAO, G., ROSEN, C. J., EFSTRATIADIS, A. & CLEMENS, T. L. 2002a. Osteoblast-specific knockout of the insulin-like growth factor (IGF) receptor gene reveals an essential role of IGF signaling in bone matrix mineralization. *Journal of Biological Chemistry,* 277**,** 44005-12.

ZHANG, M., YAN, Y., LIM, Y. B., TANG, D., XIE, R., CHEN, A., TAI, P., HARRIS, S. E., XING, L., QIN, Y. X. & CHEN, D. 2009. BMP-2 modulates beta-catenin signaling through stimulation of Lrp5 expression and inhibition of beta-TrCP expression in osteoblasts. *Journal of Cellular Biochemistry,* 108**,** 896-905.

ZHANG, P., MCGRATH, B., LI, S., FRANK, A., ZAMBITO, F., REINERT, J., GANNON, M., MA, K., MCNAUGHTON, K. & CAVENER, D. R. 2002b. The PERK eukaryotic initiation factor 2 alpha kinase is required for the development of the skeletal system, postnatal growth, and the function and viability of the pancreas. *Molecular Cell Biology,* 22**,** 3864-74.

ZHANG, Q., MURCIA, N. S., CHITTENDEN, L. R., RICHARDS, W. G., MICHAUD, E. J., WOYCHIK, R. P. & YODER, B. K. 2003. Loss of the Tg737 protein results in skeletal patterning defects. *Developmenal Dynamics,* 227**,** 78-90.

ZHANG, R., OYAJOBI, B. O., HARRIS, S. E., CHEN, D., TSAO, C., DENG, H. W. & ZHAO, M. 2013c. Wnt/beta-catenin signaling activates bone morphogenetic protein 2 expression in osteoblasts. *Bone,* 52**,** 145-56.

ZHANG, W., GUO, H., JING, H., LI, Y., WANG, X., ZHANG, H., JIANG, L. & REN, F. 2014. Lactoferrin stimulates osteoblast differentiation through PKA and p38

pathways independent of lactoferrin's receptor LRP1. *Journal of Bone and Mineral Research,* 29**,** 1232-43.

ZHANG, Y., SHEU, T., HOAK, D., SHEN, J., HILTON, M. J., ZUSCIK, M. J., JONASON, J. H. & O'KEEFE, R. J. 2016. CCN1 Regulates Chondrocyte Maturation and Cartilage Development. *Journal of Bone and Mineral Research,* 31**,** 549-59.

ZHAO, C., IRIE, N., TAKADA, Y., SHIMODA, K., MIYAMOTO, T., NISHIWAKI, T., SUDA, T. & MATSUO, K. 2006. Bidirectional ephrinB2-EphB4 signaling controls bone homeostasis. *Cell Metabolism,* 4**,** 111-21.

ZHAO, E., LI, Y., FU, X., ZHANG, J. Y., ZENG, H., ZENG, L., LIN, Y., CHEN, J., YIN, G., QIAN, J., YING, K., XIE, Y., ZHAO, R. C. & MAO, Y. M. 2004. Cloning and expression of human GTDC1 gene (glycosyltransferase-like domain containing 1) from human fetal library. *DNA and Cell Biology,* 23**,** 183-7.

ZHAO, Y., LI, X., CAI, M. Y., MA, K., YANG, J., ZHOU, J., FU, W., WEI, F. Z., WANG, L., XIE, D. & ZHU, W. G. 2013. XBP-1u suppresses autophagy by promoting the degradation of FoxO1 in cancer cells. *Cell Research,* 23**,** 491-507.

ZHOU, G., ZHENG, Q., ENGIN, F., MUNIVEZ, E., CHEN, Y., SEBALD, E., KRAKOW, D. & LEE, B. 2006. Dominance of SOX9 function over RUNX2 during skeletogenesis. *Proceedings of the National Academy of Sciences of the United States of America,* 103**,** 19004-9.

ZHOU, S. 2011. TGF-β regulates β-catenin signaling and osteoblast differentiation in human mesenchymal stem cells. *Journal of Cellular Biochemistry,* 112**,** 1651-60.

ZHOU, X., VON DER MARK, K., HENRY, S., NORTON, W., ADAMS, H. & DE CROMBRUGGHE, B. 2014. Chondrocytes transdifferentiate into osteoblasts in endochondral bone during development, postnatal growth and fracture healing in mice. *PLoS Genetics,* 10**,** e1004820.

ZHOU, Z.-Q., OTA, S., DENG, C., AKIYAMA, H. & HURLIN, P. J. 2015. Mutant activated FGFR3 impairs endochondral bone growth by preventing SOX9 downregulation in differentiating chondrocytes. *Human Molecular Genetics,* 24**,** 1764-1773.

ZILBERBERG, A., YANIV, A. & GAZIT, A. 2004. The low density lipoprotein receptor-1, LRP1, interacts with the human frizzled-1 (HFz1) and down-regulates the canonical Wnt signaling pathway. *Journal of Biological Chemistry,* 279**,** 17535-42.

ZOU, H., WIESER, R., MASSAGUÉ, J. & NISWANDER, L. 1997. Distinct roles of type I bone morphogenetic protein receptors in the formation and differentiation of cartilage. *Genes & Development,* 11**,** 2191-2203.

ZVAIFLER, N. J., MARINOVA-MUTAFCHIEVA, L., ADAMS, G., EDWARDS, C. J., MOSS, J., BURGER, J. A. & MAINI, R. N. 2000. Mesenchymal precursor cells in the blood of normal individuals. *Arthritis Research,* 2**,** 477-88.

Appendix A: Buffers and solutions

1 % (v/v) acid alcohol

for 1 litre:	5 mL	Glacial acetic acid
	995 mL	Deionised water

0.5 % (v/v) acidified water

for 1 litre:	990 mL	70 % EtOH
	10 mL	Concentrated HCl

Alizarin complexone solution

for 10 mL:	0.0375 g	Alizarin complexone	(f.c. 3.75 mg/mL)
	10 mL	2 % (w/v) sodium bicarbonate pH 7.4	

Solution must be filter sterilised by passing through a 0.2 μM filter prior to use. To obtain a final concentration of 30 mg/kg in each injection: 4 X mass mouse in grams = μL of solution to inject. .

Alizarin red staining solution

for 100 mL:	5 mg	Alizarin Red S	(f.c. 0.05 mg/mL)
	100 mL	2 % (w/v) Potassium hydroxide	

5x borate buffer, diluted to 1x (0.1 M) before use

for 1 litre:	30.9 g	Boric acid	(f.c. 0.5 M)
	13.5 mL	10 M Sodium hydroxide	

Volume to 1 litre with deionised water. pH of solution adjusted to pH 8.5.

0.2 % (w/v) Bovine hyaluronidase

for 50 mL:	100 mg	Bovine hyaluronidase
	50 mL	1x PBS

1 % (w/v) Bovine serum albumin

For 100 mL:	1 g	Bovine serum albumin	
	100 mL	1x PBS	

Calcein solution

for 10 mL:	0.025 g	Calcein	(f.c. 1.25 mg/mL)
	10 mL	2 % (w/v) sodium bicarbonate pH 7.4	

Solution must be filter sterilised by passing through a 0.2 μM filter prior to use. To obtain a final concentration of 20 mg/kg in each injection: 4 x mass mouse in grams = μL of solution to inject.

Chondrocyte digest solution

250 mg	Collagenase IA	(f.c. 25 mg/mL)
10 mL	DMEM	

Solution passed through 0.2 μM filter.

5 mL	Collagenase IA in DMEM	(f.c. 2.5 mg/mL)
45.5 mL	DMEM	
0.5 mL	Penicillin/Streptomycin	(f.c. Penicillin 1U/mL, Streptomycin 1 μg/mL)
1 mL	Fetal bovine serum	(f.c. 2 %)

Solution aliquoted into 1.5 mL aliquots and stored at – 20 °C.

Citrate buffer pH6

for 500 mL:	0.96 g	Citric acid	(f.c 10 mM)
	250 μL	Tween® 20	(f.c 0.05 %)
	500.0 mL	Deionised water	

pH adjusted to pH 6.

Cutting solution

for 100 mL:	90 mL	Deionised water	
	10 mL	70 % (v/v) EtOH	
	50 µL	Tween® 20	(f.c 0.05 %)

1 mM DSP in PBS

for 50 mL:	5 mL	10 mM DSP	(f.c. 1 mM)
	45 mL	DPBS	

10 mM DSP

for 10 mL:	44.4 mg	DSP	(f.c. 10 mM)
	10 mL	Dry Dimethyl sulfoxide (DMSO)	

DMSO is dried using Molecular sieves 4A 2-12 mesh.

0.5 M EDTA, pH 8

for 1 litre:	800 mL	Deionised water
	146.12 g	EDTA

NaOH pellets are added until EDTA dissolves and pH is adjusted to 8. Volume adjusted to 1 litre with deionised water.

Embryo fixing solution for lacZ staining

for 50 mL:	22.1 mL	0.1 M phosphate buffer	
	25 m L	4 % (v/v) formaldehyde	(f.c. 2 %)
	2.5 mL	0.1 M EDTA pH 8	(f.c. 5 mM)
	0.4 mL	25 % (v/v) glutaraldehyde	(f.c. 0.2 %)
	0.1 mL	1 M $MgCl_2$	(f.c. 2 mM)

Solution made fresh before use.

20 % (w/v) EDTA, pH 7.4

for 1 litre:	1 litre	Deionised water
	200 g	EDTA

Sodium hydroxide pellets are added until EDTA dissolves and pH is adjusted to 7.4.

4 M HCl

For 100 mL:	32.8 mL	37 % Concentrated HCl
	67.2 mL	Deionised water

HotSHOT alkaline lysis buffer

for 200 mL:	198.9 mL	Deionised water	
	1 mL	5 M Sodium hydroxide	(f.c. 25 mM)
	80 µL	0.5 M EDTA pH 8	(f.c. 0.2 mM)

Adjust pH to pH12.

HotSHOT neutralising buffer

for 200 mL:	200 mL	Deionised water	
	1.26 g	Trizma Hydrochloride	(f.c. 40 mM)

Adjust pH to pH 5-5.5.

LacZ staining solution

for 50 mL:	44 mL	LacZ staining wash buffer	
	2.5 mL	0.2 M Potassium-ferrocyanide	(f.c. 10 mM)
	2.5 mL	0.2 M Potassium-ferricyanide	(f.c. 10 mM)
	1 mL	X-Gal solution	(f.c.1 mg/mL)

Ferrocyanide and ferricyanide are stored in the dark at 4 °C. Staining solution can be filtered after use and stored in the dark at -20 °C. Solution can be reused 2-3 times.

LacZ staining wash buffer

for 200 mL:	195.6 mL	0.1 M phosphate buffer	
	2 mL	1 % (w/v) Sodium deoxycholate	(f.c. 0.01 %)
	2 mL	2 % Nonidet-P40	(f.c. 0.02 %)
	0.4 mL	1 M Magnesium chloride	(f.c. 2 mM)

LB-Agar

for 500 mL:	5 g	Tryptone
	2.5 g	Yeast Extract
	5 g	Sodium chloride (NaCl)
	7.5 g	Agar

Heated to boil before being autoclaved. Before use ampicillin is added at a concentration of 50 µg/mL.

LB-Broth

for 500 mL:	5 g	Tryptone
	2.5 g	Yeast Extract
	5 g	NaCl

Heated to boil before being autoclaved. Before use ampicillin is added at a concentration of 50 µg/mL.

MMA embedding solution 1 & 2

100 mL	Deactivated MMA
14 mL	Nonylphenyl-polyethyleneglycol acetate (NPG)
0.55 g	Prewarmed Luperox ® A75 Bonzoyl peroxidase (BPO)

MMA was deactivated by passing through column containing active basic aluminium oxide 60, particle size 0.063 – 0.200 mm (70-230 mesh ASTM). BPO was prewarmed to 37 °C prior to use. Solution 1 can be used 2-3 times. Solution 2 can only be used once.

MMA embedding solution 3

100 mL	Deactivated MMA	
14 mL	NPG	
0.55 g	Prewarmed BPO	
525 µL	N,N-Dimethyl-p-toluidine (DMPT)	

0.85 % (w/v) NaCl

For 100 mL:	0.85 g	NaCl
	100 mL	Deionised water

Osteoblast digest solution

30 mg	Collagenase IV	(f.c. 1 mg/mL)
75 mg	Porcine Trypsin	(f.c. 2.5 mg/mL)
30 mL	HBSS	

Solution passed through 0.22 µM filter. Solution made fresh before use.

PBS-T

for 1 litre:	5 tablets	Phosphate buffered saline (PBS)
	500 µL	Tween® 20
	1 litre	Deionised water

1x PBS

for 1 litre:	5 tablets	PBS (PBS)
	1 litre	Deionised water

0.1 M potassium phosphate buffer pH 7.4-8

for 1 litre:	86.6 mL	0.2 M Potassium phosphate dibasic (K_2HPO_4)
	13.4 mL	0.2 M Potassium phosphate monobasic (KH_2PO_4)
	900 mL	Deionised water

Adjust pH to pH 7.4-8

20 µg/mL proteinase K

For 10 mL:	20 µL	10 mg/mL Proteinase K
	10 mL	Deionised water

RIPA buffer

for 20 mL:	1 mL	1M Trizma-HCl pH 7.4	(f.c. 50 mM)
	1.5 mL	1 M NaCl	(f.c. 0.15 M)
	100 µL	Nonidet-P40	(f.c. 1 %)
	2.5 mL	1 % (w/v) Sodium deoxycholate	(f.c. 0.25 %)
	20 µL	0.5 M EDTA pH 8	(f.c. 1 mM)
	100 µL	0.1 M Sodium Fluoride	(f.c. 1 mM)
	500 µL	20 mM Sodium orthovanadate	(f.c. 1 mM)
	4.28 mL	Deionised water	

One cOmplete™, Mini, EDTA-free Protease Inhibitor Cocktail Tablet was added prior to use.

1 % (w/v) Silver nitrate

for 100 mL:	1 g	Silver nitrate
	100 mL	Deionised water

Solution is kept in the dark at 4 °C.

0.1 M Sodium acetate buffer (pH ~ 4)

for 1 litre:	8.2 g	Sodium Acetate	
	1 Litre	Deionised water	

Adjust pH to pH 4.

2 % (w/v) Sodium bicarbonate pH 7.4

for 100 mL:	2 g	Sodium bicarbonate	
	100 mL	Deionised water	

Adjust pH to pH 7.4.

5x Sodium dodecyl sulpahate (SDS) loading buffer

for 20 mL:	6 mL	1.0 M Tris-HCl pH 6.8	(f.c. 0.3 M)
	2 g	Sodium dodecyl sulpahate	(f.c. 10 %)
	10 mL	Glycerol	(f.c. 50 %)
	1mL	1.0 % Bromophenol blue	(f.c. 0.05 %)

Volume to 20 mL with deionised water.

Sodium formamide

12.5 g	Sodium carbonate	(f.c. ~ 0.5 M)
63 mL	37 % (w/v) formaldehyde solution	(f.c. 9.3 %)
187 mL	Deionised water	

5 % (w/v) Sodium thiosulphate

for 100 mL:	5 g	Sodium thiosulphate
	100 mL	Deionised water

Solution is kept in the dark at – 4 °C.

Stretching solution

for 50 mL:	50 mL	70 % EtOH
	50 mL	Ethylene glycol butyl ether

50x TAE, diluted to 1x before use

for 1 litre:	242 g	Tris-base	(f.c. 2 M)
	57.1 mL	Glacial acetic acid	
	100 mL	0.5 M EDTA pH 8	

Volume to 1 litre with deionised water.

0.04 % Toluidine blue pH 3.75

for 100 mL:	0.04 g	Toluidine Blue O	(f.c. 0.04 %)
	100 mL	0.1 M Sodium acetate buffer pH 4	

Adjust pH to pH 3.75.

1 % (w/v) Toluidine blue pH 4.5

for 50 mL:	0.5 g	Toludine blue O
	50 mL	Deionised water

Adjust pH to pH 4.5.

TRAcP Solution 1

for 1 litre:	9.2 g	Sodium acetate	(f.c. 0.1 M)
	11.4 g	Sodium tartrate	(f.c. 50 mM)
	750 µL	Glacial acetic acid	

Volume to 1 litre with deionised water. pH of solution adjusted to pH 5.7. This solution can be stored at room temperature for up to 2 months.

TRAcP Solution 2

for 5 mL:	0.1 g	Naphthol AS-BI phosphate	(f.c. 0.1 %)
	5 mL	Ethylene glycol monoethyl ether	
	20 mL	Deionised water	

TRAcP Solution 3

for 20 mL:	1.0 g	Sodium nitrite	(f.c. 5 %)
	20 mL	Deionised water	

TRAcP Solution 4

for 20 mL:	1 g	Pararosaniline hydrochloride	(f.c. 5 %)
	20 mL	2 M HCl	

0.2 % (v/v) Triton-X

For 100 mL:	200 µL	Triton-X	
	200 mL	Deionised water	

1x Transfer buffer

for 1 litre:	50 mL	20x Transfer buffer	(f.c. 1x)
	200 mL	Methanol	
	750 mL	Deionised water	

20x Transfer buffer

for 500 mL:	60.57 g	Tris-Base	(f.c. 1 M)
	28.9 g	Glycine	(f.c. 0.77 M)
	3.6 g	Sodium dodecyl sulpahate	(f.c. 25.0 mM)
	500 mL	Deionised water	

1 M Tris-HCl pH 6.8

<u>for 100 mL:</u>	15.76 g	Tris-HCl
	100 mL	Deionised water

Adjust pH to pH 6.8.

Appendix B: Primer sequences, cycling conditions and RNA-sequencing validation

Genotyping primer sequences.

Primer Name	Sequence (5'-3')	Cycling Conditions
***Cre* F**	TGC CAC CAG CCA GCT ATC AAC T	1. 94 °C 2 minutes 2. 94 °C 30 seconds 3. 50 °C 30 seconds 4. 72 °C 30 seconds 5. 72 °C 10 minutes Steps 2-4 repeated x28 cycles
***Cre* R**	AGC CAC CAG CTT GCA TGA TCT C	
***Creld2* F**	GGT GGA CAC CTG TCA ATG GT	1. 95 °C 2 minutes 2. 95 °C 1 minute 3. 55 °C 1 minute 4. 72 °C 1 minute 5. 72 °C 5 minutes Steps 2-4 repeated x30 cycles
***Creld2* R**	CAG CAT GAG AAA GGG AGC TTA	

Real-time PCR primer sequences.

Primer Name	Sequence (5'-3')
***Rn18s* F**	GTA ACC CGT TGA ACC CCA TT
***Rn18s* R**	CCA TCC AAT CGG TAG TAG CG
***Actb* F**	CAT CCG TAA AGA CCT CTA TGC CAA C
***Actb* R**	ATG GAG CCA CCG ATC CAC A
***Acp5* F**	TCC TGG CTC AAA AAG CAG TT
***Acp5* R**	ACA TAG CCC ACA CCG TTC TC
***B2m* F**	CTG CTA CGT AAC ACA GTT CCA CCC
***B2m* R**	CAT GAT GCT TGA TCA CAT GTC TCG
***Bmp4* F**	GCC ATT GTG CAG ACC CTA GT
***Bmp4* R**	ACC CCT CTA CCA CCA TCT CC
***Bmp7* F**	CGA GAC CTT CCA GAT CAC AGT
***Bmp7* R**	CAG CAA GAA GAG GTC CGA CT
***Calcr* F**	ACT TCT GGA TGC TCT GCG AG
***Calcr* R**	GTA GAG GGC ACG AGT GAT GG
***Cdkn1a* F**	GGG CAA CTT CGT CTG GGA G
***Cdkn1a* R**	AAT CTT CAG GCC GCT CAG AC
***Ctgf* F**	CTT CTG CGA TTT CGG CTC C
***Ctgf* R**	TAC ACC GAC CCA CCG AAG A

***Ctsk* F**	ACT GCC TTC CAA TAC GTG CA
***Ctsk* R**	AGC TTG CAT CGA TGG ACA CA
***Cyr61* F**	CAG TGC TGT GAA GAG TGG GT
***Cyr61* R**	GCC AAA GAC AGG AAG CCT CT
***Fas* F**	GTT TTC CCT TGC TGC AGA CA
***Fas* R**	TTG ACA GCA AAA TGG GCC TC
***Fbn2* F**	CAA CAC AGT GGG CTC GTT TG
***Fbn2* R**	GAA CAG TCG CCA GTC TCA CA
***Hmbs* F**	GAG TCT AGA TGG CTC AGA TAG CAT GC
***Hmbs* R**	CCT ACA GAC CAG TTA GCG CAC ATC
***Hprt* F**	CCTAAGATGAGCGCAAGTTGAA
***Hprt* R**	CCACAGGACTAGAACACCTGCTAA
***Ibsp* F**	GAG GCA GAG AAC TCC ACA CT
***Ibsp* R**	TCT TCC TCG TCG CTT TCC TT
***Id4* F**	TGC CTG CAG TGC GAT ATG AA
***Id4* R**	AGC AAA GCA GGG TGA GTC TC
***Igf1* F**	AGA CAG GCA TTG TGG ATG AG
***Igf1* R**	TGA GTC TTG GGC ATG TCA GT
***Il1a* F**	TGT ATG CCT ACT CGT CGG GA
***Il1a* R**	GCA ACT CCT TCA GCA ACA CG
***Il6* F**	AGC CAG AGT CCT TCA GAG AGA
***Il6* R**	TGG TCT TGG TCC TTA GCC AC
Mmp13 F	AAG ATG TGG AGT GCC TGA TG
Mmp13 R	AAG GCC TTC TCC ACT TCA GA
Sema3e F	CCC CTG TTT CAC CTG GAG TC
Sema3e R	GGA AGA TCG CCG AGT CTC TG
Tnf F	ACG TCG TAG CAA ACC ACC AA
Tnf R	GCA GCC TTG TCC CTT GAA GA
Tnfsf11 (RANKL F	TGT ACT TTC GAG CGC AGA TG
Tnfsf11 (RANKL R)	AGG CTT GTT TCA TCC TCC TG
Tnfrsf11b (OPG) F	GTG GTG CAA GCT GGA ACC CCA G
Tnfrsf11b (OPG) R	AGG CCC TTC AAG GTG TCT TGG TC
Twist2 F	CAG CAA GAT CCA GAC GCT CA
Twist2 R	CTA GTG GGA GGC GGA CAT G
Wnt4 F	CTG GAG AAG TGT GGC TGT GA
Wnt4 R	CAG CCT CGT TGT TGT GAA GA

Real-time PCR cycling conditions.

Step	Temperature	Time
1.	94 °C	2 minutes
2.	94 °C	30 seconds
3.	60 °C	30 seconds
4.	72 °C	30 seconds
5.	72 °C	10 minutes
Steps 2-4 repeated x40 cycles		
6.	Melt curve from 55 °C to 95 °C, Reading every 0.2 seconds, Hold 00:00:01	

Quality control statistics for chondrocyte samples submitted for RNA-sequencing.

Sample	Total reads	Discarded reads	Quality control passed reads	Mapped reads	% mapped
Control 1	93,469,146	2,333,484	88,995,412	85,239,536	95.8
Control 2	148,569,462	2,799,416	143,523,246	135,442,453	94.4
Control 3	76,641,794	1,968,540	72,860,992	69,895,700	95.9
Knockout 1	72,357,646	2,146,139	68,252,010	65,368,088	95.8
Knockout 2	178,819,100	3,285,644	172,540,762	166,006,436	96.2
Knockout 3	90,654,038	3,138,287	84,596,282	80,775,772	95.5

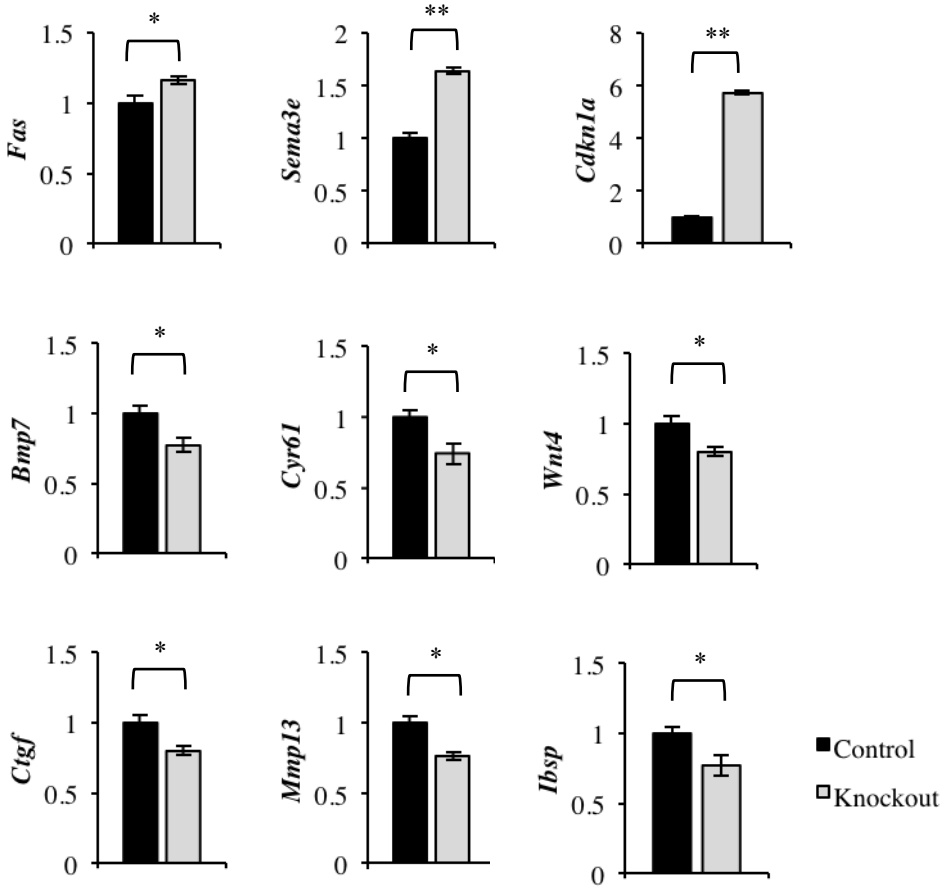

qPCR confirmed several dysregulated genes identified by RNA-seq in *Creld2* knockout chondrocytes.

Quality control statistics for osteoblast RNA samples submitted for RNA-sequencing.

Sample	Total reads	Discarded reads	Quality control passed reads	Mapped reads	% mapped
Control 1	81,048,814	2,010,744	77,425,298	71,986,927	93.0
Control 2	84,891,894	2,625,641	79,995,996	74,601,095	93.3
Control 3	78,541,692	2,079,026	74,788,290	70,579,896	94.4
Knockout 1	78,116,776	1,784,644	74,794,786	71,313,342	95.3
Knockout 2	60,008,688	1,691,956	56,834,908	53,862,437	94.8
Knockout 3	93,905,080	2,175,223	89,932,374	85,056,783	94.6

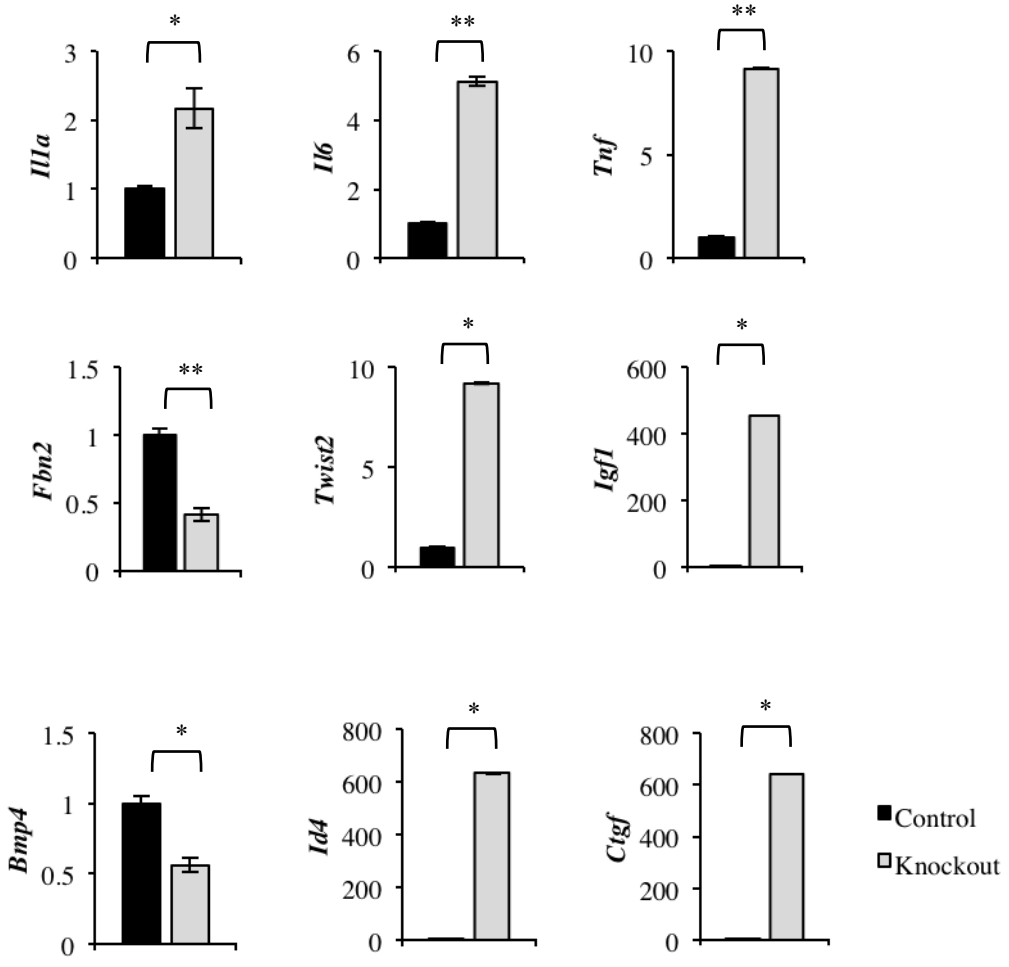

. qPCR confirmed several dysregulated genes identified by RNA-seq in *Creld2* knockout osteoblasts.

Appendix C: Tissue processing programme

Tissue processing programme.

Step	Solution	Time
1.	70 % Ethanol	6 hours
2.	90 % Ethanol	45 minutes
3.	95 % Ethanol	45 minutes
4.	100 % Ethanol	45 minutes
5.	100 % Ethanol	45 minutes
6.	100 % Ethanol	45 minutes
7.	Xylene	30 minutes
8.	Xylene	30 minutes
9.	Xylene	30 minutes
10.	Paraffin wax	1 hour
11.	Paraffin wax	1 hour

Appendix D: Antibodies

Primary antibodies

Primary Antibody Name	Company	Code	Raised in	Dilution
Anti-Acetylated Tubulin	Abcam	ab24610	Mouse monoclonal	1:1000
Anti-Aggrecan	Professor Tim Hardingham, University of Manchester	N/A	Rabbit monoclonal	1:500
Anti-CD81	Santa Cruz Biotech.	sc166029	Mouse polyclonal	1:200
Anti-Collagen I	Abcam	ab34710	Rabbit polyclonal	1:500
Anti-Collagen II	Abcam	ab34712	Rabbit polyclonal	1:500
Anti-Collagen X	Professor Karl Kadler, University of Manchester	N/A	Rabbit monoclonal	1:500
Anti-Creld2	Santa Cruz Biotech.	sc86110	Rabbit polyclonal	1:100
Anti-EEA1	R&D Systems	AF8047	Sheep polyclonal	1:100
Anti-GLG1	Biotechne Ltd.	AF7879	Sheep polyclonal	1:100
Anti-GRP94	Santa Cruz Biotech.	sc1794	Goat polyclonal	1:100
Anti-Matrilin-3	R&D Systems	AF3357	Goat polyclonal	1:500
Anti-Osteoprotegerin	Abcam	ab183910	Rabbit Polyclonal	1:200
Anti-Podocalyxin	Dr Rachael Redgrave, Newcastle University	N/A	Goat polyclonal	1:200
Anti-RANKL	Santa Cruz Biotech.	sc377079	Mouse monoclonal	1:200

Secondary antibodies

Secondary Antibody Name	Company	Code	Raised in	Dilution
Anti-rabbit IgG H+L (AlexaFluor® 594)	Thermo Fisher Scientific	A11012	Goat polyclonal	1:200
Anti-mouse IgG H+L (AlexaFluor® 488)	Thermo Fisher Scientific	A11059	Rabbit polyclonal	1:200
Anti-goat IgG H+L (AlexaFluor® 488)	Thermo Fisher Scientific	A11055	Donkey polyclonal	1:200
Anti-rat IgG H+L (AlexaFluor® 488)	Thermo Fisher Scientific	A21208	Donkey polyclonal	1:200
Anti-sheep IgG H+L (AlexaFluor® 488)	Thermo Fisher Scientific	A11015	Donkey polyclonal	1:200
Anti-mouse IgG H+L (IRDye® 800CW)	LI-COR®	925-32213	Donkey polyclonal	1:10000
Anti-Rabbit IgG H+L (IRDye® 800CW)	LI-COR®	925-32212	Donkey polyclonal	1:10000

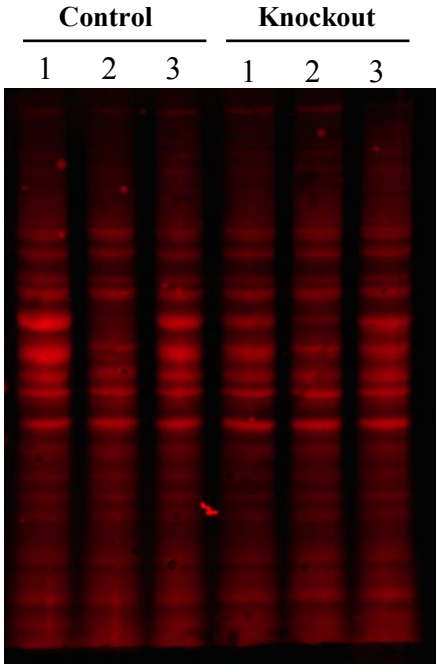

Equal loading of protein shown using REVERT™ total protein stain from LI-COR®.

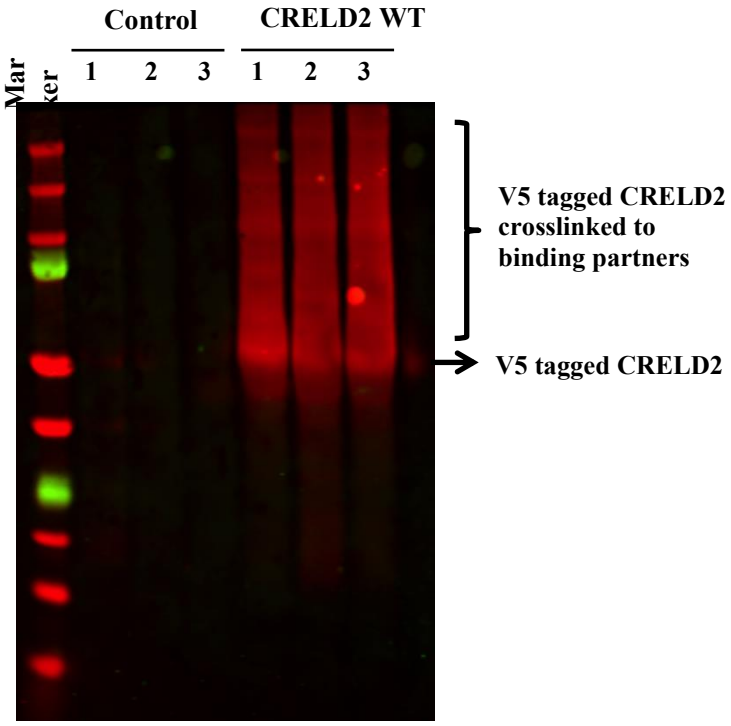

7.2.1 **Western blot of cells transfected with V5-tagged CRELD2 showing cross-linked proteins identified using anti-V5 antibody.**

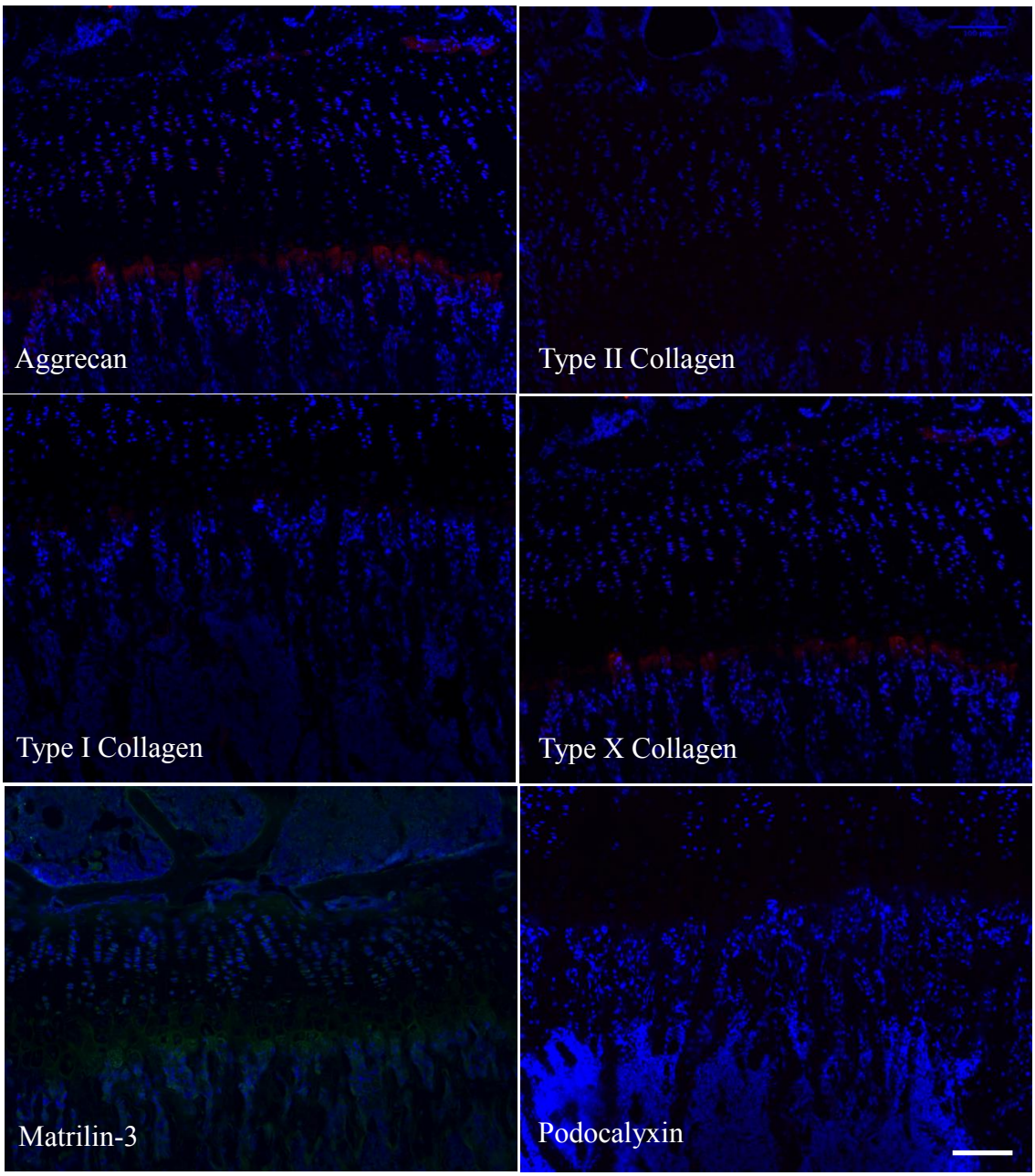

Immunohistochemistry negative controls.

Appendix E: Media

Bone cell growth media

for 500 mL	450 mL	Minimum Essential Medium α, nucleosides, no ascorbic acid	
	50 mL	Fetal bovine serum	(f.c. 10 %)
	5 mL	Penicillin/Streptomycin	(f.c. Penicillin 1 U/mL, Streptomycin 1 µg/mL)

Chondrocyte growth media

for 500 mL:	450 mL	DMEM (Dulbecco's Modified Eagle Medium), high glucose, pyruvate	
	50 mL	Fetal bovine serum	(f.c. 10 %)
	5 mL	Penicillin/Streptomycin	(f.c. Penicillin 1U/mL, Streptomycin 1 µg/mL)
	5 mL	100x Non essential amino acids	(f.c. 1x)
	5 mL	20 mM L-Ascorbate-2-phosphate	(f.c. 50 mg/L)

Osteoclastogenic media

for 50 mL:	50 mL	Bone cell growth media	
	60 µL	10 µg/mL Recombinant RANKL	(f.c. 100 ng/µL)
	15 µL	100 µg/mL Recombinant M-CSF	(f.c. 30 ng/mL)

SW1353 growth media

for 500 mL:	450 mL	DMEM/F-12 (Dulbecco's Modified Eagle Medium / Nutrient Mixture F-12), GLUTAMAX™supplement	
	50 mL	Fetal bovine serum	(f.c. 10 %)
	5 mL	Penicillin/Streptomycin	(f.c. Penicillin 1U/mL, Streptomycin 1 µg/mL)
	5 mL	100x Non essential amino acids	(f.c. 1x)